EXPERIMENTAL CHARACTERIZATION OF SHAPE-MEMORY POLYMERS: INFLUENCE OF PROCESSING METHODS AND CHEMICAL STRUCTURE

David Manuel Santiago Abraira

UNIVERSITAT ROVIRA I VIRGILI
EXPERIMENTAL CHARACTERIZATION OF SHAPE-MEMORY POLYMERS: INFLUENCE OF PROCESSING METHODS AND CHEMICAL STRUCTURE
David Manuel Santiago Abraira

UNIVERSITAT ROVIRA I VIRGILI
EXPERIMENTAL CHARACTERIZATION OF SHAPE-MEMORY POLYMERS: INFLUENCE OF PROCESSING METHODS AND CHEMICAL STRUCTURE
David Manuel Santiago Abraira

David Manuel Santiago Abraira

EXPERIMENTAL CHARACTERIZATION OF SHAPE-MEMORY POLYMERS: INFLUENCE OF PROCESSING METHODS AND CHEMICAL STRUCTURE

DOCTORAL THESIS

Supervised by:
Dr. Silvia De la Flor and Dr. Francesc Ferrando

Department of Mechanical Engineering

UNIVERSITAT ROVIRA i VIRGILI

Tarragona 2016

UNIVERSITAT ROVIRA I VIRGILI
EXPERIMENTAL CHARACTERIZATION OF SHAPE-MEMORY POLYMERS: INFLUENCE OF PROCESSING METHODS AND CHEMICAL STRUCTURE
David Manuel Santiago Abraira

UNIVERSITAT
ROVIRA i VIRGILI
Department of Mecanical Engineering
Avinguda dels Països Catalans, 26
43007, Tarragona, Spain
Tel (34) 977 559602

Dr. Silvia De la Flor López and Dr. Francesc Ferrando Piera, professors of the Mechanical Engineering Department of Universitat Rovira i Virgili,

CERTIFY that the present study, entitled,

"Experimental Characterization of Shape-Memory Polymers: Influence of Processing Methods and Chemical Structure"

presented by Mr. David Manuel Santiago Abraira to obtain the degree of Doctor, has been carried out under our supervision at the Department of Mechanical Engineering of this university and meets the requirements to qualify for the European Mention.

And, to inform you of that, and in order for it to have needed effects, we sign this certification.

Tarragona, April 2016

Doctoral Thesis Supervisor/s:

Dra. Silvia De la Flor López

Dr. Francesc Ferrando Piera

UNIVERSITAT ROVIRA I VIRGILI
EXPERIMENTAL CHARACTERIZATION OF SHAPE-MEMORY POLYMERS: INFLUENCE OF PROCESSING METHODS AND CHEMICAL STRUCTURE
David Manuel Santiago Abraira

Agradecimientos

Hace cuatro años me ofrecieron la posibilidad de empezar un doctorado en Tarragona. "¿Empezar un doctorado en una ciudad extraña para mí, lejos de mi familia y de mis amigos?" pensé. Entonces recordé las palabras que dijo un sabio: "Es muy peligroso, […], cruzar la puerta. Vas hacia el camino y si no cuidas tus pasos no sabes hacia dónde te arrastrarán". Pues bien, yo decidí cruzar la puerta y la verdad es que ha merecido la pena. Ha sido una aventura fantástica, tanto en lo profesional como en lo personal. Con estas líneas me gustaría dar las gracias a todas las personas que me han acompañado durante este tiempo y que tanto me han ayudado.

En primer lugar me gustaría expresar mi más sincero agradecimiento a la Dra. *Silvia De la Flor* y al Dr. *Francesc Ferrando*, que han sido mis supervisores durante el desarrollo de esta tesis. Sus puertas siempre han estado abiertas y su tiempo siempre ha estado disponible para mí. Muchas gracias por vuestra guía, consejo y paciencia ya que han sido una ayuda inestimable.

También me gustaría dar las gracias a la Dra. *Àngels Serra*, al Dr. *Xavier Ramis* y al Dr. *Xavier Fernández-Francos*. En sus despachos desaparecían todas las dudas que me surgían y su sabiduría impregna todas las páginas de este trabajo. Gracias por guiar mis pasos hacia el mundo de la investigación y mostrarme lo apasionante que es. Quiero darle las gracias también al Dr. *Marco Sangermano*, del *Politecnico di Torino*, por darme la oportunidad de trabajar con él durante mi estancia en Turín.

Para mí ha sido todo un honor colaborar con un profesional tan magnífico.

El mayor de todos los logros y el tesoro más valioso que he encontrado durante este doctorado ha sido la amistad de mis compañeros de aventuras. *Albert*, *Javier*, *Yolanda*, *Maria, Valentín e Irene*, ellos me han acompañado desde el primer día y han hecho que esta etapa haya merecido la pena. Con ellos he compartido muchas alegrías y no pocas penas y espero seguir haciéndolo durante mucho tiempo. Gracias chicos, gracias por todo vuestro apoyo y por vuestra amistad.

También quiero dedicarles unas líneas al resto de mis compañeros del *Departamento de Ingeniería Mecánica* y del *Departamento de Química Analítica y Química Orgánica*. Muchas gracias por los buenos momentos que hemos compartido dentro y fuera del despacho y del laboratorio. Me gustaría darles las gracias también a mis compañeros del *Dipartamento di Scienza Applicata e Tecnologia* del *Politecnico di Torino*. Muchas gracias por vuestra compañía y por vuestra hospitalidad. De vosotros es el recuerdo más bonito que guardo de Turín. Grazie mille a tutti.

También le quiero dar las gracias a todo el personal del *Departamento de Ingeniería Mecánica*, pues son unos profesionales fantásticos y unas personas estupendas.

Hay muchas otras personas que no han compartido laboratorio o despacho conmigo, quizá no podían ayudarme con la química o la mecánica, sin embargo sin su colaboración no habría podido llevar a cabo este trabajo.

En primer lugar me gustaría darles las gracias a mis *amigos de Barcelona*, mis amigos de toda la vida, y a mis amigos "*especiales*". Todos los momentos que he compartido con ellos me daban fuerzas para seguir adelante.

También le quiero dar las gracias a la familia *Velasco Aznar* por todo su cariño y todo su apoyo. Ellos siempre me han tratado como a uno más

de su familia y eso ha sido de gran ayuda, no sólo para llevar a cabo este doctorado sino también para hacerme disfrutar más de la vida.

A mi familia, en especial a mis padres *Manuel* y *Áurea* y a mis hermanos *Inés*, *Adelaida* y *Carlos*. Ellos me apoyaron cuando decidí empezar este doctorado y son todo un ejemplo para mí. Gracias a vosotros he aprendido el valor de la humildad, del esfuerzo y del trabajo bien hecho. Espero haber plasmado todas vuestras enseñanzas en esta tesis.

Y por último, a *Noemí*. Ella es mi compañera en una aventura mucho más larga e intrépida, una aventura que decidimos emprender juntos y que es la vida. Muchas gracias por todo tu apoyo, que ha sido la energía que me impulsaba a seguir trabajando día a día. Por tu cariño, que me hace ser mejor persona día tras día. Y simplemente por ser como eres, ya que eso da sentido a mi vida.

Muchas gracias a todos,

David.

UNIVERSITAT ROVIRA I VIRGILI
EXPERIMENTAL CHARACTERIZATION OF SHAPE-MEMORY POLYMERS: INFLUENCE OF PROCESSING METHODS AND CHEMICAL STRUCTURE
David Manuel Santiago Abraira

"Dimidium facti, qui coepit, habet;
sapere aude, incipe"

UNIVERSITAT ROVIRA I VIRGILI
EXPERIMENTAL CHARACTERIZATION OF SHAPE-MEMORY POLYMERS: INFLUENCE OF PROCESSING METHODS AND CHEMICAL STRUCTURE
David Manuel Santiago Abraira

Abstract

In this thesis a selected group of thermoplastic and thermosetting shape-memory polymers were experimentally characterized. The influence of different processing methods and the chemical structure of the shape-memory polymers on thermal, mechanical and shape-memory properties was analysed and discussed.

The thermomechanical conditions selected during shape-memory cycling have a considerable influence on the shape-memory properties of thermoplastic shape-memory polymers. The programming temperature, the maximum stress applied, the temporary shape or the number of cycles strongly affects the results in terms of shape recovery and stabilization of the shape-memory properties. The influence of these thermomechanical conditions on shape-memory properties was evaluated by performing numerous consecutive shape-memory cycles under stress-controlled conditions. The extent of recovery decreased when the shape-memory polymer was subjected to consecutive cycles but this decrease gradually slowed and finally reached steady state. We applied a stabilization criterion to determine which thermomechanical combination gave the best shape-memory properties over the highest number of cycles.

Another important thermomechanical parameter that affects shape-memory performance is the stress-holding time at high temperature. The study of the stress-holding time required a separate investigation because of the significant effect on the shape-memory properties. The decrease in

shape recovery was significantly greater when a stress-holding time was applied and degradation was accentuated when successive cycles were performed.

Chemical structure is an important factor for thermosetting shape-memory polymers. Their crosslinked structure usually restricts their shape-memory properties because of their lack of deformation. Incorporating rubbery domains that increase the length of the polymer chains between netpoints is the most common method for enabling thermosetting polymers to show a shape-memory effect. However, this usually implies poor mechanical properties. In this thesis, new thermosetting shape-memory polymers which combine high mechanical properties and high shape-memory properties were synthesized.

Two different networks were studied: hyperbranched-modified epoxy-based shape-memory polymers and acrylate-based shape-memory polymers with bisphenol A-based monomers as crosslinking agents. The implications that the structure and molecular weight of hyperbranched polymers have on the thermal, mechanical, viscoelastic and shape-memory properties were evaluated. They led to good shape-memory properties and mechanical properties in terms of tensile strength at the onset of the glass transition temperature. However, the hyperbranched polymer content and molecular weight had to be controlled because of their effect on network homogeneity.

In view of the excellent mechanical and shape-memory properties shown, hyperbranched-modified epoxy-based shape-memory polymers are good candidates for demanding mechanical applications such as thermomechanical actuators. It is likely that in these kinds of application the shape-memory polymer must operate under constrained conditions (that is, against an external force or under fixed strain). Consequently, the potential use of hyperbranched-modified epoxy-based shape-memory polymers as actuator was fully characterized. The recovery stress and the mechanical work generated during fully and partially constrained shape

recovery were evaluated as a function of the maximum stress applied and the level of constraint, respectively. The network structure of shape-memory polymers proved to be a key factor for actuator-like applications.

Mechanical properties in terms of maximum stress and strain give important information about the failure limits of the shape-memory polymers when the temporary shape is programmed. However, bearing in mind that the shape-memory polymer might not be programmed in the same place as in which it will operate or might be stored for some time, the shape-memory polymer should be resistant to cracks or scratches that can damage the shape-memory effect. For this reason, the less focused mechanical properties of shape-memory polymers were completely characterized. Tensile testing at different temperatures, Young's modulus, hardness and impact testing were studied. The onset of the glass transition temperature proved to be a desirable programming temperature for shape-memory applications. However, it is possible that in real applications the programming temperature cannot be adjusted at this temperature. Therefore, we also studied the implications on the shape-memory properties when other programming temperatures are used.

With respect to acrylate-based shape-memory polymers, networks synthesized from poly(ethylene glycol)-based monomers have been widely studied for emerging SMP-based medical devices because of their high degree of biocompatibility. The shape-memory properties of these materials show excellent values of shape recovery, shape fixity, recovery stress and mechanical work. However, other multifunctional monomers, such as bisphenol A-based monomers, should be explored for more mechanically demanding applications. The presence of aromatic rings in the structure may lead to higher glass transition temperatures and an increase in the mechanical properties in comparison to classical acrylate-based shape-memory polymers. Accordingly, in this study the implications of the chemical structure of bisphenol A-based monomers

as crosslinking agents and various monofunctional monomers as chain builders on the thermomechanical and shape-memory properties were analyzed and discussed. Tensile tests and shape-memory performances revealed shape-memory materials with good mechanical properties at room and high temperatures and excellent shape-memory properties with high shape-recovery and shape-fixity ratios and fast recovery velocities under isothermal and transient temperature conditions.

The influence of the thermomechanical conditions and the chemical structure of shape-memory polymers have been analysed and discussed. The results show which combination of thermomechanical parameters maximizes the shape-memory properties over the highest number of cycles in thermoplastic shape-memory polymers. In addition, it can be concluded that hyperbranched polymers and bisphenol-A diacrylate-based crosslinking agents can be used to enhance the thermomechanical and shape-memory properties of thermosetting shape-memory polymers.

Table of Contents

List of Abbreviations

$\dot{T}$	Heating rate
$\dot{\varepsilon}$	Deformation rate
$\dot{\sigma}$	Stress rate
A	Area
BADA	Diglycidyl ether of bisphenol A diacrylate
BAEDA	Diglycidyl ether of bisphenol A ethoxylate diacrylate
CED	Cohesive energy density
CTE	Coefficient of thermal expansion
D400	Jeffamine® D400
DETA	Diethylene triamine
DG, DGEBA	Diglycidyl ether of bisphenol A
DMA	Dynamical mechanical analysis
DSC	Differential scanning calorimetry
E	Energy loss of the pendulum with sample
E^*	Complex modulus
E'	Storage modulus
E''	Loss modulus
E'_g	Storage modulus at glassy region
E'_r	Storage modulus at rubbery region
E_0	Energy loss of the pendulum with no sample
E_f	Young modulus calculated under flexural conditions

EMA	Ethyl (meth)acrylate
F	Force
FTIR	Fourier transform infrared spectroscopy
FWHM	Full width at half maximum
HBPs	Hyperbranched polymers
HV	Vickers hardness
L	Length
L_0	Initial length
L_f	Final length
L_l	Corresponding length at σ_m
L_m	Maximum length
L_p	Permanent length
LP	Lupasol®
L_p'	Permanent length at partially constrained recovery
LP2000, LP PR	Lupasol® PR8515
LP800, LP FG	Lupasol® FG
L_u	Length after unloading
L_u'	Length after partially unloading
MMA	Methyl (meth)acrylate
M_w	Molecular weight
N	Cycle
N_e	Stabilization cycle
PGM	Poly(ethylene glycol) methylether methacrylate
R_f	Shape fixity ratio
R_r	Shape recovery ratio
S	Section of the sample
SCE	Shape-changing effect
SEM	Scanning electron microscopy
SMAs	Shape-memory alloys
SME	Shape-memory effect
SMPs	Shape-memory polymers

T	Temperature
t	Time
T_g	Glass transition temperature
$T_{g,mix}$	Glass transition temperature of mixed phase
$T_g^{E'}$	Onset of the glass transition
t_H	Holding time
T_{low}	Low temperature
T_m	Melting temperature
TMA	Thermal mechanical analysis
T_{perm}	Transition temperature of the hard-segment
T_{prog}	Programming temperature
$T_{recovery}$	Recovery temperature
T_{room}	Room temperature
T_{sw}	Switching temperature
T_{trans}	Transition temperature
$T_{trans,A}$	Transition temperature of the domain A
$T_{trans,B}$	Transition temperature of the domain B
$T_{\sigma rec}$	Temperature of maximum recovery stress
V_r	Shape-recovery velocity
W_a	Work output
W_p	Work required to deform the SMP
ε	Deformation
ε_0	Initial deformation
ε_b	Deformation at break
ε_c	Deformation caused by a creep phenomenon
ε_l	Corresponding deformation at σ_m
ε_m	Maximum deformation
ε_p	Permanent deformation
ε_p'	Deformation after partial recovery
ε_{rec}	Strain recovered
$\varepsilon_{rec,15\%}$	Deformation corresponding to 15% of shape

	recovery
$\varepsilon_{rec,85\%}$	Deformation corresponding to 85% of shape recovery
ε_u	Deformation after unloading
ε_u'	Deformation after partial unload
$\varepsilon_{\sigma max}$	Corresponding strain at ultimate strength
θ	Bending angle
ν_c	Crosslinking density
σ	Stress
σ_0	Initial stress
σ_b	Stress at break
σ_{const}	Constraining stress
σ_m	Maximum stress
σ_{max}	Ultimate strength
σ_{rec}	Recovery stress

Chapter I

General Introduction and Objectives

I.1. Introduction

I.1.1. Shape-memory polymers

Shape-memory polymers (SMPs) are materials that are capable of changing their shape upon application of an external stimulus. SMPs can be deformed to a new or temporary shape in their low modulus state and fixed into this new shape in their high modulus state. The temporary shape will remain stable until the application of the external stimulus, which induces the recovery of the original shape [1].

The first appearance of the shape recovery effect was proposed by Vernon in 1941 in a US patent [2], in which a material with "*elastic memory*" could resume its original shape upon heating [3]. However, it was not until the 1960s, before the terminology was being used, when appeared the first applications of SMPs which consisted of heat shrinkable polyethylene tubes and films [4-6]. The term "*shape-memory*" was officially first used in 1984 with the development of a polynorborene based SMP by CdF Chimie Company (France) [7]. Starting from the late 1980s the interest in SMPs has increased significantly. One of the reasons of this trend was the discovery of segmented polyurethane SMPs by Mitsubishi Heavy Industries Ltd. due to the versatility of urethane chemistry and its practical potential [3,8].

The developments in nanotechnology and biotechnology have enabled the use of SMPs in many applications. In biomedicine, SMPs have been applied in form of cardiovascular stents or smart sutures; deployable structures and morphing skins are used in the aerospace field; and the possibility of activate the shape recovery with various stimuli (heat, electricity or magnetism) enables the introduction of SMPs as sensors [1,9].

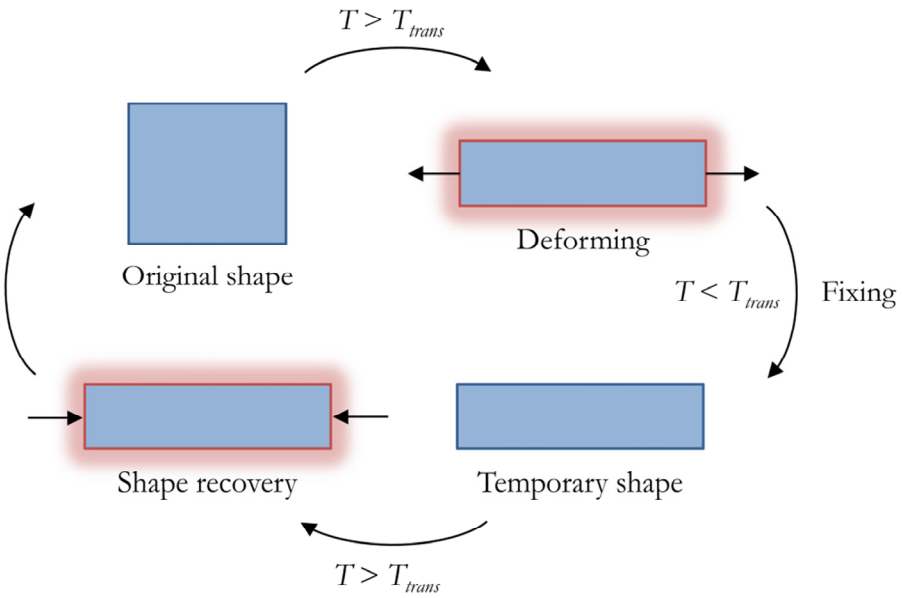

Figure I.1 Schematic representation of the shape-memory effect.

The shape-memory effect (SME) is schematically represented in Figure I.1. The original shape of the polymer is obtained by conventional processing techniques and the temporary shape is obtained by means of a thermomechanical procedure. This consists of heating the polymer to a high temperature, higher than the transition temperature of the SMP (T_{trans}), and deforming it to the specific temporary shape. This new shape is fixed by cooling the SMP to a low temperature, lower than T_{trans}. The SMP will show its new temporary shape until an appropriate stimulus is

applied. In the case of heat-triggered SMPs, the SME will be induced by reheating the SMP above its T_{trans}. After the SME, the SMP shows again its original or permanent shape and can be re-programmed to a new temporary shape [10].

I.1.2. Shape-memory effect

SMPs are not the only materials with shape-changing capabilities. The SME was observed for the first time in a shape-memory alloy (SMA) in 1951 in a AuCd alloy by Chang and Read [11]. The SME in SMAs is given by the martensitic phase transition. The martensitic phase is obtained by cooling from a high temperature austenitic phase. The temporary shape is obtained by deforming the SMA in its martensitic phase. Upon re-heating above the transitions temperatures, the deformed shape will recover its initial shape. The discovery of the SME in nickel-titanium alloys (Nitiniol®) in 1963 [12] led to a great interest toward commercial applications due to transitions temperatures close to the human body, superelasticity and biocompatibility of these alloys.

Compared to SMAs, SMPs possess some advantages such as lower cost, lower density, adjustable T_{trans}, easier processing and larger recovered deformations. SMPs can recover strains up to 200% while in SMAs is less than 10%. However SMPs exhibit lower actuation stresses (less than 10 MPa) than SMA (around 100 MPa) and lower shape-recovery velocity (around an order of magnitude lower, depending on the size of test specimen).

The SME in SMPs is totally different from SMAs and relies on the entropy elasticity. According to the Boltzmann equation:

$$S = k \cdot \ln W \tag{I.1}$$

where S is the entropy, k is the Boltzmann constant and W represents the probability of a conformation, W represents the most probable

conformation that is, the highest entropy conformation which, in the glassy state, is given by random coiled conformation. In the glassy state the movement of the polymer chains are highly impeded. When increasing the temperature above the transition temperature of the polymer, it acquires a rubber-elastic state and the molecular dynamics are greatly enhanced. In this state the polymer can be easily deformed and the polymer chains are aligned in the direction of the applied external force. Therefore, the polymer goes from an equilibrium high entropy random coil state to a non-equilibrium low entropy aligned state. If the external force is released, the polymer springs back and recovers its original shape. However, if the polymer is cooled down while maintaining the external applied force, the recovery of the polymer chains is prohibited because of the formation of reversible secondary crosslinking points. These crosslinking points are able to fix the temporary shape when the external force is released. This non-equilibrium low entropy temporary shape will remain stable until the temperature surpasses the transition temperature of the polymer. When heated above T_{trans}, the reversible secondary crosslinking points which fix the temporary shape disappear and the strain energy stored during cooling is liberated. This energy provides the polymer the driving force to recover its equilibrium high entropy original shape.

I.1.3. Activation methods of shape-memory polymers

The SME is usually heat-triggered but can also be induced by means of other stimuli. The SME in thermally triggered SMPs is activated by the Joule effect from a source of heat such as air or water. However, in many applications it is not possible to directly activate the SME with hot water or air. In the recent years, several articles on alternative activation methods for SMPs have been reported with the aim of eliminate external heat sources.

Functional fillers can be incorporated into the SMPs which can trigger the SME by means of electrical currents or magnetic fields (Figure I.2). The SME is indirectly induced by the Joule effect in these alternative stimuli SMPs and the heat is produced by various methods. In the case of electro-activated SMPs, they are filled with conductive fillers which increase the electrical conductivity [13-15]. The electrical current passes through the SMPs and heats up the polymer [16]. Similar behaviour is shown in magnetically induced SMPs, which are prepared by incorporating magnetic fillers. In these materials the SME is triggered by inductive heating when subjected to a magnetic field [17-19].

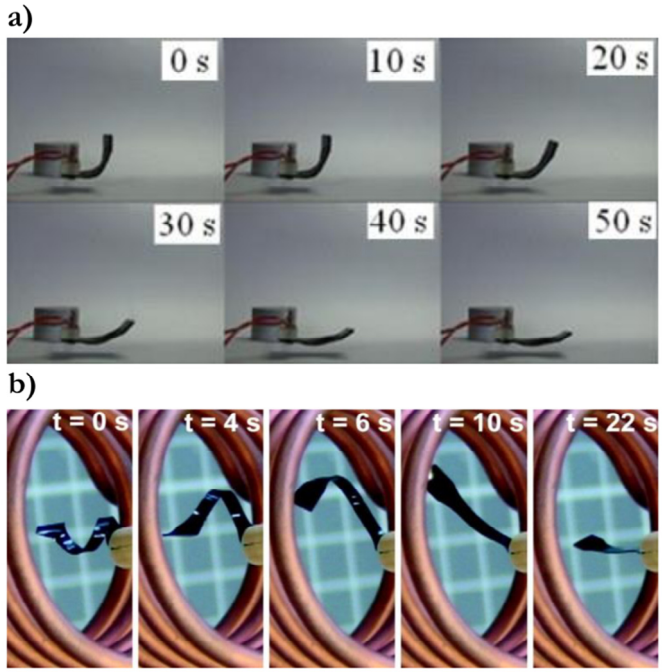

Figure I.2 (a) Shape-memory effect of electro-activated SMPs, from Liu *et al.* [16]. (b) Shape-memory effect magneto-activated SMPs, from Mohr *et al.* [17].

In the case of water or other solvents triggered SMPs the solvent acts as a plasticizers which causes a reduction in the T_{trans} of the SMPs [20]. Bound water can be removed by heating above 120 ºC. Solvent-

triggered SME can also be classified as an indirectly thermal-induced actuation method.

Light induced SMPs incorporate light sensitive molecular switches which can fix the temporary shape and trigger the SME [21]. The main advantage of light activated SMPs is that the SME can be activated at room temperature by remote light activation. Light induced SMEs should not be considered a thermal process.

I.1.4. Network structure of shape-memory polymers

Although all polymers show viscoelastic behaviour not all polymers show shape-memory behaviour [22]. In fact, adequate network structure design is necessary for polymeric systems to exhibit shape-memory behaviour that is, to restore the temporary fixed deformation once reheated to the rubbery state.

In contrast, ordinary polymers do not at all, or only to a low extent, recover from such deformation. Elastomers show a kind of memory effect. The polymer chains become aligned in the direction of an applied external force and, if the external force is applied in a short period of time, the entanglements will spring back the polymer chains and thus recover its original shape. However, if the external force is applied during longer time, the elastomer will show plastic irrecoverable deformation due to a relaxation process [10].

Other materials show another different shape changing phenomenon which is known as shape-changing effect (SCE). The SCE refers to the ability of some materials to alter their shape when an external stimulus is applied and return to their original shape upon releasing of the stimulus. The difference between the SME and the SCE relies on the energy gap between the two different shapes (Figure I.3). If the energy gap is approachable to zero (*H'*), the material recovers its original shape upon removal of the stimulus (SCE). However if the energy gap is high (*H*), the material will maintain its new shape unless a

driving force helps to overcome the energy gap as in the case of SMPs [23].

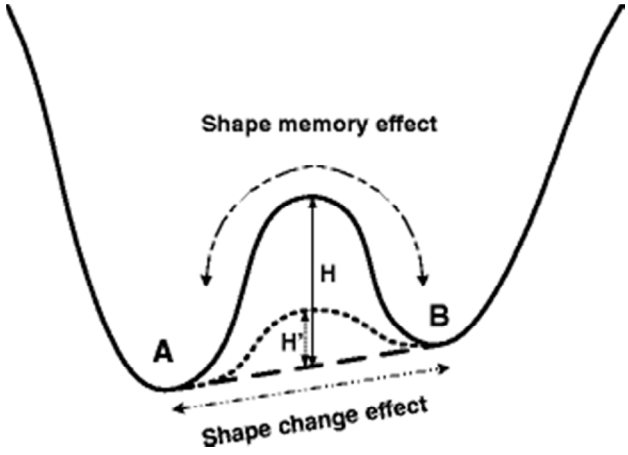

Figure I.3 Schematic representation of the shape-memory effect (SME) and the shape-changing effect (SCE), from Huang *et al.* [23].

The SME results from a combination of a determined network structure and morphology along with a thermomechanical procedure (Section I.1.6). The network structure of the SMPs must allow them to be deformed and fixed into a particular shape relevant for the application and must allow them to memorize their original shape in order to recover the imposed deformation. In general, SMPs architecture consists of netpoints and molecular switches. The netpoints determine the permanent shape and can be chemical (covalent bonds) or physical (molecular interactions, *i.e.* entanglements, hydrogen bonding, van der Waals forces) in nature. Chemical netpoints are formed by the reaction of two functional groups which form a covalent bond. Physical netpoints are obtained in polymers which have two segregated domains. In such SMPs, the phase showing the highest thermal transition (T_{perm}) is known as hard-segment and act as physical netpoints which exerts the driving force to recover the permanent shape. Molecular switches are sensitive to the stimulus and must be able to fix the temporary shape. In thermally-

triggered SMPs, the transition temperature of the molecular switches (T_{trans}) acts as a switch which activates the SME. In phase-segregated SMPs this phase is known as soft-segment [1].

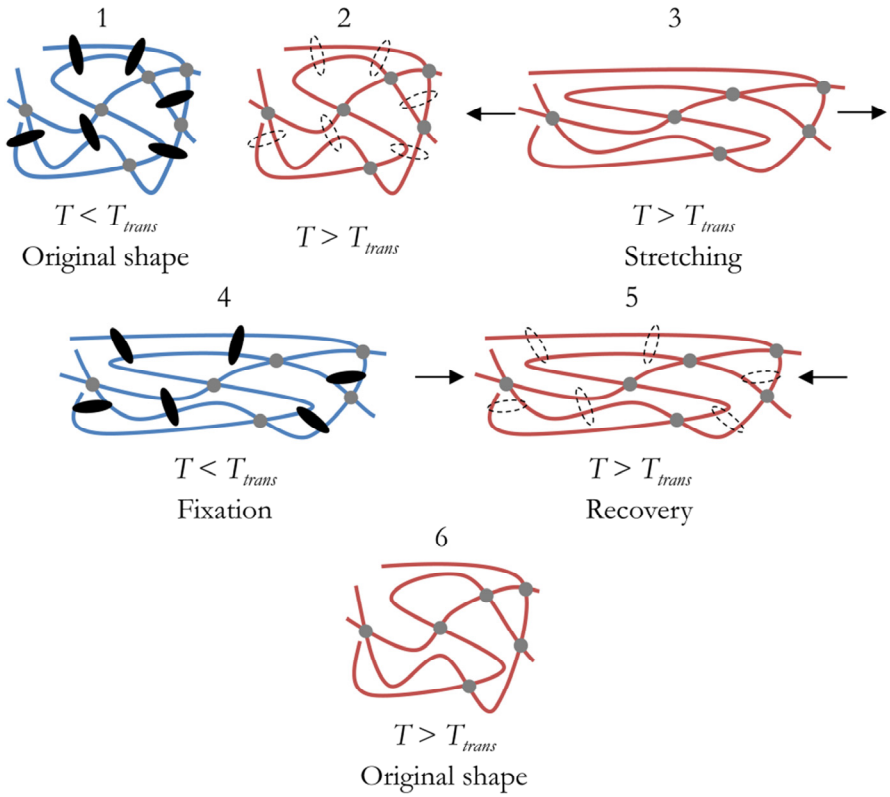

Figure I.4 Schematic representation of the network structure during the shape-memory effect. Grey dots represent netpoints, black filled dots represent secondary reversible crosslinking points, dashed hollow dots represent missing secondary reversible crosslinking points, blue lines represents polymer chains at $T < T_{trans}$ and red lines represents polymer chains at $T > T_{trans}$.

In Figure I.4 are represented the molecular structure of a SMP and the SME for thermally-triggered SMPs. The molecular motion of the SMP depends on the temperature. Below T_{trans}, the motion of the polymer chains (blue lines) is partially impeded (1) whereas above the T_{trans} the polymer chains can move freely (red lines) (2) and can be easily deformed

to the temporary shape (3). The temporary shape is fixed by the formation of reversible secondary crosslinks points (black filled dots). This reversible fixation is formed by the vitrification or crystallization of the molecular switches, depending on whether they are amorphous or semi-crystalline. Therefore, the transition temperature of the SMP can be a glass transition temperature (T_g) or a melting temperature (T_m). The crystallites or the glassy domains formed during cooling will prevent the rearrangement of the polymer chains and the recovery of the applied deformation (4). When the polymer is heated above T_{trans}, the crystallites melt or the glassy domains become rubber (dashed hollow dots) (5) and the permanent shape is recovered due to the driving force exercised by the netpoints (grey dots) (6). In the case of thermoplastic SMPs, the recovery of the permanent shape is carried out by the hard-segment and in the case of thermosetting SMPs the recovery is carried out by the covalent netpoints.

I.1.5. Classification of shape-memory polymers

According to Liu *et al.* [3], SMPs can be classified into four different classes depending on their chemical structure and transition temperature.

I.1.5.1. Class I: covalently crosslinked glassy thermoset networks

This class of SMPs consists of covalently crosslinked networks with a glass transition temperature T_g as T_{trans}. Class I SMPs is characterized by a high degree of shape fixity due to the high modulus at the glassy region and a high degree of shape recovery due to an excellent rubber elasticity at the rubbery region and the absence of chain slippage. As an inconvenient, it is difficult to reshape after the curing reaction because the original shape is covalent bonded [22].

Figure I.5 shows the molecular mechanism of the SME of this class of SMPs. The permanent shape is formed during the curing process of the monomers that form the system. The temporary shape is obtained by deforming the material above its T_g, facilitated by the increase in flexibility of the polymer chains in the rubbery state and is fixed by cooling the SMP below the T_g. In the glassy state, the molecular motion of the SMP is totally impeded, preventing the energy stored to be released and the SMP to recover its permanent shape.

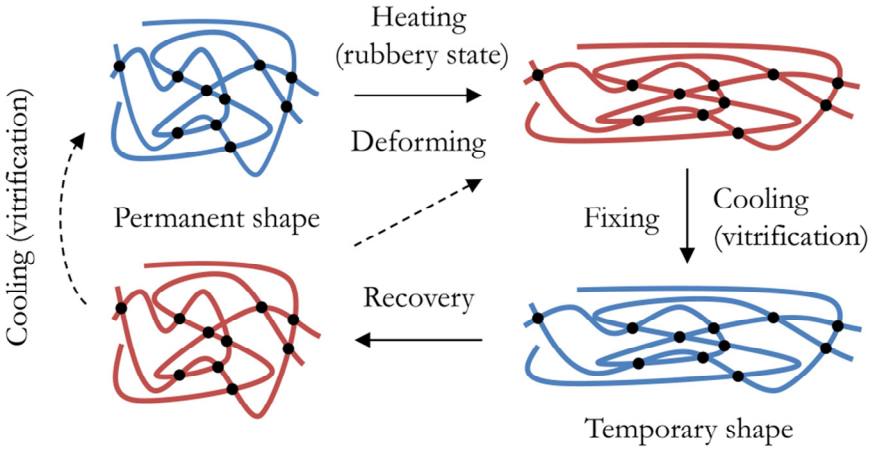

Figure I.5 Molecular mechanism of the shape-memory effect of covalently crosslinked glassy thermoset networks. Black dots represent covalent netpoints, blue lines represent glassy domains and red lines represent rubbery domains.

Epoxy-based SMPs and acrylate-based SMPs are the most common examples of this class of SMPs. In epoxy-based SMPs it is necessary to incorporate rubbery domains in the network in order to increase the distance between crosslinking points and enhance the deformability of the SMP. The most common way to achieve this effect is by aliphatic or aromatic amines [24-27].

From Section IV.3 to Section IV.6 are presented the investigations on epoxy-based SMPs modified with hyperbranched polymers of

different molecular weight, which represent a new kind of Class I SMPs with enhanced mechanical and shape-memory properties.

Acrylate-based SMPs have attracted a lot of interest due to their high degree of biocompatibility, which make them suitable for biomedical applications. The primary backbone of acrylate-based shape-memory networks are formed through free radical polymerization of crosslinking monomers and pendant segments formed by mono-functional chain builder monomers. Several articles can be found from the Gall research group about the thermal and mechanical properties [28-32] and biomedical applications [33-36] of acrylate-based SMPs.

In Section IV.7 is presented the investigation on acrylate-based SMPs synthesized from bisphenol A-based crosslinking agents, which lead to enhanced mechanical and shape-memory properties.

I.1.5.2. Class II: covalently crosslinked semi-crystalline thermoset networks

The SMPs of this class are covalently crosslinked polymers with a melting temperature T_m as T_{trans}. This class is characterized by a high dependence of the shape-memory properties on the degree of crystallinity and the crosslinking density. As in the case of Class I SMPs, these materials cannot be reshaped after processing due to their covalently crosslinked nature. The shape-recovery velocity is faster than in class I SMPs due to their first-order transition temperature (T_m) [3].

Figure I.6 shows the molecular mechanism of the SME of Class II SMPs. The permanent shape is formed during the cure reaction and the temporary shape is fixed by the crystallization of the crystalline domains during the cooling process.

Semi-crystalline rubbers are the most common example of Class II SMPs. They have been favoured as SMPs as a result of their excellent rheological properties, fast shape recovery and flexible modulus below the T_{trans}. Examples of semi-crystalline rubbers include crosslinked

polyethylene systems, with T_{trans} around 120 ºC and shape recovery and shape fixity values around 95% [37,38]; crosslinked polycyclooctene with almost complete shape recovery and shape fixity and T_{trans} around 45 ºC [39]; and crosslinked ethylene-vinyl-acetate rubbers [40,41].

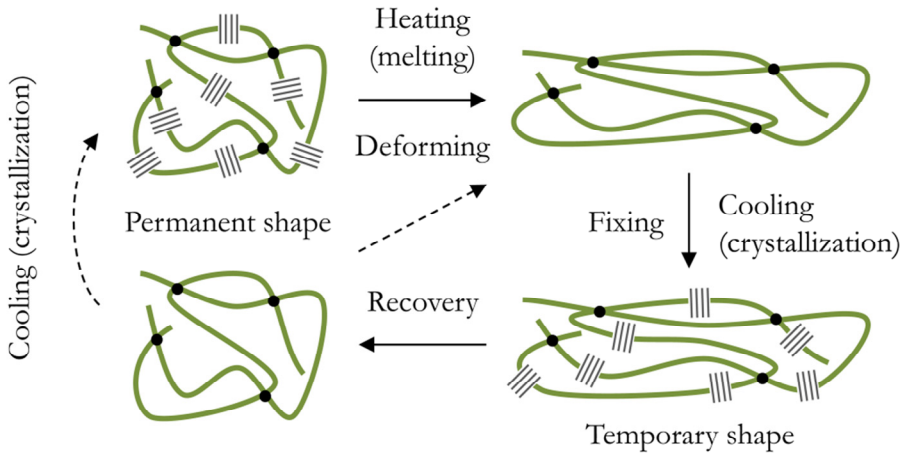

Figure I.6 Molecular mechanism of the shape-memory effect of covalently crosslinked semi-crystalline thermoset networks. Black dots represent covalent netpoints, black lines represent crystalline domains and green lines represent amorphous domains.

I.1.5.3. Class III: physically crosslinked glassy copolymers

The network structure of physically crosslinked SMPs are formed by, at least, two different segregated domains. Figure I.7 schematically represents the molecular mechanism of Class III SMPs. The permanent shape is provided by the physical netpoints of the hard-segment through molecular interactions. The transition temperature of the hard-segment (T_{perm}) can be either a melting temperature (T_m) or a glass transition temperature (T_g). The SME is attributed to the glass transition temperature of the amorphous soft-segments. The temporary shape is obtained by deforming the SMP at a temperature $T_g < T < T_{perm}$, in which the soft-segment is in a rubbery state, and is fixed by cooling to $T < T_g$

[3,22]. The glassy domains formed during cooling prevent the rearrangement of the polymer chains.

Class III SMPs shows lower shape-memory properties as Class I or Class II SMPs mainly because of the absence of chemical crosslinks, which may produce chain slippage during deforming. However their viscoelastic properties make them suitable for several thermoplastic processing methods and in contrast to covalently crosslinked SMPs, when the temperature surpasses the transition temperature of the hard-segment (T_{perm}) the SMP flows and can be reshaped [3].

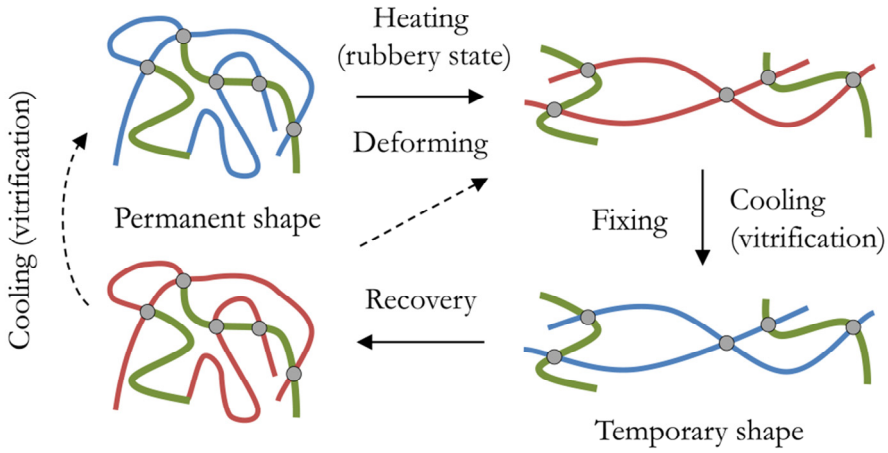

Figure I.7 Molecular mechanism of the shape-memory effect of physically crosslinked glassy copolymers. Grey dots represent physical netpoints, blue lines represent glassy domains of the soft-segment, red lines represent rubbery domains of the soft-segment and green lines represent the hard-segments.

Amorphous polyurethanes represent the majority of this class of SMPs [42-45]. They are usually synthesized from a diisocynate as hard-segment and a polyol as soft-segment by direct coupling of pre-synthesized polymer blocks with a low-molecular weight junction unit, by applying the pre-polymer method or by melt blending [46].

Some studies have reported the influence of the molecular weight of the soft-segment and the hard-segment content [47-49]. Generally, the

extent of shape recovery increases when the hard-segment content and the molecular weight of the soft-segment are decreased; and the extent of shape fixation increases when the molecular weight of the soft-segment is increased and the hard-segment content is decreased.

I.1.5.4. Class IV: physically crosslinked semi-crystalline block copolymers

Class IV SMPs have a very similar structure to Class III SMPs but they have semi-crystalline switching domains and thus a melting temperature T_m as T_{trans}. Figure I.8 shows the molecular mechanism of Class IV SMPs. The temporary shape is obtained by deforming the SMP at $T_m < T < T_{perm}$ and it is fixed due to the crystallization of the soft-segment when cooled to $T < T_m$.

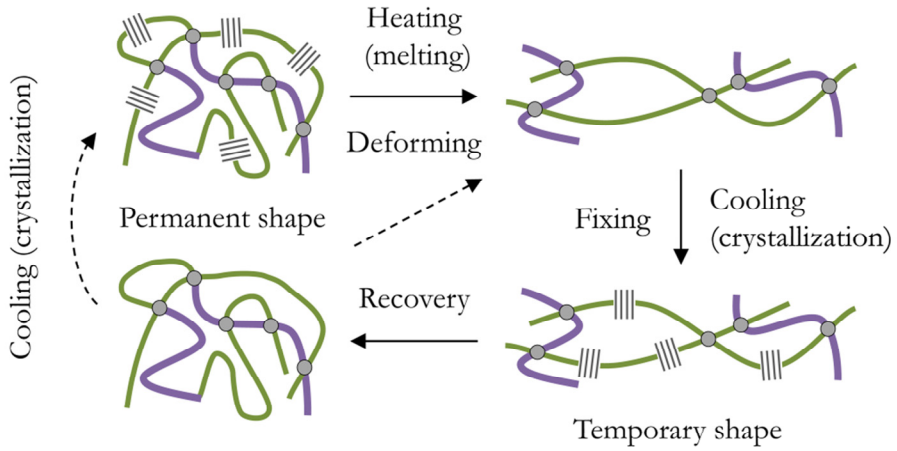

Figure I.8 Molecular mechanism of the shape-memory effect of physically crosslinked semi-crystalline block copolymers. Grey dots represent physical crosslinks, black lines represent semi-crystalline domains of the soft-segment, green lines represent amorphous domains of the soft-segment and purple lines represent the hard-segment.

Semi-crystalline polyurethane-based SMPs represent the most common examples of this class of SMPs [50-52]. They are generally

synthesized from diisocyanates as hard-segment and a polyol or polyester as soft-segment. An average molecular weight around 2000 g/mol is necessary in order to obtain properly phase separation and thus the crystallization of the switching domains [10].

One of the main disadvantages of these materials is that, although shape-memory properties of Class III and Class IV SMPs can be tailored to reach performance levels comparable to those of Class I and Class II SMPs, they require shape-memory training through a minimum of 2–3 shape-memory cycles. Thus, an optimized behaviour for Class IV SMPs is achieved after the sample has been cycled several times according to the application requirements prior to utilization. In addition, in contrast to covalently crosslinked SMPs, a significant irrecoverable strain generally results from the first cycle which persists through subsequent thermomechanical cycles [22].

I.1.6. Shape-memory cycle

The shape-memory cycle is a thermomechanical procedure used to impose or to program a temporary shape to the SMP and to trigger the recovery process. The most common method to perform a shape-memory cycle is the thermomechanical tensile cyclic test. It can be carried out with a universal testing machine equipped with a thermal chamber or with a dynamic mechanical analyser (DMA).

The shape-memory cycle is the most important procedure to determine the shape-memory properties of a SMP. This section presents an overview of the most important characteristics of shape-memory cycling. Shape-memory cycling can be divided into two modules: *programming the temporary shape* and *recovery of the permanent shape*. In Figure I.9 is represented a shape-memory thermomechanical cycle in a strain – temperature – stress plot. This procedure allows obtaining the percentage of strain fixing and strain recovery among other shape-memory properties. The influence of the thermomechanical testing parameters is

discussed and other procedures such as bending, torsion or compression test are presented.

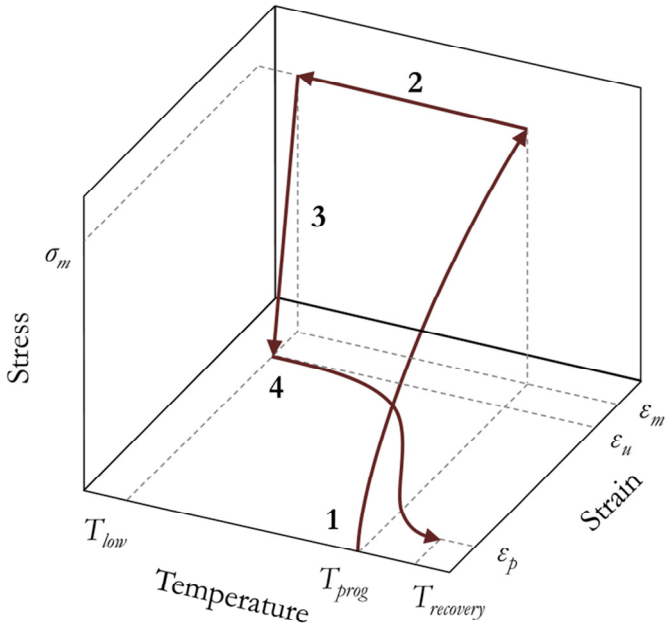

Figure I.9 Schematic representation in a three-dimensional plot of the temporary shape creation procedure or programming.

I.1.6.1. Programming the temporary shape

The programming of the temporary shape can be carried out with a stress-controlled or strain-controlled procedure. The difference between them is based on whether the temporary shape is obtained by deforming the SMP to a prescribed value of stress or strain.

The programming of the temporary shape consists of three steps:

1. Firstly, the SMP is heated to a programming temperature T_{prog} which is usually higher than T_{trans}, and deformed to a determined value of maximum stress (σ_m) or strain (ε_m) at a certain stress or strain rate ($\dot{\sigma}$ o $\dot{\varepsilon}$), depending on whether the programming is stress- or strain-controlled.

2. The SMP is cooled to a low temperature T_{low}, which is lower than T_{trans}, while maintaining the imposed σ_m or ε_m in order to fix the temporary shape. In a stress-controlled programming a creep phenomenon may occur and the resulting deformation may be higher than ε_m whereas in a strain-controlled programming a stress relaxation phenomenon may occur and the resulting stress may be lower than σ_m. A relatively high cooling rate is necessary in order to avoid these phenomena. For the sake of simplicity these two phenomena are not included in Figure I.9.
3. The stress applied to deform the sample (either σ_m or the corresponding stress to achieve ε_m) is released. A spontaneous recovery may occur while unloading the stress and the resulting deformation at the end of the unloading process is ε_u.

I.1.6.2. Recovery of the permanent shape

Once the temporary shape is fixed the next step of the cycle is the recovery of the permanent shape.

4. The SMP is heated to a recovery temperature $T_{recovery}$, which is higher than T_{trans}, at a certain heating rate ($\dot{T}$). The SMP may show a certain amount of irrecoverable or permanent deformation (ε_p) at the end of the cycle. The cycle can be repeated by simply programming the SMP again (step 1).

Once the shape-memory cycle is finished the SME can be quantified that is, the percentage of shape fixity and shape recovery, the switching temperature, the recovery stress or the work output. The evaluation of the shape-memory properties is presented in Section I.1.7.

I.1.6.3. Impact of the thermomechanical testing parameters

The shape-memory properties are greatly influenced by the thermomechanical programming conditions such as the programming

temperature or the maximum stress o strain applied and the thermomechanical recovery conditions such as the heating rate or the recovery temperature. This section presents the influence of some testing parameters on shape-memory properties.

One of the most important programming parameters is the programing temperature T_{prog}, which has a strong effect on the shape recovery and shape fixity. Mohr *et al.* [17] reported shape-recovery ratios around 80% in PDC multiblock copolymers in traditional shape-memory cycles, where the programming temperature is higher than transition temperature of SMP. However when the programming temperature is lower than transition temperature, the extent of recovery is around 50%. In the case of shape fixation, when programming at $T_{prog} > T_{trans}$ it shows values of around 90%; and when the programming temperature is lower than the transition temperature, the extent of fixation is in the range of 50% to 75%.

Accordingly, a programming temperature above the transition temperature is desired. However a number of studies reported a decrease in the extent of recovery on increasing the programming temperature above the transition temperature. Hu *et al.* [53] and Santiago *et al.* [54] reported a descend of shape recovery when programming at T_g + 25, T_g + 50 and T_g + 80 in the first case and when programming at T_g and T_g + 10 in the second case.

The maximum prescribed stress or strain imposed during the programming of the temporary shape is another important testing parameter with great influence on shape-memory properties. Generally speaking, the higher is the deformation achieved during programming the lower is the shape recovery. Hu *et al.* [53] reported a decrease in shape-recovery when applying a maximum deformation ε_m = 300% with respect to maximum deformations of ε_m = 100% and 200% in a polyurethane SMP. The same results were obtained by Schmidt *et al.* [55], where the

shape recovery decreased when ε_m is increased from 100% to 400% in a polyurethane SMP.

The fatigue cycling is an important parameter for the design of applications. It represents somehow the lifetime of the application. Some studies reported the evolution of shape recovery and shape fixity when the SMP is subjected to consecutive thermomechanical cycles [54,56,57]. The percentage of shape recovery decreases in each consecutive cycle due to the accumulation of permanent or plastic deformation at the end of each cycle. This effect is more accentuated in thermoplastic SMPs due to possible slippage of the polymer chains. In the case of shape fixation, the performance of various consecutive cycles does not significantly affects the extent of fixation [54,58].

The effect of these thermomechanical parameters on a commercial aliphatic polyether-based thermoplastic polyurethane (Tecoflex®) is deeply studied in Chapter III. As mentioned before, consecutive cycles cause a degradation of the shape recovery. This degradation is severe during the first cycles and softens as the cycling advances until reaches a steady behaviour. In Section III.3 is analysed how T_{prog} and σ_m affect the stabilization of the shape-memory properties with cycling. Another important thermomechanical parameter that has a great effect on shape-memory properties is the stress-holding time at high temperature. The effect of this parameter is widely analysed in Section III.4.

The recovery temperature $T_{recovery}$ is probably the most influential parameter on shape recovery. The $T_{recovery}$ has to be necessarily above the T_{trans} of the SMP in order to obtain good shape recovery values. As described in Section I.1.2, when the temperature surpasses the transition temperature the polymer chains acquire enough mobility to allow their rearrangement and recovering the original shape of the SMP. Azra *et al.* [59] reported the extent of recovery with different $T_{recovery}$s. Results revealed poor shape-recovery ratios (less than 50%) with $T_{recovery} < T_{trans}$ and around 80%-90% when $T_{recovery} > T_{trans}$.

I.1.6.4. Cold-working programming

The programming temperature for shape-memory cycling is usually higher than the transition temperature of the SMP in order to enhance the molecular mobility of the polymer. This thermomechanical cycle is recognized to be potentially a difficult and expensive operation for practical applications, in particular when large structures have to be employed [60]. The cold-working programming represents a more simplified method that is, deforming the material at temperature below the transition temperature of the SMP [60,61] (Figure I.10).

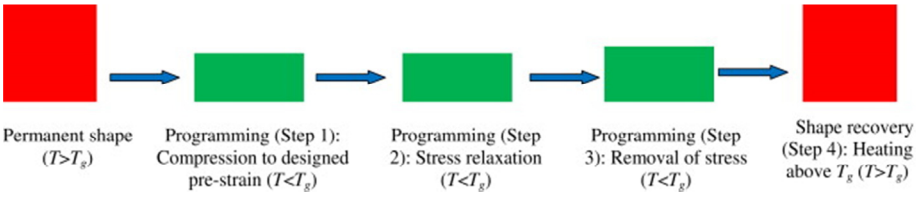

Figure I.10 Schematic representation of the thermomechanical procedure of cold-working programming, from Li and Xu [61].

This non-conventional technique consists of deforming the material above their yielding point in order to maintain a significant amount of deformation after fixation. This deformation can be partially or totally recovered when heating the SMPs above their transition temperature. This effect is known as "*reversible plasticity shape-memory effect*" [8]. The cold-working programming cannot obtain the same extent of shape fixation than traditional, however it present some advantages such as increased recoverable strains or higher stress capacity.

I.1.6.5. Constrained shape-memory recovery

In Section I.1.6.2 is described the recovery process of the permanent shape under unconstrained or free conditions. However the programming can also be carried out under constraining conditions that is, with a fixed strain or under a constraining stress.

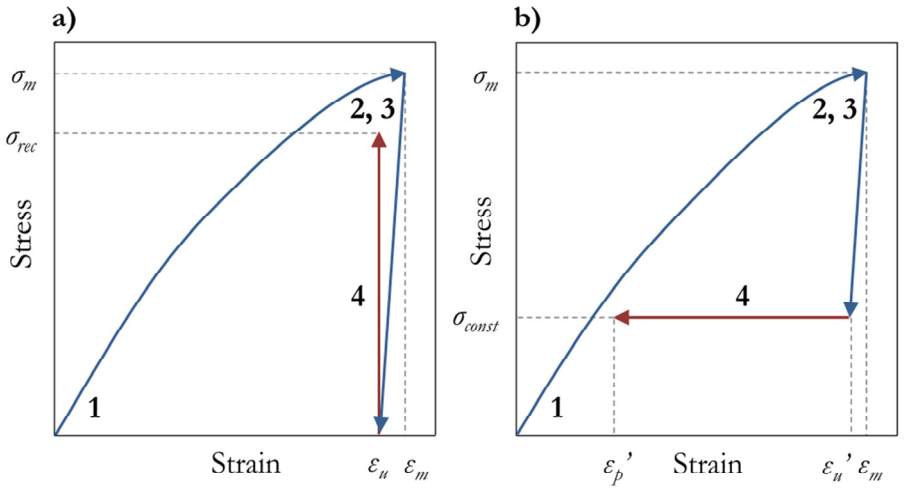

Figure I.11 Schematic representation of the constrained recoveries: a) totally constrained recovery and recovery stress generation; b) partially constrained recovery and work output. The numbers correspond to: 1) deforming to temporary shape, 2) cooling and fixing the temporary shape, 3) unloading the stress applied and 4) heating to $T_{recovery}$ under constrained conditions.

In Figure I.11 is schematically represented the programming under fully constrained conditions (Figure I.11a) and under partially constrained conditions (Figure I.11b). In both cases, the temporary shape creation follows the same path than the programming under free conditions (heating to T_{prog} and cooling to T_{low} while maintaining the stress applied). In the case of programming under fully constrained conditions, the deformation after unloading (ε_u) is held constant while the sample is heated to $T_{recovery}$. In this way, the SMP generates a recovery stress (σ_{rec}) instead of recovery their original shape. In the case of partially constrained recovery, the SMP is not unloaded to $\sigma = 0$ but it is unloaded to a determined value of constraining stress σ_{const}. The deformation of the SMP after partially unloading is ε_u'. σ_{const} is held constant while the SMP is heated to $T_{recovery}$. Under these conditions the SMP generates mechanical work which can be calculated according to Equation I.2:

$$W\left(\frac{kJ}{m^3}\right) = \sigma \cdot \varepsilon \qquad (I.2)$$

The deformation of the SMP after the recovery process is ε_p'.

I.1.6.6. Isothermal temperature shape-memory recovery

In the majority of publications on SMPs, the recovery of the permanent shape is carried out with a determined heating rate to the recovery temperature. This is presumably because most applications investigated in the literature require highly reproducible shape fixity and shape recovery, or high recovery stresses [59]. However, in some applications, usually biomedical applications, a precise control of the recovery temperature is preferred over high shape recovery in order to avoid tissue damage. With this aim, some research studies on the SME under isothermal temperature recovery conditions can be found in the literature [59,62-64].

The shape-memory properties are strongly influenced by T_{prog} and $T_{recovery}$. Generally speaking, the higher the $T_{recovery}$, the higher shape recovery and the faster shape-recovery velocity. For programming temperatures $T_{prog} < T_{trans}$ the shape recovery is more rapid than with $T_{prog} > T_{trans}$. In the case of constrained recovery, the recovery stress shows a maximum as a function of time when the material is programmed $T_{prog} < T_g$, whereas when programmed at $T_{prog} > T_g$ leads to monotonic stress relaxation towards the level defined by the rubbery modulus.

I.1.6.7. Bending, compression and torsion shape-memory tests

Although shape-memory tensile testing are the most common method for the quantification of the SME, other procedures for programming the temporary shape, *i.e.* bending, compression and torsion test can be found in the literature.

The bending shape-memory cycles present some advantages in comparison to tensile tests such as simpler sample and test preparation and many applications involve bending [1]. However the maximum deformation in bending test is much lower than in tensile test. Bending shape-memory cycles can be carried out as simply bending test or as three-point bending test. In a bending test the temporary shape is obtaining by bending the SMP to an angle θ and the shape recovery is monitored in terms of the deformation angle as a function of temperature [26,65,66]. Gall *et al.* [33] used a three-point flexural configuration to study shape-memory properties of acrylate-based SMPs under free and constrained conditions (Figure I.12). Three-point flexural tests allow reasonable stress/strain levels in the sample for the temperature range spanning from the glassy to rubbery state.

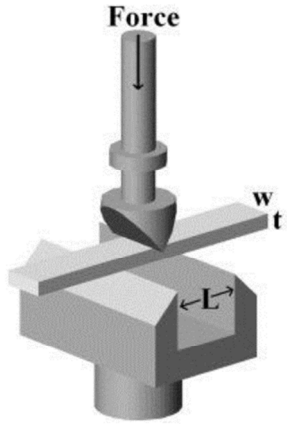

Figure I.12 Schematic representation of the three-point flexural test, from Gall *et al.* [33].

Torsion and compression tests are less used procedures because of the complexity of the equipment necessary to implement the experiment. Diani *et al.* [67] designed a torsion device for testing shape-memory properties at large deformations (Figure I.13a). The mechanical device was designed to apply torsional loading to rectangular specimens and

further monitor their torsion angle recovery through video capture and quantified by image analysis when heated. Westbrook *et al.* [68] presented an improved testing system for thermomechanical cycling in compression (Figure I.13b) which provides faster temperature response and a more uniform sample temperature distribution with respect to existing systems. When characterizing materials with low thermal conductivity, such as polymer compression samples, classic equipments lead to large variations between the measured air temperature and the temperature of the sample. That paper presented an improved system design for thermal management in uniaxial compression experiments that significantly reduces the temperature difference between the air in the chamber and within the sample so that the sample temperature can be assumed to be near that of the reported temperatures.

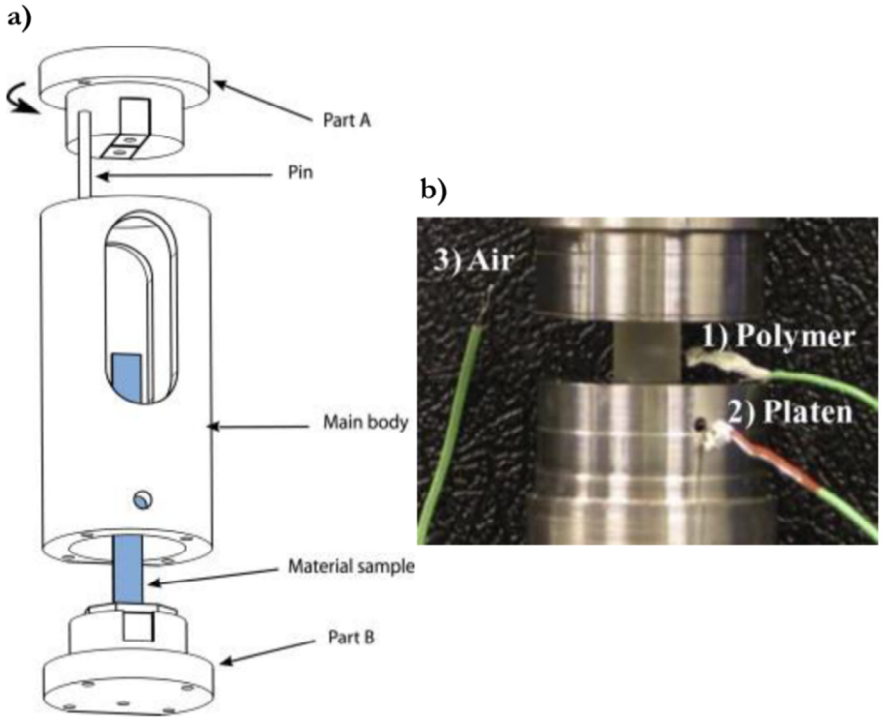

Figure I.13 a) Torsion device, from Diani *et al.* [67]. b) Experimental setup for thermomechanical cycling in compression, from Westbrook *et al.* [68].

I.1.7. Characterization of shape-memory polymers

The extent of shape fixation and shape recovery are the most important properties for quantifying the SME. The characterization of these properties is carried out through the thermomechanical shape-memory cycle described in Section I.1.6. However other characterization methods, such as viscoelastic or thermomechanical methods, are necessary in order to understand structure – operation relations.

I.1.7.1. Storage modulus *E'* and tan δ

Experimental study of temperature- and frequency-dependent properties, such as the storage modulus *E'* and tan δ, using dynamic mechanical analysis (DMA), allows to study molecular mobility of polymeric chains and to draw conclusions about crystallinity, molecular weight or crosslinking density of polymer materials [69]. In addition, some studies noted that it is possible to predict shape-memory properties from the dynamical mechanical analysis [69-72].

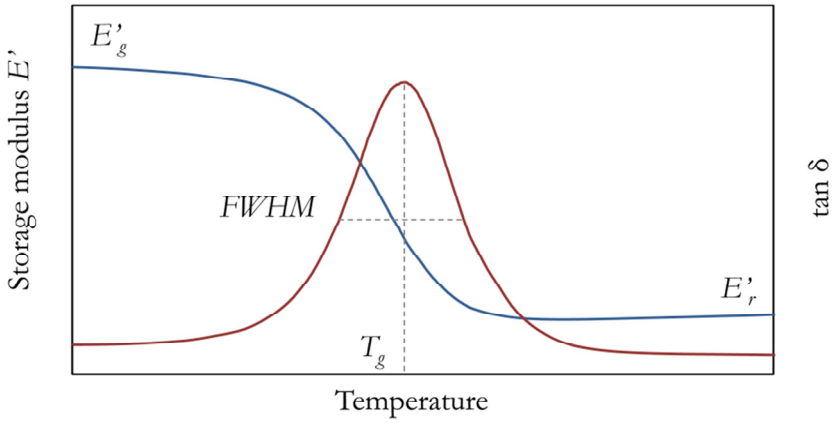

Figure I.14 Schematic representation of the important parameters obtained from dynamic mechanical analysis (DMA).

In Figure I.14 are represented the most relevant parameters for SMPs obtained from DMA analysis. The glass transition temperature T_g is determined from the peak of the tan δ curve and the modulus at glassy region (E'_g) and at rubbery region (E'_r) is determined directly from the curve of the storage modulus. The sharpness of the transition can be determined with the full width at half maximum (FWHM).

A high storage modulus at rubbery region (E'_r) is advantageous for the shape recovery and the shape-recovery velocity. E'_r can be tailored through the crosslinking density of the network (in Class I and Class II SMPs) (ν_c). According to the theory of rubber elasticity, E'_r is related to the crosslinking density by Equation I.3:

$$E'_r = 3 \cdot R \cdot T \cdot \varrho \cdot \nu_c \qquad \text{(I.3)}$$

where R is the universal gas constant, T is the temperature at which E'_r was determined, ϱ is the density of the material and ν_c is the crosslinking density. SMPs with high ν_c will provide a higher driving force during the shape recovery [73]. Although Equation I.3 refers to ideal rubbers and some non-ideal factors should be considered such as physical entanglements and non-Gaussian deformation, it gives a good correlation between E'_r and ν_c [72].

A high storage modulus at glassy region (E'_g) is advantageous for shape fixity. Overall, a difference of two orders of magnitude between E'_g and E'_r (or $E'_g/E'_r > 100$) will ensure properly shape recovery and shape fixity [74].

The peak of the tan δ curve is accepted as indicator for the glass transition temperature of the polymer and the shape of the curve during material relaxation can be correlated with its network structure. The peak height is an indication of the viscous character of the material during the relaxation and the total peak area is related to the total amount of energy dissipated during the relaxation. Moreover, the sharpness of the relaxation is related with the shape-recovery velocity [72]. Materials with a

more heterogeneous network structure and a broader relaxation profile (higher FWHM and lower tan δ peak) have a slower relaxation process, limiting the molecular motion and thus adversely affecting the shape recovery process.

I.1.7.2. Mechanical properties

The characterization of the mechanical properties of SMPs is an important stage before the operation of the SME. It is necessary to know which are the failure limits in order to not to overcome them during the programming of the temporary shape. For thermomechanical tensile shape-memory cycles this is carried out by tensile stretching until failure. The stress at break, strain at break, Young's modulus or elastic energy density capacity can be obtained from this experiment.

Several studies on enhanced mechanical properties of SMPs can be found in the literature. Increasing the maximum deformation achievable is the most widely studied feature, especially in Class I and Class II SMPs [25,75,76]. However mechanical requirements of SMPs go beyond the showing of high values for stress and strain at break. Some SMP applications like biomedical applications (*i.e.* cardiovascular stents, smart sutures) may require the material to operate in a conditioned environment. Thus it is necessary to know the implications of the environment on shape-memory properties [77]. Other mechanical property that might be interesting for the design of shape-memory applications is the impact strength or hardness [78,79]. Bearing in mind other applications such as thermomechanical actuators or self-deployable structures, it is likely the SMPs may operate in an aggressive mechanically demanding environment. Some applications may require the temporary shape to be programmed at a different site from the one in which it will operate. High impact strength may be desirable in order to avoid cracks produced during shipping which can damage the shape-memory behaviour of the material. In Section IV.6 is presented a complete

characterization of these mechanical properties in a series of thermosetting SMPs, including the Young's modulus, impact strength and hardness evaluation.

I.1.7.3. Shape-recovery ratio

The shape-recovery ratio (R_r) quantifies the ability of SMPs to recover the imposed deformation during the programming of the temporary shape or, in other words, the ability of the SMPs to memorize their permanent shape. Two expressions of R_r have been reported. The first one, reported by Tobushi *et al.* [80] is expressed in Equation I.4 in accordance to notation in Figure I.9:

$$R_r(\mathrm{N}) = \frac{\varepsilon_m(\mathrm{N}) - \varepsilon_p(\mathrm{N})}{\varepsilon_m(\mathrm{N}) - \varepsilon_p(\mathrm{N}-1)} \cdot 100 \qquad \text{(I.4)}$$

This ratio compares the deformation recovered during the *N*th cycle $\varepsilon_m(\mathrm{N}) - \varepsilon_p(\mathrm{N})$ with the deformation recovered during the previous cycle $\varepsilon_m(\mathrm{N}) - \varepsilon_p(\mathrm{N}-1)$. The drawback of this definition is that it does not give a full picture of the material capability. Usually, in studies where Tobushi's ratio is used, the permanent strain following the shape-memory cycle increases from cycle 1 to 10. Tobushi's shape-recovery ratio indicates a recovery performance which begins low and increases toward 100% as the cycling is continued. This increase may lead to believe that the material recovery is improving while it is simply stabilizing to a constant state of performance which is comprised of a lower magnitude of strain recovered than in the first shape-memory cycle [81].

The second one, reported by Lendlein and Kelch [10] is expressed in Equation I.5:

$$R_r(\mathrm{N}) = \frac{\varepsilon_m(\mathrm{N}) - \varepsilon_p(\mathrm{N})}{\varepsilon_m(\mathrm{N})} \cdot 100 \qquad \text{(I.5)}$$

This ratio compares the deformation recovered during the *N*th cycle $\varepsilon_m(N) - \varepsilon_p(N)$ with the maximum prescribed deformation applied $\varepsilon_m(N)$. The shape-recovery ratio defined in Equation I.5 uses the original pre-deformed configuration as the reference value, and therefore provides a measure of the performance of the material in reference to its original state when cycled multiple times [81]. This parameter has been adopted for the shape-memory performances realized during the realization of this thesis.

I.1.7.4. Shape-fixity ratio

The shape-fixity ratio quantifies the ability of SMPs to fix the temporary shape and it is calculated according to Equation (I.6):

$$R_f(N) = \frac{\varepsilon_u(N)}{\varepsilon_m(N)} \cdot 100 \qquad \text{(I.6)}$$

I.1.7.5. Shape-recovery velocity

Another important parameter is the velocity at which SMPs recover their original shape (V_r). Rousseau and Xie [82] described the V_r as a percentage of recovery per unit time accomplished by a SMP in the temperature window where 10–90% recovery is accomplished between the corresponding temperatures $T_{10\%}$ and $T_{90\%}$ (Equation I.7).

$$V_r\,(\%/\text{min}) = \frac{0.8 \cdot R_f \cdot \varepsilon_u}{T_{90\%} - T_{10\%}} \cdot \left(\frac{dT}{dt}\right) \qquad \text{(I.7)}$$

More recently, another way to calculate V_r was described by our research group [83] as the relation of a 15% to 85% of strain recovered between the corresponding time $t_{15\%}$ and $t_{85\%}$ (Equation I.8):

$$V_r\,(\%/\mathrm{min}) = \frac{\left(\frac{\varepsilon_{rec,15\%} - \varepsilon_{rec,85\%}}{\varepsilon_{rec,15\%}}\right) \cdot 100}{\Delta t_{15\%-85\%}} \qquad \text{(I.8)}$$

I.1.7.6. Switching temperature

The switching temperature (T_{sw}) is the temperature at which the shape recovery is initiated. T_{sw} can be determined as the inflexion point of the recovery curve in a temperature – strain axis (Figure I.15). T_{sw} is related to the T_{trans} of the SMP, however it is necessary to differentiate it from T_{trans} because some conditions may affect the temperature at which the SME is activated, such as the T_{prog} [84].

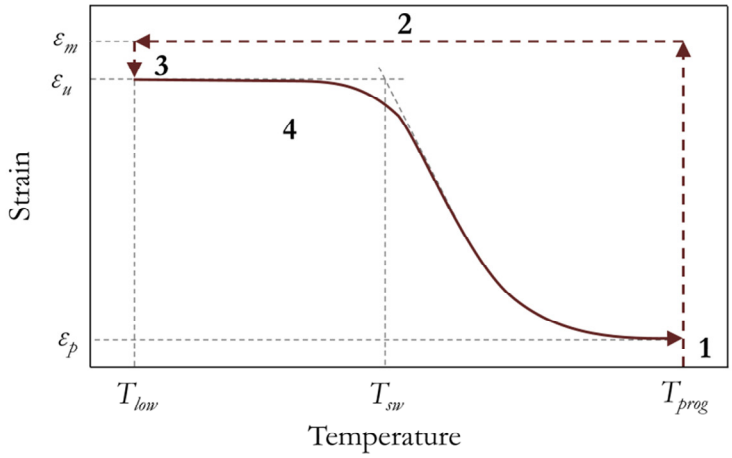

Figure I.15 Schematic representation of the determination of the switching temperature T_{sw} in temperature – strain axis. The numbers correspond to: 1) deforming to temporary shape, 2) cooling and fixing the temporary shape, 3) unloading the stress applied and 4) heating to $T_{recovery}$.

I.1.7.7. Recovery stress

The energy stored after the fixation of the temporary shape can be used to generate recovery stress σ_{rec}. The methodology for recovery stress generation was described in Section I.1.6.5. The recovery stress

generation can be monitored as a function of temperature. σ_{rec} progressively increases as the temperature increases until it reaches a maximum at a determined temperature known as $T_{\sigma rec}$.

Many factors affect the recovery stress generation. On one hand, the recovery stress is strongly dependent on the applied thermomechanical conditions of the programming. In a constrained recovery, the energy stored during fixation is released in form of recovery stress. Thus a higher applied deformation during programming will lead to a higher entropy gain during recovery and higher recovery stress [85]. T_{prog} can also affect the recovery stress generation. That is, deforming the SMP at different T_{prog}s will require different amount of energy, even if the SMP is deformed to the same σ_m or ε_m, and thus different recovery stresses [8]. Allowing the SMP to undergo some molecular relaxation leads to a lower recovery stress generation [86]. Therefore, limiting the loss of energy both during fixation and recovery leads to better results in the recovery stress generation.

On the other hand, the molecular structure of the SMP plays an important role on the recovery stress. Various studies have explored ways to enhance the recovery stress by increasing the rubbery modulus of the SMP. This have been accomplished by increasing the crosslinking density of the SMP [32] or reinforce the SMP with fillers [85].

In addition to crosslinking density, network homogeneity also plays an important role in recovery stress generation. The influence of both parameters as well as the maximum stress applied during programming on the recovery stress generation is presented in Section IV.5, in which a series of thermosetting SMPs are subjected to totally and partially constrained shape recovery.

I.1.7.8. Work output

Neither unconstrained nor fully constrained conditions are likely to be realized for the majority of SMP applications. It is more probable that in

actual service, the SMP will be partially constrained, meaning that the material will be allowed to recover under an applied stress below the maximum stress required for programming the temporary shape [31]. The methodology of partially constrained shape recovery was described in Section I.1.6.5. Under these conditions, the SMP will recover part of the deformation stored under a constraining stress and thus will generate mechanical work according to Equation I.2.

The majority of studies have investigated the SME under free or totally constrained conditions. However, just a few research studies have investigated the work output generated by SMPs when the shape recovery is performed under partially constrained conditions. Lakhera *et al.* [31] quantified the recoverable work and the efficiency of the recovery process in (meth)acrylate-based shape-memory thermosets. Results obtained showed that the maximum work output scaled with the magnitude of the rubbery modulus but the efficiency was similar for all materials for the same programming temperature. The authors observed that to obtain highest efficiency from the SMP, samples should be allowed to recover approximately half the initial deformation under constraining stress. Kolesov *et al.* [87] measured the mechanical work generated by release of the stored energy and resulting stress during shape recovery under 0.1 or 0.2 MPa applied load in short-chain branched polyethylenes. The work generated by the programmed specimen during recovery slightly increased with crosslinking density, despite the substantial increase in programming stress. Rapp and Baier [88] introduced an experimental procedure to determine the work output using closed-loop force controlled thermo-mechanical cycling. This study discovered that for moderate maximum strains, the performance of SMP actuators in compression is better than in tension because of the superposition of the thermal expansion and the SME.

With the aim of contributing to the knowledge of this understudied area, in Section IV.5 is presented a complete study of partially

constrained recovery and mechanical work generation in thermosetting SMPs.

I.1.8. Multi shape-memory effect

Multi shape-memory effect is based on multiphase polymer network structures with at least two phase-separated domains. These domains are associated to individual transition temperatures (T_gs or T_ms). Upon cooling below T_{trans} of a specific domain, this domain solidifies forming physical crosslinks. As these additional crosslinks dominate the covalent netpoints below T_{trans}, they enable the temporary fixation of an elastic deformation, which can be recovered by reheating [89]. Accordingly, in addition to the original shape, multi shape-memory polymers can exhibit more than one temporary shape.

The coexistence of two thermal transitions in a single polymer is not uncommon. For instance, semicrystalline polymers typically possess an amorphous phase (thus a glass transition) in addition to their crystalline phase [8]. Some examples of triple and multi shape-memory polymers can be found in the literature [90-92].

Figure I.16 shows a schematic representation of the operation of a triple shape-memory polymer. While the original shape C is determined by the covalent netpoints during polymer network formation, shapes B and A are fixed by physical crosslinks created in a thermomechanical process. The shape B is determined by the highest transition temperature $T_{trans,B}$, while the second highest transition temperature $T_{trans,A}$ is associated to shape A. During the thermomechanical procedure to program the temporary shapes, the polymer is heated to $T_{high} > T_{trans,B}$ and is deformed to shape B. Physical crosslinks related to $T_{trans,B}$ are formed when the material is cooled under external stress to a temperature $T_{trans,A} < T < T_{trans,B}$. Shape B is obtained after releasing the external stress. Shape A is created subsequently by deformation of shape B at $T_{trans,A} < T < T_{trans,B}$ and cooling to $T_{low} < T_{trans,A}$ under external stress and successive release of

it. Reheating to a temperature $T_{trans,A} < T < T_{trans,B}$ the polymer recovers shape B and consequent heating to T_{high} results in shape C [89].

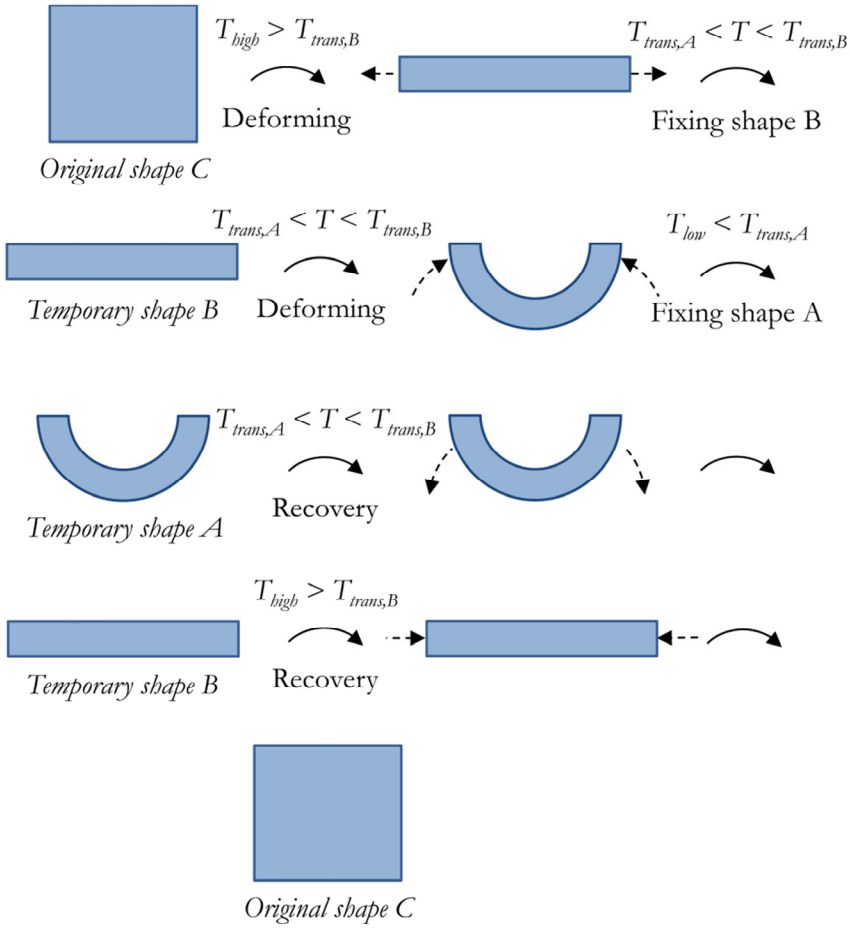

Figure I.16 Schematic representation of the operation of a triple shape-memory polymer.

I.1.9. Shape-memory polymers applications

Since their discovery, many applications have been designed based on the unique characteristics of SMPs. Excellent articles and reviews about SMPs applications can be found in the literature [93-95]. In the following

section only the most representative and featured applications described in the literature are presented.

I.1.9.1. Biomedical applications

SMPs have been promoted for biomedical applications due to their potential in minimal invasive surgery, the possibility of combine many functionalities such as biodegradability or drug release and the easiness which they can be adapted to a singular patient [1].

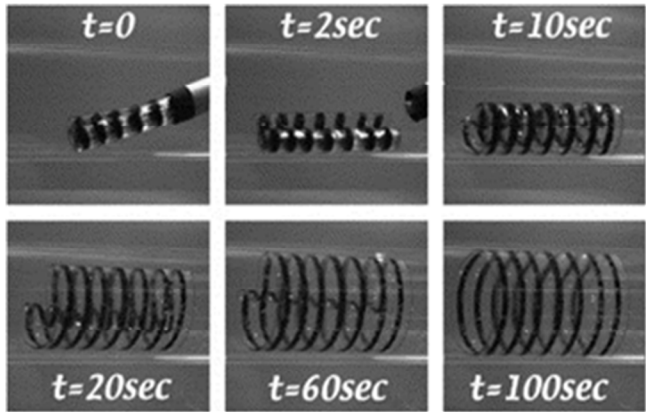

Figure I.17 Photo sequence of the deployment of the SMP cardiovascular stent, from Yakacki *et al.* [34]. The deployment took place in 18 Fr. catheter in a 37 ºC water bath.

One of the most interesting SMP biomedical applications is intravascular stents. Expandable vascular stents are devices used to expand blood vessels in the treatment of arterial stenosis. Most of the vascular stents are metallic and are deployed by balloon expansion or self-expansion. The advantages of using SMPs stents instead of classic metal stents are increased biocompatibility and biodegradability, lower cost and the possibility of be deployed at body temperature. Yakacki *et al.* [34] published the characterization of unconstrained recovery of SMP stents of thermosetting methacrylates (Figure I.17). They studied shape recovery

as a function of T_g, crosslinking density and geometrical perforation which can be independently tailored. The time for full deployment and shape fixity was found to be highly dependent on T_g, crosslinking density and T_{prog}.

Baer *et al.* [96] reported a laser-activated thermoplastic polyurethane SMP stent. The stent did not full deploy under flow conditions due to convective cooling, however this research has important implications in terms of photothermal activation and avoiding tissue damage.

Smart sutures may facilitate the manipulation of surgical sutures in order to prevent necrosis of the surrounding tissue when the force is too strong or the formation of hernia when the force is too weak. The temporary shape is obtained by elongating the fiber under controlled stress. When the temperature is raised above the T_{trans} of the fiber (which is close to body temperature), the suture will shrink and tighten the knot, applying an optimal force (Figure I.18) [97].

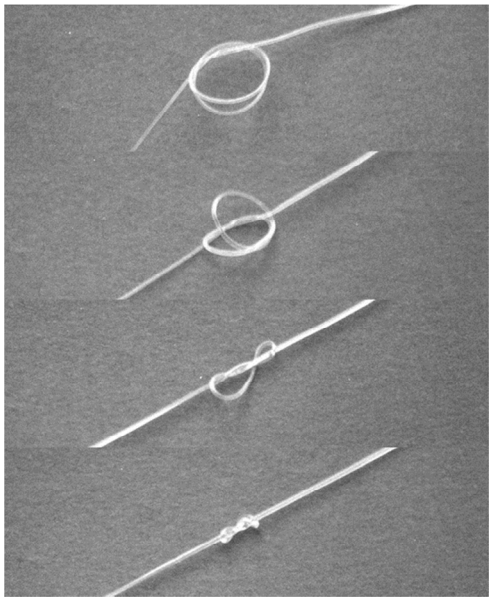

Figure I.18 Photo sequence of the recovery process of a thermoplastic shape-memory polymer fiber for smart sutures, from Lendlein and Langer [97]. The photo series shows how the knot tightened in 20 seconds when heated to 40°C.

Another interesting application is actuators for clot removing. Patients who have suffered a thrombotic stroke should be immediately treated in order to prevent irreparable cell damage or event death. SMPs for clot-removal devices are a promising alternative of pharmaceutical clot removing treatment for stroke patients. Small *et al.* [98] developed a intravascular device to mechanically retrieve thrombus using a laser-activated polyurethane-based SMP (Figure I.19). The device is delivered through a catheter distal in its temporary shape, which is a straight rod, in the thrombotic vascular occlusion. Then the SME is activated by laser heating and the device returns to its original shape in form of corkscrew. By retracting the device the thrombus is captured and removed.

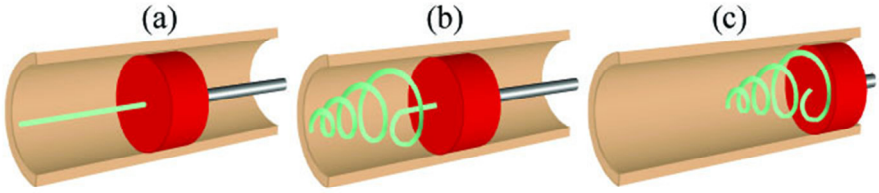

Figure I.19 Depiction of the intravascular laser-activated SMP device used in thrombectomy, from Small *et al.* [98]. a) The actuator is coupled to an optical fiber in its straight rod temporary shape; b) the actuator is transformed in its corkscrew original shape by laser heating; c) the actuator is retracted to remove the thrombus.

I.1.9.2. Aerospace applications

SMPs are also good candidates for future aerospace applications. Structures and devices made from these materials present some advantages in front of the classic ones: lower weight, lower cost and take up less space in the spacecraft because can be packaged in their reduced volume temporary shape and can be deployed under a variety of stimulus [94]. The variety of devices reported for aerospace applications are numerous for this reason in this section only a representative part of them are described, including hinges, boom and antennas.

Hinges are used as driving devices in the deployment of deployable structures. Traditionally it was carried out by steel tape spring hinges. However, they show some disadvantages such as large shock effect and complexity. SMP and SMP-composite hinges are increasingly applied in deployable structures in order to reduce the moving parts [94]. Lan *et al.* [99] developed a carbon fiber reinforced SMP composite hinge (Figure I.20). The hinge was subjected to 140º bending angle and showed almost complete recovery in approximately 100s.

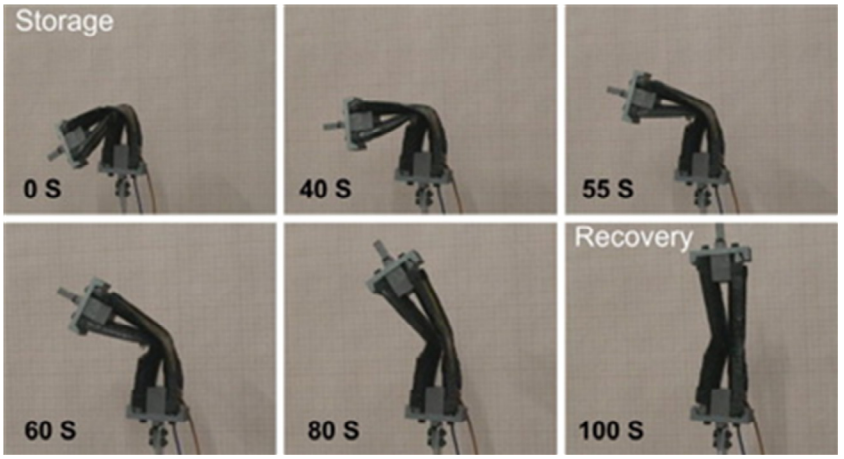

Figure I.20 Photo sequence of the deployment of the SMP composite hinger, from Land *et al.* [99]. The storage angle was 140º and it took 100s for whole deployment at 80 ºC.

Booms are used in satellites and spacecrafts to deploy solar arrays, antennas or other supporting instruments once they have reached their destiny. Researches have explored the replacement of traditional booms for SMP and SMP-composites booms. They possess simpler structure because do not have mechanical devices, less weight and can support big payloads. The Composite Technology Development Inc. (CDT) developed a SMP-composite extendable boom to support a micro-propulsion attitude control system in micro-satellite (Figure I.21) [100].

The longerons of the boom are programmed in a 'z shape' and once in orbit, a series of resistor heaters trigger the SME and deploy the boom.

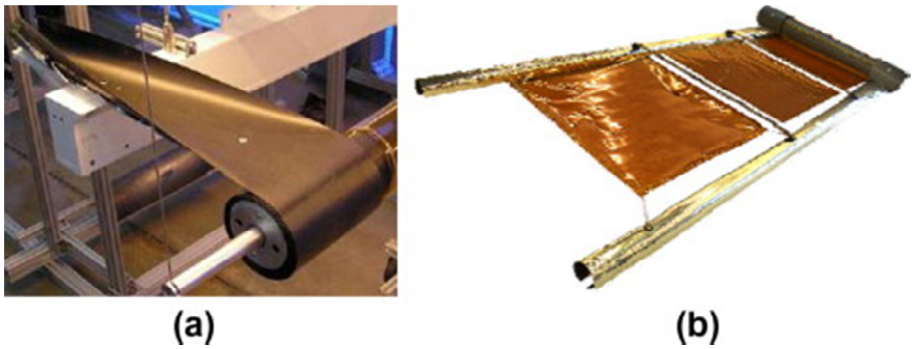

Figure I.21 Deployment of a SMP composite boom, from Campbell *et al.* [100]. a) SMP composite boom and b) partially deployed solar array supported by the SMP composite boom.

Antennas are one of the most important parts in a satellite or spacecraft because allows the communication with the Earth. Many researchers have investigated novel types of structure which satisfy a correct deployment. The antenna can be stowed in the spacecraft and then deployed to finally hold the surface of the antenna. Harrys Corporation developed a solid surface deployable reflector called Flexible Precision Reflector (FPR) (Figure I.22) [101].

Figure I.22 SMP composite reflector, from Keller *et al.* [101]. a) Pre-deformed shape and b) recovered shape.

I.1.9.3. Other applications

SMPs are also attractive materials for textile applications. The SME can be used to control the breathability and waterproofness and windproofness [102-104]. SMPs for breathable fabrics have a T_g and a change of permeability around human body temperature. When the body temperature is above the T_g, the molecular free volume of the film increases and enables the transfer of heat and vapor through perspiration. When the body temperature is below the T_g, the molecular free volume decreases and prevents air and water molecules from passing through. Thus the SMP can help in maintaining a stable body temperature [95].

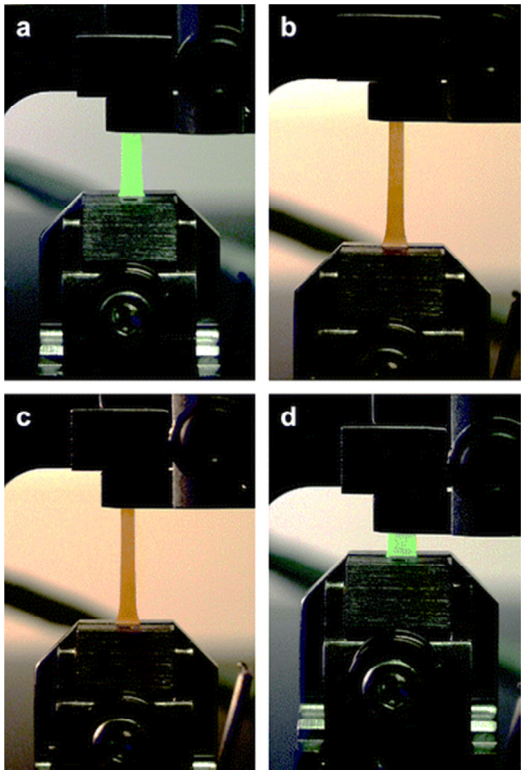

Figure I.23 Photo sequence of the shape-memory cycle of a poly(cyclooctene)/1,4-bis(a-cyano-4-octadecyloxystyryl)-2,5-dimethoxybenzene SMP, from Kunzelman *et al.* [105]. a) Deforming, b) fixing and cooling, c) unloading and d) recovery.

The stimuli sensitiveness gives to SMPs the ability to respond to environmental changes such as an increase in temperature. Thus the SME can be used for sensor-like applications. Kunzelman *et al.* [105] reported a SMP with built-in temperature sensing capabilities by incorporating a fluorescent dye into the poly(cyclooctene) (PCO) crosslinked network (Figure I.23). Exposure of the SMP to temperatures above the melting temperature leads to dissolution of the dye molecules causing a pronounced change of their absorption and fluorescence colour. The aggregate absorption and emission are restored upon cooling below the melting temperature due to the crystallization of the PCO. The colour is dictated by the phase behaviour and is independent of the mechanical state of the SMP allowing observing the set/release temperature of the polymer.

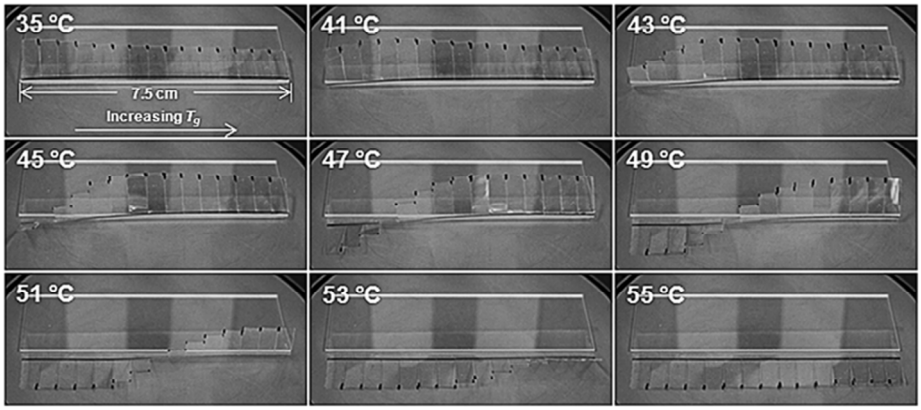

Figure I.24 Photo sequence of the gradient recovery behaviour of the graded SMP, from Diorio *et al.* [106].

The SMP applications as temperature sensors have usually limited to one single T_{trans} and are unable to respond to a range of operation temperatures. Diorio *et al.* [106] reported a functionally graded SMP with a range of transition temperatures (Figure I.24). This was achieved by post-curing a glassy SMP in a linear temperature gradient that imposes

different vitrification temperatures. The resulting material can respond to a range of temperatures (from T_{min} to T_{max}) upon application of external heating.

SMPs can also be used as packaging materials. SMPs can shrink when being heated and are able to adapt any shape. In addition, they can provide protection from the environment and insulation [107]. Heat-shrinkable films and heat-shrinkable tubing are examples of this kind of application [108,109].

I.2. Objectives

The main objective of this thesis is to experimentally analyse the influence of thermomechanical conditions and chemical structure on the shape-memory performances of a selected group of thermoplastic and thermosetting shape-memory polymers.

This general objective was achieved by setting a series of more specific objectives.

In terms of the influence of thermomechanical cycling conditions on shape-memory properties, our specific objectives were:

- To evaluate the impact of different thermomechanical conditions in stress-controlled shape-memory cycling on the shape-memory properties of thermoplastic SMPs.
- To find the thermomechanical conditions in stress-controlled programming that stabilize the shape-memory properties of thermoplastic shape-memory polymers in the fewest cycles while obtaining the best mechanical properties.

The results obtained in these investigations are presented in Chapter III.

In order to accomplish the objectives about the impact of the chemical structure of shape-memory polymers, two different thermosetting shape-memory networks were studied.

In terms of hyperbranched-modified epoxy-based shape-memory polymers, our specific objectives were:

- To study the implications of the hyperbranched polymer molecular weight and content on the thermomechanical and viscoelastic properties of thermosetting shape-memory polymers.

- To study the shape-memory effect of hyperbranched-modified epoxy-based shape-memory polymers under free and constrained recovery conditions.
- To evaluate the mechanical properties of hyperbranched-modified epoxy shape-memory polymers for their potential use in mechanically demanding shape-memory applications.

The results obtained in these investigations are presented in Chapter IV, from Section IV.3 to Section IV.6.

In terms of acrylate-based bisphenol A-based shape-memory polymers, our specific objectives were:

- To study the thermomechanical and shape-memory properties of acrylate-based thermosetting shape-memory polymers synthesized from bisphenol A-based crosslinking agents and different monofunctional monomers.

The results obtained in these investigations are described in Chapter IV, Section IV.7.

I.3. References

[1] A. Lendlein, *Shape Memory Polymers*, Springer, **2010**.

[2] L. B. Vernon, H. M. Vernon, *Process of manufacturing articles of thermoplastic synthetic resins*, US Pat. 2234993A, **1941**.

[3] C. Liu, H. Qin, P. T. Mather, *Review of progress in shape-memory polymers*, J. Mater. Chem. **2007**, *17*, 1543–1558.

[4] W. C. Rainer, E. M. Redding, J. J. Hitov, A. W. Sloan, W. D. Stewad, *Polyethylene product and process*, US Pat. 3144398, **1964**.

[5] R. J. Perrone, *Heat-shrinkable articles made from silicone rubber–polyethylene compositions*, US Pat. 3326869, **1967**.

[6] P. E. Wray, *Elastic memory articles*, US Pat. GB1075704, **1967**.

[7] D. Ratna, J. Karger-Kocsis, *Recent advances in shape memory polymers and composites: a review*, J. Mater. Sci. **2008**, *43*, 254–269.

[8] T. Xie, *Recent advances in polymer shape memory*, Polymer **2011**, *52*, 4985–5000.

[9] J. Leng, X. Lan, Y. Liu, S. Du, *Shape-memory polymers and their composites: Stimulus methods and applications*, Prog. Mater. Sci. **2011**, *56*, 1077–1135.

[10] A. Lendlein, S. Kelch, *Shape-Memory Polymers*, Angew. Chem. Int. Ed. **2002**, *41*, 2034–2057.

[11] L. C. Chang, T. A. Read, *Plastic deformation and diffusionless phase changes in metals*, Trans. AIME, **1951**, *189*, 47–52.

[12] W. J. Bühler, J. W. Gilfrich, R. C. Wiley, *Effect of low-temperature phase changes on mechanical properties of alloys near composition TiNi*, J. Appl. Phys. **1963**, *34*, 1475.

[13] M. Raja, A. M. Shanmugharaj, S. H. Ryu, J. Subha, *Influence of metal nanoparticle decorated CNTs on polyurethane based electro active shape memory nanocomposite actuators*, Mater. Chem. Phys. **2011**, *129*, 925–931.

[14] C. L. Huang, M. J. He, M. Huo, L. Du, C. Zhan, C. J. Fan, K. K. Yang, I. J. Chin, Y. Z. Wang, *A facile method to produce PBS-PEG/CNTs nanocomposites with controllable electro-induced shape memory effect*, Polym. Chem. **2013**, *4*, 3987–3997.

[15] Y. Wang, G. Zhu, X. Cui, T. Liu, Z. Liu, K. Wang, *Electroactive shape memory effect of radiation cross-linked SBS/LLDPE composites filled with carbon black*, Colloid Polym. Sci. **2014**, *292*, 2311–2317.

[16] Y. Liu, H. Lv, X. Lan, J. Leng, S. Du, *Review of electro-active shape-memory polymer composite*, Smart Compos. Nanocomposites Spec. Issue Regul. Papaers, **2009**, *69*, 2064–2068.

[17] R. Mohr, K. Kratz, T. Weigel, M. Lucka-Gabor, M. Moneke, A. Lendlein, *Initiation of shape-memory effect by inductive heating of magnetic nanoparticles in thermoplastic polymers*, Proc. Natl. Acad. Sci. U.S.A. **2006**, *103*, 3540–3545.

[18] Y. Cai, J. S. Jiang, Z. W. Liu, Y. Zeng, W. G. Zhang, *Magnetically-sensitive shape memory polyurethane composites crosslinked with multi-walled carbon nanotubes*, Compos. Part Appl. Sci. Manuf. **2013**, *53*, 16 – 23.

[19] S. Xia, X. Li, Y. Wang, Y. Pan, Z. Zheng, X. Ding, Y. Peng, *A remote-activated shape memory polymer network employing vinyl-capped Fe3O4 nanoparticles as netpoints for durable performance*, Smart Mater. Struct. **2014**, *23*, 085005.

[20] W. M. Huang, B. Yang, Y. Zhao, Z. Ding, *Thermo-moisture responsive polyurethane shape-memory polymer and composites: a review*, J. Mater. Chem. **2010**, *20*, 3367–3381.

[21] A. Lendlein, H. Jiang, O. Jünger, R. Langer, *Light-induced shape-memory polymers*, Nature **2005**, *434*, 879–882.

[22] I. A. Rousseau, *Challenges of shape memory polymers: A review of the progress toward overcoming SMP's limitations*, Polym. Eng. Sci. **2008**, *48*, 2075–2089.

[23] W. M. Huang, Y. Zhao, C. C. Wang, Z. Ding, H. Purnawali, C. Tang, J. L. Zhang, *Thermo/chemo-responsive shape memory effect in*

polymers: a sketch of working mechanisms, fundamentals and optimization, J. Polym. Res. **2012**, *19*, 9952.

[24] D. M. Feldkamp, I. A. Rousseau, *Effect of Chemical Composition on the Deformability of Shape-Memory Epoxies*, Macromol. Mater. Eng. **2011**, *296*, 1128–1141.

[25] A. B. Leonardi, L. A. Fasce, I. A. Zucchi, C. E. Hoppe, E. R. Soulé, C. J. Pérez, R. J. J. Williams, *Shape memory epoxies based on networks with chemical and physical crosslinks*, Eur. Polym. J. **2011**, *47*, 362–369.

[26] Y. Liu, C. Han, H. Tan, X. Du, *Thermal, mechanical and shape memory properties of shape memory epoxy resin*, **2010**, *527*, 2510–2514.

[27] W. B. Song, L. Y. Wang, Z. D. Wang, *Synthesis and thermomechanical research of shape memory epoxy systems*, Mater. Sci. Eng. **2011**, *529*, 29–34.

[28] A. M. Ortega, S. E. Kasprzak, C. M. Yakacki, J. Diani, A. R. Greenberg, K. Gall, *Structure-property relationships in photopolymerizable polymer networks: Effect of composition on the crosslinked structure and resulting thermomechanical properties of a (meth)acrylate-based system*, J. Appl. Polym. Sci. **2008**, *110*, 1559–1572.

[29] D. L. Safranski and K. Gall, *Effect of chemical structure and crosslinking density on the thermo-mechanical properties and toughness of (meth)acrylate shape memory polymer networks*, Polymer **2008**, *49*, 4446–4455.

[30] C. M. Yakacki, S. Willis, C. Luders, K. Gall, *Deformation limits in shape-memory polymers*, Adv. Eng. Mater. **2008**, *10*, 112–119.

[31] N. Lakhera, C. M. Yakacki, T. D. Nguyen, C. P. Frick, *Partially constrained recovery of (meth)acrylate shape-memory polymer networks*, **2012**, *126*, 72–82.

[32] A. M. Ortega, C. M. Yakacki, S. A. Dixon, R. Likos, A. R. Greenberg, K. Gall, *Effect of crosslinking and long-term storage on the shape-memory behavior of (meth)acrylate-based shape-memory polymers*, Soft Matter. **2012**, *8*, 7381–7392.

[33] K. Gall, C. M. Yakacki, Y. Liu, R. Shandas, N. Willett, K. S. Anseth, *Thermomechanics of the shape memory effect in polymers for biomedical applications*, J. Biomed. Mater. Res. Part A **2005**, *73*, 339–348.

[34] C. M. Yakacki, R. Shandas, C. Lanning, B. Rech, A. Eckstein, K. Gall, *Unconstrained recovery characterization of shape-memory polymer networks for cardiovascular applications*, **2007**, *28*, 2255–2263.

[35] K. E. Smith, J. S. Temenoff, K. Gall, *On the toughness of photopolymerizable (meth)acrylate networks for biomedical applications*, J. Appl. Polym. Sci. **2009**, *114*, 2711–2722.

[36] K. E. Smith, S. S. Parks, M. A. Hyjek, S. E. Downey, K. Gall, *The effect of the glass transition temperature on the toughness of photopolymerizable (meth)acrylate networks under physiological conditions*, Polymer **2009**, *50*, 5112–5123.

[37] D. A. Chernous, S. V. Shil'ko, Y. M. Pleskachevskii, *Description of the shape memory effect of radiation-modified polymers under thermomechanical action*, J. Eng. Phys. Thermophys. **2004**, *77*, 6–10.

[38] H. A. Khonakdar, S. H. Jafari, S. Rasouli, J. Morshedian, H. Abedini, *Investigation and Modeling of Temperature Dependence Recovery Behavior of Shape-Memory Crosslinked Polyethylene*, Macromol. Theory Simulations **2007**, *16*, 43–52.

[39] C. Liu, S. B. Chun, P. T. Mather, L. Zheng, E. H. Haley, E. B. Coughlin, *Chemically cross-linked polycyclooctene: Synthesis, characterization, and shape memory behavior*, Macromolecules **2002**, *35*, 9868–9874.

[40] S. R. Chowdhury, J. K. Mishra, C. K. Das, *Study of heat shrinkability and flame retardancy of poly(ethylene vinyl acetate)/epichlorohydrin blends*, Macromol. Mater. Eng. **2001**, *286*, 243–247.

[41] S. R. Chowdhury, C. K. Das, *Structure-property correlations of heat-shrinkable polymer blends based on ethylene vinyl acetate/carboxylated nitrile rubber in the presence of different curatives*, J. Appl. Polym. Sci. **2003**, *87*, 1414–1420.

[42] M. Ahmad, J. Luo, B. Xu, H. Purnawali, P. J. King, P. R. Chalker, Y. Fu, W. Huang, M. Miraftab, *Synthesis and characterization of polyurethane-based shape-memory polymers for tailored Tg around body temperature for medical applications*, Macromol. Chem. Phys. **2011**, *212*, 592–602.

[43] F. L. Ji, J. L. Hu, S. S.-Y. Chui, *Influences of phase composition and thermomechanical conditions on shape memory properties of segmented polyurethanes with amorphous reversible phase*, Polym. Eng. Sci. **2012**, *52*, 1015–1026.

[44] S. Weng, Z. Xia, J. Chen, L. Gong, *Shape memory properties of polycaprolactone-based polyurethanes prepared by reactive extrusion*, J. Appl. Polym. Sci. **2013**, *127*, 748–759.

[45] X. Jing, H. Y. Mi, X. F. Peng, L. S. Turng, *The morphology, properties, and shape memory behavior of polylactic acid/thermoplastic polyurethane blends*, Polym. Eng. Sci. **2015**, *55*, 70–80.

[46] M. Behl, M. Y. Razzaq, A. Lendlein, *Multifunctional Shape-Memory Polymers*, Adv. Mater. **2010**, *22*, 3388–3410.

[47] J. R. Lin, L. W. Chen, *Study on shape-memory behavior of polyether-based polyurethanes. I. Influence of the hard-segment content*, J. Appl. Polym. Sci. **1998**, *69*, 1563–1574.

[48] J. R. Lin, L. W. Chen, *Study on shape-memory behavior of polyether-based polyurethanes. II. Influence of soft-segment molecular weight*, J. Appl. Polym. Sci. **1998**, *69*, 1575–1586.

[49] S. Mondal, J. L. Hu, *Shape Memory Study of Thermoplastic Segmented Polyurethane: Influence of Hard Segment*, Polym.Plast. Technol. Eng. **2007**, *46*, 939–942.

[50] W. Wang, Y. Jin, P. Ping, X. Chen, X. Jing, Z. Su, *Structure Evolution in Segmented Poly(ester urethane) in Shape-Memory Process*, Macromolecules **2010**, *43*, 2942–2947.

[51] E. Del Río, G. Lligadas, J. C. Ronda, M. Galià, V. Cádiz, M. A. R. Meier, *Shape memory polyurethanes from renewable polyols obtained by*

ATMET polymerization of glyceryl triundec-10-enoate and 10-undecenol, Macromol. Chem. Phys. **2011**, *212*, 1392–1399.

[52] L. Peponi, I. Navarro-Baena, A. Sonseca, E. Gimenez, A. Marcos-Fernandez, J. M. Kenny, *Synthesis and characterization of PCL-PLLA polyurethane with shape memory behavior*, Eur. Polym. J. **2013**, *49*, 893–903.

[53] J. L. Hu, F. L. Ji, and Y. W. Wong, *Dependency of the shape memory properties of a polyurethane upon thermomechanical cyclic conditions*, Polym. Int. **2005**, *54*, 600–605.

[54] D. Santiago, F. Ferrando, S. De La Flor, *Effect of different shape-memory processing methods on the thermomechanical cyclic properties of a shape-memory polyurethane*, J. Mater. Eng. Perform. **2014**, *23*, 2561–2566.

[55] C. Schmidt, A. M. S. Chowdhury, K. Neuking, G. Eggeler, *Studies on the cycling, processing and programming of an industrially applicable shape memory polymer Tecoflex® (or TFX EG 72D)*, High Perform. Polym. **2011**, *23*, 300–307.

[56] C. Schmidt, K. Neuking, G. Eggeler, *Functional fatigue of shape-memory polymers*, Adv. Eng. Mater. **2008**, *10*, 922–927.

[57] S. Mogharebi, R. Kazakeviciute-Makovska, H. Steeb, G. Eggeler, K. Neuking, *On the cyclic material stability of shape memory polymer*, Mater. Werkst. **2013**, *44*, 521–526.

[58] A. J. W. McClung, G. P. Tandon, J. W. Baur, *Fatigue Cycling of Shape Memory Polymer Resin*, Conference Proceedings of the Society for Experimental Mechanics Series **2011**, *3,* 119–127.

[59] C. Azra, C. J. G. Plummer, J. A. E. Månson, *Isothermal recovery rates in shape memory polyurethanes*, Smart Mater. Struct. **2011**, *20*, 082002.

[60] S. Pandini, F. Bignotti, F. Baldi, S. Passera, *Network architecture and shape memory behavior of cold-worked epoxies*, J. Intell. Mater. Syst. Struct. **2013**, *24*, 1583–1597.

[61] G. Li, W. Xu, *Thermomechanical behavior of thermoset shape memory polymer programmed by cold-compression: Testing and constitutive modeling*, J. Mech. Phys. Solids **2011**, *59*, 1231–1250.

[62] F. Castro, K. K. Westbrook, J. Hermiller, D. U. Ahn, Y. Ding, H. J. Qi, *Time and temperature dependent recovery of epoxy-based shape memory polymers*, J. Eng. Mater. Technol. **2011**, *133*, 021025.

[63] H. Tan, T. Zhou, Y. Liu, L. Lan, *Isothermal recovery response and constitutive model of thermoset shape memory polymers*, Proc. SPIE **2012**, *8409*, 8409H.

[64] C. Azra, Y. Ding, C. J. G. Plummer, J.-A. E. Månson, *Influence of molecular architecture on the isothermal time-dependent response of amorphous shape memory polyurethanes*, Eur. Polym. J. **2013**, *49*, 184–193.

[65] D. Zhang, Y. Liu, K. Yu, J. Leng, *Influence of cross-linking agent on thermomechanical properties and shape memory effect of styrene shape memory polymer*, J. Intell. Mater. Syst. Struct. **2011**, *22*, 2147–2154.

[66] D. Santiago, S. De la Flor, F. Ferrando, X. Ramis, M. Sangermano, *Thermomechanical Properties and Shape-Memory Behavior of Bisphenol A Diacrylate-Based Shape-Memory Polymers*, Macromol. Chem. Phys. **2016**, *217*, 39–50.

[67] J. Diani, C. Frédy, P. Gilormini, Y. Merckel, G. Régnier, I. Rousseau, *A torsion test for the study of the large deformation recovery of shape memory polymers*, Polym. Test. **2011**, *30*, 335–341.

[68] K. K. Westbrook, F. Castro, K. N. Long, A. J. Slifka, H. J. Qi, *Improved testing system for thermomechanical experiments on polymers using uniaxial compression equipment*, Polym. Test. **2010**, *29*, 503–512.

[69] R. Kazakevičiute-Makovska, S. Mogharebi, H. Steeb, G. Eggeler, K. Neuking, *A critical assessment of experimental methods for determining the dynamic mechanical characteristics of shape memory polymers*, Adv. Eng. Mater. **2013**, *15*, 732–739.

[70] I. A. Rousseau, T. Xie, *Relationship between materials properties and shape memory behavior in epoxy-amine polymers*, MRS Proc. **2009**, *1190*, 31–36.

[71] J. Diani, P. Gilormini, C. Frédy, I. Rousseau, *Predicting thermal shape memory of crosslinked polymer networks from linear viscoelasticity*, Int. J. Solids Struct. **2012**, *49*, 793–799.

[72] A. Belmonte, D. Guzmán, X. Fernández-Francos, S. De la Flor, *Effect of the Network Structure and Programming Temperature on the Shape-Memory Response of Thiol-Epoxy 'Click' Systems*, Polymers **2015**, *7*, 2146-2164.

[73] X. L. Wu, S. F. Kang, X. J. Xu, F. Xiao, X. L. Ge, *Effect of the crosslinking density and programming temperature on the shape fixity and shape recovery in epoxy-anhydride shape-memory polymers*, J. Appl. Polym. Sci. **2014**, *131*, 40559.

[74] J. Xu, W. Shi, W. Pang, *Synthesis and shape memory effects of Si–O–Si cross-linked hybrid polyurethanes*, Polymer **2006**, *47*, 457–465.

[75] T. Xie, I. A. Rousseau, *Facile tailoring of thermal transition temperatures of epoxy shape memory polymers*, Polymer **2009**, *50*, 1852–1856.

[76] X. Jing, Y. Liu, Y. Liu, Z. Liu, H. Tan, *Toughening-modified epoxy-amine system: Cure kinetics, mechanical behavior, and shape memory performances*, J. Appl. Polym. Sci. **2014**, *131*, 40853.

[77] G. P. Tandon, K. Goecke, K. Cable, J. Baur, *Durability assessment of styrene- and epoxy-based shape-memory polymer resins*, J. Intell. Mater. Syst. Struct. **2009**, *20*, 2127–2143.

[78] C. Park, J. Yul Lee, B. Chul Chun, Y. C. Chung, J. Whan Cho, B. Gyoo Cho, *Shape memory effect of poly(ethylene terephthalate) and poly(ethylene glycol) copolymer cross-linked with glycerol and sulfoisophthalate group and its application to impact-absorbing composite material*, J. Appl. Polym. Sci. **2004**, *94*, 308–316.

[79] H. Deka, N. Karak, *Shape-memory property and characterization of epoxy resin-modified Mesua ferrea L. seed oil-based hyperbranched polyurethane*, J. Appl. Polym. Sci. **2010**, *116*, 106–115.

[80] H. Tobushi, H. Hara, E. Yamada, S. Hayashi, *Thermomechanical properties in a thin film of shape memory polymer of polyurethane series*, Smart Mater. Struct. **1996**, *5*, 483–491.

[81] A. J. W. McClung, G. P. Tandon, J. W. Baur, *Deformation rate-, hold time-, and cycle-dependent shape-memory performance of Veriflex-E resin*, Mech. Time-Depend. Mater. **2011**, *17*, 1–14.

[82] I. A. Rousseau, T. Xie, S*hape memory epoxy: Composition, structure, properties and shape memory performances*, J. Mater. Chem. **2010**, *20*, 3431–3441.

[83] D. Santiago, X. Fernández-Francos, F. Ferrando, S. De la Flor, *Shape-memory effect in hyperbranched poly(ethyleneimine)-modified epoxy thermosets*, J. Polym. Sci. Part B Polym. Phys. **2015**, *53*, 924–933.

[84] J. Cui, K. Kratz, M. Heuchel, B. Hiebl, A. Lendlein, *Mechanically active scaffolds from radio-opaque shape-memory polymer-based composites*, Polym. Adv. Technol. **2011**, *22*, 180–189.

[85] J. Cui, K. Kratz, A. Lendlein, *Adjusting shape-memory properties of amorphous polyether urethanes and radio-opaque composites thereof by variation of physical parameters during programming*, Smart Mater. Struct. **2010**, *19*, 065019.

[86] J. S. Arrieta, J. Diani, P. Gilormini, *Cyclic and monotonic testing of free and constrained recovery properties of a chemically crosslinked acrylate*, J. Appl. Polym. Sci. **2014**, *131*, 39813.

[87] I. S. Kolesov, K. Kratz, A. Lendlein, H. J. Radusch, *Kinetics and dynamics of thermally-induced shape-memory behavior of crosslinked short-chain branched polyethylenes*, Polymer **2009**, *50*, 5490–5498.

[88] S. Rapp, H. Baier, *Determination of recovery energy densities of shape memory polymers via closed-loop, force-controlled recovery cycling*, Smart Mater. Struct. **2010**, *19*, 045018.

[89] M. Behl, A. Lendlein, *Triple-shape polymers*, J. Mater. Chem. **2010**, *20*, 3335–3345.

[90] I. Bellin, S. Kelch, R. Langer, A. Lendlein, *Polymeric triple-shape materials*, Proc. Natl. Acad. Sci. USA. **2006**, *103*, 18043–18047.

[91] I. S. Kolesov, H. J. Radusch, *Multiple shape-memory behavior and thermal-mechanical properties of peroxide cross-linked blends of linear and short-chain branched polyethylenes*, Express Polym. Lett. **2008**, *2*, 461–473.

[92] M. Behl, I. Bellin, S. Kelch, W. Wagermaier, A. Lendlein, *One-step process for creating triple-shape capability of AB polymer networks*, Adv. Funct. Mater. **2009**, *19*, 102–108.

[93] W. Small IV, P. Singhal, T. S. Wilson, D. J. Maitland, *Biomedical applications of thermally activated shape memory polymers*, J. Mater. Chem. **2010**, *20*, 3356–3366.

[94] Y. Liu, H. Du, L. Liu, J. Leng, *Shape memory polymers and their composites in aerospace applications: A review*, Smart Mater. Struct. **2014**, *23*, 023001.

[95] J. Hu, H. Meng, G. Li, S. I. Ibekwe, *A review of stimuli-responsive polymers for smart textile applications*, Smart Mater. Struct. **2012**, *21*, 053001.

[96] G. M. Baer, W. Small IV, T. S. Wilson, W. J. Benett, D. L. Matthews, J. Hartman, D. J. Maitland, *Fabrication and in vitro deployment of a laser-activated shape memory polymer vascular stent*, Biomed. Eng. Online **2007**, *6*, 43.

[97] A. Lendlein, R. Langer, *Biodegradable, elastic shape-memory polymers for potential biomedical applications*, Science **2002**, *296*, 1673–1676.

[98] W. Small IV, T. S. Wilson, W. J. Benett, J. M. Loge, D. J. Maitland, *Laser-activated shape memory polymer intravascular thrombectomy device*, Opt. Express **2005**, *13*, 8204–8213.

[99] X. Lan, Y. Liu, H. Lv, X. Wang, J. Leng, S. Du, *Fiber reinforced shape-memory polymer composite and its application in a deployable hinge*, Smart Mater. Struct. **2009**, *18*, 024002.

[100] D. Campbell, M. S. Lake, M. R. Scherbarth, E. Nelson, R. W. Six, *Elastic memory composite material: An enabling technology for future furlable space structures*, Collection of Technical Papers - AIAA/ASME/ASCE/AHS/ASC Structures, Structural Dynamics and Materials Conference **2005**, *10*, 6735–6743.

[101] P. N. Keller, M. S. Lake, D. Codell, R. Barrett, R. Taylor, M. R. Schultz, *Development of elastic memory composite stiffeners for a flexible precision reflector*, Collection of Technical Papers - AIAA/ASME/ASCE/AHS/ASC Structures, Structural Dynamics and Materials Conference **2006**, *10*, 6984–6994.

[102] S. Mondal, J. L. Hu, *Structural characterization and mass transfer properties of nonporous-segmented polyurethane membrane: Influence of the hydrophilic segment content and soft segment melting temperature*, J. Membr. Sci. **2006**, *276*, 16–22.

[103] S. Mondal, J. L. Hu, *A novel approach to excellent UV protecting cotton fabric with functionalized MWNT containing water vapor permeable PU coating*, J. Appl. Polym. Sci. **2007**, *103*, 3370–3376.

[104] H. R. Han, S. E. Chung, C. H. Park, *Shape memory and breathable waterproof properties of polyurethane nanowebs*, Text. Res. J. **2013**, *83*, 76–82.

[105] J. Kunzelman, T. Chung, P. T. Mather, C. Weder, *Shape memory polymers with built-in threshold temperature sensors*, J. Mater. Chem. **2008**, *18*, 1082–1086.

[106] A. M. Diorio, X. Luo, K. M. Lee, P. T. Mather, *A functionally graded shape memory polymer*, Soft Matter. **2011**, *7*, 68–74.

[107] J. Hu, Y. Zhu, H. Huang, J. Lu, *Recent advances in shape-memory polymers: Structure, mechanism, functionality, modeling and applications*, Prog. Polym. Sci. **2012**, *37*, 1720–1763.

[108] N. Takagi, A. Takeda, *Heat-shrinkable film*, US Pat. 7182998, **2007**.

[109] T. Saito, *System for holding a heat shrinkable tube during a heat shrinkage operation*, US Pat. 6531659, **2003**.

UNIVERSITAT ROVIRA I VIRGILI
EXPERIMENTAL CHARACTERIZATION OF SHAPE-MEMORY POLYMERS: INFLUENCE OF PROCESSING METHODS AND CHEMICAL STRUCTURE
David Manuel Santiago Abraira

Chapter II

Experimental Methods and Materials

II.1. Experimental methods

II.1.1. Dynamic Mechanical Analysis (DMA)

Dynamic mechanical analysis (DMA) involves applying a small oscillating force to a sample and analysing the material's response to that force [1]. DMA can be used to study the relaxation of the polymer chains and to determine inherent mechanical or flow properties as a function of time and temperature.

Figure II.1 shows the basic principles of DMA. This technique studies the viscoelastic nature of a material by applying an oscillatory stress:

$$\sigma(t) = \sigma_0 \cdot \sin(\omega t) \tag{II.1}$$

where σ is the stress as a function of time, σ_0 is the maximum stress, ω is the frequency and t is the time.

The response of the material will show a phase lag δ between the applied stress and the resultant strain:

$$\varepsilon(t) = \varepsilon_0 \cdot \sin(\omega t) \tag{II.2}$$

where ε_0 is maximum deformation and δ is the phase angle.

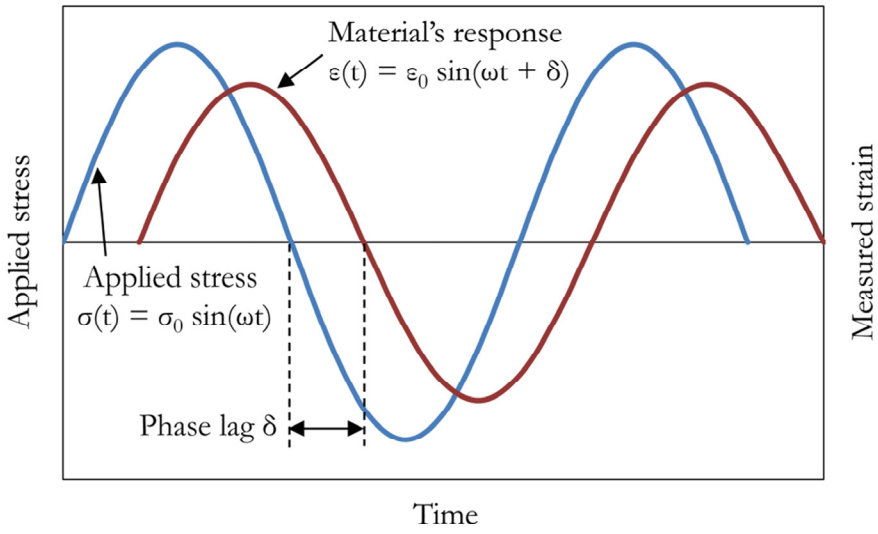

Figure II.1 Basic principles of the dynamical mechanical analysis (DMA).

Based on this discussion, a storage or elastic modulus E' and a loss or viscous modulus E'' can be calculated:

$$E' = \frac{\sigma_0}{\varepsilon_0} \cdot \cos\delta \tag{II.3}$$

$$E'' = \frac{\sigma_0}{\varepsilon_0} \cdot \sin\delta \tag{II.4}$$

The storage modulus E' represents the ability of the material to return or store energy, whilst the loss modulus E'' represents the ability of the material to lose energy.

The tangent of the phase angle tan δ is an indicator of the damping properties of the material and the peak of tan δ curve is accepted as the glass transition temperature T_g of the material although it changes with the frequency used in the experiment. tan δ is calculated as the ratio of the loss modulus to storage modulus:

$$\tan\delta = \frac{E''}{E'} \tag{II.5}$$

Figure II.2 shows a DMA analysis of a general crosslinked polymer. Several parameters can be obtained from the DMA analysis. The storage modulus at glassy region E'_g has important implications for the shape fixation ability of the SMP and the storage modulus at rubbery region E'_r is advantageous for the shape recovery and the shape-recovery velocity. Moreover, the ratio of glassy modulus to rubbery modulus E'/E'' is an important indicative of whether a material is going to present shape-memory properties [2]. A ratio $E'_g/E'_r \geq 100$ is desired for proper shape-memory properties. During the realization of this thesis, E'_g was obtained at $T_g - 40$ and E'_r was obtained at $T_g + 40$.

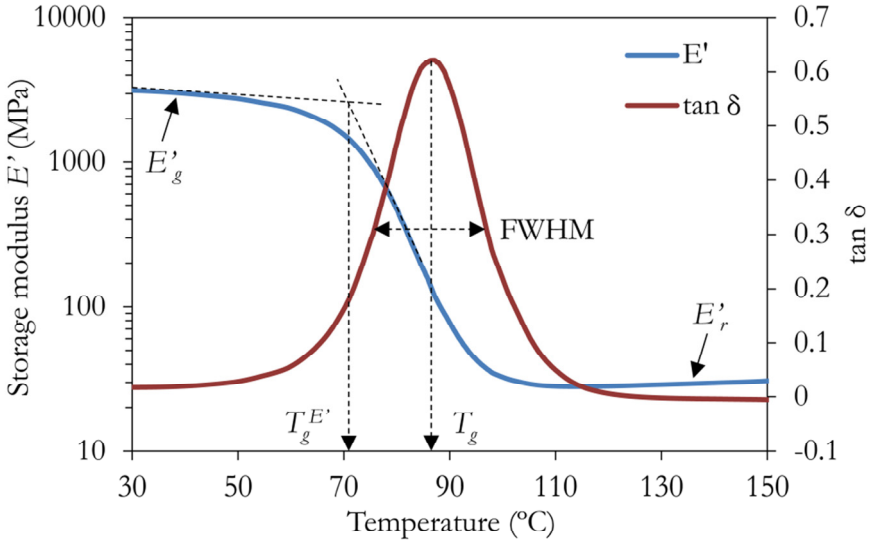

Figure II.2 Viscoelastic response of a material subjected an oscillatory stress.

As mentioned before, the peak of the tan δ curve is accepted as indicator for the glass transition temperature of the polymer and the shape of the curve is also indicative of the structure of the material: the

peak height is an indication of the viscous character of the material during the relaxation and the total peak area is related to the total amount of energy dissipated during the relaxation [3]. In general, the higher and narrower is the peak of tan δ, the more homogeneous and mobile is the network structure. The parameter used to compare the width of the curves of tan δ in different materials is the "full width at half maximum" (FWHM). The area of the curve of tan δ was calculated as:

$$\tan\delta \text{ area} = \tan\delta \text{ peak} \cdot \text{FWHM} \qquad \text{(II.6)}$$

Another important temperature is the onset of the glass transition temperature $T_g^{E'}$. This temperature can be obtained as the onset in the storage modulus decrease during mechanical relaxation. Yakacki *et al.* [4] and Feldkamp and Rousseau [5] reported that the deformability of acrylated-based and epoxy-based shape-memory thermosetting polymers is greatly improved when deformed at $T_g^{E'}$.

Figure II.3 DMA Q800 (left) and detail of the 3-point bending clamp (right).

The DMA measurements were carried out with a DMA Q800 (TA Instruments) at *Departament de Química Analítica i Química Orgànica* of *Universitat Rovira i Virgili* (Tarragona) equipped with a 3-point bending clamp (Figure II.3). Prismatic samples of 30 mm x 5.5 mm x 2.5 mm were used for hyperbranched-modified epoxy-based shape-memory polymers and prismatic samples of 20 mm x 2 mm x 0.5 mm were used for acrylate-based shape-memory polymers. The experimental procedure of sample preparation is described in the corresponding chapter.

II.1.2. Shape-memory properties

The quantification of the shape-memory properties involves imposing a temporary shape to the material and the recovery of the permanent shape in a shape-memory cycle. In this thesis, three different methods for shape-memory properties characterization were used: transient temperature stress-controlled free recovery experiments, transient temperature stress-controlled constrained recovery experiments and isothermal temperature self-deploy experiments.

II.1.2.1. Transient temperature stress-controlled free recovery experiments

Transient temperature free recovery experiments represent the most common procedure to study the shape-memory properties. They are usually carried out either with a dynamical-mechanical analyser or a universal testing machine equipped with a thermal chamber.

The programming of the temporary shape can be carried out under stress-controlled conditions or strain-controlled conditions. The difference between both protocols relies in imposing a maximum prescribed stress σ_m or a maximum prescribed strain ε_m to the sample in order to obtain the temporary shape. In this thesis only the stress-controlled protocol has been used.

In this procedure, the recovery of the original or permanent shape is carried out under free conditions. After unloading the applied stress, the SMP is heated to the recovery temperature $T_{recovery}$ with no restriction and thus the sample is able to return to its original shape.

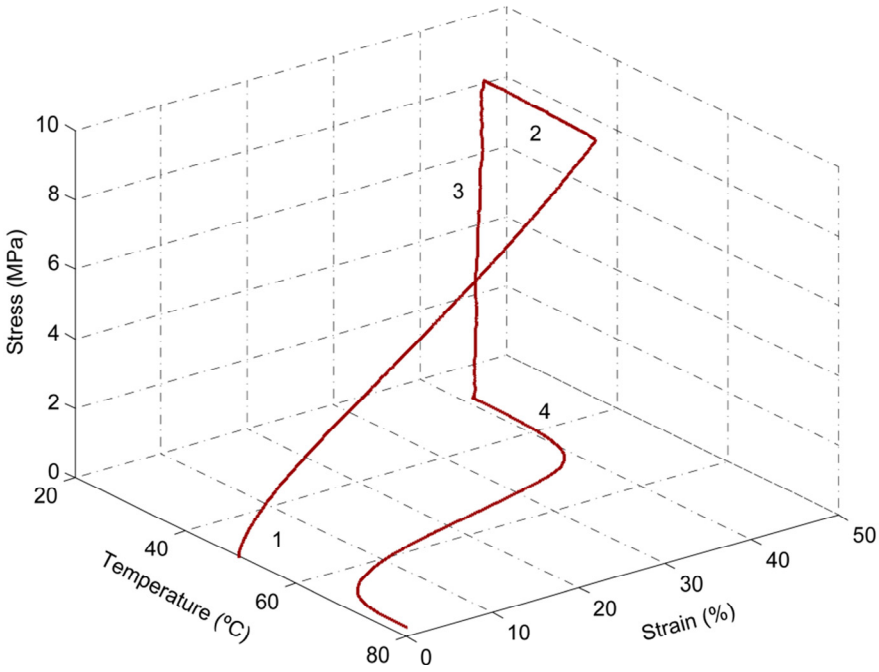

Figure II.4 Three-dimensional representation of transient temperature stress-controlled free recovery shape-memory performances. The numbers correspond to: 1) deforming to temporary shape, 2) cooling and fixing the temporary shape, 3) unloading the stress applied and 4) heating to $T_{recovery}$.

The procedure for developing a shape-memory cycle with a stress-controlled protocol and under free conditions consisted of various steps:

1. Equilibrate at the programming temperature: the equipment is equilibrated at the programming temperature T_{prog} selected.
2. Isothermal step: isothermal step of 5 minutes in order to ensure proper heat transfer to the sample.

3. Stretching the sample: the sample is stretched to the prescribed maximum stress σ_m at a fixed stress rate of 1 MPa/min.
4. Equilibrate at room temperature: the sample is cooled to room temperature (~25 ºC) while maintaining the stress applied in order to fix the temporary shape.
5. Stress holding time: a stress holding time t_H is applied (if desired).
6. Isothermal step: isothermal step of 15 minutes in order to ensure the sample is cooled.
7. Unloading the sample: the prescribed maximum stress applied σ_m is unloaded at a fixed stress rate of 1 MPa/min.
8. Isothermal step: isothermal step of 3 minutes.
9. Heating the sample: the sample is heated to the recovery temperature $T_{recovery}$ at a fixed heating rate of 3 ºC/min.

In Figure II.4 are represented the resulting shape-memory cycle represented in a strain-temperature-stress plot.

The stress, the temperature and the length are monitored during the experiment (Figure II.5). L_m, L_u and L_p and are obtained from the experiment data (Figure II.5a) in order to calculate ε_m, ε_u and ε_p. The deformation was calculated according to Equation II.7:

$$\varepsilon(\%) = \frac{L - L_0}{L_0} \cdot 100 \qquad \text{(II.7)}$$

where L is the length of interest (*i.e.* L_m, L_u, L_p, etc.) and L_0 is the initial length. The shape-recovery ratio R_r and shape-fixity ratio R_f can be calculated as follows:

$$R_r(\%) = \frac{\varepsilon_m - \varepsilon_p}{\varepsilon_m} \cdot 100 \qquad \text{(II.8)}$$

$$R_f(\%) = \frac{\varepsilon_u}{\varepsilon_m} \cdot 100 \qquad \text{(II.9)}$$

The switching temperature T_{sw} is obtained from the inflexion point in a temperature-length curve (Figure II.5b).

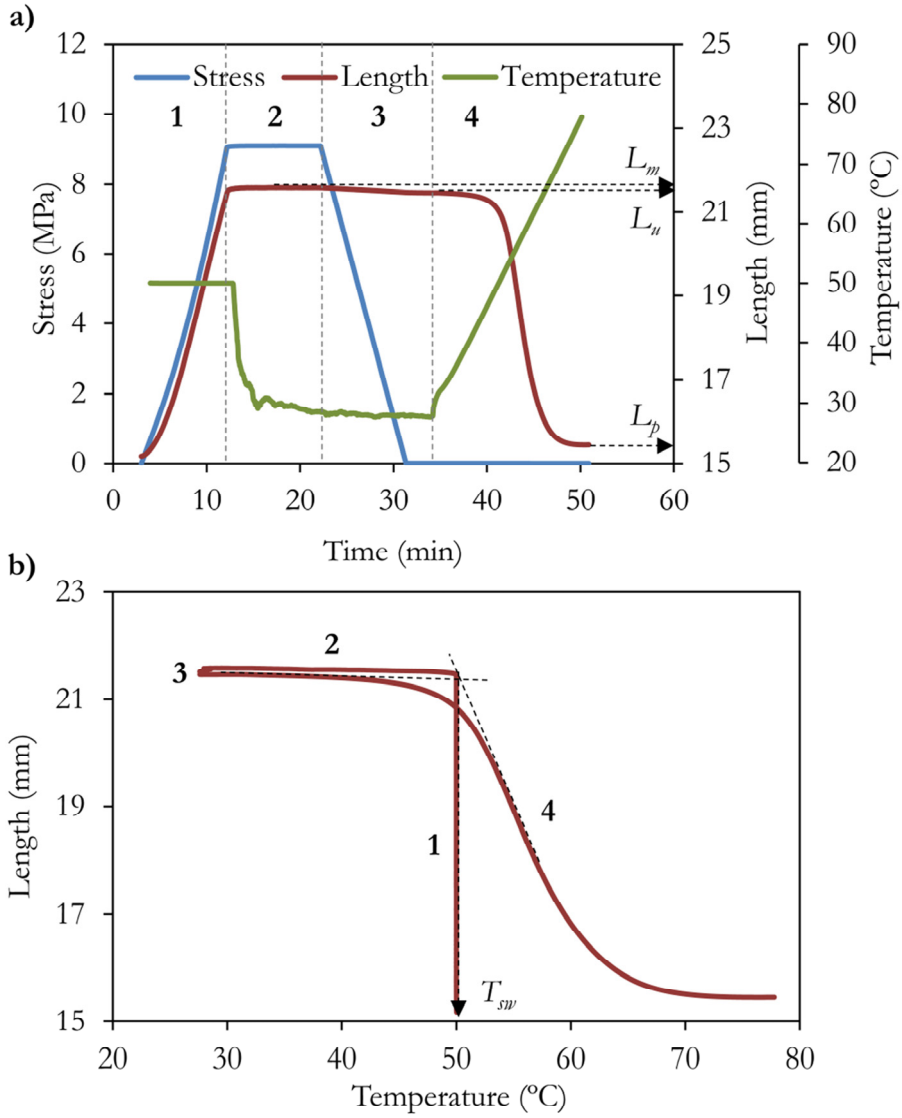

Figure II.5 Examples of the data obtained during a shape-memory cycle. The numbers correspond to: 1) deforming to temporary shape, 2) cooling and fixing the temporary shape, 3) unloading the stress applied and 4) heating to $T_{recovery}$.

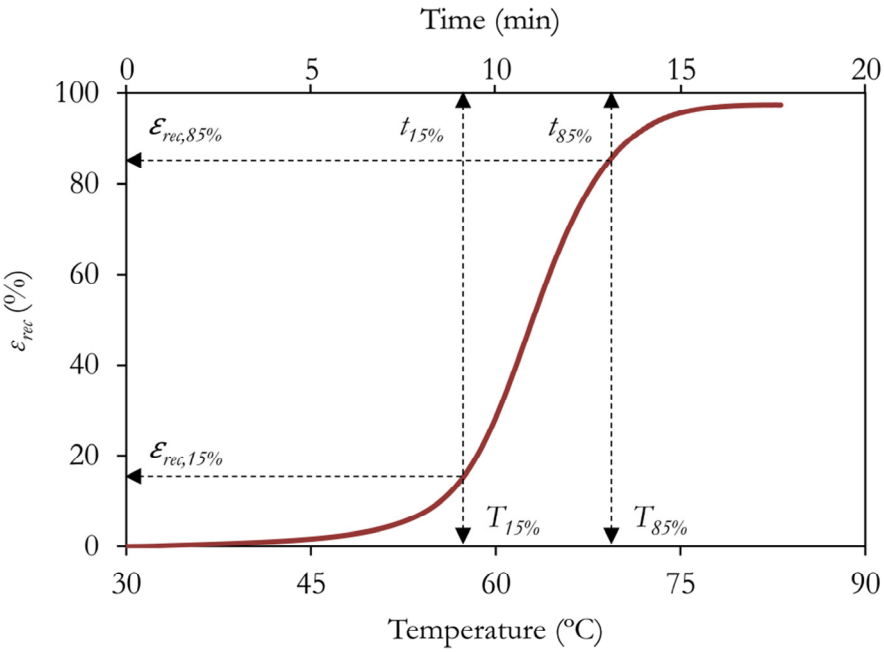

Figure II.6 Example of the determination of the parameters $\varepsilon_{rec,15\%}$, $\varepsilon_{rec,85\%}$, $t_{15\%}$, $t_{85\%}$, $T_{15\%}$ *and* $T_{85\%}$ for the calculation of the shape-recovery velocity V_r.

The shape-recovery velocity V_r can be calculated in two different ways, according to Equation II.10 and Equation II.11:

$$V_r\,(\%/\text{min}) = \frac{\left(\frac{\varepsilon_{rec,15\%} - \varepsilon_{rec,85\%}}{\varepsilon_{rec,15\%}}\right) \cdot 100}{\Delta t_{15\%-85\%}} \qquad \text{(II.10)}$$

$$V_r\,(\%/^{\circ}\text{C}) = \frac{\left(\frac{\varepsilon_{rec,15\%} - \varepsilon_{rec,85\%}}{\varepsilon_{rec,15\%}}\right) \cdot 100}{\Delta T_{15\%-85\%}} \qquad \text{(II.11)}$$

where $\varepsilon_{rec,15\%}$ is the deformation corresponding to a shape recovery of 15%, $\varepsilon_{rec,85\%}$ is the deformation corresponding to a shape recovery of 85% and $\Delta t_{15\%-85\%}$ and $\Delta T_{15\%-85\%}$ are the time interval and temperature range between these two points. These parameters can be obtained from the

curve of strain recovered as a function of time or temperature during the shape recovery process (Figure II.6).

The difference between deformations corresponding to a shape recovery of 15% and 85%, $\varepsilon_{rec,15\%} - \varepsilon_{rec,85\%}$, was calculated with respect to $\varepsilon_{rec,15\%}$ in order to avoid the influence of the maximum deformation on the shape-recovery velocity.

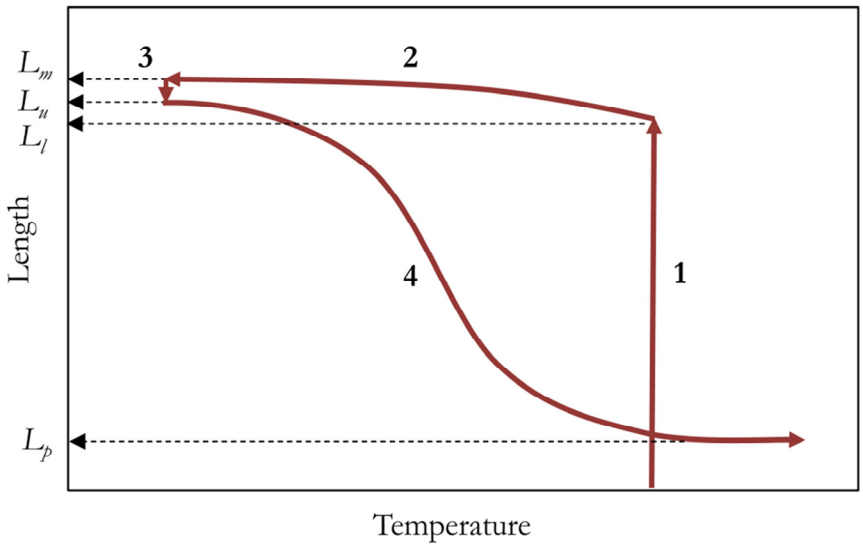

Figure II.7 Example of the creep phenomenon occurred during a stress-controlled shape-memory cycle and the determination of L_m and L_l. The numbers correspond to: 1) deforming to temporary shape, 2) cooling and fixing the temporary shape, 3) unloading the stress applied and 4) heating to $T_{recovery}$.

In a stress-controlled protocol, the fixation of the temporary shape is carried out while a stress is applied and a creep phenomenon may occour. Thus, the maximum length increases during the fixation of the temporary shape (Figure II.7). Depending on the kind of SMP tested (*i.e.* thermoplastic SMPs, thermosetting SMPs) the creep phenomenon may be misprised. In those cases in which the increase in the maximum length is considerabe, it should be distinguished the length of the sample when

σ_m is reached L_l and the maximum length obtained during the cycle L_m and so the shape-recovery ratio can be calculated as:

$$R_r(\%) = \frac{L_l(\mathrm{N}) - L_p(\mathrm{N})}{L_l(\mathrm{N}) - L_0} \cdot 100 \qquad \text{(II.12)}$$

and the shape-fixity ratio as:

$$R_f(\%) = \frac{L_u(\mathrm{N}) - L_0}{L_m(\mathrm{N}) - L_0} \cdot 100 \qquad \text{(II.13)}$$

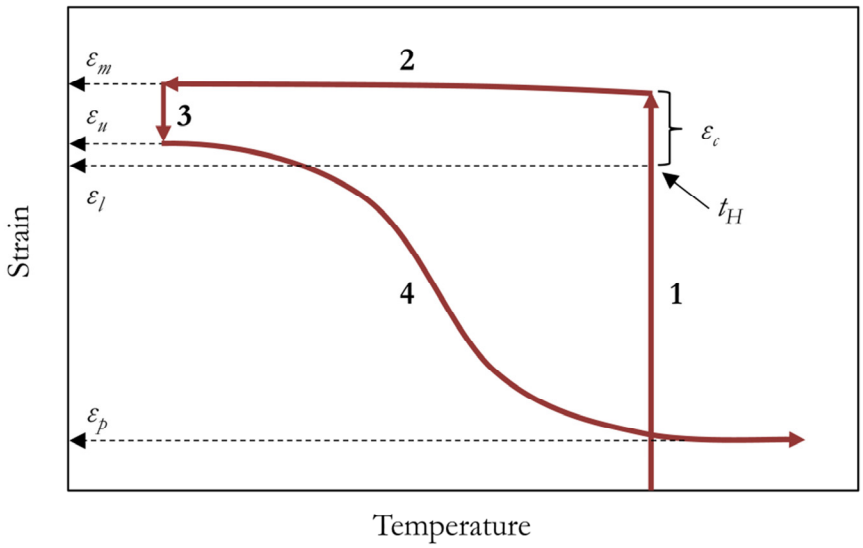

Figure II.8 Example of a shape-memory cycle applying a stress holding time t_H and the corresponding deformation ε_c caused by a creep phenomenon. The numbers correspond to: 1) deforming to temporary shape, 2) cooling and fixing the temporary shape, 3) unloading the stress applied and 4) heating to $T_{recovery}$.

If a stress-holding time t_H is applied, the maximum stress applied σ_m is held during a certain amount of time just before the cooling step. The application of a t_H causes an additional deformation ε_c to the sample due

to a creep phenomenon (Figure II.8). Thus maximum deformation obtained during programming the temporary shape can be calculated as:

$$\varepsilon_m(\%) = \varepsilon_l + \varepsilon_c \quad \text{(II.14)}$$

Samples of ca. 20 mm x 2.5 mm x 0.5 mm were used for transient temperature stress-controlled free recovery procedures. These experiments were carried out with a DMA Q800 (TA Instruments) (Figure II.3) at *Departament de Química Analítica i Química Orgànica* of *Universitat Rovira i Virgili* (Tarragona). The shape-memory cycles were performed with a force-controlled mode and equipped with a film-tension clamp (Figure II.9).

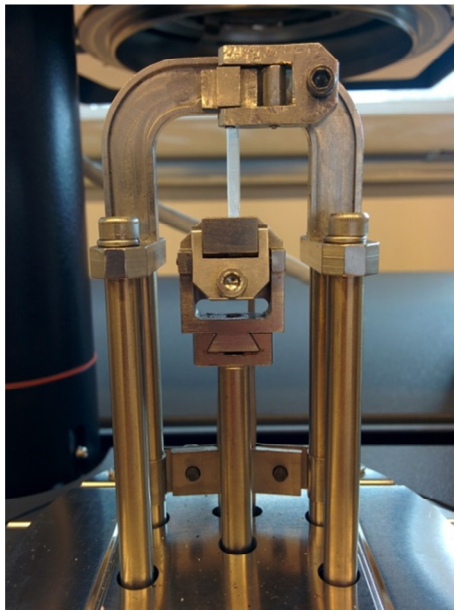

Figure II.9 Detail of the film-tension clamp of the DMA Q800

II.1.2.2. Transient temperature stress-controlled constrained recovery experiments

The constrained recovery testing consists of performing the shape recovery process under a fixed strain (fully constraint) or under a constraining stress (partially constraint). These procedures allow characterizing the ability of the SMP to perform recovery stress or mechanical work, which is essential for actuator-like applications.

Fully constraining conditions

The procedure for developing a shape-memory cycle under fixed strain conditions consisted of various steps:

1. Equilibrate at the programming temperature: the equipment is equilibrated at the programming temperature T_{prog} selected.
2. Isothermal step: isothermal step of 5 minutes in order to ensure proper heat transfer to the sample.
3. Stretching the sample: the sample is stretched to the prescribed maximum stress σ_m at a fixed stress rate of 1 MPa/min.
4. Equilibrate at room temperature: the sample is cooled to room temperature (~25 ºC) while maintaining the stress applied in order to fix the temporary shape.
5. Isothermal step: isothermal step of 15 minutes in order to ensure the sample is cooled.
6. Unloading the sample: the prescribed maximum stress applied σ_m is unloaded at a fixed stress rate of 1 MPa/min.
7. Isothermal step: isothermal step of 3 minutes.
8. Strain fixing: the deformation after unloading ε_u is fixed.
9. Heating the sample: the sample is heated to the recovery temperature $T_{recovery}$ at a fixed heating rate of 3 ºC min.

An example of a fully constrained recovery test is shown in Figure II.10. If deformation after unloading ε_u is fixed during the recovery process, the material generates a recovery stress as the temperature

increases. The maximum recovery stress σ_{rec} as well as the corresponding temperature $T_{\sigma rec}$ can be obtained from the generated curve.

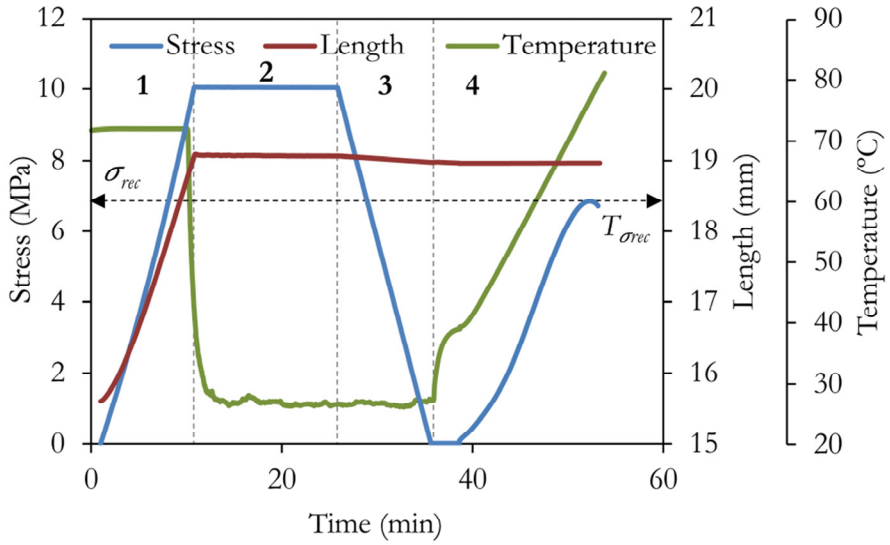

Figure II.10 Example of the data obtained during a fully constrained recovery test. The numbers correspond to: 1) deforming to temporary shape, 2) cooling and fixing the temporary shape, 3) unloading the stress applied and 4) heating to $T_{recovery}$ while ε_u is fixed.

Partially constraining conditions

The procedure for developing a shape-memory cycle under partially constrained conditions consisted of the following steps:

1. Equilibrate at the programming temperature: the equipment is equilibrated at the programming temperature T_{prog} selected.
2. Isothermal step: isothermal step of 5 minutes in order to ensure proper heat transfer to the sample.
3. Stretching the sample: the sample is stretched to the prescribed maximum stress σ_m at a fixed stress rate of 1 MPa/min.
4. Equilibrate at room temperature: the sample is cooled to room temperature (~25 ºC) while maintaining the stress applied in order to fix the temporary shape.

5. Isothermal step: isothermal step of 15 minutes in order to ensure the sample is cooled.
6. Unloading the sample: the prescribed maximum stress applied σ_m is unloaded to a determined value of constraining stress σ_{const} at a fixed stress rate of 1 MPa/min.
7. Isothermal step: isothermal step of 3 minutes.
8. Heating the sample: the sample is heated to the recovery temperature $T_{recovery}$ at a fixed heating rate of 3 ºC/min while σ_{const} is applied.

An example of a partially constrained recovery test is shown in Figure II.11. If the maximum deformation σ_m is unloaded to $\sigma = 0$, the recovery process takes place under free conditions. However, σ_m can be partially unloaded to a determined value of constraining stress σ_{const}. This value of constraining stress is held constant during the recovery process.

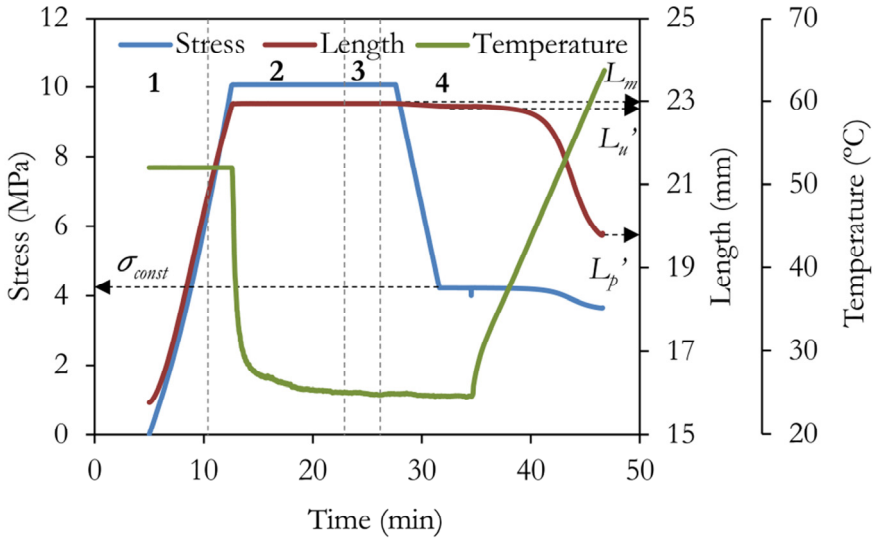

Figure II.11 Example of the data obtained during a partially constrained recovery test. The numbers correspond to: 1) deforming to temporary shape, 2) cooling and fixing the temporary shape, 3) unloading to constraining stress σ_{const} and 4) heating to $T_{recovery}$.

The maximum length reached L_m, the length after partial unload L_u' and the length after partially constrained recovery L'_p can be obtained from the experimental data (Figure II.11) in order to obtain ε_m, ε_u' and ε_p' (Equation II.7). The shape-recovery ratio under partially constrained conditions can be calculated as follows:

$$R_r(\%) = \frac{\varepsilon_m - \varepsilon_p'}{\varepsilon_m} \cdot 100 \qquad \text{(II.15)}$$

In a partially constrained recovery the SMP recovers a certain amount of deformation against an external stress, thus the material performs actuator work W_a according to Equation II.16:

$$W_a\left(\frac{\text{kJ}}{\text{m}^3}\right) = \sigma_{const} \cdot (\varepsilon_u' - \varepsilon_p') \qquad \text{(II.16)}$$

The work required to program the sample W_p can be calculated as:

$$W_p\left(\frac{\text{kJ}}{\text{m}^3}\right) = \sigma_m \cdot \varepsilon_m \qquad \text{(II.17)}$$

Samples of ca. 20 mm x 2.5 mm x 0.5 mm were used for transient temperature stress-controlled constrained recovery procedures. These experiments were carried out with a DMA Q800 (TA Instruments) at *Departament de Química Analítica i Química Orgànica* of *Universitat Rovira i Virgili* (Tarragona) (Figure II.3). Totally and partially constrained shape-memory cycles were performed with a force-controlled mode and equipped with a film-tension clamp (Figure II.9).

II.1.2.3. Isothermal temperature self-deploy experiments

For isothermal temperature self-deploy tests prismatic rectangular samples of ca. 30 mm × 3.75 mm × 0.75 mm were used. The samples were immersed in a hot water bath at a temperature equal to the glass

transition temperature of the material tested and held for 30 seconds. The samples were deformed into 'U' shape (θ = 180º) with a specially designed device (Figure II.12). The samples were immersed in cold water (~10 ºC) for 5 minutes in order to fix the 'U' shape. Once the 'U' shape was fixed, the sample was immersed in hot water at the corresponding recovery temperature $T_{recovery}$. The angle θ and the time until complete recovery t were monitored (Figure II.13).

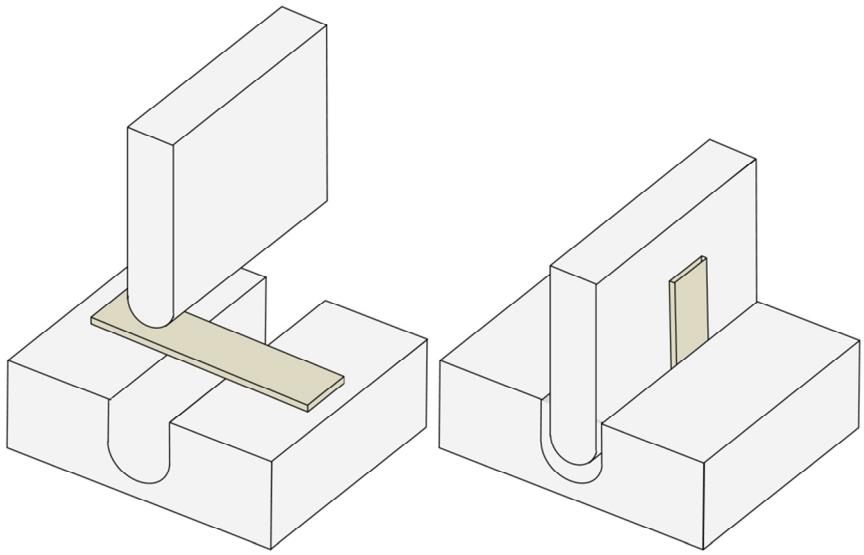

Figure II.12 Schematic representation of the deformation into 'U' shape in isothermal temperature self-deploy experiments.

Isothermal temperature self-deploy shape-memory experiments were performed at *Dipartamento di Scienza Applicata e Tecnologia* of *Politecnico di Torino* (Turin) with special designed equipment (Figure II.14).

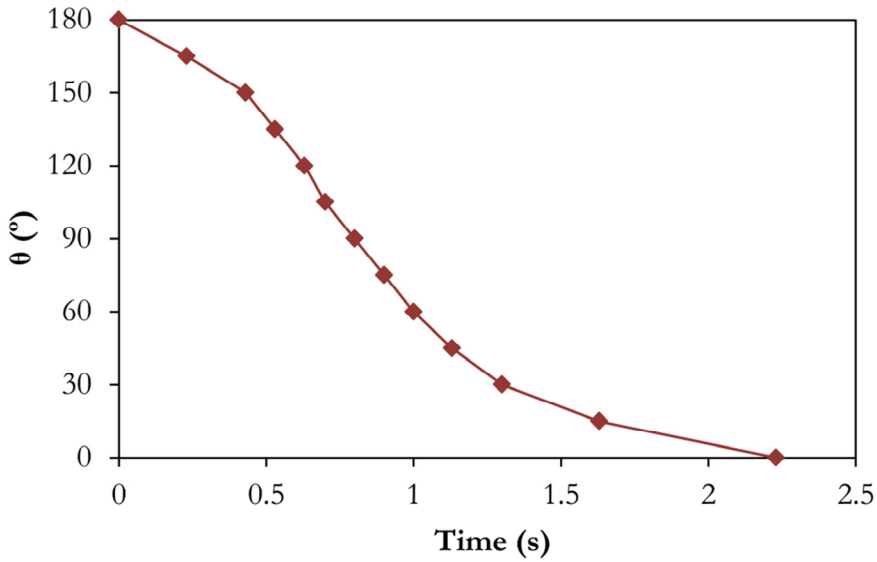

Figure II.13 Example of the data obtained during a isothermal self-deploy shape-memory experiment.

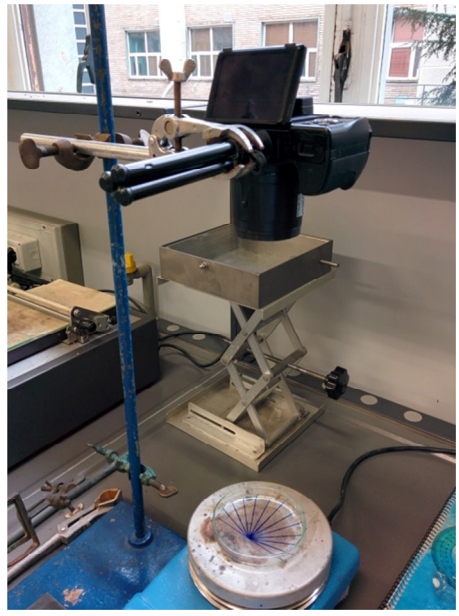

Figure II.14 Equipment used for isothermal temperature self-deploy shape-memory experiments.

II.1.3. Stabilization of the shape-memory properties

As mentioned in Section I.1.6.3, shape-memory properties vary significantly when successive thermomechanical shape-memory cycles are performed. Particularly, the degradation of the R_r is markedly in the initial cycles and softens as the cycling advances until reaches a steady behaviour. To determine whether a sample reached a steady behaviour we used a stabilization criterion previously used for SMAs by some members of our research group. This consisted of calculating the average value and the standard deviation of R_r over 10 successive cycles. R_r was considered to be stable when the standard deviation value was under 2%, and this condition was repeated for at least five consecutive values.

II.1.4. Tensile testing

Tensile testing refers to tests in which a controlled uniaxial stress is applied to a specimen until failure occurs [6]. In a tension test, the opposite ends of the specimen are gripped and elongated in the direction of the applied load. Tensile testing allows determining tensile properties of the materials at different conditions (*i.e.* temperature, humidity, testing rate).

For this thesis two different methodologies were used either for tensile tests performed at room temperature or at high temperature.

II.1.4.1. Tensile testing at room temperature

Figure II.15 shows the results of a typical tensile test performed at room temperature. The stress at break σ_b and deformation at break ε_b are obtained when sample failure, the elastic modulus E is obtained as the tangent of the curve in strain-stress plot and the elastic energy density is obtained as:

$$\text{Elastic energy density}\left(\frac{\text{MJ}}{\text{mm}^3}\right) = \frac{\sigma_b \cdot \varepsilon_b}{2} \qquad \text{(II.18)}$$

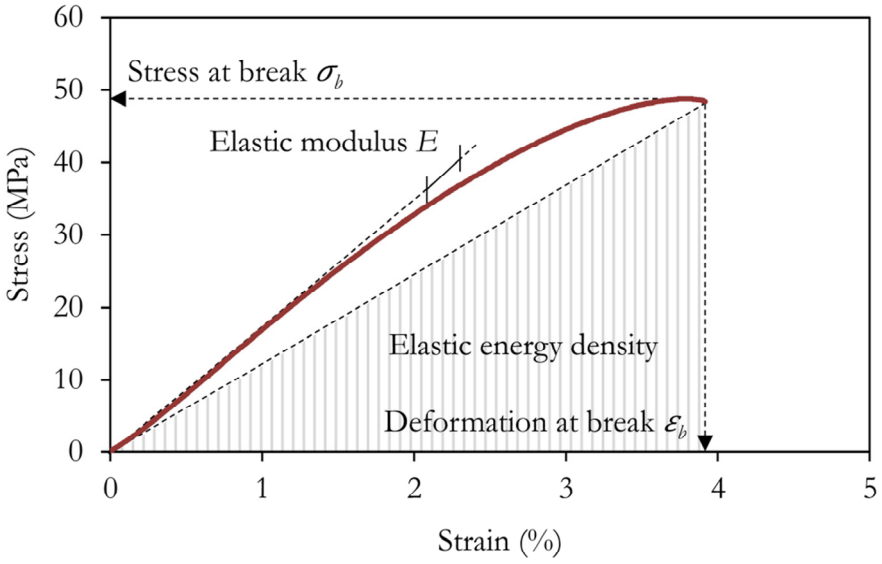

Figure II.15 Example of a tensile test performed at room temperature.

The size of the samples for this method was adapted from ASTM D638 requirements, adopting a Type IV dog-bone shape (Figure II.16). The experiments were performed at a crosshead speed of 1 mm/min.

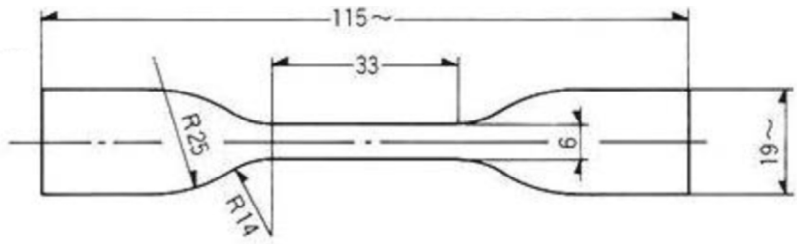

Figure II.16 Detail of the sample dimensions (in mm) according to ASTM D638 Type IV.

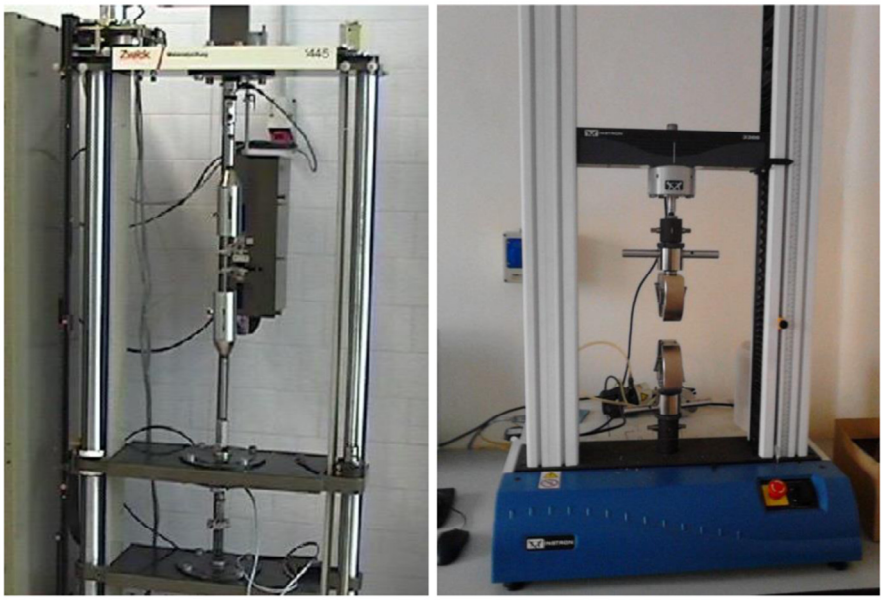

Figure II.17 Universal testing machines Zwick 1445 (left) and Instron 3366 (right).

Two different equipments were used to perform tensile testing at room temperature (Figure II.17). Firstly, a universal testing machine Zwick 1445 was used at *Departament d'Enginyeria Mecànica* of *Univeristat Rovira i Virgili* (Tarragona) and secondly, a universal testing machine Instron 3366 was used at *Dipartamento di Scienza Applicata e Tecnologia* of *Politecnico di Torino* (Turin).

II.1.4.2. Tensile testing at high temperature

Figure II.18 shows the results of a typical tensile test performed at high temperature. The stress at break σ_b and deformation at break ε_b were obtained when sample failure, the tensile modulus was obtained as the tangent of the curve in the elastic regime and the elastic energy density was calculated according to Equation II.18.

Prismatic rectangular samples of 20 mm x 2.5 mm x 0.5 were analyzed at a force rate of 1 N/min. The strain was calculated according to Equation II.7.

Tensile testing at high temperature was carried out with a DMA Q800 (TA Instruments) at *Departament de Química Analítica i Química Orgànica* of *Universitat Rovira i Virgili* (Tarragona). Experiments were performed with a force-controlled mode and equipped with a film-tension clamp (Figure II.9).

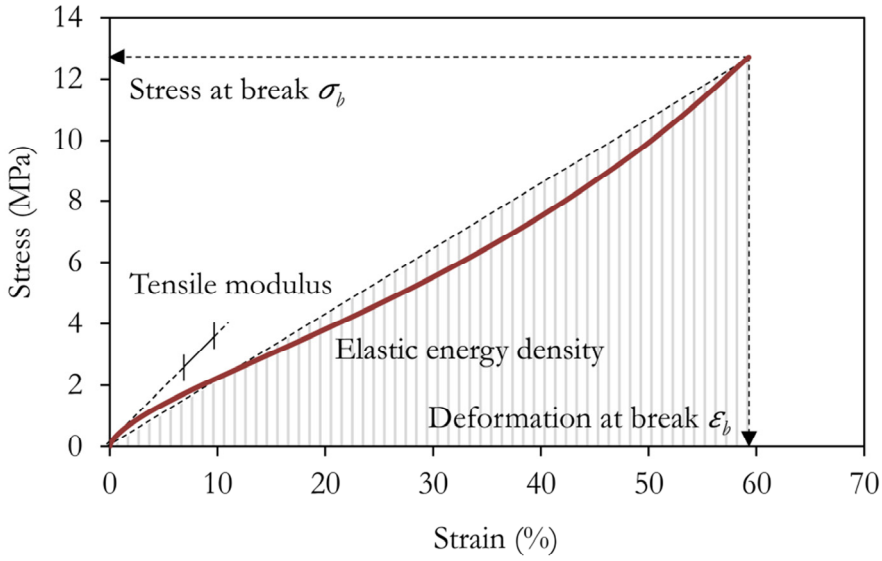

Figure II.18 Examples of a tensile test performed at high temperature.

II.1.5. Young's modulus determination

The Young's or elastic modulus defines the relationship between stress and strain in a material and can be determined as the slope of a stress-strain curve, usually by tensile testing (as indicated in Figure II.15). However determining the Young's modulus in plastics by tensile testing is complicated due to the difficulty of determining distinctly the proportional part of the elastic deformation. This proportional part is

more clearly observed by 3-point bending testing because the whole test can be performed in the elastic regime. Moreover, the determination of the Young's modulus using 3-point bending assembly has some advantages with respect to tensile testing, *i.e.* easier sample preparation and testing.

The modulus of elasticity is calculated using the slope of the force-deflection curve in accordance with Equation II.19:

$$E_f\,(\mathrm{MPa}) = \frac{L^3 \cdot m}{4 \cdot b \cdot d^3} \qquad \text{(II.19)}$$

where, E_f is the flexural modulus of elasticity (MPa), L is support span (mm), b is width of test beam (mm), d is thickness of the tested beam (mm) and m is the slope of the initial straight-line portion of the force-deflection curve.

In this thesis the Young's modulus were determined using DMA Q800 (TA Instruments) equipped with a 3-point bending clamp of 20 mm of span (Figure II.3) at *Departament de Química Analítica i Química Orgànica* of *Universitat Rovira i Virgili* (Tarragona). Experiments were performed with a force-controlled mode and a force rate of 1 N/min up to 15 N.

II.1.6. Izod impact testing

Impact testing is used to measure the resistance to failure of a material to a suddenly applied load, such as the impact of a moving mass [7]. In an impact test, a specimen is struck and broken by the action of a single blow and the energy absorbed by the specimen is measured. The Izod testing is one of the most commonly used and has become the standard testing procedure for comparing the impact resistances of plastics.

The modified Izod impact testing employs the pendulum principle and the test is made on a sample supported as a cantilever. The load is

applied in flexion by the action of the swinging pendulum, which impacts the specimen at the bottom of its swing (Figure II.19).

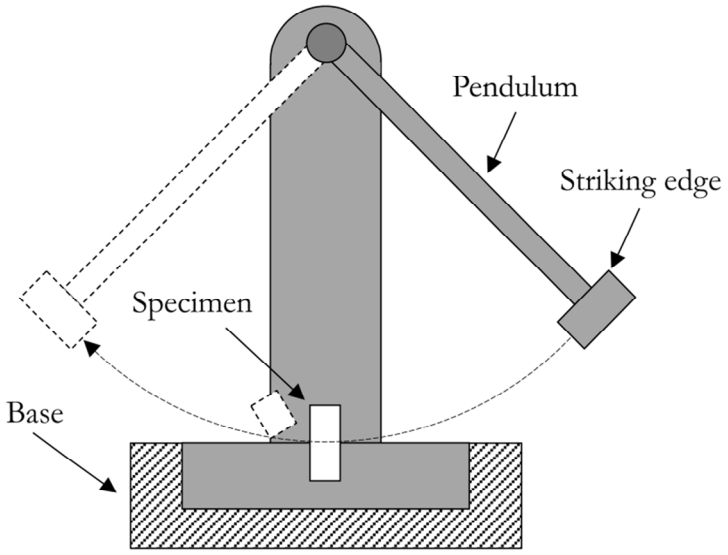

Figure II.19 Schematic representation of the modified Izod impact testing instrument.

The impact strength (*IS*) is calculated as follows:

$$\mathrm{IS}\left(\frac{\mathrm{kJ}}{\mathrm{m}^2}\right) = \frac{(E - E_0) \cdot E_p}{100 \cdot S} \qquad \text{(II.20)}$$

where E is the energy loss of the pendulum with the sample, E_0 is energy loss of the pendulum with no sample (due to friction, deformation of the supports, vibration of the testing machine, etc.), E_p is the energy of the pendulum and S is cross section of the sample.

Impact testing was carried out at *Departament d'Enginyeria Mecànica* of *Universitat Rovira i Virgili* (Tarragona) using a Zwick 5110 impact tester at room temperature (Figure II.20). Impact test were carried out according to ASTM D4508-10 with prismatic rectangular samples of 25 mm x 15 mm x 2 mm.

Figure II.20 Impact tester Zwick 5110.

II.1.7. Microhardness

Microhardness testing is used for very brittle materials where only a small indentation may be made for testing purposes. A pyramidal diamond point is pressed into the polished surface of the test material with a known force for a specified time. The length of the long diagonal produced by the indentation of a rhomboidal tip can be related with the hardness of the material [8]. The Vickers microhardness (HV) can be calculated as follows:

$$HV = \frac{F}{A_p} \tag{II.21}$$

where F is the load applied to the indenter in kilograms-force, A_p is the projected area of indentation in mm^2.

Figure II.21 Microhardness tester Wilson Wolpert 401MAV.

Microhardness testing was carried out at *Departament d'Enginyeria Mecànica* of *Universitat Rovira i Virgili* (Tarragona) using a Wilson Wolpert 401MAV (Figure II.21) according to the ASTM D1474-98(2002) standard procedure.

II.1.8. Differential Scanning Calorimetry (DSC)

Differential scanning calorimetry (DSC) is a technique in which the heat flow rate difference into a substance and a reference is measured as a function of temperature while the sample is subjected to a controlled temperature program [9].

The most common DSC applications are the easy and fast determination of the glass transition temperature, melting and crystallization temperatures, heat of fusion, heat of reactions, characterization of thermosets and measurements of liquid crystal transitions among others.

In this thesis, DSC was used to determine the time necessary to ensure the complete disappearance of any exothermic peak related to residual crosslinking reactions and ensure the complete polymerization of the materials.

A Mettler DSC821e equipped with a robotic arm TSO801RO (Figure II.22) was used for DSC analysis at *Departament de Química Analítica i Química Orgànica* of *Universitat Rovira i Virgili* (Tarragona). Samples of ~10 mg of weight were placed in covered aluminium pans.

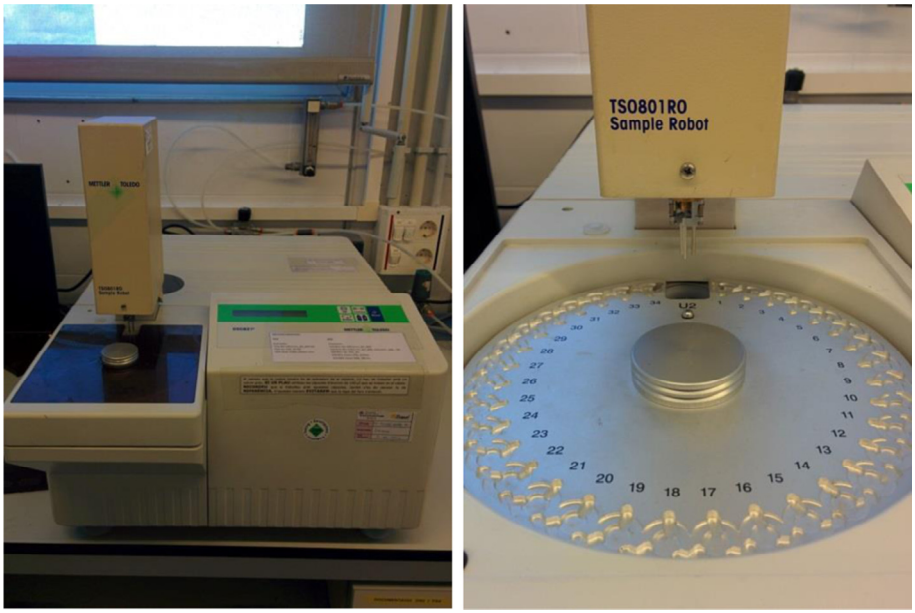

Figure II.22 Calorimeter DSC821e (left) and detail of the robotic arm TSO801 RO (right).

II.1.9. Thermal Mechanical Analysis (TMA)

Thermomechanical analysis (TMA) measures changes in sample length or volume as a function of temperature or time under a static or variable load at atmospheric pressure [9]. In Figure II.23 is shown a schematic representation of the thermal mechanical analysis. The most important

TMA measurements include determination of the coefficient of linear thermal expansion (CTE) and the glass transition temperature, stress relaxation, creep tensile properties of films and fibers, flexural properties and volume dilatometry.

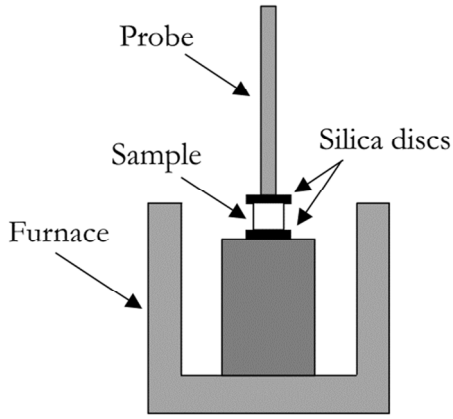

Figure II.23 Schematic representation of a TMA instrument.

In this thesis the TMA was used for the determination of the CTE. Prismatic rectangular samples of 3 mm x 3 mm x 2 mm were sandwiched between two silica discs and heated at 3 ºC/min from 30 to T_g + 30 with a contact force of 0.01 N for a first scan in order erase thermal history, followed by a second scan at the same conditions. Figure II.24 shows a typical example of the determination of the CTE. The CTE at glassy region and at rubbery region were obtained from the second scan as:

$$\mathrm{CTE}\left(\frac{1}{\mathrm{C}^\circ}\right) = \frac{1}{L_0} \cdot \frac{dL}{dT} \qquad \text{(II.22)}$$

where L_0 is the initial thickness at room temperature, L is the thickness at any temperature and T is the temperature.

The TMA analyses were carried out with a TMA/SDTA 840 at *Laboratori de Màquines i Motors Tèrmics* of *Universitat Politècnica de Catalunya* (Barcelona) (Figure II.25).

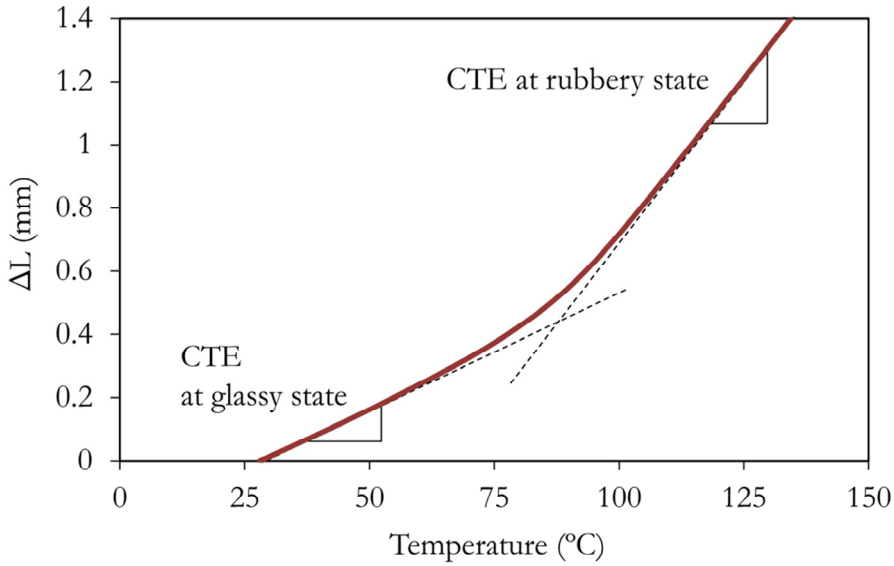

Figure II.24 Example of a TMA analysis for the determination of the coefficient of thermal expansion (CTE) at glassy state and at rubbery state.

Figure II.25 TMA/SDTA 840 (left) and detail of the analysing probe (right).

II.1.10.Fourier Transmission Infrared Spectroscopy (FTIR)

The basic principle of the Fourier transmission infrared spectroscopy (FTIR) is that the IR radiation passes through the sample where it is selectively absorbed, depending on the vibrations excited the sample, and obtaining the absorption and transmission spectrum [10].

According to the Lambert-Beer law:

$$A = \varepsilon \cdot C \cdot L \tag{II.23}$$

the absorbance of a specimen A at a certain frequency is related with its absorptivity ε, its concentration C and with the optical pathway L. Identifying the signals corresponding to reactive groups involved in a curing process which disappears as the curing process advances and monitoring them, it is possible to follow the reaction.

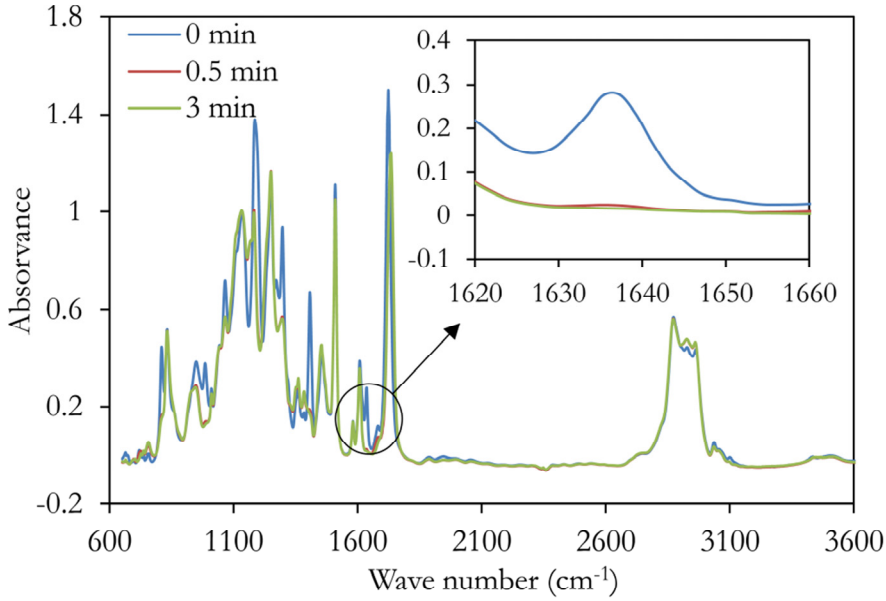

Figure II.26 Example of a IR spectrum and detail of the disappearance of a reactive group during a curing process.

In this thesis the FTIR was used to check the composition of the materials provided by manufacturers and to evaluate the final conversion of UV-curing processes. The samples for UV-curing were coated onto a sample holder and exposed to UV-light. After 30 seconds of UV irradiation, the sample was irradiated with IR to analyse the extent of the reaction and then irradiated again during 30 seconds with UV-light. This process was repeated until final conversion. The disappearance of the peak corresponding to acrylate double bond at 1635 cm^{-1} was monitored and, as the IR absorbance is proportional to the monomer concentration, the final conversion could be obtained (Figure II.26).

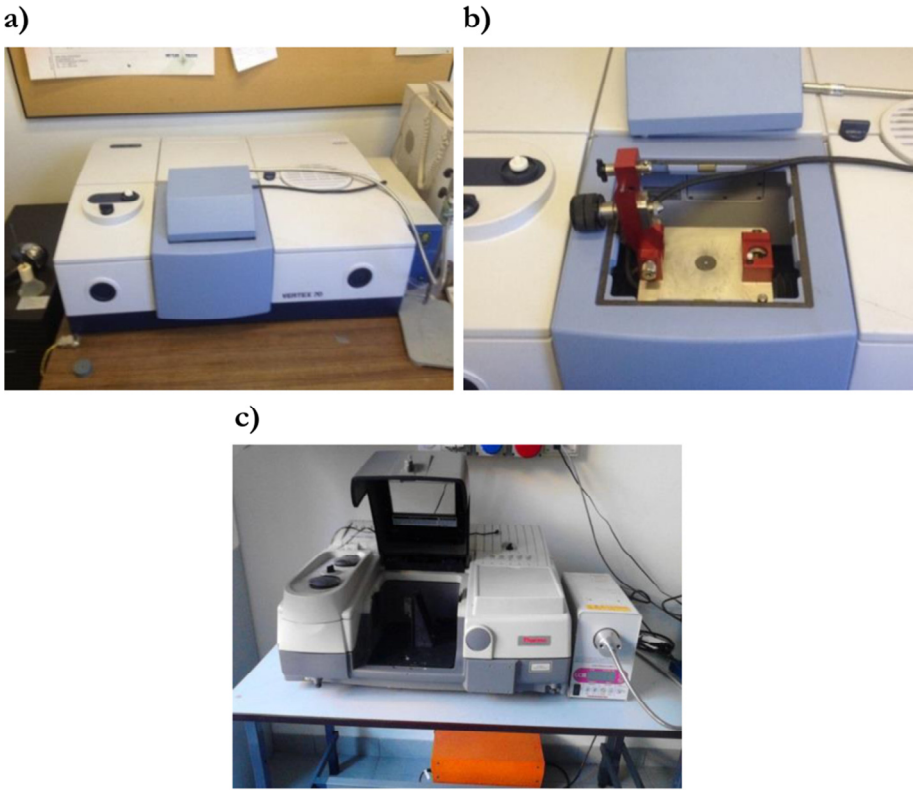

Figure II.27 FTIR Bruker Vertex 70 (a), detail of the golden gate heated single reflection diamond ATR (b) and FTIR Thermo-Nicolet 5700 (c).

Two different FT-IR devices were used. Firstly, a FTIR spectrometer Bruker Vertex 70 (Figure II.27a) with an attenuated total reflection accessory with thermal control and a diamond crystal (Golden Gate Heated Single Reflection Diamond ATR, Specac-Teknokroma) (Figure II.27b) at *Laboratori de Màquines i Motors Tèrmics* of *Universitat Politècnica de Catalunya* (Barcelona). Secondly, a Thermo-Nicolet 5700 FTIR (Figure II.27c) at *Dipartamento di Scienza Applicata e Tecnologia* of *Politecnico di Torino* (Turin).

II.1.11. Scanning Electron Microscopy (SEM)

The principle of scanning electron microscopy (SEM) consists of an electron beam generated by an electron cathode and electromagnetic lenses of the column which swept across the surface of a sample (Figure II.28). The main signals which are generated by the interaction of the primary electrons of the electron beam and the specimen´s bulk are secondary electrons and backscattered electrons and furthermore X rays. The secondary electrons come from a small layer on the surface and yield the best resolution, which can be realized with a scanning electron microscope. The electrons interact with the atoms that make up the sample producing signals that contain information about the sample's surface topography, composition, and other properties such as electrical conductivity [11].

In this thesis, the SEM microscopy was used to analyse the surface fracture of materials broken by impact testing at room temperature. For standard SEM analysis, samples were coated with gold.

A microscope Jeol JSM 6400 with a resolution of 3.5 nm was used for SEM analyses at *Servei de Recursos Científics i Tècnics* of *Universitat Rovira i Virgili* (Tarragona) (Figure II.29).

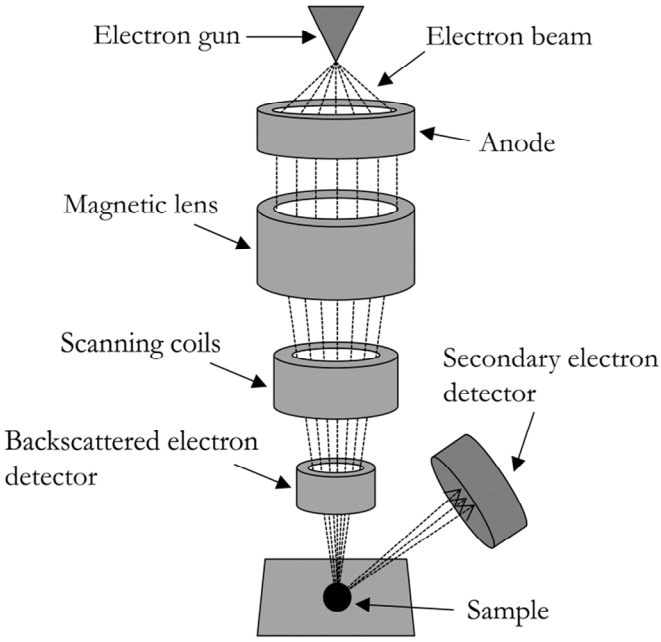

Figure II.28 Schematic representation of a scanning electron microscope.

Figure II.29 SEM equipment used for obtaining fracture surface images (left) and detail of electron emitter and samples (right).

II.2. Materials

II.2.1. Tecoflex®

In Chapter III are studied the influence of different processing methods on shape-memory properties of thermoplastic shape-memory polymers. The material used to carry out this study was a commercial aliphatic polyether-based thermoplastic polyurethane named Tecoflex® (Lubrizol).

There is a wide range of formulations available including clear and filled grades. The formulation selected for this thesis is Tecoflex® EG-72D (Figure II.30). The technical supplied by the manufacturer is listed in Table A.1.

The material was obtained as pellets and processed by injection moulding with a Injector Moulder 25 (CR Clarke) (Figure II.31) to obtain final samples of 20 mm x 5 mm x 1.5mm.

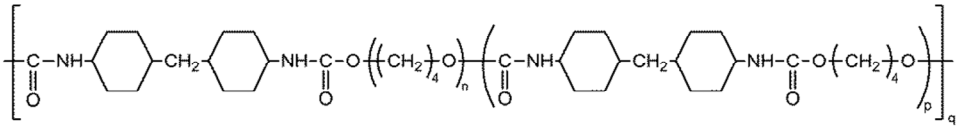

Figure II.30 Chemical structure of Tecoflex® EG-72D.

Figure II.31 Injector Moulder 25.

II.2.2. Epoxy-based thermosetting polymers

In Chapter IV hyperbranched modified-epoxy shape-memory polymers are studied. These materials were prepared at *Departament de Química Analítica i Química Orgànica* of *Universitat Rovira i Virgili*. The reactants used to prepare the formulations for study were a diglycidyl ether of bisphenol A Araldyte® GY 240 (Huntsman) with a weight per epoxy equivalent of 182 g/mol as base epoxy and an aliphatic diamine Jeffamine® D-400 (Huntsman) with M_w = 430 g/mol and hyperbranched poly(ethyleneimine)s Lupasol® (BASF) as crosslinking agents. Two different types of Lupasol® were used: Lupasol® FG with M_w = 800 g/mol and Lupasol® PR8515 with M_w = 2000 g/mol.

The physical and chemical specifications supplied by the manufacturer of each reactant are listed in Table A.2, Table A.3 and Table A.4. The chemical structure and the proportion of the reactants in each formulation are shown in the corresponding section.

II.2.3. Acrylate-based thermosetting polymers

In Chapter IV acrylate-based shape-memory thermosetting are studied. These materials were synthesized at *Dipartamento di Scienza Applicata e Tecnologia* of *Politecnico di Torino* (Turin). The reactants used to perform this study were a diglycidyl ether of bisphenol A diacrylate Ebecryl® 605 (Allnex) (based on 75/25 w/w bisphenol A diacrylate/tripropylene glycol diacrylate) with $M_w = 500$ g/mol and a diglycidyl ether of bisphenol A ethoxylate diacrylate (Sigma-Aldrich) with $M_n = 512$ g/mol as crosslinking agents. Methyl methacrylate (Sigma-Aldrich), ethyl methacrylate (Sigma-Aldrich) and poly(ethylene glycol) methylether methacrylate (Sigma-Aldrich) with $M_n = 475$ g/mol were used as monofunctional chain builders. Darocur 1173 (BASF) was used as photoinitiator.

The physical and chemical specifications supplied by the manufacturer of each reactant are listed from Table A.5 to Table A.9. The chemical structure and the proportion of the reactants in each formulation are shown in the corresponding section.

II.3. References

[1] K. P. Menard, *Dynamic Mechanical Analysis: a Practical Introduction*, CRC Press, **2002**.

[2] C. Liu, H. Qin, P. T. Mather, *Review of progress in shape-memory polymers*, J. Mate. Chem. **2007**, *17*, 1543-1558.

[3] Y. C. Chern, S. M. Tseng, K. H. Hsied, *Damping properties of interpenetrating polymer networks of polyurethane-modified epoxy and polyurethanes*, J. App. Pol. Sci. **1999**, *74*, 328-335.

[4] C. M. Yakacki, S. Willis, C. Luders, K. Gall, *Deformation limits in shape-memory polymers*, Adv. Eng. Mater. **2008**, *10*, 112-119.

[5] D. M. Feldkamp, I. A. Rousseau, *Effect of the Deformation Temperature on the Shape-Memory Behavior of Epoxy Networks*, Macromol. Mater. Eng. **2010**, *295*, 726-734.

[6] A. Lendlein, *Shape Memory Polymers*, Springer, **2010**.

[7] H. E. Davis, G. E. Troxell, G. Hauck, *The Testing of Engineering Materials*, McGraw Hill, **1982**.

[8] R. Brown, *Handbook of Polymer Testing - Short-Term Mechanical Tests*, Rapra Technology, **2002**.

[9] J. D. Menczel, R. B. Prime, *Thermal Analysis of Polymers*, John Wiley & Sons, Inc., **2009**.

[10] P. R. Griffiths, J. A de Haseth, *Fourier Transform Infrared Spectroscopy*, John Wiley & Sons, Inc., **2006**.

[11] J. Goldstein, D. E. Newbury, D. C. Joy, C. E. Lyman, P. Echlin, E. Lifshin, L. Sawyer, J. R. Michael, *Scanning Electron Microscopy and X-ray Microanalysis*, Springer, **2007**.

UNIVERSITAT ROVIRA I VIRGILI
EXPERIMENTAL CHARACTERIZATION OF SHAPE-MEMORY POLYMERS: INFLUENCE OF PROCESSING METHODS AND CHEMICAL STRUCTURE
David Manuel Santiago Abraira

Chapter III

Thermoplastic Shape-Memory Polymers

III.1. Introduction

As described in Section I.1.4, the mechanism of thermally induced thermoplastic shape-memory polymers is based on the formation of a phase segregated morphology, with one phase acting as a molecular switches and one phase acting as netpoints (Figure III.1.1). The phase with the highest transition temperature T_{perm} or hard-segment provides mechanical strength and determines the permanent shape. The phase with the lowest transition temperature T_{trans} or soft-segment allows the formation of the temporary shape through the formation of secondary reversible physical crosslinks [1]. These materials are divided into two categories according to the thermal transition of the switching segment on which the shape-memory effect is based that is, a melting temperature T_m or a glass transition temperature T_g. In the case of a melting temperature, a relatively sharp transition in most cases is observed while glass transitions always extend over a broad temperature range. Mixed glass transition temperatures $T_{g,mix}$ between the glass transition of the hard-segment and the soft-segment determining blocks may occur in the cases where there is no sufficient phase separation between the hard-segment and the soft-segment. Mixed glass transition temperatures can also act as switching transitions for the thermally induced shape-memory effect in thermoplastic SMPs [2].

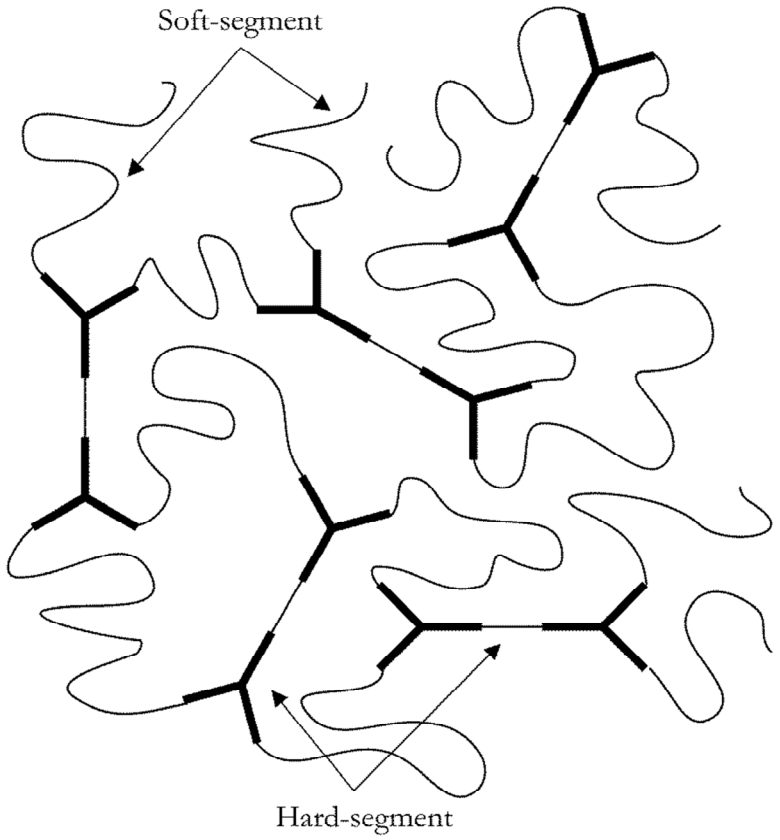

Figure III.1.1 Schematic representation of the network structure of thermoplastic shape-memory polymers.

III.1.1. Effect of thermomechanical cyclic conditions

The relationship between shape-memory properties of thermoplastic SMPs and the thermomechanical cyclic conditions has been widely studied [3-6]. The resulting shape-memory properties that is, the shape-recovery ratio R_r, the shape-fixity ratio R_f or the switching temperature T_{sw} are strongly influenced by the choice of test parameters like maximum stress σ_m or strain ε_m or the programming temperature T_{prog}.

This chapter analyses the influence of the thermomechanical conditions during shape memory cycling on shape-memory properties of

a commercial aliphatic polyether-based thermoplastic polyurethane (Tecoflex® EG-72D). The effect of these parameters is different whether the programming is performed under stress-controlled or strain-controlled conditions. Most of the research studies on SMPs are carried out under strain-controlled conditions; however a stress-controlled protocol is a more appropriate method for characterizing a SMP which has to operate under a constant stress. The results obtained during the realization of this study are presented in two research articles published in *Journal of Material Engineering and Performance* on 2014.

The first of these articles (Section III.3) describes the influence of the maximum stress applied, the programming temperature and the number of cycles performed on shape-memory properties and stabilization of shape recovery. The shape-recovery ratio showed higher values with lower programming temperatures and lower maximum programming stresses. In the case of shape fixation, it was not significantly affected by maximum stresses but it showed higher values when the programming temperature was lower than the transition temperature of the SMP. The switching temperature was not affected by maximum stress but increased when the programming temperature was increased.

It is observed that shape-memory properties can vary significantly with successive thermomechanical cycles [3,7]. The shape-recovery ratio decreases significantly during the first cycles until it reaches a steady behaviour. Bearing in mind SMP applications in which multiple shape-memory cycles have to be performed, the degradation of the shape-memory polymers has to be controlled. Consequently, a stabilization criterion was used in order to determine whether the shape-memory properties reached a steady behaviour. Higher maximum prescribed stresses and higher programming temperatures accentuated the degradation of shape recovery with cycling. The shape fixity and the switching temperature were not significantly affected by cycling. The

stabilization of the shape-memory properties was achieved earlier with lower maximum stress values and the programming temperature did not affect the stabilization.

The results of this study give an overview of how the combination of different thermomechanical programming parameters can affect the shape-memory properties and the lifetime of SMP applications.

The second article (Section III.4) describes the influence of the stress-holding time and the temperature at which it is applied during the programming of the temporary shape. To the best knowledge of the authors, only the holding time under strain-controlled conditions that is, the strain-holding time, has been studied. Tobushi *et al.* [8] studied the influence of the strain-holding conditions on shape recovery and secondary-shape forming in polyurethane-SMP films. It was confirmed in research on the long-term characteristics of the polyurethane SMP foam that the shape fixity and shape recovery became imperfect, and secondary-shape forming appears, depending on the strain-holding conditions. McClung *et al.* [9] studied the strain-holding time on a commercial two-part epoxy-based SMP (Veriflex®). Although the testing material was not a thermoplastic SMP, the effect of the strain-holding time can be understood and related to thermoplastic SMPs. The authors reported a slight decrease in the average total strain recovery and no changes in shape fixity as the strain-holding time was increased. Based on these results, the strain-holding time at elevated temperature causes a stress-relaxation phenomenon on the SMP which adversely affects the extent of shape recovery. The less time the material is given for configurational changes to take place at elevated temperature, the less resistance the material produces against locking in the strain and the better total strain recovery [9].

In those research studies, the strain-holding time was in the range of a few minutes to a few hours. The stress-holding time applied at elevated temperature produces an increase in the maximum deformation

due to a creep phenomenon. The study presented in Section III.4 shows that shape recovery decreased drastically when a stress-holding time at high temperature was applied, even though it was applied just for a few seconds. This degradation was more accentuated when the programming temperature was lower than the glass transition temperature of the SMP. The shape fixation and the switching temperature were not affected by the stress-holding time or by cycling.

The effect of the stress-holding time has important implications for the design of applications in which the SMP needs to work under a constant stress. The cooling process should be as fast as possible in order to reduce the effect of the stress-holding time. The programming of the temporary shape might be compromised due to an increase in the maximum deformation in each cycle when a stress-holding time is applied.

III.2. References

[1] Lendlein, S. Kelch, *Shape-Memory Polymers*, Angew. Chem. Int. Ed. **2002**, *41*, 2034-2057.

[2] J. Leng, S. Du, *Shape-Memory Polymers and Multifunctional Composites*, CRC Press, **2010**.

[3] S. Mogharebi, R. Kazakeviciute-Makovska, H. Steeb, G. Eggeler, K. Neuking, *On the cyclic material stability of shape memory polymer*, Mat.-wiss. u. Werkstofftech. **2013**, *44*, 521–526.

[4] T. Sauter, M. Heuchel, K. Kratz, A. Lendlein, *Quantifying the shape-memory effect of polymers by cyclic thermomechanical tests*, Polym. Rew. **2013**, *53*, 6-40.

[5] S. Abdallah-Elhirtsi, J. Fitoussi, B.-J. Rashmi, K. Prashantha, S. Farzaneh, M.-F Lacrampe, P. Krawczak, A. Tcharkhtchi, *Study of partial shape memory effect of polymers by multicycle tests*, Polym. Comp. **2015**, *36*, 1145-1151.

[6] D. A. Collins, C. M. Yakacki, D. Lightbody, R. R. Patel, C. P. Frick, *Shape-memory behavior of high-strength amorphous thermoplastic poly(para-phenylene)*, J. Appl. Polym. Sci. **2016**, DOI: 10.1002/APP.42903.

[7] C. Schmidt, A. M. S. Chowdhury, K. Neuking, G. Eggeler, *Studies on the cycling, processing and programming of an industrially applicable shape memory polymer Tecoflex® (or TFX EG 72D)*, High Perform. Polym. **2011**, *23*, 300-307.

[8] H. J. Tobushi, S. Hayashi, K. Hoshio, N. Miwa, *Influence of strain-holding conditions on shape recovery and secondary-shape forming in polyurethane-shape memory polymer*, Smart Mater. Struct. **2006**, *15*, 1033-1038.

[9] A. J. W. McClung, G. P. Tandon, J. W. Baur, *Deformation rate-, hold time-, and cycle-dependent shape-memory performance of Veriflex-E resin*, Mech. Time-Depend. Mater. **2011**, *17*, 39-52.

III.3. Effect of Different Shape-Memory Processing Methods on the Thermomechanical Cyclic Properties of a Shape-Memory Polyurethane

David Santiago, Francesc Ferrando, Silvia De la Flor

Journal of Materials Engineering and Performance ***2014****, 23, 2561-2566*

UNIVERSITAT ROVIRA I VIRGILI
EXPERIMENTAL CHARACTERIZATION OF SHAPE-MEMORY POLYMERS: INFLUENCE OF PROCESSING METHODS AND CHEMICAL STRUCTURE
David Manuel Santiago Abraira

J. Mater. Eng. Perform. 2014, 23, 2561-2566

Effect of Different Shape-Memory Processing Methods on the Thermomechanical Cyclic Properties of a Shape-Memory Polyurethane

David Santiago[1], Francesc Ferrando[1], Silvia De la Flor[1]

[1]Department of Mechanical Engineering, Universitat Rovira i Virgili, Av. Països Catalans 26, 43007, Tarragona (Spain)

Abstract

Shape-memory polymers are materials that are capable of changing their shape when an external stimulus is applied. This effect is called the shape-memory effect (SME) and takes place by means of a thermomechanical cycle called programming. The SME depends on the thermomechanical conditions at which programming is performed, and the influence of these conditions differs depending on whether the programming is performed with a strain- or stress-controlled protocol. This study focuses on finding the thermomechanical cycling conditions in stress-controlled programming (T_{prog} and σ_m) that stabilize the material in the fewest cycles while obtaining the best mechanical and shape-memory properties over the highest number of cycles. Using a T_{prog} above or below, the glass transition temperature makes a big difference in terms of shape recovery and the maximum stress is a key factor in the stabilization of shape-memory properties.

Keywords: *Creep and stress rupture, cycling, mechanical, shape-memory polymer, shape-memory polyurethane, stress-controlled programming, Tecoflex®*

1. Introduction

Shape-memory polymers (SMPs) are materials that can be deformed and fixed in a new or temporary shape and return to their original shape, once

the appropriate stimulus is applied [1]. This effect is called the shape-memory effect (SME) and can be induced by an electrical current, a magnetic field or light [2,3], however, the most common SMPs are heat triggered. The SME also appears in other materials like metallic alloys, but SMPs become an excellent substitute when low density and easy conformation are needed as well as the possibility of tailoring the transition temperature. The main fields of applications of SMPs are packaging, electronics, textiles, and aerospace applications [2].

The SME is not an intrinsic property of these kind of polymers. It needs a specific molecular structure and the performance of a thermomechanical procedure to 'program' the new shape and to recover the original. The shape-memory polymer architecture consists of netpoints, or the "hard-segment," and switches, or the "soft-segment." The hard-segment determines the permanent shape and has the highest thermal transition (T_{perm}), and the soft-segment allows the deformation and the fixation of the temporary shape and has a lower thermal transition (T_{trans}). The fixation of the temporary shape occurs by the formation of secondary reversible physical crosslinks. These crosslinks can be formed by the vitrification or crystallization of the switching domains, depending on their chemical nature. Therefore, T_{trans} can be a melting temperature or a glass transition temperature. Once the temperature exceeds T_{trans}, the crystallites melt or the glassy regions become rubber and the crosslinks, which had stabilized the temporary shape, disappear.

The procedure for creating the temporary shape and triggering the SME is a thermomechanical cycle called programming (Figure III.3.1). Programming begins by heating up the material from an elastic state to a rubbery state, which causes a great decrease in the Young modulus [4]. At this high temperature (T_{prog}), the material is deformed into the temporary shape. At this stage, the polymer chains are deformed from a high entropy random coil state to a low entropy-aligned state [5,6]. The

material can be stretched into a prescribed value of strain (ε_m) or stress (σ_m). The strain or stress is held constant while the material is cooled down to a low temperature (T_{low}). During the cooling stage, secondary reversible crosslinks are formed due to the vitrification or crystallization of the switching domains. Once the SMP is cooled down, the stress is released and the temporary shape is fixed. To trigger the SME, the material is heated up again ($T_{recovery}$), allowing the recovery of the original or permanent shape. This thermomechanical cycle can be repeated any number of times.

The SME is strongly influenced by different cyclic conditions such as the maximum imposed strain (ε_m) or stress (σ_m), the programming temperature (T_{prog}) or the number of cycles performed [4-9]. By varying these programming conditions, it is possible to alter shape-memory properties of the SMP. However, the study of these parameters needs to distinguish whether this programming is performed with a strain- or stress-controlled protocol. In the literature, most of the works that study the influence of the thermomechanical conditions on shape-memory properties were performed using a strain-controlled procedure [9-11]. However, stress-controlled programming is more appropriate for applications that require working under constant stress, such as a thermomechanical actuator with partially impeded recovery or deployable structures for aerospace applications.

When programming is performed with a stress-controlled protocol, the programming temperature (T_{prog}) and the maximum prescribed stress (σ_m) applied are two of the most important parameters. Therefore, this study focuses on finding the thermomechanical cycling conditions in stress-controlled programming (*i.e.*, T_{prog} and σ_m) that stabilize the material in the fewest cycles while obtaining the best mechanical and shape-memory properties over the highest number of cycles.

2. Materials and Experimental Method

2.1 Materials

The experiments were performed using Tecoflex® (Lubrizol, USA) thermoplastic amorphous shape-memory polyurethane. The strip dimensions for testing were 20 mm x 5 mm x 1.5 mm. Tecoflex® (TFX EG-72D) was obtained by synthesizing methylene bis(*p*-cyclohexylisocyanate) (H_{12}MDI), 1,4-butanediol (1,4-BD) and poly(tetramethylene glycol) (PTMG) [12].

2.2 Thermomechanical Characterization

Glass transition temperature (T_g) was measured using a DMA Q800 (TA Instruments, USA) equipped with 3-point bending clamp. The sample was heated from 30 to 150 ºC at a heating rate of 3 ºC/min and a frequency of 1 Hz. IR measurements were carried out using a FTIR Vertex 70 (Bruker, Germany) equipped with a Golden Gate ATR (Specac-Teknokroma) accessory. The measurements were taken with a range from 4000 to 600 cm^{-1}, a resolution of 2 cm^{-1}, and a scan time of 10 scans.

2.3 Determination of Shape-Memory Properties

Thermomechanical cycling was performed using a DMA Q800 (TA Instruments) equipped with a film-tension clamp in force-controlled mode. The shape-memory thermomechanical cycle performed is shown in Figure III.3.1. First, the sample is heated to T_{prog} with a heating rate of 3 K/min and then stretched into the prescribed stress (σ_m) at a constant stress rate of 0.4 MPa/min. In this state, the length of the sample at σ_m is L_r. Once the specimen has been stretched, the next step is to cool it down to T_{low} (30 ºC), to fix the temporary shape. This process should be done as fast as possible (5 K/min in our experiments) in order to avoid possible non-desired creep effects. Even so, there is a little variation in the deformation and the length of the specimen after cooling reaches L_m.

After fixation, the stress is released at the same stress rate of 0.4 MPa/min. Once the sample is unloaded, the length of the sample is L_u. The cycle is completed by reheating the sample to $T_{recovery}$ (70 ºC) at 3 K/min. A certain deformation, which the material cannot recover, is stored and the length of the sample at the end of the cycle is L_p. The time between two consecutive cycles is three minutes.

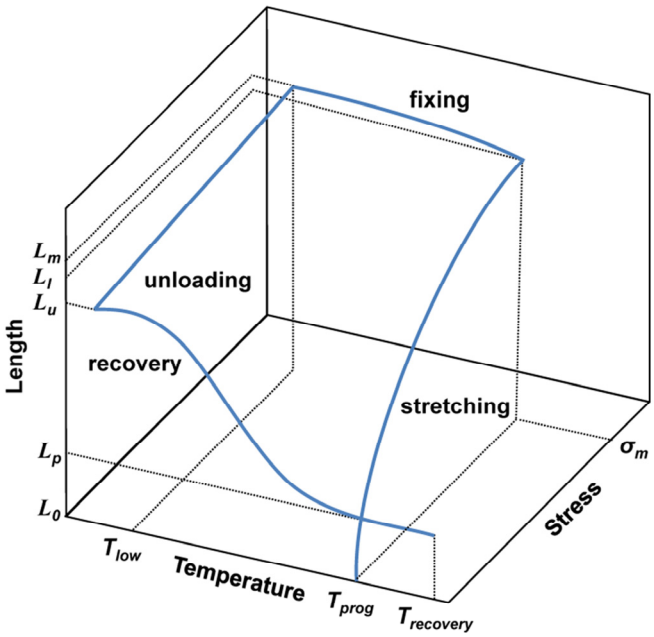

Figure III.3.1 Scheme of the thermomechanical cycle performed with a stress-controlled mode.

Three different T_{prog} were chosen in the vicinity of T_g in order to compare the behavior of TFX EG-72D when T_{prog} is above and below the T_g (50, 60, and 70 ºC) as well as when $T_{prog} \sim T_g$. The specimens were stretched using two different prescribed maximum stresses, 0.7 and 1.4 MPa. The thermomechanical programming was repeated for 25 consecutive cycles in order to analyze the influence of these parameters and stabilization with cycling.

The most significant parameter for quantifying shape-memory properties is the shape-recovery ratio (R_r). The shape-recovery ratio is used to quantify how well an SMP recovers its original shape [2]. There are two significant ways to define this parameter, one defined by Tobushi *et al.* [13] and the other defined by Lendlein and Kelch [2], and both of them seem appropriate when the programming is strain-controlled. Nevertheless, these parameters are not suitable when the programming is performed with a stress-controlled protocol as stated by Liu *et al.* [1]. Therefore, in this work, the following shape-recovery ratio (Equation III.3.1) to quantify permanent shape-recovery was used.

$$R_r(\mathrm{N}) = \frac{L_l(\mathrm{N}) - L_p(\mathrm{N})}{L_l(\mathrm{N}) - L_0} \cdot 100 \qquad \text{(III.3.1)}$$

where L_l(N) is the maximum length reached in the cycle N, L_p(N) is the length of the sample at the end of the cycle (N), and L_0 is the initial length of the sample at the beginning of the programming. In a stress-controlled procedure, the samples are stretched into a fixed σ_m, which means the maximum length reached increases with each cycle. So R_r compares the elongation recovered during the Nth cycle L_l(N) – L_p(N) with the maximum elongation, L_l(N) – L_0, reached before cooling the sample during the Nth cycle. The shape-recovery quantification was calculated with L_l and not with L_m because this variation of deformation is very low and tends to disappear with cycling.

Shape-memory properties vary significantly with successive thermomechanical cycles [6,8,14]. R_r decreases markedly in the initial cycles and remains stable during the following cycles. To determine whether a sample had reached a steady behavior, the average value and the standard deviation of R_r over 10 successive cycles were calculated. R_r was considered to be stable when the standard deviation value was under 2%, and this condition was repeated for at least five consecutive values. Regardless of the number of cycles needed to reach the stability, all

programmings were performed with N = 25 cycles (which is above the highest stabilization cycle of any sample).

Another important property for an SMP is the ability to fix a temporary shape [2]. The shape-fixity ratio (R_f) quantifies this ability. The shape-fixity ratio (Equation III.3.2) compares the deformation of the sample after unloading with the maximum deformation reached in each cycle.

$$R_f(\mathrm{N}) = \frac{L_u(\mathrm{N}) - L_0}{L_m(\mathrm{N}) - L_0} \cdot 100 \qquad \text{(III.3.2)}$$

Another parameter that can be affected by the thermomechanical conditions is the switching temperature (T_{sw}). T_{sw} is the temperature at the inflection point during the recovery stage of the length-temperature curve (Figure III.3.1) and it is similar to T_{trans}. The change in T_{sw} upon cycling has also been quantified for each test condition.

3. Results and Discussion

The glass transition temperature of TFX EG-72D was measured by means of dynamic mechanical analysis (Figure III.3.2a). Two relaxations occurred. The first peak of tan δ at 61 ºC corresponds to the glass transition temperature of a mixed-phase formed by hard- and soft-segments. The second relaxation occurred at 120 ºC and corresponds to the glass transition of the hard-segment [12]. The stiffness of TFX EG-72D dramatically changes when the temperature is above the glass transition temperature. The storage modulus E' in the glassy state is two orders of magnitude higher than the modulus in the rubbery state. This important difference of the mechanical properties between the glassy and rubbery states is crucial if a polymer is going to present the SME [1]. Below the glass transition temperature, the polymer chains adopt a high entropy random coil state. Above the glass transition temperature, the polymer is easily deformed into a low entropy state, because the polymer

chains acquire a more aligned state. If the SMP is cooled down while the stress is still applied, then reversible secondary crosslinks are formed. They can hold the deformation because the polymer is in a low entropy state and the driving entropic forces cannot overcome the crosslinks [15]. Once temperature exceeds the T_g, the crosslinks disappear and the SMP tends to a more stable high entropy state, and the polymer returns to the original shape.

Figure III.3.2b shows the IR spectrum of TFX EG-72D. The main absorption bands are 3340 cm^{-1}, NH stretching; 2925 cm^{-1}, β CH2 stretching; 2853 cm^{-1}, α CH2 stretching; 1697 cm^{-1}, C=O stretching (amide I band); 1571 cm^{-1}, CN stretching (1º amide) and NH bending (amide II band); 1219 cm^{-1}, CN stretching (amide III band); 1095 cm^{-1}, C-O-C stretching (urethane); and 778 cm^{-1}, ring puckering. The results of the IR spectrum indicate that the composition of TFX EG-72D corresponds with that provided by the manufacturer.

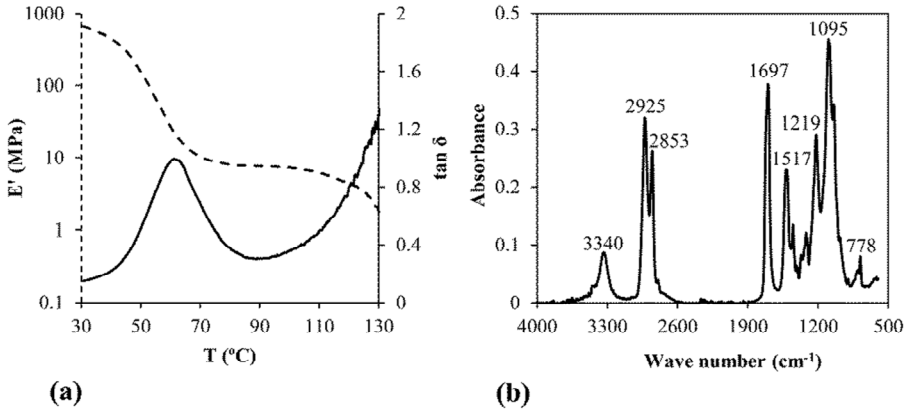

Figure III.3.2 (a) Storage modulus *E'* and tan δ as a function of temperature; (b) IR spectrum of TFX EG-72D

As shown in Figure III.3.3, the SMP shows shape-recovery ratio degradation with cycling for both σ_m and all T_{prog}. With σ_m = 0.7 MPa, R_r decreases drastically during the first seven cycles, and then taking on a steady behavior with a slight decrease to the stabilization cycle (N_e) for all

T_{prog}. The programmings performed with T_{prog} = 50 and 70 ºC show an early stabilization at N_e = 18 and N_e = 19, while with T_{prog} = 60 ºC, stabilization is reached at N_e = 25. With σ_m = 1.4 MPa and again for all T_{prog}, the initial drop of R_r is notably higher and lasted until N = 10. From this point to N_e, R_r also decreases slightly. The stabilization cycles for T_{prog} = 50, 60, and 70 ºC are N_e = 22, 24, and 21, respectively.

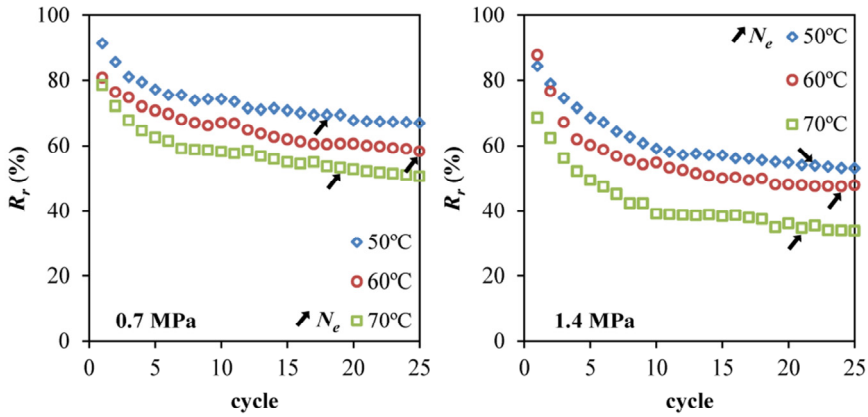

Figure III.3.3 Shape-recovery ratios upon cycling of the experiments performed

Similar results were also reported by Schmidt *et al.* [6], but those were obtained with a strain-controlled procedure. This degradation of R_r is caused by the accumulation of irrecoverable strain at the end of the cycles that the SMP cannot recover and is notably more pronounced with σ_m = 1.4 MPa than with σ_m = 0.7 MPa. Comparing the first cycle with N_e, with σ_m = 0.7 MPa, R_r only drops a 24% for T_{prog} = 50 ºC and a higher value (but similar) with T_{prog} = 60 and 70 ºC around 30%). However, when σ_m = 1.4 MPa this drop is higher for all T_{prog} (36% for 50 ºC and, again, similar values for 60 and 70 ºC, around 50%).

The stabilization cycle N_e of R_r is reached later with σ_m = 1.4 MPa. This may be related to the higher degradation of R_r with higher σ_m. The accumulation of irrecoverable strain grows with each cycle, thereby

preventing steady behavior from being achieved. It seems that T_{prog} does not strongly influence N_e, however stabilization is reached later with T_{prog} = 60 ºC at both σ_m. The reason for these results might be explained by the programming of the SMP at $T_{prog} \sim T_g$, which may have prevented the glassy-rubbery ratio of the mixed-phase from being well established, thereby resulting in the instability of shape-memory properties.

Comparing the values of R_r between T_{prog}s, R_r is higher with lower T_{prog}. The highest recovery values are reached with 50 ºC and the lowest with 70 ºC. This could be explained because the rubbery domains of the mixed-phase support the fixation of the temporary shape while the glassy domains support the recovery of the permanent shape. Therefore, when $T_{prog} < T_g$, the mixed-phase is in a predominantly glassy state and better recovery is achieved [12]. Nevertheless, the programmings performed with T_{prog} = 60 ºC show unexpected R_r values during the first cycle: at σ_m = 0.7 MPa a higher value would be expected than with T_{prog} = 70 ºC; and at σ_m = 1.4 MPa a lower value than with T_{prog} = 50 ºC. These results may be caused by the possible instability of shape-memory properties in the vicinity of T_g.

Figure III.3.4 shows the shape-fixity ratios upon cycling for both maximum σ_m and different T_{prog}. With σ_m = 0.7 MPa, R_f shows a notable decrease when T_{prog} = 50 ºC and very similar values with T_{prog} = 60 ºC and T_{prog} = 70 ºC. R_f does not seem to be affected by cycling (for all T_{prog}) as also described by McClung *et al.* [8], but using a strain-controlled procedure. However, with σ_m = 1.4 MPa a different behavior can be observed, in which R_f increases notably during the first four cycles. It seems that higher σ_m causes instability at the beginning of the thermomechanical cycling and the fixation needs a few cycles to establish a steady behavior. Once the SMP has passed this initial transitional regime, the values of R_f with σ_m = 1.4 MPa are similar to those with σ_m = 0.7 MPa.

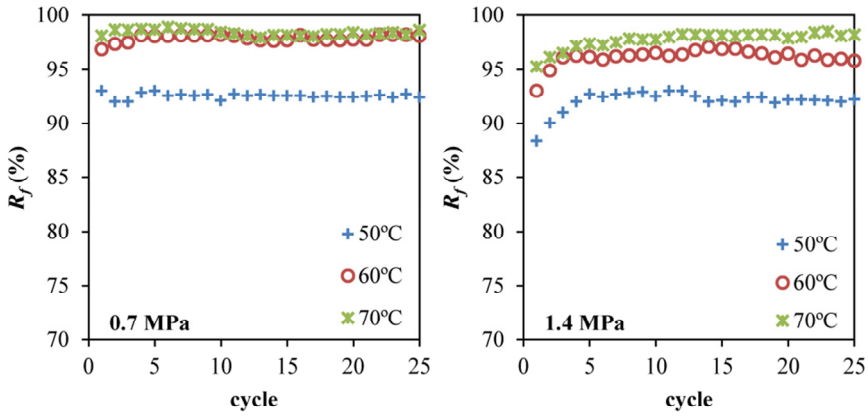

Figure III.3.4 Shape-fixity ratios upon cycling of each experiment performed.

Regardless of σ_m, R_f is higher with higher T_{prog}. This is because, as mentioned earlier, the fixation of the temporary shape is carried out by the rubbery domains of the mixed-phase [12]. With T_{prog} = 50 ºC, which is below the T_g, the mixed-phase is predominantly in a glassy-state, and thus R_f is significantly lower than with T_{prog} = 60 and 70 ºC. With T_{prog} = 70 ºC, R_f is slightly higher than with T_{prog} = 60 ºC, because at 70 ºC the mixed-phase is in a completely rubbery state while at 60 ºC some glassy domains that have not yet become rubbery may still be present.

Figure III.3.5 shows the evolution of the switching temperature upon cycling for both maximum σ_m and different T_{prog}. With σ_m = 0.7 MPa, T_{sw} shows similar values for T_{prog} = 60 ºC and T_{prog} = 70 ºC and slightly lower values with T_{prog} = 50 ºC. T_{sw} is not affected by cycling, however, with σ_m = 1.4 MPa, T_{sw} increases with cycling to approximately N = 15. From this point forward, no more changes with cycling are observed and T_{sw} has almost the same values as with σ_m = 0.7 MPa. This initial increase with σ_m = 1.4 MPa is similar to that shown in R_f, however, it seems that switching temperature is more sensitive with higher σ_m because the transitional regime is notably longer than in the case of R_f. A comparison

of the values of T_{sw} between the different T_{prog} shows that T_{sw} increases with higher T_{prog}, as mentioned by Cui *et al.* [16].

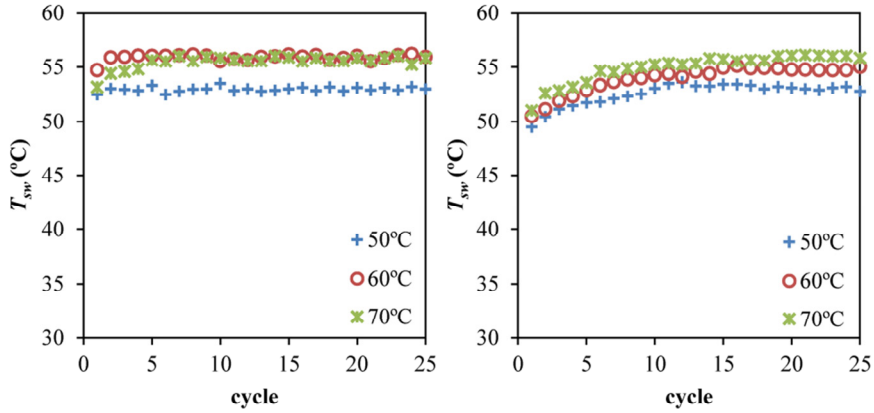

Figure III.3.5 Switching temperature upon cycling of each condition

An important phenomenon that takes place when the samples are subjected to successive cycles is a progressive strain-hardening. Figure III.3.6 shows the strain-stress curves of the stretching stage of each condition of testing. The deformation represented in the x axis of Figure III.3.6 corresponds to the amount of deformation reached in each cycle, calculated as $\varepsilon = (L_f(\mathrm{N}) - L_0(\mathrm{N}))/L_0(\mathrm{N})$, where $L_f(\mathrm{N})$ is the length of the sample reached at the prescribed stress during the cycle N and $L_0(\mathrm{N})$ is the initial length of the sample at beginning of the cycle N. When repeated thermomechanical strain-controlled cycles are carried out, there is an increase in the maximum stress in each cycle [8,14]. However, when the programming is performed with a stress-controlled protocol, a progressive decrease in the strain el (deformation of the sample at σ_m and T_{prog}) with cycling is observed.

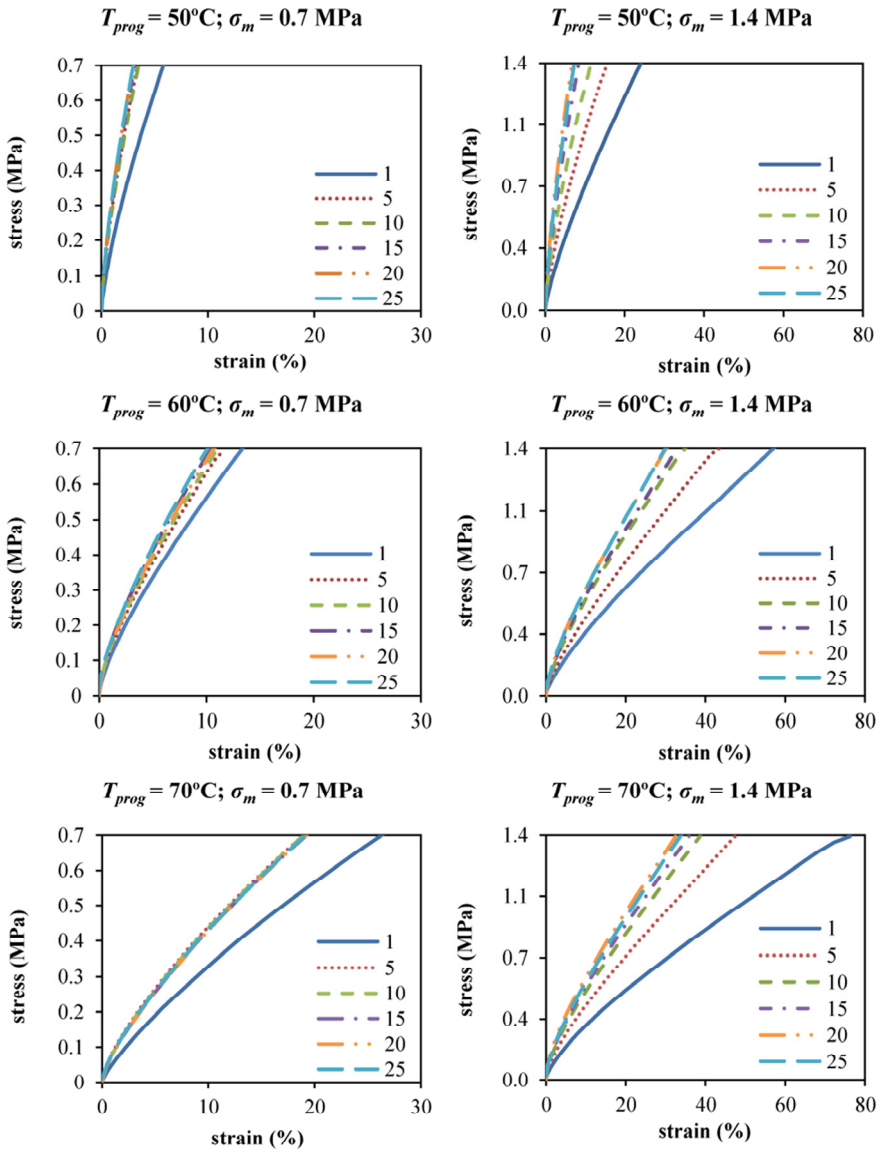

Figure III.3.6 Strain-stress curves of the stretching stage of the 1st, 5th, 10th, 15th, 20th, and 25th cycles of each programming performed

With σ_m = 0.7 MPa, the slope of the curve increases progressively to N = 5 and from that point forward, the hardening phenomenon saturates and the slope does not significantly change. However, with σ_m =

1.4 MPa, the strain-hardening is more pronounced. The increasing of the slopes of the curves is progressive to $N = 10$ and from this point to $N = 20$, where the hardening phenomenon saturates, the slopes increase only slightly. This behavior of hardening saturation seems to be the same regardless of the T_{prog} used for each σ_m.

Strain-hardening with cycling can be related to the alignment of the polymer chains and the accumulation of plastic deformation [17]. At first glance, it seems that the hardening is more pronounced at $T_{prog} = 70$ ºC, however, the decrease in the deformation in relative terms is notably higher at $T_{prog} = 50$ ºC. Comparing the deformation between the 1st cycle and the stabilization cycle (N_e), with $\sigma_m = 0.7$ MPa, the deformation drops to around 49% ($N_e = 18$), 23% ($N_e = 25$), and 26% ($N_e = 19$) and with $\sigma_m = 1.4$ MPa to around 70% ($N_e = 22$), 47% ($N_e = 24$), and 55% ($N_e = 21$) for $T_{prog} = 50$, 60, and 70 ºC, respectively. These results may be explained by the fact that when the specimen is stretched at $T_{prog} < T_g$, there is a higher accumulation of plastic deformation because the polymer chains cannot flow easily.

Conclusions

Shape-memory properties of a shape-memory polyurethane (TFX EG-72D) programmed with a stress-controlled procedure have been investigated. The influence of different programming conditions on shape-recovery and the shape-fixity, switching temperature and the stabilization over successive cycles is analyzed and discussed.

The shape-recovery ratio showed higher values with lower T_{prog} and lower σ_m. When the SMP was subjected to successive cycles, R_r degraded with cycling due to the accumulation of irrecoverable deformation. Higher maximum prescribed stress accentuated this degradation, causing a higher drop in R_r and delaying stabilization. Higher T_{prog} also caused a higher decrease in R_r with cycling. This effect was slight in comparison with σ_m and did not affect the stability of R_r, however when the SMP is

programmed in the vicinity of T_g, shape-memory properties can be instable, hindering stabilization.

With low σ_m, neither the shape-fixity ratio R_f nor the switching temperature T_{sw} was affected by cycling. However, with higher σ_m, R_f, and T_{sw} became instable during the first cycles, increasingly slightly until reaching steady behavior. Once stability was reached, R_f and T_{sw} showed similar values at each σ_m. If $T_{prog} > T_g$, TFX EG-72D showed better values of fixation than $T_{prog} < T_g$ and T_{sw} increased with increasing T_{prog}.

Another important phenomenon was observed when the SMP was programmed over successive cycles: progressive strain-hardening. This phenomenon was more pronounced when $T_{prog} < T_g$. When low σ_m was applied, the strain-hardening saturated early, but with higher σ_m it was prolonged for more cycles and the percentage of hardening was higher.

As a global conclusion for future applications that need to work in a stress-controlled procedure over successive cycles, it would be imperative to carefully select the most appropriate thermomechanical conditions (*i.e.*, σ_m and T_{prog}) to ensure correct operation, as they greatly influence the shape-recovery and stabilization of shape-memory properties when the SMP is subjected to successive cycles.

Acknowledgment

The authors would like to thank MINECO (MAT2011-27039-C03-01, MAT2011-27039-C03-02) for giving financial support.

References

[1] C. Liu, H. Qin, and P.T. Mather, Review of Progress in Shape-Memory Polymers, *J. Mater. Chem.*, 2007, **17**(16), p 1543–1558

[2] A. Lendlein and S. Kelch, Shape-Memory Polymers, *Angew. Chem. Int. Ed.*, 2002, **41**(12), p 2034–2057

[3] R. Mohr, K. Kratz, T. Weigel, M. Lucka-Gabor, M. Moneke, and A. Lendlein, Initiation of Shape-Memory Effect by Inductive

Heating of Magnetic Nanoparticles in Thermoplastic Polymers, *Proc. Natl. Acad. Sci. USA*, 2006, **103**(10), p 3540–3545

[4] A.J.W. McClung, G.P. Tandon, and J.W. Baur, Deformation Rate-, Hold Time-, and Cycle-Dependent Shape-Memory Performance of Veriflex-E Resin, *Mech. Time-Depend. Mater.*, 2011, **17**, p 39–52

[5] V.A. Beloshenko, V.N. Varyukhin, and Y.V. Voznyak, The Shape Memory Effect in Polymers, *Usp. Khim.*, 2005, **74**(3), p 285–306

[6] C. Schmidt, K. Neuking, and G. Eggeler, Functional Fatigue of Shape-Memory Polymers, in *Materials Research Society Symposium Proceedings*, San Francisco, CA, 2009, vol. 1190, pp. 43–48

[7] F. Castro, K.K. Westbrook, K.N. Long, R. Shandas, and H.J. Qi, Effects of Thermal Rates on the Thermomechanical Behaviors of Amorphous Shape Memory Polymers, *Mech. Time-Depend. Mater.*, 2010, **14**(3), p 219–241

[8] A.J.W. McClung, G.P. Tandon, and J.W. Baur Air, Fatigue Cycling of Shape Memory Polymer Resin, in *Conference Proceedings of the Society for Experimental Mechanics Series*, Uncasville, 2011, vol. 3, pp. 119–127

[9] J.L. Hu, F.L. Ji, and Y.W. Wong, Dependency of the Shape Memory Properties of a Polyurethane upon Thermomechanical Cyclic Conditions, *Polym. Int.*, 2005, **54**(3), p 600–605

[10] C. Schmidt, A.M.S. Chowdhury, K. Neuking, and G. Eggeler, Stress- Strain Behavior of Shape Memory Polymers by 1WE Method: Application to Tecoflex®, *J. Macromol. Sci. A*, 2011, **48**(3), p 204–210

[11] A.J.W. McClung, G.P. Tandon, and J.W. Baur, The Strain Rate- and Temperature-Dependent Mechanical Behavior of Veriflex-E in tension, in *ASME 2010 Conference on Smart Materials, Adaptive Structures and Intelligent Systems, SMASIS 2010*, Philadelphia, PA, 2010, vol. 1, pp. 69–78

[12] J. Cui, K. Kratz, M. Heuchel, B. Hiebl, and A. Lendlein, Mechanically Active Scaffolds from Radio-Opaque Shape-Memory Polymer-Based Composites, *Polym. Adv. Technol.*, 2011, **22**(1), p 180–189

[13] H. Tobushi, H. Hara, E. Yamada, and S. Hayashi, Thermomechanical Properties in a Thin Film of Shape Memory Polymer of Polyurethane Series, *Smart Mater. Struct.*, 1996, **5**(4), p 483–491

[14] S. Mogharebi, R. Kazakeviciute-Makovska, H. Steeb, G. Eggeler, and K. Neuking, On the Cyclic Material Stability of Shape Memory Polymer, *Mater. wis. Werkstofftech.*, 2013, **44**(6), p 521–526

[15] B. Atli, F. Gandhi, and G. Karst, Thermomechanical Characterization of Shape Memory Polymers, in *Proceedings of SPIE - The International Society for Optical Engineering*, San Diego, CA, 2007, vol. 6524

[16] J. Cui, K. Kratz, and A. Lendlein, Adjusting Shape-Memory Properties of Amorphous Polyether Urethanes and Radio-Opaque Composites Thereof by Variation of Physical Parameters during Programming, *Smart Mater. Struct.*, 2010, **19**(6), p 065019

[17] S. Farzaneh, J. Fitoussi, A. Lucas, M. Bocquet, and A. Tcharkhtchi, Shape Memory Effect and Properties Memory Effect of Polyurethane, *J. Appl. Polym. Sci.*, 2013, **128**(5), p 3240–3249

UNIVERSITAT ROVIRA I VIRGILI
EXPERIMENTAL CHARACTERIZATION OF SHAPE-MEMORY POLYMERS: INFLUENCE OF PROCESSING METHODS AND CHEMICAL STRUCTURE
David Manuel Santiago Abraira

III.4. Influence of Holding Time on Shape Recovery in a Polyurethane Shape-Memory Polymer

David Santiago, Francesc Ferrando, Silvia De la Flor

Journal of Materials Engineering and Performance ***2014****, 23, 2567-2573*

UNIVERSITAT ROVIRA I VIRGILI
EXPERIMENTAL CHARACTERIZATION OF SHAPE-MEMORY POLYMERS: INFLUENCE OF PROCESSING METHODS AND CHEMICAL STRUCTURE
David Manuel Santiago Abraira

J. Mater. Eng. Perform. 2014, 23, 2567-2573

Influence of Holding Time on Shape Recovery in a Polyurethane Shape-Memory Polymer

David Santiago[1], Francesc Ferrando[1], Silvia De la Flor[1]

[1]Department of Mechanical Engineering, Universitat Rovira i Virgili, Av. Països Catalans 26, 43007, Tarragona (Spain)

Abstract

Shape-memory polymers have attracted a lot of interest in recent years. A shape-memory polymer can be deformed and fixed into a temporary shape and subsequently made to recover its original shape when a suitable stimulus is applied. This is accomplished by means of a thermomechanical cycle called programming. Programming can be performed in a stress-or strain-controlled mode. The thermomechanical conditions of the programming affect shape-memory properties differently in each programming mode. One of the parameters which significantly affects shape-memory properties in a stress-controlled procedure is stress-holding time (t_H) at high temperature. This paper studies how stress-holding time affects the most significant shape-memory properties under successive thermomechanical cycles. The experiments were conducted using two different programming temperatures in the vicinity of the T_g. The shape-recovery ratio decreased dramatically with cycling even when the holding time was just a few seconds, however, the impact of the stress-holding time depends on the temperature at which it has been applied. Shape-fixity ratio and switching temperature were also studied, but stress-holding time and successive cycles do not seem to affect either of these factors.

Keywords: *creep and stress rupture, cyclic behavior, mechanical, nondestructive testing, polyurethane, shape-memory polymers, stress-holding time*

1. Introduction

Shape-memory polymers (SMPs) are materials that are capable of changing shape when an external stimulus is applied. This effect is called the shape-memory effect (SME) and it is usually thermally induced, but it can also be induced by means of an electrical current, light, or a magnetic field if the polymer is properly filled [1]. SME can also appear in other materials like metallic alloys, but SMPs are an excellent replacement in applications where low density and easy conformation are needed as well as the possibility of tailoring the transition temperature. The main fields of applications of shape-memory polymers are packaging, electronics, textiles, and biomedical and aerospace applications [1].

The SME requires a specific polymer network and a thermomechanical procedure called programming. The shape-memory polymer architecture consists of netpoints, or the "hard-segment", and switches called the "soft-segment". The hard-segment determines the permanent shape and has the highest thermal transition (T_{perm}), while the soft-segment allows the material to deform and take on a fixed temporary shape and has a lower thermal transition (T_{trans}) [1].

The thermomechanical procedure to create the temporary shape and to trigger the recovery effect, called programming, is shown in Figure III.4.1a. The cycle consists of four steps: stretching the specimen to σ_m at a high temperature (T_{prog}); cooling to a low temperature (T_{low}) in order to fix the temporary shape, maintaining σ_m; releasing the stress σ_m at T_{low}; and, finally, heating to $T_{recovery}$ (which is usually equal or greater than T_{prog}) to trigger the SME. Programming begins with heating up the material from a glassy state to a rubbery state, which causes a great decrease in the Young modulus [2]. At T_{prog}, the material is deformed into the temporary shape and the polymer chains are deformed from a high-entropy random coil state to a low-entropy aligned state. The deformation is maintained while the material is cooled down to T_{low} in order to fix the temporary shape. Fixation occurs by means of the formation of secondary reversible

crosslinks [1]. These crosslinks are formed, depending on the nature of the soft-segment, by the vitrification or crystallization of the switching domains. Therefore, the transition temperature of the soft-segment (T_{trans}) can be a melting temperature or a glass transition temperature. The stress is then released and the new crosslinks that are formed are imposed on the netpoints, which means the material remains stable in its new shape [2]. To trigger the SME and recover the permanent shape, the material is heated up to $T_{recovery}$. Once the temperature exceeds T_{trans}, the crystallites melt or the glassy regions become rubber and the crosslinks which stabilize the temporary shape disappear. The recovery force is led by the entropy elasticity of the soft-segment, because, over the T_{trans}, the soft-segment gains entropy by moving from an aligned state to a random coil [3].

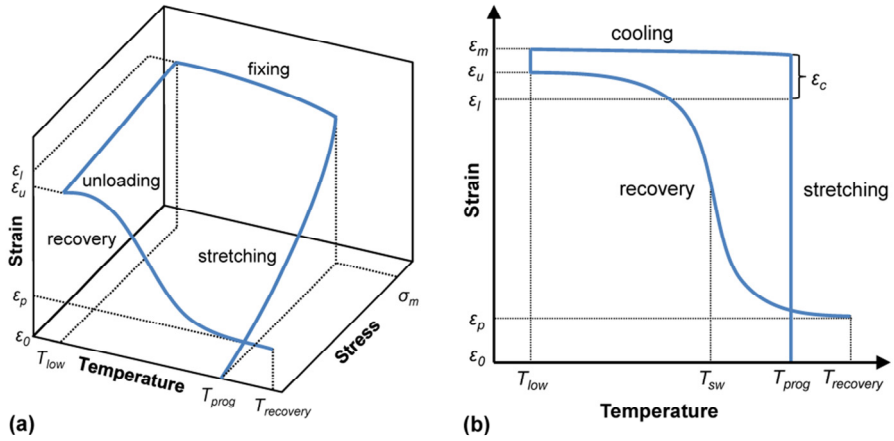

Figure III.4.1 (a) Scheme of the thermomechanical cycle performed with a stress-controlled mode under stress-holding conditions; (b) scheme of the strain-temperature plot performed with a stress-controlled mode under stress-holding conditions.

Several thermomechanical conditions affect shape-memory properties during programming, such as the maximum imposed strain or stress, programming temperatures (T_{prog}, T_{low}, or $T_{recovery}$), the stretching rate

($\dot{\varepsilon}$ or $\dot{\sigma}$), and the number of cycles performed [4-7]. However, the effects of these parameters can differ depending on whether programming is performed with a strain-or a stress-controlled protocol. In strain-controlled programming, the SMP is deformed into a desired strain, while in a stress-controlled programming, it is stretched to a prescribed stress. Most of the studies in the literature that focus on the shape-memory properties of SMPs are performed with strain-controlled programming. However, if the SMP needs to work as a thermomechanical actuator, the most appropriate programming mode is stress-controlled. In this study, a stress-controlled protocol is used in order to improve understanding of this kind of procedure.

One of the most significant parameters mentioned above that affects shape-memory properties is the strain or stress-holding time. Several authors have studied strain-holding conditions and their effect on shape-memory properties [4,6-9]. Strain-holding time causes a decrease in shape recovery due to stress relaxation; however, the effect of holding stress at a high temperature has not been investigated.

Therefore, the primary objective of this paper is to analyze the influence of stress-holding time on shape-memory properties. The effect of different t_H and the temperature at which they are applied when the SMP is subjected to successive thermomechanical cycles is also discussed.

Stress-holding times at a high temperature can produce undesired effects, such as overrunning the yield point or storing too much irrecoverable deformation, even if the t_H is just a few seconds. Therefore, the proper understanding of the effect of stress-holding time would be useful for shape-memory applications which need to work under constant stress, such as actuators or reconfigurable structures.

J. Mater. Eng. Perform. 2014, 23, 2567-2573

2. Material and Methods

2.1 Material

The experiments were performed using Tecoflex® (Lubrizol, USA) thermoplastic amorphous shape-memory polyurethane. The strip dimensions for testing were 20 mm x 5mm x 1.5 mm. Tecoflex® (TFX EG-72D) was obtained by synthesizing methylene bis(*p*-cyclohexylisocyanate) (H_{12}MDI), 1,4-butanediol (1,4-BD), and poly(tetramethylene glycol) (PTMG) [10].

2.2 Thermomechanical Characterization

T_g was measured using a DMA Q800 (TA Instruments, USA) equipped with a 3-point bending clamp. The sample was heated from 30 to 150 ºC at a heating rate of 3 ºC/min and a frequency of 1 Hz. IR measurements were carried out using a FTIR Vertex 70 (Bruker, Germany) equipped with a Golden Gate ATR (Specac-Teknokroma) accessory. The measurements were taken with a range from 4000 to 600 cm^{-1}, a resolution of $2cm^{-1}$, and a scan time of 10 scans.

2.3 Determination of Shape-Memory Properties

Thermomechanical cycling or programming was carried out using a DMA Q800 (TA Instruments, USA) equipped with a film-tension clamp in force-controlled mode. The shape-memory thermomechanical cycle performed with stress-holding time (t_H) is shown in Figure III.4.1b. First, the sample is heated to the programming high temperature (T_{prog}). The sample is stretched into the prescribed stress, σ_m, at a constant stress rate of 0.4 MPa/min. In this state, the deformation of the sample is el. Once the sample is stretched, the stress-holding time, t_H, is applied. This causes an additional deformation ε_c caused by a creep phenomenon. Thus, the total deformation is $\varepsilon_m = \varepsilon_l + \varepsilon_c$. The next step is to fix the temporary shape. To achieve this, the specimen is cooled to T_{low}. During cooling, secondary reversible crosslinks are formed by the vitrification of the soft-

segment. Once the sample is cooled down, the stress is released at the same stress rate of 0.4 MPa/min. After unloading, the strain of the sample is ε_u. The cycle is completed by reheating again the sample to $T_{recovery}$ (70 ºC) at 3 ºC/min. At this temperature, the physically reversible crosslinks which fix the temporary shape disappear (the soft-segments become rubbery again) and the material recovers its permanent shape. A certain degree of deformation, which the material cannot recover, is stored, and the strain at the end of the cycle is ε_p. Programming is repeated for 30 consecutive cycles. The time between two consecutive cycles is 3 min.

The different parameters used in the experiments performed are presented in Table III.4.1. The number of cycles performed was N = 30 in order to study the evolution of the shape-memory properties with cycling, and the maximum stress σ_m was 0.7 MPa. Two different temperatures were chosen as T_{prog}, 50 and 60 ºC, in order to compare the response of the material when $T_{prog} < T_g$ and $T_{prog} = T_g$. For each T_{prog}, experiments with different t_H were carried out from t_H = 10 s until t_H = 120 s. The times seem short in comparison with those used in strain-holding programming, but it is important to note that even very short times produce significant effects in shape-memory properties.

Table III.4.1 Stress-holding times applied in each experiment

T_{prog}, ºC	t_H, s					
50	0	10	30	60	90	120
60	0	10	30	60	90	-

The most significant parameter for quantifying how well the SMP memorizes the permanent shape is the shape-recovery ratio (R_r) [1]. There are two significant ways to define this parameter, one defined by Tobushi *et al.* [11] and another defined by Lendlein and Kelch [1]. Both of them seem appropriate when programming is strain controlled.

However, these parameters are not suitable when programming is performed with a stress-controlled protocol as stated by Liu *et al.* [12]. Therefore, in this work, the following expression to quantify permanent shape recovery was used (Equation III.4.1).

$$R_r(\mathrm{N}) = \frac{\varepsilon_m(\mathrm{N}) - \varepsilon_p(\mathrm{N})}{\varepsilon_m(\mathrm{N})} \cdot 100 \qquad \text{(III.4.1)}$$

In this ratio, the amount of deformation recovered during the Nth cycle, $\varepsilon_m(N)$ - $\varepsilon_p(N)$, is compared with the deformation after the stress-holding time $\varepsilon_m(N)$ of the Nth cycle (referred to as the initial length, L_0).

Successive thermomechanical cycles cause a degradation in the shape-memory properties [5,9]. The accumulation of irrecoverable strain causes a decrease in R_r with cycling until it reaches a steady behavior. To determine whether a sample had reached this steady behavior, the average value and the standard deviation of R_r over 10 successive cycles were calculated. R_r was considered to be stable when the standard deviation value was under 2% and this condition was repeated for at least five consecutive cycles. Regardless of the number of cycles needed to reach stability, all programmings were performed with N = 30 cycles (which is above the highest stabilization cycle of any sample).

Another important property for an SMP is its ability to fix the temporary shape. The shape-fixity ratio (R_f) quantifies this ability [1]. The shape-fixity ratio compares the maximum deformation reached in each cycle and the deformation of the sample once it has been unloaded. If the specimen is subjected to stress-holding conditions, in addition to the deformation caused by the prescribed stress, there is a certain amount of deformation caused due to creep, as explained above. Therefore, in order to study the fixation of the temporary shape, the shape-fixity ratio was calculated using the maximum deformation reached in each cycle ε_m. The shape-fixity-used ratio is presented in Equation III.4.2.

$$R_f(\%) = \frac{L_u(\mathrm{N}) - L_0}{L_m(\mathrm{N}) - L_0} \cdot 100 \qquad \text{(III.4.2)}$$

Another parameter that can be affected by the thermomechanical process and stress-holding time is switching temperature (T_{sw}). T_{sw} is the temperature at the inflection point during the recovery stage of the strain-temperature curve (Figure III.4.1b), and it is similar to T_{trans}. The change in T_{sw} upon cycling and stress holding is also quantified.

3. Results and Discussion

The glass transition temperature of TFX EG-72D was measured by means of dynamic mechanical analysis (Figure III.4.2a). Two relaxations occurred. The first peak of tan δ at 61 ºC corresponds to the glass transition temperature of a mixed phase formed by hard and soft-segments. The second relaxation occurred at 120 ºC and corresponds to the glass transition of the hard-segment [13]. The storage modulus *E'* in the glassy state is two orders of magnitude higher than the modulus in the rubbery state. This important difference in the mechanical properties of the glassy and rubbery states is crucial for a polymer to present the SME [12]. If the SMP is deformed at a high temperature and cooled down to a low temperature under a constant strain or stress, the driving entropic forces are not able to surpass the secondary reversible crosslinks formed during fixation and the temporary shape remains stable [2].

Figure III.4.2b shows the IR spectrum of TFX EG-72D. The main absorption bands are 3340 cm^{-1}, NH stretching; 2925 cm^{-1}, β CH2 stretching; 2853 cm^{-1}, α CH2 stretching; 1697 cm^{-1}, C=O stretching (amide I band); 1571 cm^{-1}, CN stretching (1º amide) and NH bending (amide II band); 1219 cm^{-1}, CN stretching (amide III band); 1095 cm^{-1}, C-O-C stretching (urethane); and 778 cm^{-1}, ring puckering. The results of the IR spectrum indicate that the composition of TFX EG-72D

corresponds to that provided by the manufacturer and, therefore, a significant SME can be expected.

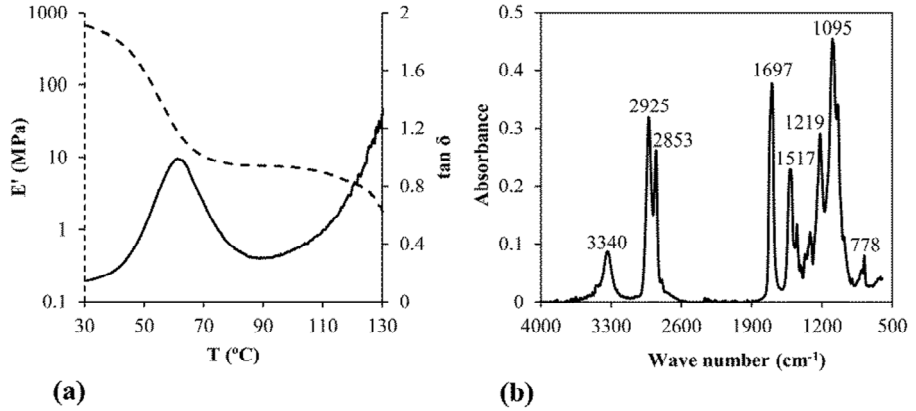

Figure III.4.2 (a) Storage modulus E' and tan δ as a function of temperature; (b) IR spectrum of TFX EG-72D.

Figure III.4.3 shows the deformation el (corresponding to the strain at the prescribed stress σ_m without t_H) and the additional deformation ε_c added in each cycle due to the creep phenomenon that takes places during the t_H for programming cycles at T_{prog} = 50 ºC and 60 ºC. ε_c is calculated as the percentage of deformation added at each t_H with respect to the deformation el. With T_{prog} = 50 ºC, the deformation ε_c added is higher for longer t_H. In general, ε_c is not significantly affected by cycling, however, it seems to increase slightly with t_H = 10 and 30s. With t_H = 60, 90, and 120 s, ε_c decreases slightly until approximately N = 20 and then increases slightly to N = 30. Overall, ε_c shows average values ranging from a 40% at t_H = 10 s up to 85% at t_H = 120 s.

With T_{prog} = 60 ºC (Figure III.4.3b), ε_c does not vary with cycling and progressively increases from average values of around 20% with t_H = 10s up to 58% with t_H = 90 s. The deformation added with t_H at 60 ºC is notably lower than at 50 ºC. This is because the deformation el at 50 ºC is very low in each cycle and, as ε_c is calculated in relation to ε_b, a few seconds of t_H produce a notable increment in deformation. At 60 ºC, the

deformation el is higher because the temperature is also higher, however, the absolute deformation added during t_H is not as significant with respect to ε_l.

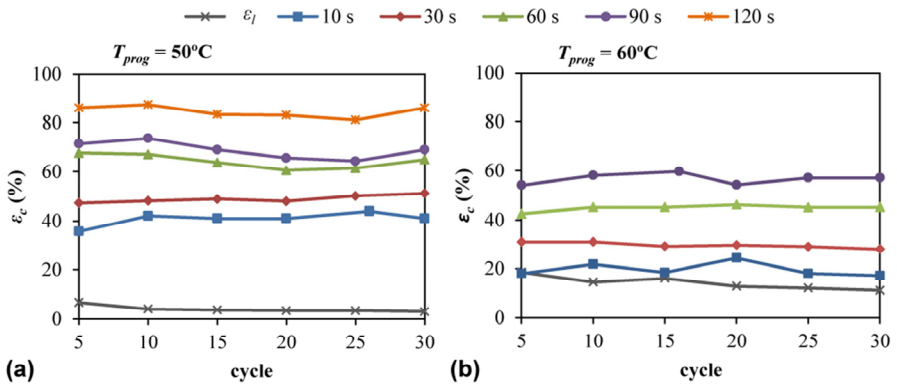

Figure III.4.3 Evolution of deformation added (ε_c) with cycling during the stress-holding time (t_H) at T_{prog} = 50 ºC (a) and T_{prog} = 60 ºC (b).

Figure III.4.4 shows the shape-recovery ratio for both T_{prog} and each stress-holding time applied. With T_{prog} = 50 ºC, the decrease in R_r with cycling is dramatic when t_H is applied. However, this drop in R_r is similar for all t_H. Analyzing the first cycle, when no stress-holding time is applied, R_r shows the highest value, but it is not significantly affected by t_H: with t_H = 10, 30, and 120 s, R_r is around 85% and, with t_H = 60 and 90 s, R_r is around 90%. Nevertheless, when the samples are subjected to successive cycles with or without t_H, the degradation of R_r is marked. Again, when t_H = 0 s, the behavior is considerably better, with an early stabilization (N_e = 18) and less degradation (R_r drops to 70% at N_e). With t_H = 10 and 30 s, stabilization is reached later (N_e = 24 and 27, respectively) and R_r drops significantly (38 and 30% at N_e). It would be expected that longer t_H would result in greater degradation of R_r; however, with t_H = 60 and 90 s, the stable behavior is reached in almost the same cycles as with t_H =10 and 30s (N_e = 25 for 60 sand N_e = 27 for 90 s). Moreover, the drop in R_r

is less pronounced: 44 and 51%, respectively. The behavior observed with t_H = 120 s is almost the same as with 60 s: stabilization is reached at N_e = 25, and R_r is 43% at that point.

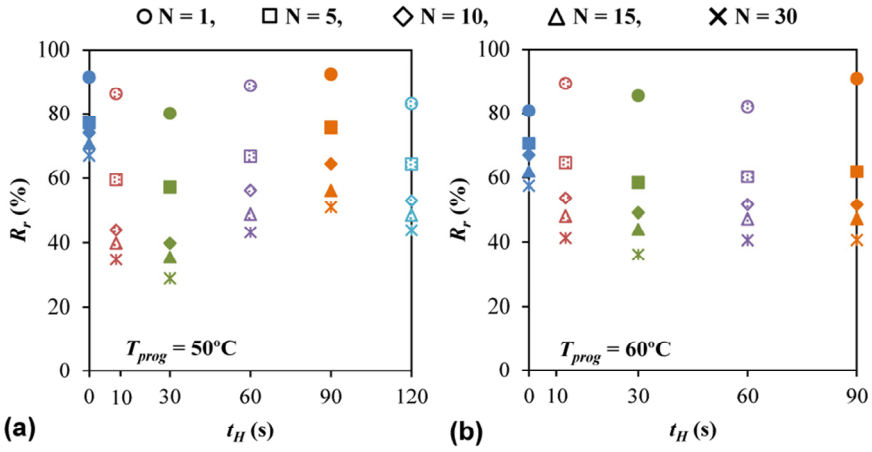

Figure III.4.4 Shape-recovery ratio (R_r) for each stress-holding time (t_H) corresponding to the 1st, 5th, 10th, 15th, and 30th cycle for the experiments performed at 50 °C (a) and 60 °C (b).

These results can be explained as follows. The stress-holding time causes an increase in deformation due to a creep phenomenon. At 50 °C, as $T_{prog} < T_g$, this deformation is predominantly stored as elastic energy; so, t_H does not greatly affect R_r during the first cycle. However, it seems that t_H causes degradation in R_r as the SMP is subjected to successive cycles due to a slippage of the polymer chains. This relative movement between polymer chains causes a reconfiguration of the morphology of the SMP. However, as $T_{prog} < T_g$, the movement of the polymer chains is partially restricted. The fact that there is an increase in R_r during cycling with t_H = 60 and 90 s compared to t_H = 10 and 30 s might be explained by the fact that, from a certain t_H, the polymer chains have enough time to adapt to their new morphology and this results in a better R_r. With t_H = 120 s, R_r decreases compared to t_H = 90 s, probably because with long

t_H, the slippage of the polymer chains predominates over the adaptation to the new morphology.

With T_{prog} = 60 ºC (Figure III.4.4b), R_r also shows a dramatic decrease with cycling when t_H is applied. As in the case of T_{prog} =50 ºC, longer t_H does not cause a greater decrease in R_r but, in this case, the difference between t_H is much less significant. Focusing on the first cycle, without t_H, R_r does not present the highest value (80%) but increases slightly with t_H up to 91% with t_H = 90 s. Despite this initial increase, R_r decreases drastically when the samples are subjected to successive cycles with t_H. Again, this drop is not so marked for t_H = 0 s and the stabilization is reached earlier (N_e = 24 with a R_r = 55%). For higher t_H, R_r exhibits a similar behavior during cycling to the case of T_{prog} = 50 ºC: with t_H = 10 and 30 s, R_r progressively decreases and the stabilization is reached later (N_e = 29 for 10s and N_e = 28 for 30 s), while with t_H = 60 and 90 s, stabilization is reached earlier, (N_e = 24 and 26, respectively). However, there are barely any differences in R_r during cycling no matter what t_H is applied, reaching an average value around 40% at N_e. This similar behavior of R_r with cycling for all t_H at T_{prog} = 60 ºC might be explained by the fact that, at this temperature, the movement of the polymer chains is not restricted ($T_{prog} \sim T_g$) and thus, the ability to adapt to the new morphology is greater.

Comparing the behaviors observed at both temperatures, the lower the T_{prog}, the higher the recovery with t_H = 0s. This result is in agreement with previous study by Cui *et al.* [13]. Stability is also reached earlier with T_{prog} =50 ºC than with T_{prog} = 60 ºC for t_H = 0 s. This could be observed in the values of R_r and N_e with t_H = 0 s. However, it seems that the t_H has a greater influence on R_r for T_{prog} = 50 ºC. When t_H is applied, the values of R_r are very similar or even higher with T_{prog} = 60 ºC than with T_{prog} = 50 ºC and stability is reached in very similar cycles. This could be due to the higher relative deformation added during t_H at 50 ºC (Figure III.4.3). Such additional high relative deformation added causes a greater decrease in R_r,

which in turn causes an increase in the irrecoverable strain that the SMP cannot recover [10].

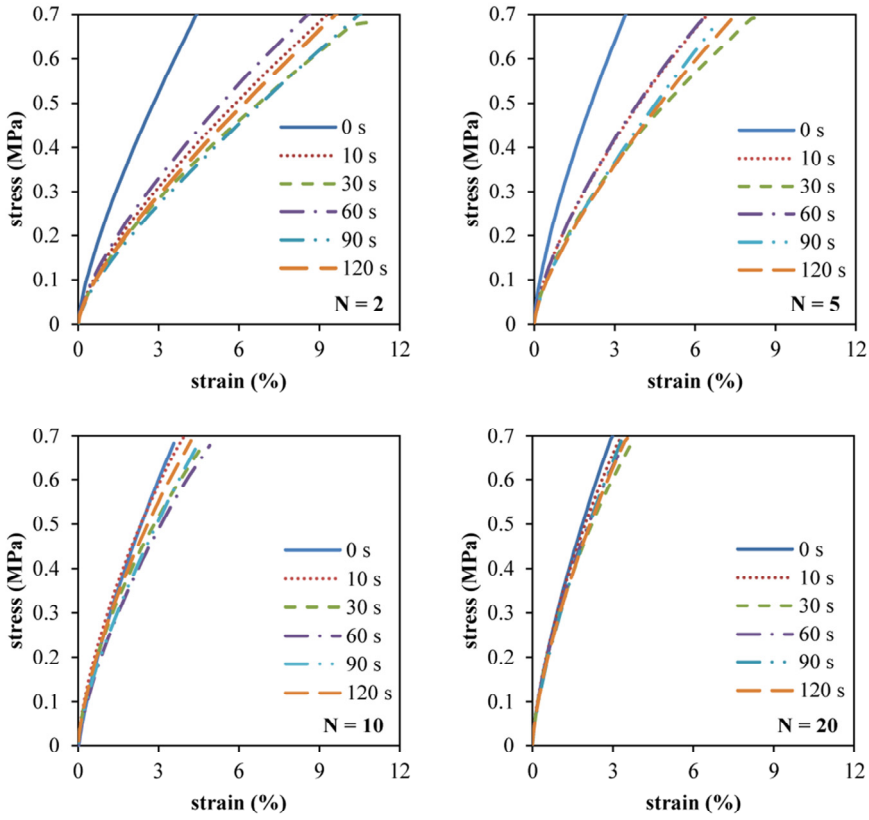

Figure III.4.5 Stretching curves for the 2nd, 5th, 10th, and 20th cycles at T_{prog}.

Another important effect observed with the stress-holding time is a progressive strain hardening of the specimens with cycling. Figure III.4.5 shows the curves of the stretching stage of the experiments performed at 50 ºC. Similar results were found for T_{prog} = 60 ºC; so, those results are not presented. The first cycle is not shown, because it is not representative and it was used to erase the thermal history of the samples. The specimens subjected to t_H show an initial softening as seen in N = 2. This softening may be explained by a slippage of the polymer chains during the stress-holding time, as mentioned above. A progressive

increase in the slope of the curve was found with cycling. This hardening is more pronounced in the experiments subjected to stress-holding conditions, probably caused by the progressive alignment of the polymer chains. It seems that the magnitude of the hardening is the same for each stress-holding time. From $N = 10$ forward, the strain hardening saturates, and no further significant changes occur. This saturation can be observed in the cycle $N = 20$, where the slopes are almost the same as in $N = 10$.

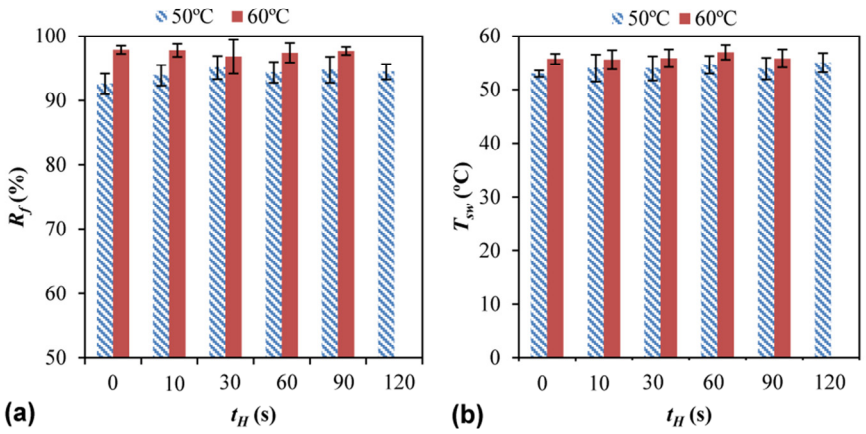

Figure III.4.6 (a) Average value of shape-fixity ratio (R_f) for every stress-holding time (t_H) and both programming temperature (T_{prog}); (b) average value of switching temperature (T_{sw}) for every stress-holding time (t_H) and both programming temperature (T_{prog}).

The variations of the shape-fixity ratio (R_f) and switching temperature (T_{sw}) with t_H were also studied and are presented in Figure III.4.6. Both R_f and T_{sw} show no significant changes with cycling. Therefore, the average values for N cycles of each experiment with different stress-holding times are plotted in Figure III.4.6. Figure III.4.6a shows that the stress-holding time does not affect the fixation of the temporary shape. TFX EG-72D shows better fixation if T_{prog} = 60 ºC rather than T_{prog} = 50 ºC. This might be explained by the fact that the

temporary shape is fixed by rubbery domains of the mixed phase [13] and with $T_{prog} < T_g$ the mixed phase is predominantly in a glassy state.

Figure III.4.6b shows the influence of t_H in the switching temperature. T_{sw} is not affected by either the stress-holding conditions or by cycling, however, T_{sw} is slightly higher at T_{prog} = 60 ºC rather than with T_{prog} = 50 ºC. This difference could be explained by the difference in the glassy-rubbery ratio of the mixed phase when T_{prog} is below or above T_{trans}, as also mentioned by Cui *et al.* [3].

Conclusions

In this paper, shape-memory properties of commercial shape-memory polyurethane (TFX EG-72D) programmed with a prescribed stress and subjected to a certain stress-holding time t_H at a high temperature have been investigated. The effect of t_H on shape recovery and fixity, as well as on the switching temperature, when the SMP is subjected to successive cycles is discussed.

The prescribed stress was held constant during different t_H at two different programming temperatures T_{prog} = 50 and 60 ºC. The maximum deformation of each cycle increased during the t_H due to a creep phenomenon, but the relative deformation added remained virtually unchanged with cycling. This deformation added during t_H is significantly higher with T_{prog} = 50 ºC than with T_{prog} = 60 ºC in relation to the deformation that corresponds to the prescribed stress.

t_H caused considerable degradation of the shape-recovery ratio when successive thermomechanical cycles were performed, even if t_H was just for a few seconds. With T_{prog} = 50 ºC, the degradation was less severe with higher t_H, possibly because the polymer chains were able to adapt to the new morphology created during the creep phenomenon. With T_{prog} = 60 ºC, the higher molecular mobility allowed the SMP to adapt to the new morphology and there were no significant differences in degradation between the t_H applied.

The specimens subjected to t_H also softened considerably during the first cycle, and, with cycling, a progressive strain hardening of the SMP is observed. This hardening was of the same magnitude regardless of the t_H applied.

The shape-fixity ratio and switching temperature were not affected by either the t_H or by successive cycles. However, a higher T_{prog} resulted in higher R_f and T_{sw}.

The study has demonstrated that shape recovery decreases drastically when an SMP is subjected to stress-holding times at high temperature. Moreover, the degradation of the recovery seems to be more accentuated when $T_{prog} < T_g$. Accordingly, in potential applications where an SMP needs to work under a constant stress and over successive cycles, it is imperative to quench the temperature as fast as possible in order to reduce the effect of the stress-holding time and, preferably, to use T_{prog} over the glass transition temperature.

Acknowledgments

The authors would like to thank MINECO (MAT2011-27039C03-01, MAT2011-27039-C03-02) for giving financial support.

References

[1] A. Lendlein and S. Kelch, Shape-Memory Polymers, *Angew. Chem. Int.*, 2002, **41**(12), p 2034–2057

[2] B. Atli, F. Gandhi, G. Karst, Thermomechanical characterization of shape memory polymers, *Proceedings of SPIE - The International Society for Optical Engineering*, San Diego, CA, Vol 6524, 2007

[3] J. Cui, K. Kratz, and A. Lendlein, Adjusting shape-memory properties of amorphous polyether urethanes and radio-opaque composites thereof by variation of physical parameters during programming, *Smart Mater. Struct.*, 2010, **19**(6), p 065019

[4] J.L. Hu, F.L. Ji, and Y.W. Wong, Dependency of the shape memory properties of a polyurethane upon thermomechanical cyclic conditions, *Polym. Int.*, 2005, **54**(3), p 600–605

[5] C. Schmidt, K. Neuking, G. Eggeler, Functional fatigue of shape-memory polymers, *Materials Research Society Symposium Proceedings*, San Francisco, CA, Vol 1190, 2009, p 43–48

[6] A.J.W. McClung, G.P. Tandon, and J.W. Baur, Deformation rate-, hold time-, and cycle-dependent shape-memory performance of Veriflex-E resin, *Mech. Time Depend. Mater.*, 2013, **17**, p 39–52

[7] C. Azra, C.J.G. Plummer, and J. -A.E.Månson, Isothermal recovery rates in shape memory polyurethanes, *Smart Mater. Struct.*, 2011, **20**(8), p 082002

[8] H.J. Tobushi, S. Hayashi, K. Hoshio, and N. Miwa, Influence of strain holding conditions on shape recovery and secondary-shape forming in polyurethane-shape memory polymer, *Smart Mater. Struct.*, 2006, **15**(4), p 1033–1038

[9] A.J.W. McClung, G.P. Tandon, and J.W. Baur, Fatigue cycling of shape memory polymer resin, *Conference Proceedings of the Society for Experimental Mechanics Series*, Vol 3, 2011, p 119–127

[10] C. Schmidt, A.S. Chowdhury, K. Neuking, and G. Eggeler, Studies on the cycling, processing and programming of an industrially applicable shape memory polymer Tecoflex® (or TFX EG 72D), *High Perform. Polym.*, 2011, **23**(300), p 300–307

[11] H. Tobushi, H. Hara, E. Yamada, and S. Hayashi, Thermomechanical properties in a thin film of shape memory polymer of polyurethane series, *Smart Mater. Struct.*, 1996, **5**(4), p 483–491

[12] C. Liu, H. Qin, and P.T. Mather, Review of progress in shape-memory polymers, *J. Mater. Chem.*, 2007, **17**(16), p 1543–1558

[13] J. Cui, K. Kratz, M. Heuchel, B. Hiebl, and A. Lendlein, Mechanically active scaffolds from radio-opaque shape-memory

polymer-based composites, *Polym. Adv. Technol.*, 2011, **22**(1), p 180–189

Chapter IV

Thermosetting Shape-Memory Polymers

IV.1. Introduction

Thermosetting shape-memory polymers are covalently crosslinked materials in which the temporary shape is obtained by deforming the SMP at a high temperature T_{prog} and subsequently fixed by cooling the SMP to a low temperature T_{low}. By reheating above T_{trans}, the polymer chains between crosslinking points acquire mobility and the energy stored during deformation is released to return the SMP to its original or permanent shape [1].

The most common networks of thermosetting SMPs are epoxy-based and acrylate-based shape-memory thermosets. This chapter presents the studies made with examples of both types of networks: hyperbranched-modified epoxy-based shape-memory polymers and acrylate-based bisphenol A-based shape-memory polymers.

IV.1.1. Hyperbranched-modified epoxy-based shape-memory polymers

Usually, shape-memory epoxy polymers are synthesized from epoxy resins modified with aliphatic amines (*i.e.* Jeffamine®). Several research studies on mechanical and shape-memory properties of this kind of networks can be found in the literature. Maximum deformations above 50% and shape-recovery and shape-fixity ratios in the range of 90-100%

have been reported [2-4]. However, these networks are still lagging behind in terms of high stress capacity (that is, high stress at break) and the ability to generate high values of recovery stress.

In this sense, hyperbranched polymers (HBPs) are proposed to be used as crosslinking agents for epoxy-based SMPs. HBPs are a class of dendritic polymers which are promising polymeric modifiers that exhibit higher solubility and lower viscosity than their linear analogues. In addition, the large number of functional groups offers the possibility for further modification and special applications, and the type of end groups determines to a considerable extent the properties such as the glass transition temperature [5].

Previous studies performed before the realization of this thesis on curing kinetics and thermomechanical properties of epoxy resins modified with HBPs, indicated that HBPs could be used as efficient modifiers for epoxy thermosets [6-8]. According to these results, the addition of HBPs in the structure of epoxy shape-memory thermosets can be used to enhance their mechanical and shape-memory properties. It is known that the crosslinking density of shape-memory thermosets plays an important role on exercising driving forces for shape recovery and generation of recovery stress [9,10]. The local concentration of crosslinking points originated by the branched structure of HBPs (Figure IV.1.1) may influence these magnitudes.

As far as this author knows, the only references on hyperbranched-modified SMPs are those reported by Deka *et al.* [11] and Han *et al.* [12]. Deka *et al.* reported a complete characterization on hyperbranched polyurethanes modified with epoxy resins and Han *et al.* reported a preliminary study on shape-memory properties of epoxy resins modified with up to a 10 wt. % of hyperbranched polyester. Both studies reported good mechanical properties and the presence of shape-memory effect. However, the implications of the hyperbranched structure on these properties and a thorough study of the shape-memory effect has yet to be

carried out in order to determine the viability of HBPs as modifiers for epoxy-based SMPs.

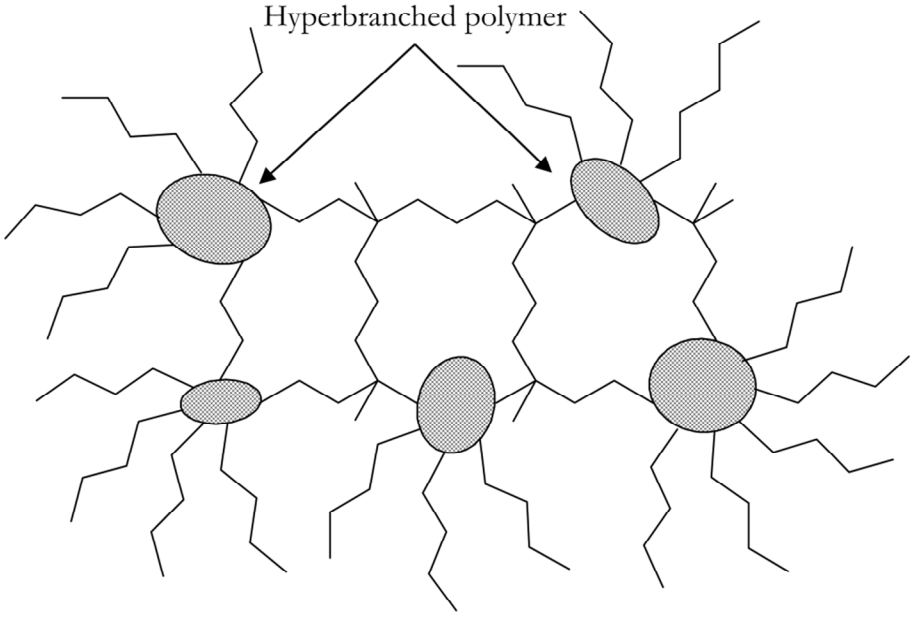

Figure IV.1.1 Schematic representation of the hyperbranched-modified structure of an epoxy SMP.

With this aim, commercial hyperbranched poly(ethyleneimine)s (Lupasol®, BASF) of different molecular weight were used as crosslinking agents for SMPs. Thermal, mechanical and shape-memory properties of epoxy resins modified with HBPs and a commercial polyetheramine (Jeffamine® D400) were studied and the results obtained are presented from Section IV.3 to Section IV.6 in four research articles.

Section IV.3 presents an article published in *Journal of Polymer Science, Part B: Polymer Physics* on 2015 in which thermal, mechanical and shape-memory properties of epoxy-based SMPs modified with low molecular weight commercial hyperbranched poly(ethyleneimine) Lupasol® FG were studied.

The thermomechanical measurements showed that an increase in the HBP content led to more heterogeneous networks with higher crosslinking density and higher glass transition temperatures. The ratio between the glassy modulus and the rubbery modulus, which is an important metric of the shape-memory effect, decreased in accordance with the increase in the crosslinking density.

Tensile testing showed excellent values of stress at break and strain at break at room temperature, rising to 55 MPa and 5% respectively, and specially at the onset of the glass transition temperature. As stated earlier, several studies on shape-memory thermosetting polymers with high maximum deformations can be found in the literature. However the mechanical properties in terms of tensile strength still remain a limitation in epoxy-based shape-memory thermosetting polymers. At the onset of the glass transition temperature, the stress at break increased from 12 MPa to 15 MPa, which represents a significant enhance in stress at break with respect to other epoxy-based SMPs. The deformation at break decreased from 60% to 17% as the HBP content was increased. These results can be explained by the increase in the crosslinking density.

The shape-memory performances showed high shape-recovery and shape-fixity ratios, around 96% and 97% respectively and high values of shape-recovery velocity rising to 22 %/min. In classical epoxy-based SMPs that is, modified with aliphatic or aromatic diamines or with epoxies with improved chain mobility, the crosslinking density and thus the rubbery modulus governs the shape recovery. However, the results proved that the network structure is also a key factor for shape-memory properties. The shape-recovery and shape-fixity ratios and the shape-recovery velocity slightly decreased when the HBP content was increased because it restricted chain-conformational changes during deformation and molecular dynamics.

All formulations studied showed high values of shape recovery and shape fixity over a broad range of transition temperatures. Despite these

good results, the HBP content should be controlled because of its effect on network homogeneity.

Given the good results obtained with the low molecular weight HBP Lupasol® FG, Section IV.4 presents a comparison between epoxy-based SMPs modified with Lupasol® FG (800 g/mol) and one of its higher molecular weight counterpart Lupasol® PR8515 (2000 g/mol). This study was published in the journal *Shape Memory and Superelasticity* on 2016.

As mentioned before, an increase in HBP content leads to more heterogeneous networks with higher glass transition temperatures. However, formulations modified with the high molecular weight Lupasol® PR8515 (which implies higher length of the branches) showed lower glass transition temperatures and wider transitions than formulations modified with Lupasol® FG.

Tensile tests at room temperature and at the onset of the glass transition temperatures showed slightly lower values of stress at break and strain at break in formulations modified with Lupasol® PR8515. The higher crosslinking density and the presence of possible molecular interactions in these formulations can explain these results.

As in the case of tensile strength, the shape-memory properties of formulations modified with Lupasol® PR8515 showed slightly lower values than in formulations modified with Lupasol® FG. As stated before, network structure is a key factor for shape-memory properties. The higher heterogeneity of formulations with Lupasol® PR8515 caused higher restriction on chain-conformational changes and molecular dynamics than formulations modified with Lupasol® FG.

While materials modified with low molecular weight Lupasol® showed slightly better mechanical and shape-memory properties, materials modified with high molecular weight Lupasol® had lower glass transition temperatures.

The results presented in Section III and Section IV note that HBPs are excellent modifiers for epoxy-based SMPs. The good mechanical properties of these materials point them as good candidates for applications that require high mechanical solicitations, such as thermomechanical actuators. However, SMPs probably will not operate under free conditions in these applications that is, SMPs will operate with a constraining stress or strain. Section IV.5 presents a study on constrained recoveries in hyperbranched-modified SMPs and the generation of recovery stress and mechanical work published in *Journal of Polymer Science, Part B: Polymer Physics* on 2016.

Partially and fully constrained recoveries were carried out in this study in order to quantify the recovery stress and work output generated by epoxy-based SMPs modified with Lupasol® FG. The recovery stress generated during fully constrained recovery increased as the maximum stress applied during programming was increased due to the higher chain orientation of the temporary shape, which resulted in a higher entropy gain during the recovery stage. Although a number of studies have reported that the crosslinking density and rubbery modulus is the most important factor in the recovery stress generation, a compromise between crosslinking density and network homogeneity should to be reached in order to guarantee sufficient driving recovery forces and to allow molecular mobility. In this way, exceptional values of recovery stress up to 7 MPa were achieved in formulations that fulfil these requirements.

The shape recovery decreased significantly when a constraining stress was applied. This decrease was more acute in formulations with a higher HBP content due to their lower molecular mobility. The work output showed a maximum when the constraining stress was around a 40% of the maximum programming stress. The descent of shape recovery shifted the maximum work generated toward lower constraining levels and decreased the efficiency of the process that is, the ratio of work output to work required to program the sample. Regarding the

mechanical work generation, the molecular mobility is probably the most important factor. The formulations with the highest molecular mobility showed remarkably high values of work output density of more than 750 kJ/m^3.

The molecular morphology of SMPs that are intended for use as thermomechanical actuators must be thoroughly studied to ensure both high recovery forces and sufficient molecular mobility.

Finally, Section IV.6 presents a wide characterization of the mechanical properties of hyperbranched-modified SMPs. Usually, research studies on SMPs focus on the shape-memory effect of novel materials or on the relationship between network structure and shape-memory properties. However, minus work has been published on mechanical properties of SMPs. The aim of this study is to provide a characterization of the mechanical properties using less conventional techniques in the study of SMPs that could be relevant for the design of applications. Shape-memory properties evaluated at less favourable programming temperatures than the onset of glass transition temperature were also evaluated. This study has been submitted in *Journal of Polymer Science* on 2016 and is currently under review.

Mechanical properties are greatly depending on the testing temperature. Well into the glassy regime, the stress at break and strain at break increased as the HBP content was increased. The higher presence of hydroxyl groups in formulations with a higher HBP content and the hyperbranched structure itself contributed to this behaviour. Well into the rubbery regime, both the stress at break and strain at break decreased as the HBP content was increased. The increasing crosslinking density of formulations with a higher HBP content and the disperse nature of the hyperbranched structure restricted molecular mobility resulting in lower values of failure strain and caused a reduction in the stress capability of these materials.

At the onset of the glass transition temperature, the stress at break increased and the strain at break decreased as the HBP content was increased. This temperature coincides with the beginning of mechanical relaxation and the effect of the crosslinking density was different to that shown well above or below the glass transition temperature. An increase in the crosslinking density resulted in a less mobile and ductile network, leading in the macroscopic scale to a lower failure strain and a higher stress at break. A peak in deformability and stored energy density was observed when testing at this temperature. Thus, in terms of limit values for programming the temporary shape, the onset of the glass transition temperature seems to be a desirable programming temperature.

The Young's modulus values revealed more rigid structures in formulations with a higher HBP content and hardness testing showed higher values in formulations with a higher DGEBA and HBP content due to increased crosslinking density and the less presence of the plasticizing effect of the polyetheramine flexible structure. In the case of impact testing, increasing the polyetheramine content caused an increase in impact strength due to the high energy dissipation upon impact provided by its long aliphatic flexible structure. The analysis of the surface fracture by SEM microscopy confirmed the higher rigid structure of formulations with a higher HBP content.

It is possible that in real applications the programming temperature cannot be adjusted at the onset of the glass transition temperature. Therefore, the implications of using other programming temperatures on shape-memory properties should be studied. Increasing the programming temperature had minor effect on shape-memory properties of formulations with low HBP content but the effect on formulations with a higher HBP content was significant. Increasing the programming temperature from the onset of the glass transition temperature to T_g + 15 caused a significant drop in shape-memory properties of these

formulations caused by restricted chain-conformational changes and low driving recovery forces.

The results obtained in this study point that these materials are available for their operation under high mechanically demanding conditions while still showing good shape-memory properties.

IV.1.2. Acrylate-based shape-memory polymers

Acrylate-based shape-memory polymers represent an important class of SMPs. Usually acrylate-based SMPs are formed through free radical polymerization of a multifunctional monomer as crosslinking agent and monofunctional monomers as chain builders (Figure IV.1.2) [13].

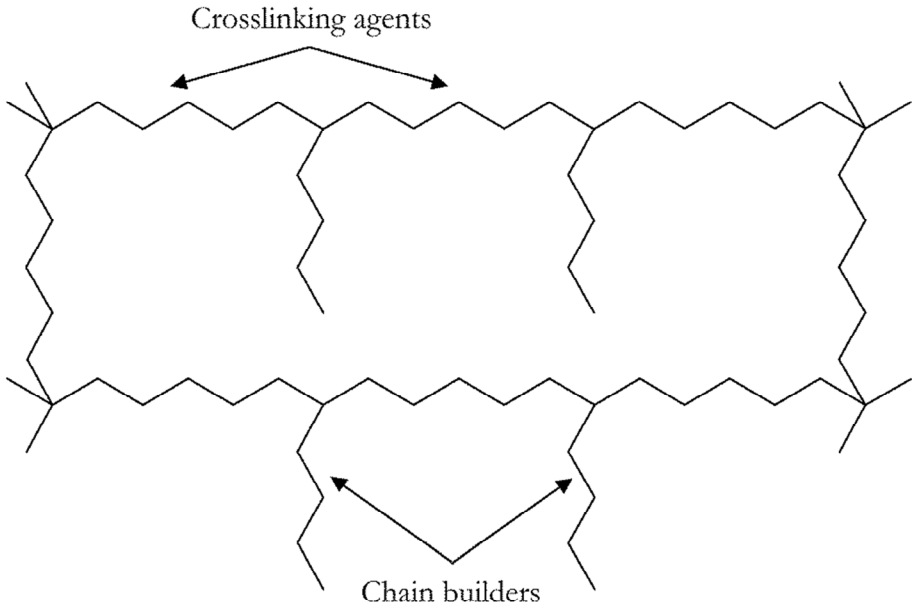

Figure IV.1.2 Schematic representation of the formation of an acrylate-based SMP.

The design of emerging SMPs-based medical devices has raised the interest in acrylate-based SMPs due to their high degree of

biocompatibility. Consequently, several research studies on the characterization of acrylate-based SMPs for biomedical applications can be found in the literature, including the study of the mechanical properties under physiological conditions, the long term storage or the generation of recovery stress [14-16].

Besides the high degree of biocompatibility, this class of SMPs presents some advantages derived from the UV-curing in front of thermally cured SMPs [17].

Usually, research studies on acrylate-based shape-memory networks use poly(ethylene glycol)-based monomers as crosslinking agents. The shape-memory properties of these materials are excellent, with high shape-recovery and shape-fixity ratios and high values of recovery stress and mechanical work. However, other multifunctional monomers should be explored, such as bisphenol A-based monomers, for more mechanically demanding applications. By substituting typical poly(ethylene glycol)-based crosslinking agents by bisphenol A-based monomers it is expected higher glass transition temperatures as well as an increase in the mechanical properties due to the presence of aromatic rings in the structure.

According to this discussion, the aim of this study is to take advantage of the UV-curing with respect to classic thermal curing that is, faster polymerization rates, lower energy consumption and the use of solvent-free formulations; and to study the enhanced mechanical and shape-memory properties of acrylate-based SMPs synthesized from bisphenol A-based crosslinking agents.

Section IV.7 presents a research study on acrylate-based SMPs using two different bisphenol A-based crosslinking agents (diglycidyl ether of bisphenol A diacrylate and diglycidyl ether of bisphenol A ethoxylate diacrylate) and different monofunctional monomers as chain builders, including methyl methacrylate, ethyl methacrylate and

poly(ethylene glycol) methylether methacrylate. This study was published in the journal *Macromolecules Chemistry and Physics* on 2016.

The thermomechanical measurements revealed more heterogeneous networks and lower glass transition temperatures in formulations with a higher poly(ethylene glycol) methylether methacrylate content and a lower methyl methacrylate and ethyl methacrylate content. Formulations with diglycidyl ether of bisphenol A ethoxylate diacrylate showed lower glass transition temperatures and more homogeneous networks than formulations with diglycidyl ether of bisphenol A diacrylate.

Mechanical properties at room temperature showed two different behaviours depending on the crosslinking agent used. Formulations with diglycidyl ether of bisphenol A ethoxylate diacrylate showed a large plateau of plastic deformation while formulations with diglycidyl ether of bisphenol A diacrylate barely showed plastic deformation. At the onset of the glass transition temperature, all formulations showed stress at break values higher than 10 MPa. Formulations with diglycidyl ether of bisphenol A ethoxylate diacrylate showed higher failure strains than formulations with diglycidyl ether of bisphenol A ethoxylate diacrylate due to the presence of mobile oxyethylene units and hydrogen-bond interactions.

Shape-memory properties showed shape-recovery and shape-fixity ratios of around 95% and 97% respectively and very fast shape-recovery velocities in transient temperature conditions (up to 24 %/min) and very short recovery times in isothermal conditions (up to 1.5 s).

The results of this study pointed that acrylate-based SMPs synthesized from bisphenol A-based crosslinking agents are promising shape-memory materials that combine excellent mechanical and shape-memory properties.

IV.2. References

[1] D. Santiago, X. Fernández-Francos, F. Ferrando, S. De la Flor, *Shape-memory effect in hyperbranched poly(ethyleneimine)-modified epoxy thermosets,* J. Polym. Sci. Part B Polym. Phys. **2015**, *53*, 924–933.

[2] A. B. Leonardi, L. A. Fasce, I. A. Zucchi, C. E. Hoppe, E. R. Soulé, C. J. Pérez, R. J. J. Williams, *Shape memory epoxies based on networks with chemical and physical crosslinks*, Eur. Polym. J. **2011**, *47*, 362-369.

[3] D. M. Feldkamp, I. A. Rousseau, *Effect of Chemical Composition on the Deformability of Shape-Memory Epoxies*, Macromol. Mater. Eng. **2011**, *296*, 1128-1141.

[4] M. Fan, H. Yu, X. Li, J. Cheng, J. Zhang, *Thermomechanical and shape-memory properties of epoxy-based shape-memory polymer using diglycidyl ether of ethoxylated bisphenol-A*, Smart Mater. Struct. **2013**, *22*, 055034.

[5] B. Voit, *New developments in hyperbranched polymers*, J. Polym. Sci., Part A: Polym. Chem. **2000**, *38*, 2505–2525.

[6] D. Santiago, M. Morell, X. Fernández-Francos, A. Serra, J.M. Salla, X. Ramis, *Influence of the end groups of hyperbranched poly(glycidol) on the cationic curing and morphology of diglycidylether of bisfenol A thermosets*, React Funct Polym. **2011**, *71*, 380-389.

[7] D. Santiago, X. Fernández-Francos, X. Ramis, J. M. Salla, M. Sangermano, *Comparative curing kinetics and thermal-mechanical properties of DGEBA thermosets cured with a hyperbranched poly(ethyleneimine) and an aliphatic triamine*, Thermochim. Acta. **2011**, *526*, 9–21.

[8] X. Fernández-Francos, D. Santiago, F. Ferrando, X. Ramis, J.M. Salla, A. Serra, M. Sangermano, *Network structure and thermomechanical properties of hybrid DGEBA networks cured with 1-methylimidazole and hyperbranched poly(ethyleneimine)s*, J. Polym. Sci., Part B: Polym. Phys. **2012**, *50*, 1489-1503.

[9] C. M. Yakacki, R. Shandas, D. Safranski, A. M. Ortega, K. Sassaman, K. Gall, *Strong, tailored, biocompatible shape-memory polymer networks*, Adv. Funct. Mater. **2008**, *18*, 2428-2435.

[10] A. M. Ortega, S. E. Kasprzak, C. M. Yakacki, J. Diani, A. R. Greenberg, K. Gall, *Structure-property relationships in photopolymerizable polymer networks: Effect of composition on the crosslinked structure and resulting thermomechanical properties of a (meth)acrylate-based system*, J. Appl. Polym. Sci. **2008**, *110*, 1559-1572.

[11] H. Deka, N. Karak, *Shape-memory property and characterization of epoxy resin-modified Mesua ferrea L. seed oil-based hyperbranched polyurethane*, J. Appl. Polym. Sci. **2010**, *116*, 106-115.

[12] C. Han, Y. Liu, H. Tan, *Preparation and investigation on properties of shape memory epoxy modified by hyperbranched polyester*, Adv. Mater. Res. **2011**, *335-336*, 851-855.

[13] D. L. Safranski, K. Gall, *Effect of chemical structure and crosslinking density on the thermo-mechanical properties and toughness of (meth)acrylate shape memory polymer networks*, Polymer **2008**, *49*, 4446-4455.

[14] C. M. Yakacki, R. Shandas, C. Lanning, B. Rech, A. Eckstein, K. Gall, *Unconstrained recovery characterization of shape-memory polymer networks for cardiovascular applications*, Biomaterials **2007**, *28*, 2255-2263.

[15] K. Gall, C. M. Yakacki, Y. Liu, R. Shandas, N. Willet, K. S. Anseth, *Thermomechanics of the shape memory effect in polymers for biomedical applications*, J. Biomed. Mater. Res., Part A **2005**, *73*, 339-348.

[16] K. E. Smith, S. S. Parks, M. A. Hyjek, S. E. Downey, K. Gall, *The effect of the glass transition temperature on the toughness of photopolymerizable (meth)acrylate networks under physiological conditions*, Polymer **2009**, *50*, 5112-51223.

[17] M. Sangermano, N. Razza, J. V. Crivello, *Cationic UV-curing: Technology and applications*, Macromol. Mater. Eng. **2014**, *299*, 775-793.

UNIVERSITAT ROVIRA I VIRGILI
EXPERIMENTAL CHARACTERIZATION OF SHAPE-MEMORY POLYMERS: INFLUENCE OF PROCESSING METHODS AND CHEMICAL STRUCTURE
David Manuel Santiago Abraira

IV.3. Shape-Memory Effect in Hyperbranched Poly(ethyleneimine)-Modified Epoxy Thermosets

David Santiago, Xavier Fernández-Francos, Francesc Ferrando, Silvia De la Flor

Journal of Polymer Science, Part B: Polymer Physics ***2015****, 53, 924-933*

UNIVERSITAT ROVIRA I VIRGILI
EXPERIMENTAL CHARACTERIZATION OF SHAPE-MEMORY POLYMERS: INFLUENCE OF PROCESSING METHODS AND CHEMICAL STRUCTURE
David Manuel Santiago Abraira

J. Polym. Sci. Part B: Polym. Phys. 2015, 53, 924-933

Shape-Memory Effect in Hyperbranched Poly(ethyleneimine)-Modified Epoxy Thermosets

David Santiago[1], Xavier Fernández-Francos[2], Francesc Ferrando[1], Silvia De la Flor[1]

[1]Department of Mechanical Engineering, Universitat Rovira i Virgili, Av. Països Catalans 26, 43007 Tarragona, Spain

[2]Centre Tecnolòogic de la Química de Catalunya, C/Marcel·lí Domingo s/n, 43007 Tarragona, Spain

Abstract

A series of shape-memory epoxy thermosets were synthesized by crosslinking diglycidyl ether of bisphenol A with mixtures of commercially available hyperbranched poly(ethyleneimine) and polyetheramine. Thermal, mechanical and shape-memory properties were studied and the effect on them of the content and structure of the hyperbranched polymer was discussed. Measurements showed that the glass transition temperature can be tailored from 60 ºC to 117 ºC depending on the hyperbranched polymer content, and all formulations showed an appropriate glassy/rubbery storage modulus ratio. Shape-memory programming was carried out at $T_g^{E'}$ given the excellent mechanical properties of the materials, with maximum stress and failure strain up to 15 MPa and 60%, respectively. The resulting shape-memory behavior was excellent, with maximum shape recovery and shape fixity of 98% as well as a fast shape-recovery rate of 22 %/min. The results show that hyperbranched poly(ethyleneimine) as a crosslinking agent can be used to enhance mechanical and shape-memory properties with different effects depending on the crosslinking density.

Keywords: *crosslinking; hyperbranched; mechanical properties; shape memory; smart polymers*

1. Introduction

Shape-memory polymers (SMPs) are materials that are capable of changing shape when an external stimulus is applied. They can be deformed and fixed in a temporary shape which is stable until such stimulus is applied [1]. This shape-changing is called the shape-memory effect (SME) and is usually heat-triggered, although it can also be induced by an electrical current, magnetic field or light [1]. These smart materials have attracted a lot of interest in recent years due to their wide range of applications, which include self-deployable structures for aerospace applications [2], smart fibers and fabrics for clothing [3], temperature sensors [4], electronic devices [5], or applications for use in biomedicine [6,7]. Other promising applications of SMPs are information carriers such as quick response code carriers (QR codes) [8,9], bidirectional actuators [10-12] or self-folding structures [13].

SMPs are usually classified according to their chemical nature (thermoplastic or thermosets) and transition temperature (glass or melting transition temperature). The most common SMPs are usually thermoplastics due to their high ductility and easy processing, making them suitable for a wide variety of potential applications. However, in recent years a number of studies have reported shape-memory epoxy-based thermosets with excellent shape-memory properties enabling the use of SMPs in more mechanically demanding applications [14-16].

Epoxy resins are widely used in many applications (coatings, adhesives, or matrix in composites) because of their chemical resistance, thermal stability and good mechanical properties [16]. In a shape-memory epoxy polymer the original or permanent shape is acquired during the curing process due to the formation of a network with permanent, covalent crosslinks. The temporary shape is obtained by deforming the material at a temperature above transition temperature and subsequently cooling it to a temperature below transition temperature. By reheating to above transition temperature, the polymer chains between crosslinking

points acquire more mobility and the energy stored during deformation is released. Thus the shape-memory epoxy polymer recovers its permanent shape.

However, the brittle behavior and low elongation at break of epoxy resins greatly limit their use as shape-memory materials. Many studies have focused on overcoming this limitation by choosing suitable shape-memory thermal programs and especially through material design. Feldkamp and Rousseau [17] studied the effect of the deformation temperature on the ultimate failure strain and found that the maximum deformation could be greatly enhanced by simply deforming the SMP at the onset of the glass transition temperature. Regarding material design, incorporating a rubbery domain within the epoxy matrix enhances the mobility of segments between crosslinking points and improves the ultimate failure strain. The most common crosslinking agents used to achieve this effect are aliphatic or aromatic amines, which increase the elongation at break while maintaining relatively elevated glass transition temperatures. Feldkamp and Rousseau [18] also studied the effect of chemical composition on the deformability of shape-memory epoxies cured with different mono-and diamines. Leonardi *et al.* [19] designed an epoxy network modified with n-dodecylamine and m-xylylenediamine that combined chemical and physical crosslinks and resulted in great deformations and recovery stresses.

In addition to epoxy-amine networks, there are other epoxy-based shape-memory polymer networks to be found in the literature. Biju and Nair [20] reported the synthesis of a shape-memory epoxy network based on a diglycidyl ether of bisphenol A (DGEBA) cured with a pyromellitic dianhydride for possible use in smart actuator systems. Rajendran *et al.* [21] synthesized an epoxy-cyanate system by coreacting a DGEBA, cyanate ester and phenol telechelic poly(tetramethylene oxide) and studied the correlation between the viscoelastic and shape-memory properties. Wei e*t al.* [22] presented a new shape memory hydro-epoxy

system made from hydro-epoxy resin, poly(propylene glycol) diclycidyl ether (PPGDGE), and menthane diamine and studied the relationships between the thermomechanical properties and structural changes in the network.

Another way to obtain a more flexible network is by introducing aliphatic diepoxides, which improve chain mobility despite the increases in crosslinking density. Xie and Rousseau [23] described a tailoring of glass transition temperature by modifying a DGEBA epoxy resin with Jeffamine® and decylamine as crosslinking agents, and by replacing DGEBA with neopentyl glycol glycidyl ether epoxy resin. Jing *et al.* [24] improved the toughness of a shape-memory epoxy resin by using PPGDGE as a toughening agent and triethylenetetramine as a curing agent.

Although the toughness of epoxies is greatly improved in these kinds of networks, achieving very high maximum strains [19,24-26], the mechanical properties in terms of tensile strength may remain a limitation for more mechanically demanding shape-memory applications such as mechanical actuators. Therefore, new structures need to be explored that combine high values of tensile strength and maximum deformation above room temperature with adequate storage modulus ratio and glass transition temperature values.

To this end, the use of hyperbranched polymers as crosslinking agents for epoxy-based SMPs is proposed in this study. Hyperbranched polymers (HBPs) are a class of dendritic polymers that are promising polymeric modifiers because of their densely branched structure, which makes them less viscous than their linear counterparts of the same molecular weight. They have a high concentration of surface reactive groups that can be modified to tune their physical/chemical compatibility to a variety of matrices and substrates [27]. Hence they have been reported to be excellent epoxy modifiers [28,29].

The only previous study on shape-memory epoxy resins modified with a hyperbranched polymer is the one by Han *et al.* [30]. They reported that the presence of hyperbranched polyester enhanced the mechanical properties (impact strength, elongation at break, and tensile strength) with respect to the neat formulation, but the shape-memory properties were only evaluated by manual bending performance. Therefore, any implications that the presence of the HBP may have for the thermomechanical and viscoelastic properties of the SMP still need to be understood. In addition, the impact on shape-memory properties of the local concentration of crosslinking points, contributed by the heterogeneous structure of the HBP, should be studied if HBPs are going to be used as toughening agents for shape-memory epoxies.

In this article, a family of materials with shape-memory properties is synthetized using an epoxy resin modified with a commercial hyperbranched poly(ethyleneimine) and an aliphatic polyetheramine as crosslinking agents with different weight fractions of each reactant. The kinetics and network structure of epoxy formulations containing hyperbranched poly(ethyleneimine)s have been studied recently [31,32]. The effect of HBP structure and content on thermal, mechanical, and shape-memory properties is experimentally analyzed and discussed in detail. This study is carried out with the aim of processing tailored SMP by varying the content of HBP in the epoxy matrix, adjusting the transition temperature of the material and obtaining enhanced tensile strength and ultimate failure strain that could lead to excellent final shape-memory properties.

2. Experimental

2.1 Materials

DGEBA (Araldite GY 240; Huntsman) with a weight per epoxy equivalent of 182 g/mol was used as the base epoxy resin (Figure IV.3.1a). A commercial hyperbranched poly(ethyleneimine) (Lupasol®

FG, BASF) with M_w = 800 g/mol and a ratio of primary:secondary:tertiary amines of 1:0.82:0.53 (Figure IV.3.1c) and an aliphatic diamine (Jeffamine® D400; Huntsman) with M_w = 430 g/mol (Figure IV.3.1b) were used as crosslinking agents.

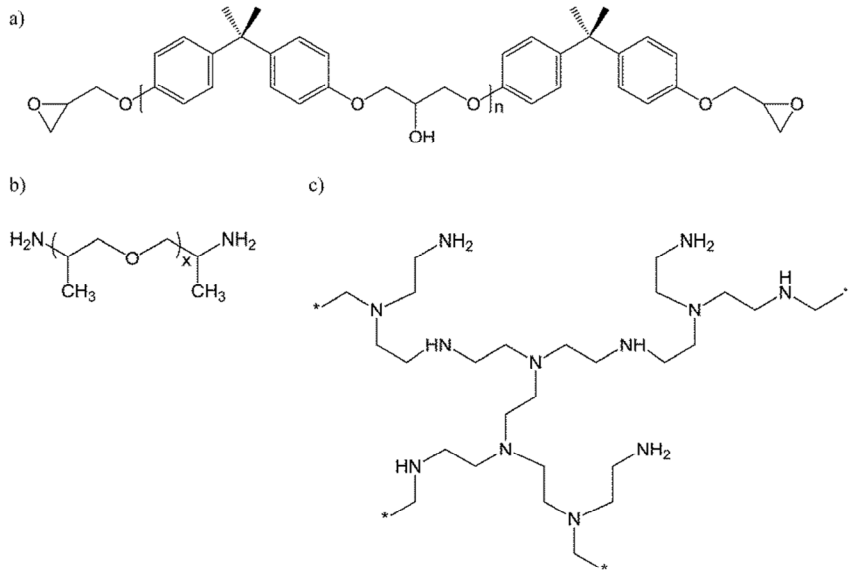

Figure IV.3.1 (a) Chemical structure of DGEBA (n = 0.08); (b) chemical structure of Jeffamine® D400 ($x \approx 6.1$); (c) chemical structure of Lupasol® FG.

Various formulations with different contents of DGEBA, Jeffamine® D400 (D400), and Lupasol FG (LP800) were prepared (Table IV.3.1). The proportions of reactants in each formulation were selected to obtain a molecular structure formed by stoichiometric DGEBA-D400 and DGEBA-LP800 networks. The sample nomenclature XD400-YLP used in Table IV.3.1 indicates the weight fraction of stoichiometric DGEBA-D400 (X) and DGEBA-LP800 (Y) networks.

The components were mixed manually in a glass vial and then poured into an open mold covered with Teflon to avoid the presence of bubbles and facilitate sample release. The samples were cured for 2 h at 120 ºC in an oven and then slowly cooled to room temperature. This

curing time was optimized on the basis of differential scanning calorimetry, by determining the time necessary to ensure the complete disappearance of any exothermic peak related to residual crosslinking reactions. The samples were then polished with sandpaper to obtain uniform final dimensions.

Table IV.3.1 Composition of the formulations studied

Sample	wt. % DGEBA	wt. % D400	wt. % LP800	D400:LP800 Amine Ratio[a]	ν_c (mol/g)
90D400-10LP	63.5	34.8	1.7	4.010	0.001915
80D400-20LP	65.7	31.0	3.3	1.782	0.002127
70D400-30LP	67.9	27.1	5.0	1.040	0.002339
60D400-40LP	70.2	23.2	6.6	0.668	0.002551
50D400-50LP	72.4	19.4	8.3	0.446	0.002763
40D400-60LP	74.6	15.5	9.9	0.297	0.002975
30D400-70LP	76.8	11.6	11.6	0.191	0.003187

ν_c is the crosslinking density calculated assuming that all amine groups turn into crosslinks.

[a] Total primary, secondary, and tertiary amine groups present in the crosslinking agent.

2.2 Thermomechanical Characterization

The thermomechanical properties were measured using a DMA Q800 (TA Instruments) equipped with a 3-point bending clamp. Prismatic rectangular samples of about 30 x mm 5.5 x mm 2.5 mm were analyzed at 1 Hz, 0.1% strain and a heating rate of 3 ºC/min. The glass transition temperature was determined from the peak in tan δ. The values of storage modulus *E'* below and above glass transition were evaluated. The onset of glass transition temperature $T_g^{E'}$ was determined as the onset in the storage modulus decrease during mechanical relaxation, as seen in Figure IV.3.2a.

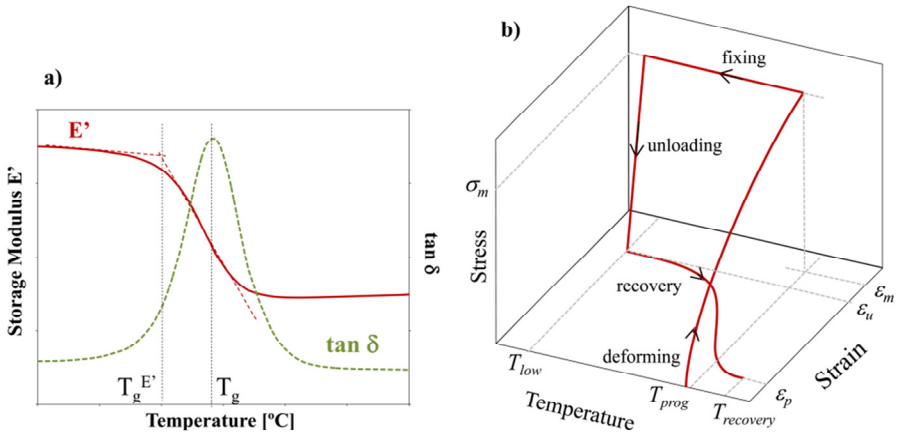

Figure IV.3.2 (a) Determination of temperatures T_g and $T_g^{E'}$ from the results obtained with DMA analysis; (b) scheme of the thermomechanical programming.

2.3 Mechanical Characterization

The mechanical properties at room temperature were evaluated using an electromechanical universal testing machine (Zwick 1445) with specially designed grips. The size of the specimens was adapted from ASTMD638 requirements, adopting a Type IV dog-bone shape. The experiments were performed at a crosshead speed of 1 mm/min.

The mechanical properties at $T_g^{E'}$ were measured using a DMA Q800 equipped with a film-tension clamp in force controlled mode. Prismatic rectangular samples of about 20 x mm 2.5 x mm 0.5 mm were analyzed at $T_g^{E'}$ at a force rate of 1 N/min. In both experiments, strain was calculated as the total elongation (displacement of the cross-head) with respect to the initial length (Equation IV.3.1).

$$\varepsilon(\%) = \frac{L_f - L_0}{L_0} \qquad \text{(IV.3.1)}$$

2.4 Shape-Memory Quantification

The shape-memory properties were measured using a DMA Q800 with a force-controlled mode and equipped with a film-tension clamp. Prismatic rectangular samples of about 20 x mm 2.5 x mm 0.5 mm were used in shape-memory performances. The method for creating a temporary shape and triggering the shape-memory effect is a thermomechanical procedure called programming (Figure IV.3.2b). This programming consists of various steps. First the sample is heated to programming temperature T_{prog} and deformed to a prescribed value of maximum stress σ_m at 1 MPa/min. In this stage the deformation of the sample is ε_m. Once the sample has been stretched, the next step is to cool it to below transition temperature T_{low} (30 ºC) in order to fix the temporary shape. After fixation the stress is released at the same stress rate of 1 MPa/min. Once the sample is unloaded, the deformation of the sample is ε_u. The shape-memory effect is triggered by heating the sample to a temperature above the transition temperature. The heating rate during shape recovery was 3 ºC/min and the final recovery temperature $T_{recovery}$ was T_g + 10 ºC to ensure complete recovery. The amount of non-recoverable deformation at the end of programming is ε_p.

Every sample was stretched to a determined value of stress corresponding to 75% of the stress at break ($\sigma_m = 0.75\sigma_b$) in order to perform a comparative study with the same level of load for each sample.

The programming temperature was chosen as the onset of the glass transition temperature $T_g^{E'}$ of each sample (Figure IV.3.2a). According to Yakacki *et al.* [33], a peak in the deformability of shape-memory acrylate-based polymer can be obtained at a temperature coinciding with the onset of glass transition temperature. Feldkamp and Rousseau [17] demonstrate that this phenomenon is also present in epoxy-based systems.

The most significant parameters for quantifying shape-memory properties are the shape-recovery ratio (R_r) and the shape-fixity ratio (R_f). The shape-recovery ratio (Equation IV.3.2) quantifies the ability of the

SMP to recover its original shape and was calculated as the total deformation recovered with respect to the maximum deformation reached during the programming.

$$R_r(\%) = \frac{\varepsilon_m - \varepsilon_p}{\varepsilon_m} \cdot 100 \qquad \text{(IV.3.2)}$$

The shape-fixity ratio, calculated from Equation IV.3.3, quantifies the ability of the SMP to fix the temporary shape. It was computed as the deformation after the stress was released with respect to the maximum deformation.

$$R_f(\%) = \frac{\varepsilon_u}{\varepsilon_m} \cdot 100 \qquad \text{(IV.3.3)}$$

Another parameter of interest in evaluating shape-memory ability is the shape-recovery rate (V_r). This quantifies the velocity at which the permanent shape is recovered. V_r was calculated in two different ways: the first (Equation IV.3.4), was calculated as the time interval between 15% and 85% of strain recovered, while the second, presented in Equation IV.3.5, was calculated as the temperature range between deformation recovered from 15% to 85%:

$$V_r(\%/\text{min}) = \frac{\left(\frac{\varepsilon_{rec,15\%} - \varepsilon_{rec,85\%}}{\varepsilon_{rec,15\%}}\right) \cdot 100}{\Delta t_{15\%-85\%}} \qquad \text{(IV.3.4)}$$

$$V_r(^{\circ}\text{C}/\text{min}) = \frac{\left(\frac{\varepsilon_{rec,15\%} - \varepsilon_{rec,85\%}}{\varepsilon_{rec,15\%}}\right) \cdot 100}{\Delta T_{15\%-85\%}} \qquad \text{(IV.3.5)}$$

where $\varepsilon_{rec,15\%}$ is the deformation corresponding to a shape recovery of 15%, $\varepsilon_{rec,85\%}$ is the deformation corresponding to a shape recovery of 85%, and $\Delta t_{15\%-85\%}$ and $\Delta T_{15\%-85\%}$ are the time interval and temperature range

between these two points. The difference between deformations corresponding to a shape recovery of 15% and 85%, $\varepsilon_{rec,15\%} - \varepsilon_{rec,85\%}$, was calculated with respect to $\varepsilon_{rec,15\%}$ in order to avoid the influence of the maximum deformation on V_r.

3. Results and Discussion

3.1 Thermomechanical Properties

The thermomechanical properties of the formulations synthesized are summarized in Table IV.3.2. As expected, it can be seen that the glass transition temperature of these materials can be controlled by varying the chemical composition of the formulation. T_g shows values ranging from 60 ºC to 117 ºC as the LP800 content increases. A T_g of 138 ºC was reported for the neat DGEBA-LP800 network [32]. Thus these epoxy thermosets can be used in applications requiring a broad range of transition temperatures.

Table IV.3.2 Thermomechanical data obtained by DMA: glass transition temperature (T_g), onset temperature of the glass transition temperature (T_g^E), storage modulus at glassy, and rubbery regions (E'_g and E'_r, respectively)

Sample	T_g (ºC)[a]	$T_g^{E'}$ (ºC)	tan δ peak	FWHM[b] (ºC)	tan δ area	E'_g (MPa)[d]	E'_r (MPa)[e]	E'_g/E'_r
90D400-10LP	60	50	0.96	15.45	14.83	2878	16	183
80D400-20LP	68	57	0.82	17.82	14.61	2880	17	166
70D400-30LP	77	63	0.71	20.29	14.41	3105	23	137
60D400-40LP	87	71	0.62	21.11	13.09	3149	29	110
50D400-50LP	96	80	0.54	23.33	12.60	3110	34	91
40D400-60LP	104	88	0.50	23.66	11.83	3221	41	79
30D400-70LP	117	98	0.41	24.58	10.08	2858	52	55

[a] Measured as the peak of tan δ.
[b] Full width at half maximum.
[c] Determination as the product of tan δ peak and FWHM
[d] Measured at T_g – 40 ºC.
[e] Measured at T_g + 40 ºC

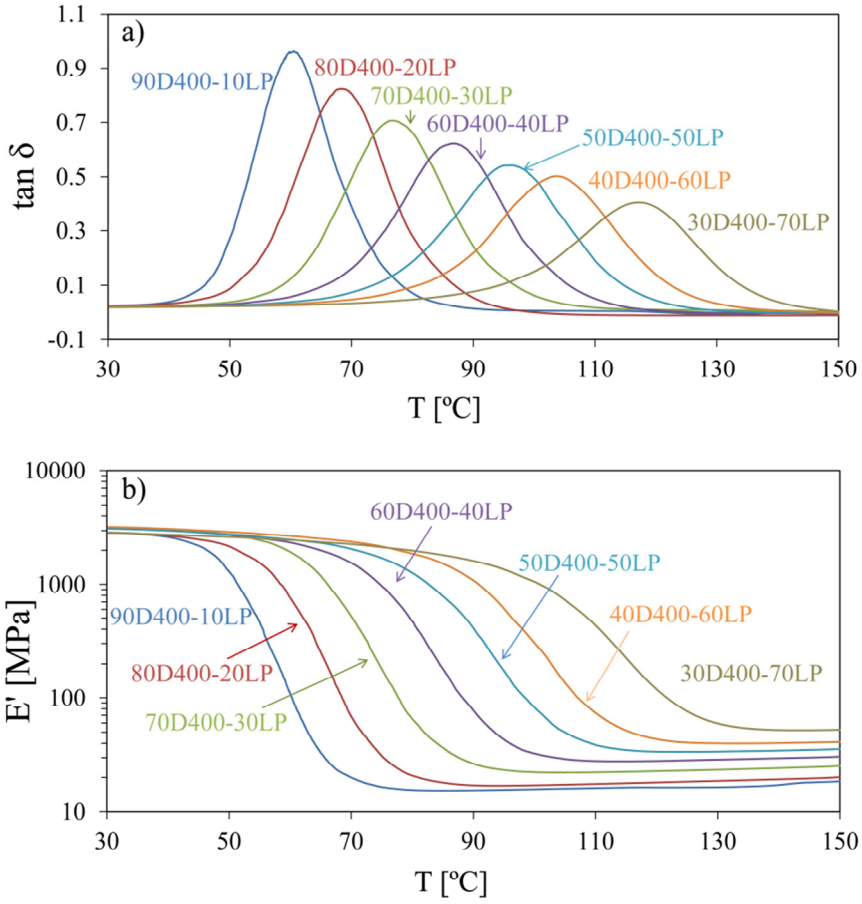

Figure IV.3.3 Tan δ and storage modulus *E'* as a function of temperature for all formulations.

A higher content of LP800 implies a higher crosslinking density (Table IV.3.1) because of the higher number of reactive amine groups per unit mass and the presence of internal branching points. This results in a decrease in the average chain length between netpoints and a more restricted molecular mobility, which leads to an increase in T_g [34]. As can be observed in Figure IV.3.3 and Table IV.3.2, an increase in LP800 also causes a lowering and a broadening of the peak of tan δ. The shape of the tan δ peak during the material relaxation can be correlated with its network structure. The peak height is an indication of the viscous

character of the material during the relaxation and the total peak area is related to the total amount of energy dissipated during the relaxation which, overall, gives an idea of the mechanical damping capabilities of the material [34]. Generally speaking, the higher and narrower the peak of tan δ, the more homogeneous and mobile the network structure [27,34]. LP800 leads to a more heterogeneous network structure due to the inherently disperse nature of the hyperbranched poly(ethyleneimine) and the presence of different types of crosslinks coming from the pre-existing tertiary amines, reacted primary and secondary amines of LP800. The decrease in tan δ peak and area on increasing the amount of LP800 is also indicative of a more densely crosslinked network with a restricted mobility.

All formulations show very high values of storage modulus at the glassy region around 3 GPa (Figure IV.3.3 and Table IV.3.2), which is higher than most of the shape-memory epoxy resins found in the literature [17-20,26,32]. The storage modulus at rubbery region E'_r increases from 16 MPa to 52 MPa as the LP800 content increases. According to the theory of rubber elasticity, E'_r is roughly proportional to the crosslinking density and the increasing trend in rubbery modulus (Table IV.3.2) with the crosslinking density is expected. However, on comparing the extreme formulations, the increase in the crosslinking density is only 60% while the increase in the apparent rubbery modulus is more than 200%. Similar deviations were already observed in epoxy networks modified with hyperbranched poly(ethyleneimine)s and explained on the basis of mobility restrictions imposed by the hyperbranched structure [28]. Given the hyperbranched structure of LP800, with a high number of internal branching points and very short ethylene segments within, in contrast to the long, flexible aliphatic structure of Jeffamine®, one can expect mobility restrictions and lower deformability on increasing the LP800 content in the cured thermosets. Similar departures from ideal long-chain, Gaussian behavior were

reported previously for other epoxy-amine systems [35]. This contrasts with the results of Xie and Rousseau [23], who showed that it could be possible to increase the crosslinking density and at the same time decrease the glass transition temperature and mechanical response of the relaxed material by using a smaller and more flexible aliphatic epoxy resin in the network structure. Their results can thus be rationalized by the higher mobility and deformability of the flexible aliphatic epoxy in the relaxed state, in comparison with DGEBA.

In any case, all the samples in the present work show a difference between the storage modulus at glassy and rubbery regions of around 2 orders of magnitude. This important difference in mechanical properties between the glassy and rubbery states is crucial if a polymer is required to present SME [36].

3.2 Mechanical Properties

The mechanical properties at room temperature of all the formulations are listed in Table IV.3.3. Both the stress at break and the deformation at break at room temperature increase with increased LP800 content, from nearly 42 MPa up to 55 MPa and from 3.5% up to nearly 5%, respectively. The values of elastic modulus are around 1800 MPa for all formulations. The trend of the Young modulus correlates well with the trend of the values of the storage modulus at glassy region (Table IV.3.2), where there is no significant difference between the formulations. With respect to the stress at break values, the observed tendency clearly shows that strength increases almost linearly with increasing crosslinking density and T_g up to sample 40D400-60LP, where it reaches its highest value (more than 55 MPa). This increase is possible up to a certain value where the increasingly crosslinked structure with restricted mobility limits its stress capability. Regarding the strain at break, this seems not to be differently affected by crosslinking density, with two distinctive regions observed: from 90D400-10LP to 60D400-20LP, with a strain value of around 3.6%, and from 50D400-50LP to 30D400-70LP, with a strain

value of around 5%. It follows that the increasing tensile strength and strain result would also result in a higher energy at break.

Table IV.3.3 Tensile data at room temperature obtained by uniaxial tensile testing: stress at break (σ_b), deformation at break (ε_b), and elastic modulus

Sample	σ_b (MPa)	ε_b (%)	Elastic Modulus (MPa)
90D400-10LP	41.76	3.52	1724.2
80D400-20LP	46.68	3.59	1825.5
70D400-30LP	47.32	3.62	1820.5
60D400-40LP	48.67	3.76	1873.4
50D400-50LP	51.46	4.98	1846.5
40D400-60LP	55.37	4.96	1803.3
30D400-70LP	54.36	4..98	1958.6

Properties below the glass transition temperature depend on a combination of factors including cohesive forces and the presence of local mobility, but the role of crosslinking density is not always clear [37]. It is usually observed that yield and ultimate stress increase with increasing T_g and depend mainly on the difference between the test temperature and T_g [37]. It should be taken into account that, on increasing the LP800 content, the DGEBA content also increases, thereby increasing the number of hydroxyl groups coming from the epoxy-amine condensation and contributing to the cohesion of the network structure. The internal flexible structure of LP800, with certain but limited local mobility below the glass transition temperature [32], may contribute to the observed behavior.

The mechanical properties evaluated at $T_g^{E'}$ are listed in Table IV.3.4. All formulations show very high values of stress at break, around 12 MPa for 90D400-10LP, 80D400-20LP and 70D400-30LP, and values up to 15.36 MPa (30D400-70LP) with increasing LP800 content. Tensile

modulus reveals a more rigid network with increasing LP800 content, which implies a decrease in strain at break: from 58% for 90D40010LP to 17% for 30D400-70LP.

Table IV.3.4 Tensile data at $T_g^{E'}$ obtained by DMA: stress at break (σ_b), deformation at break (ε_b), elastic energy density, tensile modulus, prescribed stress for shape memory programming (σ_m) and strain corresponding to σ_m (ε_m)

Sample	σ_b (MPa)	ε_b (%)	Elastic Energy Density (MJ/m^3)	Tensile Modulus (MPa)	σ_m (MPa)	ε_m (%)
90D400-10LP	12.72	58.09	3.7	19.62	9.54	41.95
80D400-20LP	11.67	44.69	2.6	23.76	8.75	33.51
70D400-30LP	11.47	33.82	1.9	31.05	8.60	30.21
60D400-40LP	12.31	29.52	1.8	38.82	9.23	22.36
50D400-50LP	13.31	25.96	1.7	48.23	9.98	21.12
40D400-60LP	14.29	21.34	1.5	62.35	10.71	18.46
30D400-70LP	15.36	17.17	1.3	84.40	11.52	13.19

Some authors have reported high ductile shape-memory epoxy networks with maximum deformations above 50% at onset of the glass transition temperature ($T_g^{E'}$), similar to formulation 90D400-10LP (ε_b = 58%) [17,19,25]. It is therefore relatively easy to obtain high ductile shape-memory epoxy networks. However, the values of stress at break are usually too unexceptional (normally below 8 MPa) for more mechanically demanding potential shape-memory applications. In this respect, note that formulations 90D400-10LP and 80D400-20LP combine great deformations at break (58% and 45%, respectively) with very high stresses at break of almost 13 MPa and 12 MPa, respectively.

The tensile modulus values shown in Table IV.3.4 correlate well with the relaxed modulus of the materials shown in Table IV.3.2. Although the behavior of the material is not at all comparable in

small/oscillatory and large/tensile deformation experiments, this is consistent with the fact that $T_g^{E'}$ is a temperature at which the material is already relaxed or has a relatively short relaxation time in comparison with the timescale of the tensile experiment. Generally speaking, an increase in the crosslinking density results in a less mobile and ductile network, leading in the macroscopic scale to a lower failure strain and a higher stress at break [34], as reported in Table IV.3.4. These results can be explained by taking into account the internal hyperbranched structure of LP800 with short ethylene segments within, with lower deformability than the long, flexible Jeffamine® structure.

In Table IV.3.4, it can also be seen that by lowering the LP800 content, the elastic energy density stored before break can be increased (with a maximum value of 3.7 MJ/m^3). This stored elastic energy density is an important metric of shape-memory behavior because it estimates an upper boundary for recoverable elastic energy, that is, the material's capability to perform mechanical work against external loads in the recovery stage. The ability of SMPs to stabilize deformed shapes and perform mechanical work upon shape recovery is limited by the strength and density of the bonds created during shape stabilization [38]. Hence reducing crosslinking density helps to improve this capability. In 90D400-10LP and 80D400-20LP, the elastic energy density reaches its highest values (3.7 MJ/m^3 and 2.6 MJ/m^3). In 70D400-30LP it further decreases down to 1.9 MJ/m^3 but, at a higher LP800 content, the decrease is gentler.

3.3 Shape-Memory Effect

In order to perform a comparative study with the same level of load for each sample, every sample was stretched during shape-memory programming to a prescribed maximum stress (σ_m) corresponding to 75% of the stress at break ($\sigma_m = 0.75\sigma_b$). Table IV.3.4 presents the prescribed maximum stress, σ_m, and the corresponding maximum deformation reached, ε_m, for each material. Figure IV.3.4 shows the typical three-

dimensional representation of the complete shape-memory process. For the sake of simplicity, only the cycles for the 90D400-10LP and 80D400-20LP samples are represented.

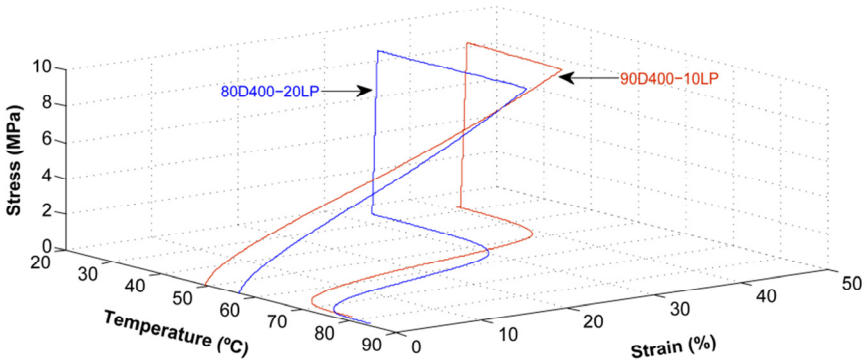

Figure IV.3.4 Three-dimensional representation of shape-memory programming of 90D400-10LP and 80D400-20LP programmed at $T_g^{E'}$ = 50 °C, σ_m = 9.54 MPa, ε_m = 41.95% and $T_g^{E'}$ = 57 °C, σ_m = 8.75 MPa, and ε_m = 33.51%, respectively.

The average shape-recovery ratio (R_r) and shape-fixity ratio (R_f) during three cycles were calculated when programming under these conditions (σ_m and $T_g^{E'}$), as plotted in Figure IV.3.5. All formulations show shape-recovery ratio values above 93% and shape-fixity ratio values around 97%, which demonstrates the excellent shape-memory properties of these shape-memory epoxies even after being stretched to near 60% (in the case of 90D400-10LP). There are hardly any cases reported in the literature of shape-memory epoxies programmed under such notable conditions of σ_m (or ε_m) and showing such excellent shape recovery and shape fixity: R_r = 96.3% and R_f = 98% for 90D400-10LP and R_r = 97.4% and R_f = 98% for 80D400-20LP.

Figure IV.3.5 shows the shape-recovery and shape-fixity ratios as a function of LP800 content. The shape-recovery ratio decreases slightly with increasing crosslinking density, from 96.3% (90D400-10LP) to

93.4% (30D400-70LP), showing a maximum for formulation 80D400-20LP with R_r = 97.4%. The shape-fixity ratio shows values higher than 94% for all formulations, decreasing from 98% (90D400-10LP) to 94.6% (30D400-70LP) as the LP800 content increases (Figure IV.3.5a).

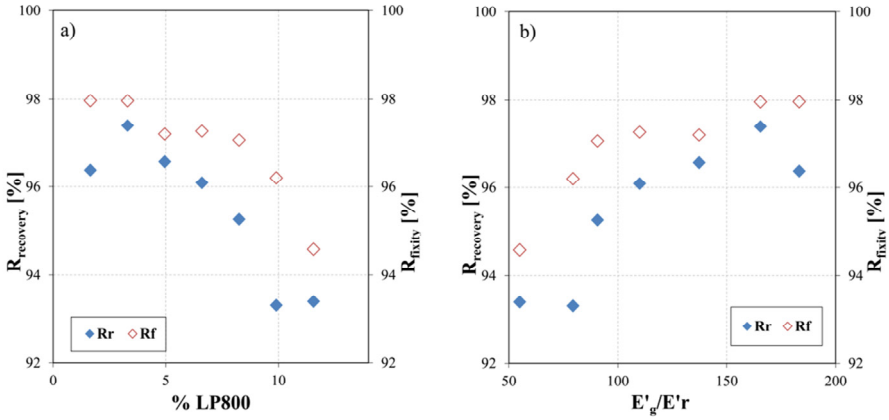

Figure IV.3.5 Shape-recovery ratio (R_r) and shape-fixity ratio (R_f) as a function of the content of LP800 (a) and as a function of the storage modulus ratio at glassy and rubbery regions E'_g/E'_r (b).

Shape-memory properties can also be correlated with thermomechanical properties and network structure (Figure IV.3.5b). Both the shape-recovery and shape-fixity ratios increase as the modulus ratio between the glassy and rubbery states increases and the glass transition temperature decreases. The samples with the lowest storage modulus ratio, R_r and R_f, present the minimum values. By decreasing the LP800 content, this ratio is widened and both ratios are increased. Rousseau and Xie [39] rationalized the shape-recovery and shape-fixity results in terms of spontaneous elastic recovery and/or stress relaxation. During the programming step, the material can be easily deformed with a significant decrease in the entropy of the system due to chain conformation rearrangement and alignment and a contribution of small elastic deformation corresponding to local chain mobility. When the applied external stress is

released at low temperature, there is a small elastic recovery coming from the immediate relaxation of local deformations. However, the lower mobility of the network structure prevents chain rearrangement and relaxation of internal stresses, balancing the conformational, entropic recovery driving force and holding the remaining deformation. Once the temperature exceeds the T_g, the network chains gain sufficient mobility, the internal stresses are eventually relaxed, and therefore the SMP is able to recover its original shape and a more stable, higher entropy state. If one bears in mind the structure of LP800 (see Figure IV.3.1c), very short ethylene segments between crosslinks can be found in formulations with a lower proportion of LP800. It is believed that the local deformation of the internal structure of LP800 in the network [32], with short ethylene segments within, has a lower contribution to conformational, entropic deformation than longer D400 chains and can therefore relax immediately after stress release. A higher amount of spontaneous elastic recovery may be expected when the sample containing higher contents of LP800 is unloaded, hence the lower shape-fixity ratio.

Figure IV.3.6 shows shape-recovery rate V_r as a function of the LP800 content (Figure IV.3.6a) and the strain recovered during the recovery stage (Figure IV.3.6b) for all samples. The recovery speed shows very high values for all formulations; it is possible to obtain more than 93% of shape recovery in a few minutes and in a narrow interval of temperatures. It is observed that V_r decreases from almost 22 %/min (or 7 %/ºC) to 15 %/min (or 5 %/ºC) as the LP800 content increases (Figure IV.3.6a). It is worth noting that the temperature range between 15% and 85% of strain recovered (Figure IV.3.6b) is also widened with increasing LP800 content: from 11.5 ºC (90D400-10LP) to 17 ºC (30D400-10LP).

As the maximum deformation during stretching has no influence on this parameter, the values and trend of V_r can be explained in viscoelastic terms. From the DMA analysis shown in Figure IV.3.3 and

Table IV.3.2, it can be seen that formulations with a higher LP800 content have broader network relaxation because of the more heterogeneous network structure. It can be assumed that network relaxation dynamics rather than the theoretical crosslinking density is the key parameter governing the recovery process [40]. Consequently it will take longer to release the stored internal stresses during the recovery process in materials with a higher LP800 content.

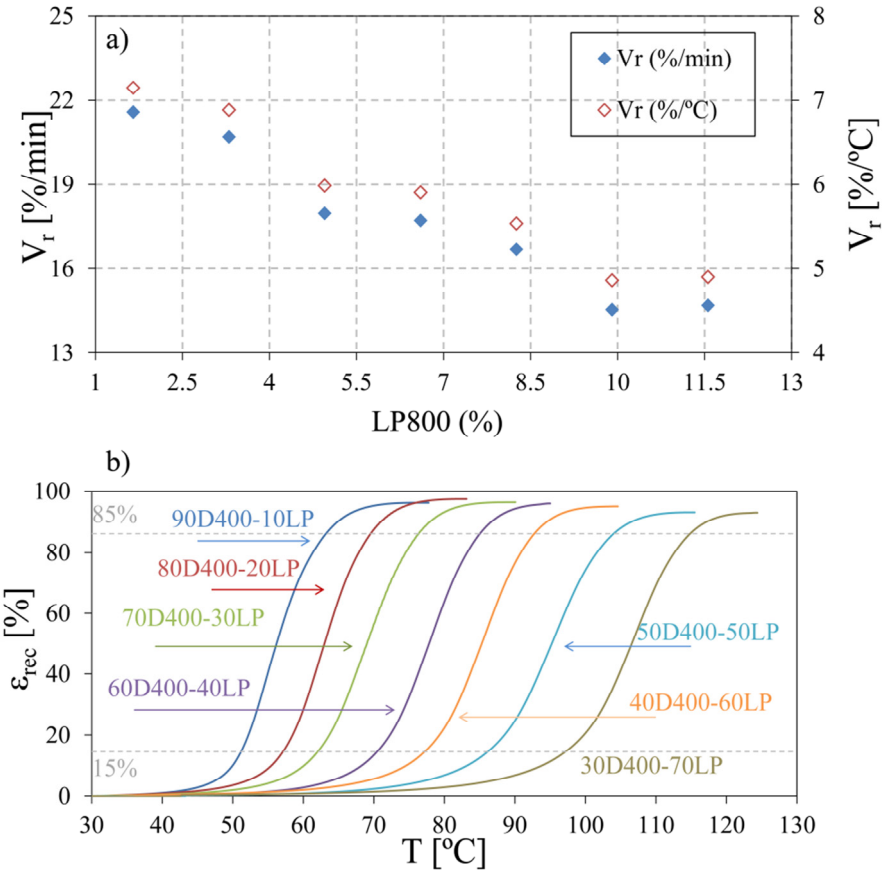

Figure IV.3.6 Shape-recovery rate V_r as a function of LP800 content (a) and strain recovered during heating for all formulations (b).

Conclusions

A series of hyperbranched-modified shape-memory epoxies were synthesized using a commercial hyperbranched poly(ethyleneimine) and an aliphatic amine as crosslinking agents. Thermal, mechanical and shape-memory properties were systematically studied and the results were interpreted in terms of the content and structure of the HBP.

The thermomechanical measurements showed that increasing LP800 content led to more heterogeneous networks with higher crosslinking density and a higher glass transition temperature. The ratio between the glassy modulus and the rubbery modulus decreased in accordance with the increase in crosslinking density, but deviations were observed due to the densely crosslinked hyperbranched structure of LP800 with short ethylene segments within.

The tensile tests at room temperature showed that an increase in LP800 resulted in an increase in the stress at break and deformation at break, reaching values of up to 55 MPa and 5%, respectively. At programming temperature, the stress at break increased from 12 to 15 MPa with increasing LP800 content, but reduced deformation at break from 60% to 17% due to an increase in the crosslinking density, The material with the lowest LP800 content reached the highest elastic energy density value of 3.7 MJ/m^3, an estimate of the potential of these materials to perform mechanical work against external loads in the recovery stage.

Shape-memory performances showed high values for the shape-recovery and shape-fixity ratios and the shape-recovery rate and demonstrated that the network structure is a key factor for shape-memory properties. The shape-recovery and shape-fixity ratios decrease slightly with increasing LP800 content because it restricted chain-conformational changes during deformation and molecular dynamics, adversely affecting the shape-recovery and shape-fixity ratios and the recovery rate.

Based on the aforementioned results, it can be concluded that hyperbranched polymers can be used to enhance the thermal and mechanical properties of epoxy-based SMPs while keeping excellent shape-memory properties. However, the hyperbranched polymer content should be controlled because of its effect on network homogeneity, the shape-recovery and shape fixity ratios and the recovery rate.

Acknowledgments

The authors would like to thank MINECO (MAT2011-27039C03-01) for its financial support. The authors are also grateful to BASF for providing Lupasol® and to Huntsman for providing Jeffamine® D400 and Araldite GY 240.

References

[1] A. Lendlein, S. Kelch, *Angew. Chem. Int. Ed.* **2002**, *41*, 2034–2057.

[2] 2. Y. Liu, H. Du, L. Liu, J. Leng, *Smart Mater. Struct.* **2014**, *23*, 023001.

[3] 3. F. Ji, Y. Zhu, J. Hu, Y. Liu, L.-Y. Yeung, G. Ye, *Smart Mater. Struct.* **2006**, *15*, 1547–1554.

[4] M. Behl, K. Kratz, U. Noechel, T. Sauter, A. Lendlein, *Proc. Natl. Acad. Sci. USA* **2013**, *110*, 12555–12559.

[5] J. Reeder, M. Kaltenbrunner, T. Ware, D. Arreaga-Salas, A. Avendano-Bolivar, T. Yokota, Y. Inoue, M. Sekino, W. Voit, T. Sekitani, T. Someya, *Adv. Mater.* **2014**, *26*, 4967–4973.

[6] K. J. Cha, E. Lih, J. Choi, Y. K. Joung, D. J. Ahn, D. K. Han, *Macromol. Biosci.* **2014**, *14*, 667–678.

[7] 7. C. Wischke, A. T. Neffe, A. Lendlein, *Adv. Polym. Sci.* **2010**, *226*, 177–205.

[8] M. Ecker, T. Pretsch, *RSC Adv.* **2014**, *4*, 46680–46688.

[9] T. Pretsch, M. Ecker, M. Schildhauer, M. Maskos, *J. Mater. Chem.* **2012**, *22*, 7757–7766.

[10] M. Bothe, T. Pretsch, *J. Mater. Chem. A*, **2013**, *1*, 14491–14497.

[11] M. Behl, K. Kratz, J. Zotzmann, U. N€ochel, A. Lendlein, *Adv. Mater.* **2013**, *25*, 4466–4469.

[12] Q. Ge, K. K. Westbrook, P. T. Mather, M. L. Dunn, H. J. Qi, *Smart Mater. Struct.* **2013**, *22*, 055009.

[13] L. Ionov, *Soft Matter.* **2011**, *7*, 6786–6791.

[14] K. K. Julich-Gruner C. Löwenberg, A. T. Neffe, M. Behl, A. Lendlein, *Macromol. Chem. Phys.* **2013**, *214*, 5272536.

[15] G. J. Berg, M. K. McBride, C. Wang, C. N. Bowman, *Polymer* **2014**, *55*, 5849–5872.

[16] K. S. Santhosh Kumar, R. Biju, C. P. Reghunadhan Nair, *React. Funct. Polym.* **2013**, *73*, 421–430.

[17] D. M. Feldkamp, I. A. Rousseau, Macromol. *Mater. Eng.* **2010**, *295*, 726–734.

[18] D. M. Feldkamp, I. A. Rousseau, *Macromol. Mater. Eng.* **2011**, *296*, 1128–1141.

[19] A. B. Leonardi, L. A. Fasce, I. A. Zucchi, C. E. Hoppe, E. R. Soulé, C. J. Pérez, R. J. J. Williams, *Eur. Polym. J.* **2011**, *47*, 362–369.

[20] R. Biju, C. P. Reghunadhan Nair, *J. Polym. Res.* **2013**, *20*, 82.

[21] B. Rajendran, K. S. Santhosh Kumar, R. S. Rajeev, C. P. Reghunadhan Nair, *Polym. Adv. Technol.* **2013**, *24*, 623– 629.

[22] K. Wei, G. Zhu, Y. Tang, L. Niu, *J. Polym. Res.* **2013**, *20*, 123.

[23] T. Xie, I. A. Rousseau, *Polymer*, **2009**, *50*, 1852–1856.

[24] X. Jing, Y. Liu, Y. Liu, Z. Liu, H. Tan, *J. Appl. Polym. Sci.* **2014**, *131*, 40853.

[25] M. Fan, H. Yu, X. Li, J. Cheng, J. Zhang, *Smart Mater. Struct.* **2013**, *22*, 055034.

[26] M. Fan, J. Liu, X. Li, J. Zhang, J. Cheng, *J. Polym. Res.* **2014**, *21*, 376.

[27] B. Voit, *J. Polym. Sci., Part A: Polym. Chem.* **2000**, *38*, 2505– 2525.

[28] D. Ratna, R. Varley, G. P. Simon, *J. Appl. Polym. Sci.* **2003**, *89*, 2339–2345.

[29] L. Boogh, B. Pettersson, J. A. E. Manson, *Polymer* **1999**, *40*, 2249–2261.

[30] C. M. Han, Y. Liu, H. Tan, *Adv. Mater. Res.* **2011**, 335–336, 851–855.

[31] D. Santiago, X. Fernández-Francos, X. Ramis, J. M. Salla, M. Sangermano, *Thermochim. Acta.* **2011**, *526*, 9–21.

[32] X. Fernández-Francos, D. Santiago, F. Ferrando, X. Ramis, J.M. Salla, A. Serra, M. Sangermano, *J. Polym. Sci. Part B: Polym. Phys.* **2012**, *50*, 1489–1503.

[33] M. Yakacki, S. Willis, C. Luders, K. Gall, *Adv. Eng. Mater.* **2008**, *10*, 112–119.

[34] X. L. Wu, S. F. Kang, X. J. Xu, F. Xiao, X. L. Ge, *J. Appl. Polym. Sci.* **2014**, *131*, 40559.

[35] J. M. Charlesworth, *Polym. Eng. Sci.* **1988**, *28*, 230–236.

[36] C. Liu, H. Qin, P. T. Mather, *J. Mater. Chem.* **2007**, *17*, 1543– 1558.

[37] J. P. Pascault, H. Sautereau, J. Verdu, R. J. J. Williams, Thermosetting Polymers; Marcel Dekker Ed.: New York, **2002**.

[38] M. Anthamatten, S. Roddecha, J. Li, *Macromolecules* **2013**, *46*, 4230–4234.

[39] I. A. Rousseau, T. Xie, *J. Mater. Chem.* **2010**, *20*, 3431–3441.

[40] J. Diani, P. Gilormini, C. Frédy, I. Rousseau, *Int. J. Solids Struct.* **2012**, *49*, 793–799.

UNIVERSITAT ROVIRA I VIRGILI
EXPERIMENTAL CHARACTERIZATION OF SHAPE-MEMORY POLYMERS: INFLUENCE OF PROCESSING METHODS AND CHEMICAL STRUCTURE
David Manuel Santiago Abraira

IV.4. Improving Mechanical and Shape Memory Properties in Hyperbranched Epoxy Shape Memory Polymers

David Santiago, Albert Fabregat-Sanjuan, Francesc Ferrando, Silvia De la Flor

Shape Memory and Superelasticity ***2016****, DOI: 10.1007/s40830-016-0067-y*

UNIVERSITAT ROVIRA I VIRGILI
EXPERIMENTAL CHARACTERIZATION OF SHAPE-MEMORY POLYMERS: INFLUENCE OF PROCESSING METHODS AND CHEMICAL STRUCTURE
David Manuel Santiago Abraira

Shap. Mem. Superelasticity 2016, DOI: 10.1007/s40830-016-0067-y 185

Improving mechanical and shape memory properties in hyperbranched epoxy shape memory polymers

David Santiago[1], Albert Fabregat-Sanjuan[1], Francesc Ferrando[1], Silvia De la Flor[1]

[1]Department of Mechanical Engineering, Universitat Rovira i Virgili, Av. Països Catalans 26, 43007 Tarragona, Spain

Abstract

A series of shape-memory epoxy polymers were synthesized using an aliphatic amine and two different commercial hyperbranched poly(ethyleneimine)s with different molecular weights as crosslinking agents. Thermal, mechanical and shape-memory properties in materials modified with different hyperbranched polymers were analyzed and compared in order to establish the effect of the structure and the molecular weight of the hyperbranched polymers used. The presence of hyperbranched polymers led to more heterogeneous networks, the crosslinking densities of which increase as the hyperbranched polymer content increases. The transition temperatures can be tailored from 56 to 117 ºC depending on the molecular weight and content of the hyperbranched polymer. The mechanical properties showed excellent values in all formulations at room temperature and, specially, at $T_g^{E'}$ with stress at break as high as 15 MPa and strain at break as high as 60%. The shape-memory performances revealed recovery ratios around 95%, fixity ratios around 97% and shape-recovery velocities as high as 22 %/min. The results obtained in this study reveal that hyperbranched polymers with different molecular weights can be used to enhance the thermal and mechanical properties of epoxy-based SMPs while keeping excellent shape-memory properties.

186 Shap. Mem. Superelasticity 2016, DOI: 10.1007/s40830-016-0067-y

Keywords: *Shape-memory, epoxy, hyperbranched, mechanical properties, smart materials*

1. Introduction

Shape-Memory Polymers (SMPs) are a class of materials that can change their shape when an external stimulus is applied. These polymers can be processed to have a permanent shape by conventional techniques, and then deformed and fixed in a new or temporary shape that can remain stable until the stimulus is applied [1]. This shape changing is called the Shape-Memory Effect (SME) and it is usually driven by heat. However, it can also be driven by light, a magnetic field, or an electrical current. These smart materials have attracted a lot of interest in recent years due to their wide range of applications including self-deployable structures for aerospace applications, biomedical devices or smart fiber and fabrics [2-4].

The most common SMPs are thermoplastics because they are extremely ductile and easy to process [5,6], and, therefore, suitable for a wide variety of potential applications. There are also some examples of SMP-composites with improved mechanical performance [7,8]. However, in recent years a number of studies have reported shape-memory thermosets with excellent mechanical and shape-memory properties, such as epoxy-based or acrylate-based SMPs [9,10].

Epoxy resins are widely used in many applications (coatings, adhesives or matrices in composites) because of their chemical resistance, thermal stability and good mechanical properties [11]. However, their brittle behavior and low elongation at break greatly limit their use as SMPs. Many studies have focused on overcoming this limitation by selecting suitable crosslinking agents which enhance local mobility and deformability of the networks [12-15]. Although the toughness of epoxies is greatly improved in such networks, the mechanical properties in terms of tensile strength may remain a limitation. So, new kinds of shape-

memory epoxy polymer need to be found that combine high values of tensile strength and maximum deformation above and below the transition temperature for more mechanically demanding applications such as thermomechanical actuators.

Our research group recently reported the use of a low molecular weight hyperbranched polymer as crosslinking agent for epoxy-based SMPs [9]. The results revealed that the presence of hyperbranched polymer led to good thermal, mechanical and shape-memory properties. These results indicate that other hyperbranched polymers should be used if shape-memory epoxy polymers are to be further improved. To this end, in this study two hyperbranched polymers with different molecular weights have been used as crosslinking agents to determine the effect of the hyperbranched structure and molecular weight on the thermomechanical and shape-memory properties of epoxy-based SMPs.

2. Materials and Experimental Methods

2.1 Materials

Diglycidyl ether of bisphenol A (Araldite GY 240, Huntsman) with a weight per epoxy equivalent of 182 g/mol was used as the base epoxy resin (Figure IV.4.1a). An aliphatic diamine (Jeffamine® D400, Huntsman) with M_w = 430 g/mol (Figure IV.4.1b) and two different commercial hyperbranched poly(ethyleneimine)s Lupasol® FG with M_w = 800 g/mol and Lupasol® PR8515 with M_w = 2000 g/mol (BASF) (Figure IV.4.1c) were used as crosslinking agents.

Various formulations with different contents of diglycidyl ether of bisphenol A (DG), Jeffamine® D400 (D400) and Lupasol® FG (LP FG) or Lupasol® PR8515 (LP PR) were prepared (Table IV.4.1) as crosslinking agents. The proportions of reactants in each formulation were selected so that the molecular structure consisted of stoichiometric DG-D400 and DG-LP networks. The sample nomenclature X-Y-Z used

in Table IV.4.1 indicates the weight fraction of stoichiometric DG-D400 (X) and DG-LP (Y) networks and the type of Lupasol® used (Z).

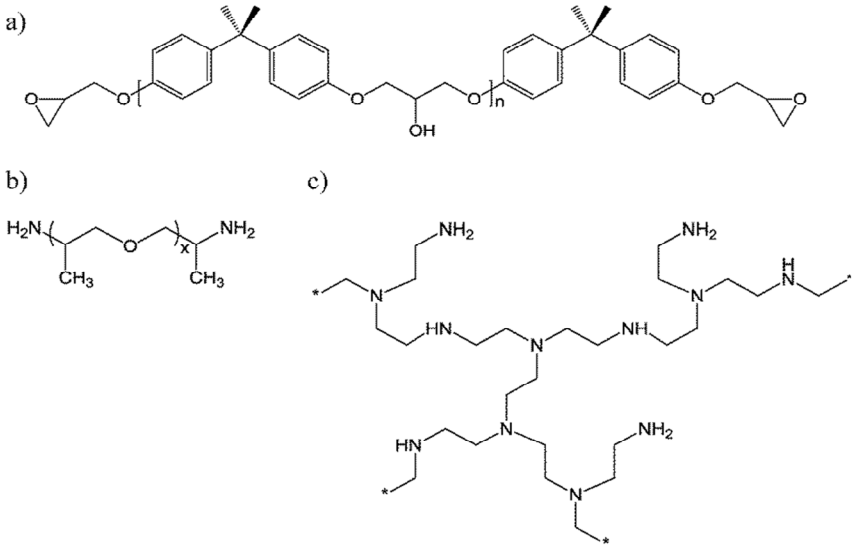

Figure IV.4.1 a) Chemical structure of DGEBA (n = 0.08); b) chemical structure of Jeffamine® D400 (x ≈ 6.1); c) chemical structure of Lupasol® FG.

Table IV.4.1 Composition of the formulations studied

Sample	wt. % DG	wt. % D400	wt. % Lupasol®	D400:LP amine ratio[a]	ν_c (mol/g)[b]
90-10-FG	63.5	34.8	1.7	4.010	0.001915
80-20-FG	65.7	31.0	3.3	1.782	0.002127
70-30-FG	67.9	27.1	5.0	1.040	0.002339
60-40-FG	70.2	23.2	6.6	0.668	0.002551
50-50-FG	72.4	19.4	8.3	0.446	0.002763
40-60-FG	74.6	15.5	9.9	0.297	0.002975
30-70-FG	76.8	11.6	11.6	0.191	0.003187
90-10-PR	63.4	34.8	1.8	3.771	0.001940
80-20-PR	65.5	31.0	3.5	1.676	0.002176
70-30-PR	67.6	27.1	5.3	0.978	0.002412
60-40-PR	69.8	23.2	7.0	0.629	0.002648
50-50-PR	71.9	19.4	8.8	0.419	0.002885
40-60-PR	74.0	15.5	10.5	0.279	0.003121
30-70-PR	76.1	11.6	12.3	0.180	0.003357

[a] Total primary, secondary and tertiary amine groups present in the crosslinking agent
[b] ν_c is the crosslinking density and it was calculated assuming that all amine groups turn into crosslinks

2.2 Thermomechanical Characterization

The thermomechanical properties were measured using a DMA Q800 (TA Instruments) equipped with a 3-point bending clamp. Prismatic rectangular samples of ca. 30 mm x 5.5 mm x 2.5 mm were analyzed at 1 Hz, 0.1% strain and a heating rate of 3 ºC/min. The glass transition temperature was determined from the peak in tan δ. The values of storage modulus *E'* were evaluated below and above glass transition.

2.3 Mechanical Characterization

The mechanical properties at room temperature were evaluated using an electromechanical universal testing machine (Zwick 1445) with specially designed grips. The specimens were sized in accordance with ASTMD638 requirements and had a Type IV dog-bone shape. The experiments were performed at a crosshead speed of 1 mm/min.

The mechanical properties at $T_g^{E'}$ were measured using a DMA Q800 equipped with a film-tension clamp in force-controlled mode. Prismatic rectangular samples of ca. 20 mm x 2.5 mm x 0.5 mm were analyzed at $T_g^{E'}$ at a force rate of 1N/min. In both cases, the stress-strain relationship was obtained by using the specifications established in ASTMD638.

2.4 Shape-Memory Properties

The shape-memory properties were measured using a DMA Q800 with a force-controlled mode and equipped with a film-tension clamp. Prismatic rectangular samples of ca. 20 mm x 2.5 mm x 0.5 mm were used in shape-memory performances. The method used to create a temporary shape and trigger the shape-memory effect was a thermomechanical procedure called programming (Figure IV.4.2). This programming consisted of four steps. 1) First the sample was heated to programming temperature T_{prog} and deformed to a prescribed value of maximum stress σ_m at 1 MPa/min. In this stage the deformation of the sample was ε_m. 2) The next step was to cool the sample to below transition temperature T_{low} (~25 ºC) so as to fix the temporary shape. 3) After fixation, the stress was released at the same stress rate of 1 MPa/min. Once the sample had been unloaded, the deformation of the sample was ε_u. 4) The SME was triggered by heating the sample to a recovery temperature $T_{recovery}$ (T_g + 10 ºC) at a heating rate of 3 ºC/min. The amount of non-recoverable deformation at the end of programming was ε_p.

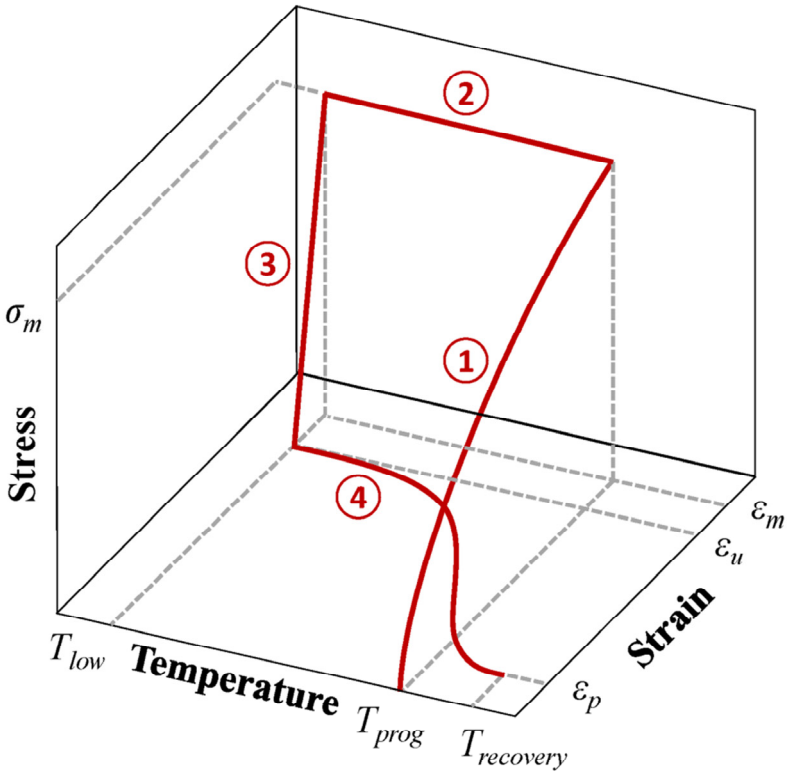

Figure IV.4.2 Scheme of the thermomechanical programming.

The programming temperature was chosen as the onset of the glass transition temperature $T_g^{E'}$ of each sample. According to Yakacki *et al.* [16] a peak in the deformability of shape-memory acrylate-based polymers can be obtained at a temperature coinciding with the onset of glass transition temperature. Feldkamp and Rousseau [17] reported the same phenomenon in epoxy-based systems.

The most significant parameters for quantifying shape-memory properties are the shape-recovery ratio (R_r) and the shape-fixity ratio (R_f). The shape-recovery ratio (Equation IV.4.1) quantifies the ability of the SMP to recover its original shape and was calculated as the total

deformation recovered with respect to the maximum deformation reached during the programming. The shape-fixity ratio, calculated from Equation IV.4.2, quantifies the ability of the SMP to fix the temporary shape. It was calculated as the deformation after the stress was released with respect to the maximum deformation.

$$R_r(\%) = \frac{\varepsilon_m - \varepsilon_p}{\varepsilon_m} \cdot 100 \qquad \text{(IV.4.1)} \qquad R_f(\%) = \frac{\varepsilon_u}{\varepsilon_m} \cdot 100 \qquad \text{(IV.4.2)}$$

Another parameter of interest in evaluating shape-memory ability is the shape-recovery rate (V_r). This quantifies the velocity at which the permanent shape is recovered and it is calculated according to Equation IV.4.3:

$$V_r\,(\%/\text{min}) = \frac{\left(\frac{\varepsilon_{rec,15\%} - \varepsilon_{rec,85\%}}{\varepsilon_{rec,15\%}}\right) \cdot 100}{\Delta t_{15\%-85\%}} \qquad \text{(IV.4.3)}$$

where $\varepsilon_{rec,15\%}$ is the deformation corresponding to a shape recovery of 15%, $\varepsilon_{rec,85\%}$ is the deformation corresponding to a shape recovery of 85%, and $\Delta t_{15\%-85\%}$ is the time interval between these two points. The difference between deformations corresponding to a shape recovery of 15% and 85%, $\varepsilon_{rec,15\%} - \varepsilon_{rec,85\%}$, was calculated with respect to $\varepsilon_{rec,15\%}$ in order to avoid the influence of the maximum deformation on V_r.

3. Results and Discussion

3.1 Thermomechanical Properties

The thermomechanical properties of formulations with Lupasol® FG and Lupasol® PR8515 are listed in Table IV.4.2. The glass transition temperatures of these materials can be controlled by varying the chemical composition of the formulations. T_gs show values between 60 ºC and 117 ºC with LP FG and 56 ºC and 112 ºC with LP PR. Formulations with LP PR have slightly lower T_gs than formulations with LP FG. The higher

molecular weight of Lupasol® PR8515 results in longer branches than Lupasol® FG, and these longer branches improve the molecular motion of the network in comparison with formulations with the lower molecular weight counterpart. Accordingly, these materials can be used in shape-memory applications that require a broad range of transition temperatures.

Table IV.4.2 Thermomechanical data obtained by DMA: glass transition temperature (T_g), onset temperature of the glass transition temperature (T_g^E), storage modulus in glassy and rubbery regions (E'_g and E'_r respectively)

Sample	T_g (°C)[a]	$T_g^{E'}$ (°C)	tan δ peak	FWHM tan δ (°C)[b]	area (°C)[c]	E'_g (MPa)[d]	E'_r (MPa)[e]	$\frac{E'_g}{E'_r}$
90-10-FG	60	50	0.96	15	14.83	2878	16	183
80-20-FG	68	57	0.82	18	14.61	2880	17	166
70-30-FG	77	63	0.71	20	14.41	3105	23	137
60-40-FG	87	71	0.62	21	13.09	3149	29	110
50-50-FG	96	80	0.54	23	12.60	3110	34	91
40-60-FG	104	88	0.50	24	11.83	3221	41	79
30-70-FG	117	98	0.41	25	10.08	2858	52	55
90-10-PR	56	48	0.98	15	15.11	3050	15	198
80-20-PR	64	55	0.78	20	15.25	3111	18	172
70-30-PR	70	60	0.62	25	15.26	3253	22	150
60-40-PR	79	65	0.57	27	15.59	3008	23	128
50-50-PR	89	73	0.50	29	14.58	3166	32	98
40-60-PR	99	78	0.38	33	12.60	2936	44	67
30-70-PR	112	89	0.34	34	11.50	2871	58	49

[a] Measured as the peak of tan δ
[b] Full Width at Half Maximum
[c] determined as the product of tan δ peak and FWHM
[d] measured at T_g - 40
[e] measured at T_g + 40

A higher content of Lupasol® means that the crosslinking density is also higher (Table IV.4.1) because of the higher number of reactive amine groups per unit mass and the presence of internal branching points. This decreases the average chain length between netpoints and restricts the molecular mobility, which leads to an increase in T_g. As can be observed in Table IV.4.2, an increase in Lupasol® also lowers and broadens the curve of tan δ. The shape of the tan δ curve can be correlated with its network structure: the higher and narrower the shape of the curve of tan δ, the more homogeneous and mobile the network structure is [18]. The presence of Lupasol® leads to a more heterogeneous network structure due to the inherently disperse nature of the hyperbranched poly(ethyleneimine) and the presence of different types of crosslinks from the pre-existing tertiary amines and the reacted primary and secondary amines. The longer branches of LP PR, which decrease the transition temperature in comparison with formulations with LP FG, increase the heterogeneity and dispersity of the networks, which have lower and wider curves of tan δ (Table IV.4.2).

All formulations show very high values of storage modulus in the glassy region around 3 GPa, which is higher than most of the shape-memory epoxy resins found in the literature [13-15]. The storage modulus in the rubbery region E'_r increases from 16 MPa to 52 MPa as the LP FG content increases and from 15 MPa to 58 MPa as the LP PR content increases. According to the theory of rubber elasticity, E'_r is roughly proportional to the crosslinking density and the rubbery modulus (Table IV.4.2) is expected to increase with the crosslinking density. Given the hyperbranched structure of Lupasol®, which has a considerable number of internal branching points and very short ethylene segments within, unlike the long and flexible aliphatic structure of Jeffamine® D400, mobility can be expected to be restricted and deformability lower when the Lupasol® content is increased in the cured thermosets.

3.2 Mechanical Properties

Most of the articles about shape-memory polymers found in the literature focus on mechanical properties at high temperature so that deformations can be high during the programing of the temporary shape. However, the characterization of the mechanical properties at room temperature is important for applications such as thermomechanical actuators, which must perform recovery stress or work against an external load. Figure IV.4.3 shows the values of stress at break and strain at break of formulations with Lupasol® FG (Figure IV.4.3a) and with Lupasol® PR8515 (Figure IV.4.3b) evaluated at T_{room}.

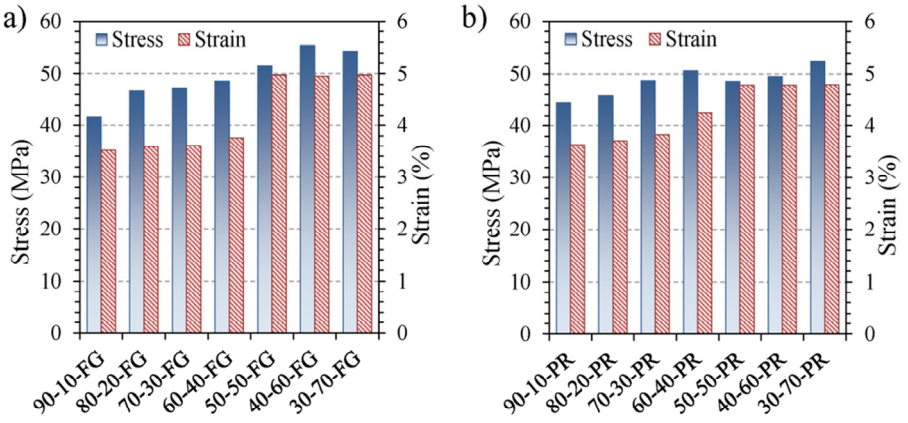

Figure IV.4.3 Stress at break and strain at break of formulations with Lupasol® FG (a) and Lupasol® PR8515 (b) evaluated at T_{room}.

Both the stress at break and the deformation at break increase from 42 MPa to 55 MPa and from 3.5% to nearly 5.0% with LP FG and from 44 MPa to 52MPa and from 3.7% to 4.8% with LP PR. The observed tendency for stress at break values clearly shows that strength increases almost linearly with increasing crosslinking density and T_g in both formulations with LP FG and LP PR. The strain at break does not seem to be affected differently by crosslinking density in formulations with LP FG. Two distinctive regions are observed: from 90-10-FG to 60-20-FG,

with values of strain at break around 3.6%, and from 50-50-FG to 30-70-FG, with values of strain at break around 5%. In formulations with LP PR, the strain at break increases linearly from 3.6% in formulation 90-10-PR to 5.0% in formulation 50-50-PR. From this point the strain at break shows values around 5.0% in the other formulations. These results suggest that the increase in the strain at break seems to be possible up to a certain value when the increasing crosslinking density limits the deformability of the network.

Properties below the T_g depend on a combination of factors such as cohesive forces and the presence of local mobility. Strain and stress at break increase with increasing T_g and depend mainly on the difference between the test temperature and T_g. It should be taken into account that when the Lupasol® content is increased, the DG content also increases (Table IV.4.1), which increases the number of hydroxyl groups from the epoxy-amine condensation and contributes to the cohesion of the network structure. The internal flexible structure of Lupasol®, which has limited local mobility below the glass transition temperature, may contribute to the observed behavior.

Figure IV.4.4 shows the values of stress at break and strain at break of formulations with LP FG (Figure IV.4.4a) and with LP PR (Figure IV.4.4b) at $T_g^{E'}$. All formulations show very high values of stress at break, above 10 MPa in all cases and up to 15 MPa in formulation 30-70-FG. Several studies have reported shape-memory epoxy networks with very high deformations at break at $T_g^{E'}$. However, the values of stress at break at $T_g^{E'}$ in shape-memory epoxy networks are usually lower than those reported in this paper [14,17,19].

The values of stress at break and strain at break have a more rigid structure as Lupasol® content increases, which mean that strain at break decreases from 58% to 17% in formulations with LP FG and from 50% to 13% in formulations with LP PR. In general, an increase in the crosslinking density results in a less mobile and ductile network. On the

macroscopic scale this leads to a lower failure strain and a higher stress at break. These results can be explained by the internal hyperbranched structure of Lupasol® which has short ethylene segments within and is less deformable than the long, flexible Jeffamine® D400 structure.

Overall, for both temperatures, formulations with LP PR have values of stress at break and strain at break that are slightly lower than formulations with LP FG. These differences may be caused by the higher crosslinking density of formulations with LP PR and the presence of possible molecular interactions due to the longer branches of LP PR.

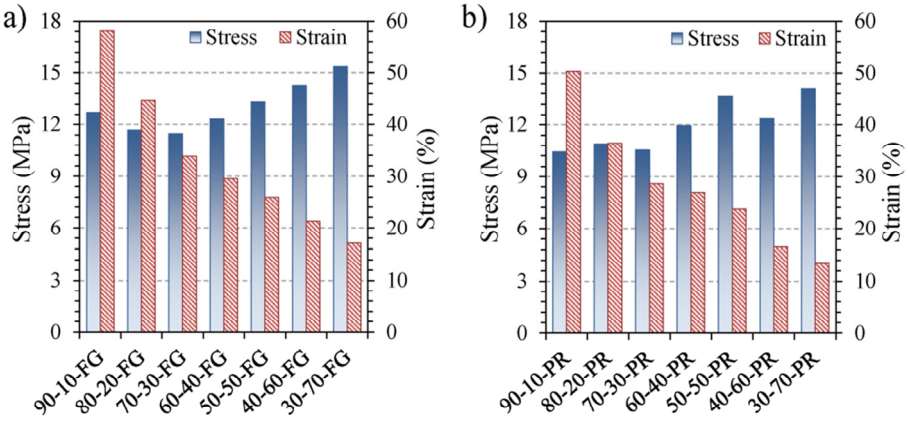

Figure IV.4.4 Stress at break and strain at break of formulations with Lupasol® FG (a) and Lupasol® PR8515 (b) evaluated at $T_g^{E'}$.

3.3 Shape-Memory Properties

To make a comparative study with the same level of load, every sample was stretched during the programming to a prescribed maximum stress (σ_m) that was 75% of the stress at break ($\sigma_m = 0.75\sigma_b$). Figure IV.4.5 shows the shape recovery ratio and the shape fixity ratio of formulations with Lupasol® FG (Figure IV.4.5a) and with Lupasol® PR8515 (Figure IV.4.5b). The average shape-recovery ratio and shape-fixity ratio over three cycles were calculated when programming under these conditions (σ_m and $T_g^{E'}$). All formulations show shape-recovery ratio values above 93% and shape-fixity ratio values around 97%, which demonstrates the

excellent shape-memory properties of materials with both Lupasol® FG and Lupasol® PR8515.

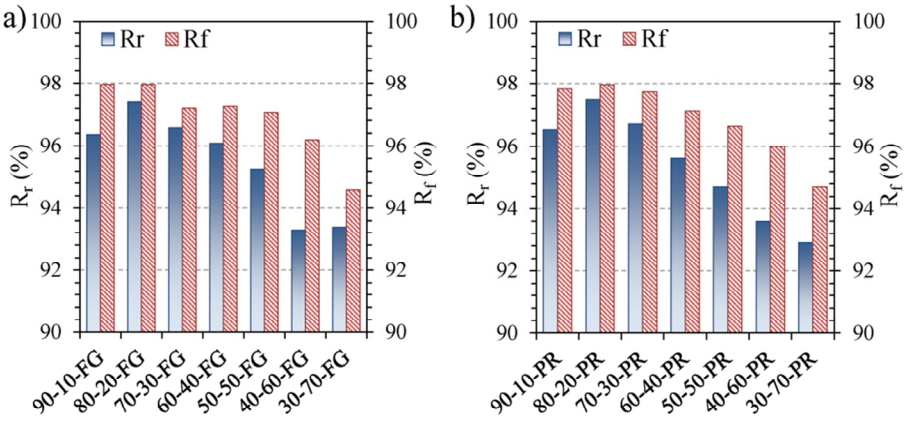

Figure IV.4.5 Shape-recovery ratio (R_r) and shape-fixity ratio (R_f) of formulations with Lupasol® FG and (a) and with Lupasol® PR8515 (b).

The shape-recovery ratio decreases slightly as the Lupasol® content increases in both groups of formulations: from 96.3% to 93.4% with LP FG and from 96.5 to 92.9% with LP PR. The maximum is for formulations 80-20-FG and 80-20-PR with R_r = 97.4% and R_r = 97.5%, respectively. The shape fixity ratio is high with both types of Lupasol® and ranges from 98% to 94% as the Lupasol® content increases.

These results can be correlated with thermomechanical properties and network structure. Formulations with a higher Lupasol® content have broader network relaxation because of the more heterogeneous network structure (Table IV.4.2) so it is more difficult to release the stored imposed stresses (step 1 in Figure IV.4.2) during the recovery process. This decreases the shape-recovery ratio R_r. The local deformation of the internal structure of Lupasol® in the network, which has short ethylene segments within, has a lower contribution to conformational, entropic deformation than longer D400 chains and can therefore relax immediately after stress release. A higher amount of spontaneous elastic

recovery may be expected when formulations with a higher Lupasol® content are unloaded. In this case, shape-fixity ratios R_f are lower.

As mentioned above, LP PR has longer branches than LP FG. This means that formulations with LP PR have a more heterogeneous structure than formulations with LP FG and have slightly lower values of R_r and R_f.

Figure IV.4.6 shows the shape-recovery velocity V_r of formulations with Lupasol® FG (Figure IV.4.6a) and Lupasol® PR8515 (Figure IV.4.6b). It is observed that V_r decreases as the Lupasol® content increases. Formulations with a higher Lupasol® content have broader network relaxation because of the more heterogeneous network structure which hinders the recovery process. Thus, it takes longer to release the stored internal stresses during the recovery process in materials with a higher Lupasol® content. Formulations with LP PR have lower values of V_r due to the more heterogeneous networks than formulations with LP FG.

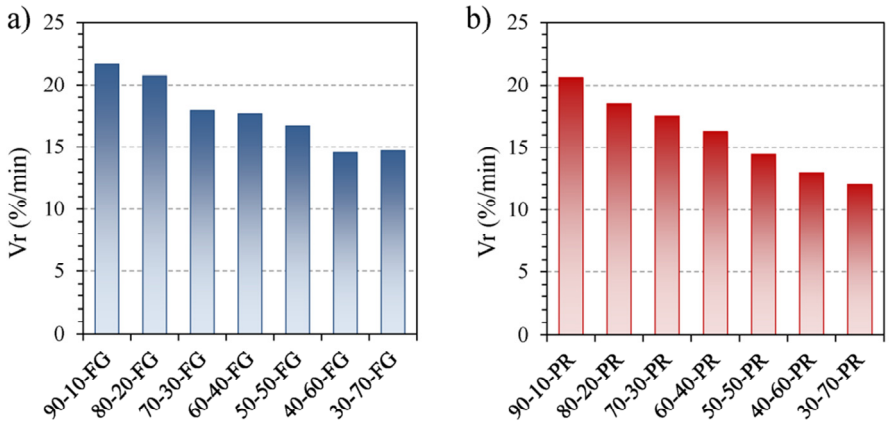

Figure IV.4.6 Shape-recovery velocity (V_r) of formulations with Lupasol® FG (a) and with Lupasol® PR8515 (b).

Conclusions

A series of shape-memory epoxy polymers was synthesized using an aliphatic amine and two commercial hyperbranched poly(ethyleneimine)s with different molecular weights as crosslinking agents. The influence of the structure of the hyperbranched polymers on the thermal, mechanical and shape-memory properties was analyzed and discussed.

The thermomechanical measurements showed that an increase in the Lupasol® content led to more heterogeneous networks with higher crosslinking densities and higher T_gs. Formulations with Lupasol® PR8515 had lower T_gs but wider transitions than formulations with Lupasol® FG.

The tensile tests at room temperature showed that an increase in the Lupasol® content resulted in an increase in the stress at break and deformation at break, showing values around 55 MPa and 5% in both groups of formulations. At the programming temperature $T_g^{E'}$, the stress at break showed excellent values above 10 MPa in all formulations and up to 15 MPa and deformations at break of almost 60%. The higher crosslinking density and the presence of possible molecular interactions of formulations with Lupasol® PR8515 resulted in slightly lower values of stress at break and strain at break than formulations with Lupasol® FG.

Shape-memory performances showed high values of shape-recovery, shape-fixity ratios and shape-recovery velocity. The shape-memory properties were reduced when the Lupasol® content was increased because it restricted chain-conformational changes during deformation and molecular dynamics, which hindered the recovery and fixity processes and decreased the recovery velocity. Formulations with Lupasol® PR8515 presented slightly lower shape-memory properties because they were more heterogeneously structured than formulations with Lupasol® FG.

The results obtained show that hyperbranched polymers can be used as crosslinking agents for epoxy-based shape-memory polymers.

The hyperbranched polymer content and molecular weight should be controlled. While materials with low molecular weight hyperbranched polymers showed slightly better mechanical and shape memory properties, materials with higher molecular weight hyperbranched polymers had lower transition temperatures. Other mechanical properties can be analyzed in future work to determine the effect of both types of hyperbranched poly(ethyleneimine)s.

Acknowledgments

The authors would like to thank MICINN (MAT2014-53706-C03-01) and the Generalitat de Catalunya (2014-SGR-67) for giving financial support.

References

[1] Lendlein, A., Kelch, S.: Shape-Memory Polymers. Angew. Chem. Int. Ed. 41(12), 2034–2057 (2002)

[2] Liu, Y., Du, H., Liu, L., Leng, J.: Shape memory polymers and their composites in aerospace applications: A review. Smart Mater. Struct. 23(2), 023001 (2014)

[3] Cha, K.J., Lih, E., Choi, J., Joung, Y.K., Ahn, D.J., Han, D.K.: Shape-memory effect by specific biodegradable polymer blending for biomedical applications. Macromol. Biosci. 14(5), 667–678 (2014)

[4] Han, H.R., Chung, S.E., Park, C.H.: Shape memory and breathable waterproof properties of polyurethane nanowebs. Text. Res. J. 83(1), 76–82 (2013)

[5] Santiago, D., Ferrando, F., De La Flor, S.: Effect of different shape-memory processing methods on the thermomechanical cyclic properties of a shape-memory polyurethane. J. Mater. Eng. Perform. 23(7), 2561–2566 (2014)

[6] Santiago, D., Ferrando, F., De La Flor, S.: Influence of holding time on shape recovery in a polyurethane shape-memory polymer. J. Mater. Eng. Perform. 23(7), 2567–2573 (2014)

[7] Ohki, T., Ni, Q.-Q., Ohsako, N., Iwamoto, M.: Mechanical and shape memory behavior of composites with shape memory polymer. Compos. Part Appl. Sci. Manuf. 35(9), 1065–1073 (2004)

[8] Lu, H., Yu, K., Sun, S., Liu, Y., Leng, J.: Mechanical and shape-memory behavior of shape-memory polymer composites with hybrid fillers. Polym. Int. 59(6), 766–771 (2010)

[9] Santiago, D., Fernandez-Francos, X., Ferrando, F., De la Flor, S.: Shape-memory effect in hyperbranched poly(ethyleneimine)-modified epoxy thermosets. J. Polym. Sci. Part B Polym. Phys. 53(13), 924–933 (2015)

[10] Santiago, D., De la Flor, S., Ferrando, F., Ramis, X., Sangermano, M.: Thermomechanical Properties and Shape-Memory Behavior of Bisphenol A Diacrylate-Based Shape-Memory Polymers. Macromol. Chem. Phys. DOI: 10.1002/macp.201500261 (2015)

[11] Santhosh Kumar, K.S., Biju, R., Reghunadhan Nair, C.P.: Progress in shape memory epoxy resins. React. Funct. Polym. 73(2), 421-430 (2012)

[12] Xie, T., Rousseau, I.A.: Facile tailoring of thermal transition temperatures of epoxy shape memory polymers. Polymer. 50(8), 1852–1856 (2009)

[13] Leonardi, A.B., Fasce, L.A., Zucchi, I.A., Hoppe, C.E., Soule, E.R., Perez, C.J., Williams, R.J.J.: Shape memory epoxies based on networks with chemical and physical crosslinks. Eur. Polym. J. 47(3), 362–369 (2011)

[14] Feldkamp, D.M., Rousseau, I.A.: Effect of Chemical Composition on the Deformability of Shape-Memory Epoxies. Macromol. Mater. Eng. 296(12), 1128–1141 (2011)

[15] Fan, M., Liu, J., Li, X., Zhang, J., Cheng, J.: Thermal, mechanical and shape memory properties of anintrinsically toughened epoxy/anhydride system. J. Polym. Res. 21(3), 376 (2014)

[16] Yakacki, C.M., Willis, S., Luders, C., Gall, K.: Deformation limits in shape-memory polymers. Adv. Eng. Mater. 10(1–2), 112–119 (2008)

[17] Feldkamp, D.M., Rousseau, I.A.: Effect of the Deformation Temperature on the Shape-Memory Behavior of Epoxy Networks. Macromol. Mater. Eng. 295(8), 726–734 (2010)

[18] Wu, X.L., Kang, S.F., Xu, X.J., Xiao, F., Ge, X.L.: Effect of the crosslinking density and programming temperature on the shape fixity and shape recovery in epoxy-anhydride shape-memory polymers. J. Appl. Polym. Sci. 131(15), 40559 (2014)

[19] Fan, M., Yu, H., Li, X.; Cheng, J., Zhang, J.: Thermomechanical and shape-memory properties of epoxybased shape-memory polymer using diglycidyl ether of ethoxylated bisphenol-A. Smart Mater. Struct. 22(5), 055034 (2013)

UNIVERSITAT ROVIRA I VIRGILI
EXPERIMENTAL CHARACTERIZATION OF SHAPE-MEMORY POLYMERS: INFLUENCE OF PROCESSING METHODS AND CHEMICAL STRUCTURE
David Manuel Santiago Abraira

IV.5. Recovery Stress and Work Output in Hyperbranched Poly(ethyleneimine)-Modified Shape-Memory Epoxy Polymers

David Santiago, Albert Fabregat-Sanjuan, Francesc Ferrando, Silvia De la Flor

Journal of Polymer Science Part B: Polymer Physics ***2016****, 54, 1002-1013*

UNIVERSITAT ROVIRA I VIRGILI
EXPERIMENTAL CHARACTERIZATION OF SHAPE-MEMORY POLYMERS: INFLUENCE OF PROCESSING METHODS AND CHEMICAL STRUCTURE
David Manuel Santiago Abraira

J. Polym. Sci. Part B: Polym. Phys. 2016, 54, 1002-1013

Recovery Stress and Work Output in Hyperbranched Poly(ethyleneimine)-Modified Shape-Memory Epoxy Polymers

David Santiago[1], Albert Fabregat-Sanjuan[1], Francesc Ferrando[1], Silvia De la Flor[1]

[1]Department of Mechanical Engineering, Universitat Rovira i Virgili, Av. Països Catalans 26, 43007 Tarragona, Spain

Abstract

In this study a series of hyperbranched modified shape-memory polymers were subjected to constrained shape recoveries in order to determine their potential use as thermomechanical actuators. Materials were synthesized from a diglycidyl ether of bisphenol A as base epoxy and a polyetheramine and a commercial hyperbranched poly(ethyleneimine) as crosslinker agents. Hyperbranched polymers within the structure of the shape-memory epoxy polymers led to a more heterogeneous network that can substantially modify mechanical properties. Thermomechanical and mechanical properties were analysed and discussed in terms of the content of hyperbranched polymer. Shape-memory effect was analysed under fully and partially constrained conditions. When shape recovery was carried out with fixed strain a recovery stress was obtained whereas when it was carried out with a constraining stress the material performs mechanical work. Tensile tests at $T_g^{E'}$ showed excellent values of stress and strain at break (up to 15 MPa and almost 60% respectively). Constrained recovery performances revealed rapid recovery stress generation and unusually high recovery stresses (up to 7 MPa) and extremely high work densities (up to 750 kJ/m^3). The network structure of shape-memory polymers was found to be a key factor for actuator-like applications. Results confirm that hyperbranched modified-epoxy shape

memory polymers are good candidates for actuator-like shape-memory applications.

Keywords: *epoxy, hyperbranched, hyperbranched polymers, polymers, recovery stress, shape-memory polymers, stimuli sensitive, thermosets, work output*

1. Introduction

Shape-memory polymers (SMPs) are materials that are capable of changing their shape upon application of an external stimulus [1]. They can be deformed and fixed in a temporary shape and then return to their original shape once the stimulus is applied. This effect is called the Shape-Memory Effect (SME) and it is usually thermally induced but it can also be induced by an electrical current, magnetic field or light [2-4]. SMPs have attracted a lot of interest in recent years due to their use in a wide range of applications such as self-deployable structures, temperature sensors, electronic devices or biomedical applications [5-8].

According to Liu *et al.* [9], SMPs can be classified in four different classes depending on their chemical structure and transition temperature. Among them, chemically crosslinked glassy thermosets (class I) have been extensively studied due to their high recovery and fixity ratio, high tensile modulus below the glass transition temperature and excellent rubber elasticity above the glass transition temperature [9,10]. Epoxy-based shape-memory thermosets are the most common examples of this type of SMPs. Epoxy resins are widely used in many applications (coatings, adhesives or matrices in composites) because of their chemical resistance, thermal stability and good mechanical properties [11]. However, their brittle behaviour and low elongation at break greatly limit their use as SMPs. Many studies have focused on overcoming this limitation by choosing suitable programming conditions and through material design [12-15].

J. Polym. Sci. Part B: Polym. Phys. 2016, 54, 1002-1013

Hyperbranched polymers (HBPs) have been reported to be excellent epoxy modifiers [16-19]. Our research group recently published the use of HBPs as modifiers for epoxy-based shape-memory thermosets [20]. HBPs have a densely-branched structure, which makes them less viscous than their linear counterparts of the same molecular weight, and a high concentration of surface reactive groups, that can be modified to tune their physical/chemical compatibility to a variety of matrices and substrates. Results have shown that the presence of HBPs within the network led to excellent mechanical properties, with stress at break up to 15 MPa and a failure strain of 60%. Shape-memory properties showed excellent results, with a fast recovery rate and shape recovery and shape fixity ratios up to 97% and 98%, respectively. Figure IV.5.1 presents a photo sequence of these thermally triggered SME developed by our research group [20].

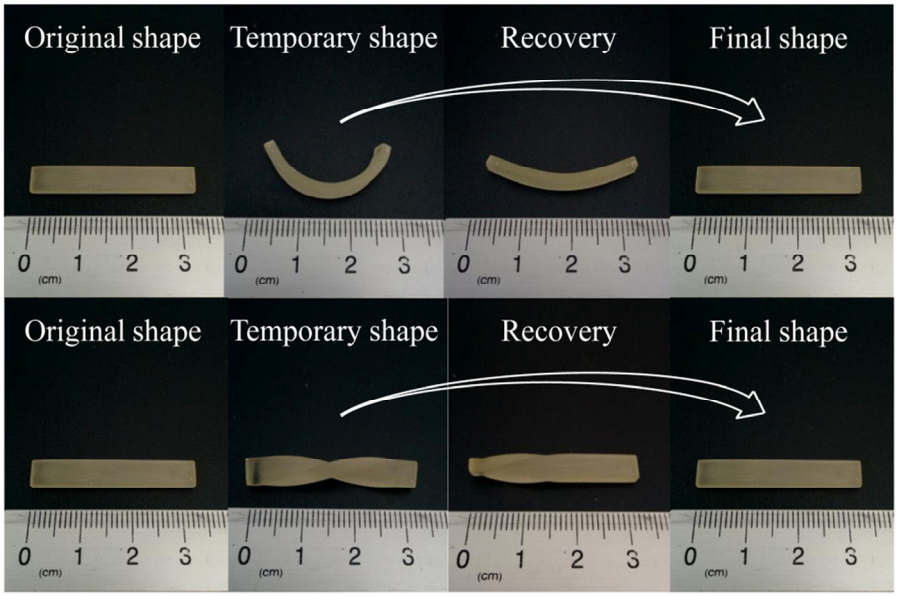

Figure IV.5.1 Photo sequence of the thermally triggered hyperbranched shape-memory polymer developed by the authors and presented in [20].

In view of these excellent mechanical and shape-memory properties, hyperbranched-modified SMPs are good candidates in mechanically demanding applications such as thermomechanical actuators [5,21,22]. However, in these kinds of application, the shape-memory effect most probably takes place under partially or fully constraining conditions. Consequently, the aim of this article is to investigate the shape recovery process under a constraining stress and under fixed strain conditions and to quantify the maximum recovery stress and the mechanical work generated in previously reported hyperbranched-modified shape-memory epoxy polymers [20].

Various articles that study shape recovery under partially or fully constraining conditions can be found in the literature. Yakacki *et al.* [23] evaluated the effect of polymer structure on free and constrained recovery in photopolymerized shape-memory thermosets. The authors reported that fully constrained recoveries were governed by the crosslinking density of the networks. Cui *et al.* [24] studied the relationship between programming parameters and shape-memory properties, including the maximum recovery stress, on neat and microparticles-modified aliphatic polyether urethane. Arrieta *et al.* [25] studied the effect of different experimental parameters on the free and totally constrained recoveries of a shape-memory acrylate-based polymer. These authors reported the ideal conditions for enhancing the recovery stress generation. Rapp and Baier [26] presented an experimental procedure to evaluate the work density using a closed-loop force-controlled thermomechanical procedure. This study concluded that for moderate maximum strains, better results are obtained when the SMPs are programmed in compression rather than in tension due to the superposition of the thermal expansion and the shape-memory effect. Kolesov *et al.* [27] reported the mechanical work generated by ethylene-1-octenecopolymers with different degrees of branching. The authors stated that the work output can be used as a shape-memory characteristic

of practical relevance. Lakhera *et al.* [28] studied partially constrained shape recovery on acrylate-based shape-memory polymers and evaluated the work per unit volume performed and the efficiency of the process. The work output increased as the rubbery modulus increased and the highest efficiency was obtained when the materials had recovered approximately half the initial deformation under constraining stress.

Accordingly, the effects of crosslinking density and thermomechanical experimental parameters on constrained shape recovery have been thoroughly investigated. However, the presence of HBPs within the shape-memory network requires a separate study due to their particular structure. In this article, partially and fully constrained shape recovery processes are studied using previously reported shape-memory epoxy thermosets modified with a commercial hyperbranched poly(ethyleneimine) and an aliphatic polyetheramine as crosslinker agents. The article evaluates the recovery stress generation during fully constrained shape recovery and the work output generation during partially constrained recovery and analyses and discusses the effect of the hyperbranched structure within the network. The presence of HBPs leads to excellent mechanical and shape-memory properties, which in turn means that they can act as excellent thermomechanical actuators.

2. Experimental Methods

2.1 Materials

Diglycidyl ether of bisphenol A (Araldite GY 240, Huntsman) with a weight per epoxy equivalent of 182 g/mol was used as the base epoxy resin (Figure IV.5.2a). The crosslinking agents used were a commercial hyperbranched poly(ethyleneimine) (Lupasol® FG, BASF) with M_w = 800 g/mol and a ratio of primary:secondary:tertiary amines of 1:0.82:0.53 (Figure IV.5.2b) and an aliphatic diamine (Jeffamine® D400, Huntsman) with M_w = 430 g/mol (Figure IV.5.2c). All data are obtained from the supplier. The molecular mechanism of the epoxy-amine condensation is

showed in Figure IV.5.3a and the final structure of the hyperbranched-modified epoxy shape-memory network is showed in Figure IV.5.3b.

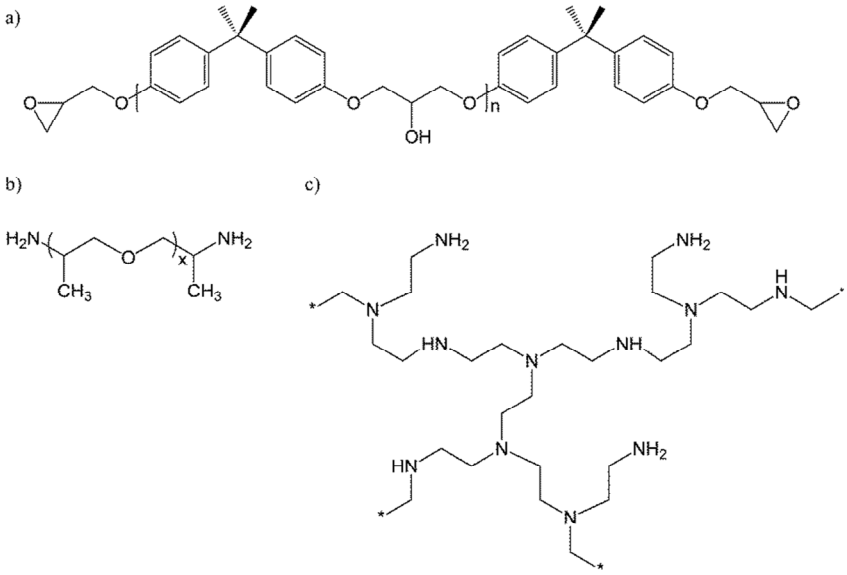

Figure IV.5.2 a) Chemical structure of DGEBA (n = 0.08); b) chemical structure of Jeffamine® D400 (x ≈ 6.1); c) chemical structure of Lupasol® FG.

J. Polym. Sci. Part B: Polym. Phys. 2016, 54, 1002-1013

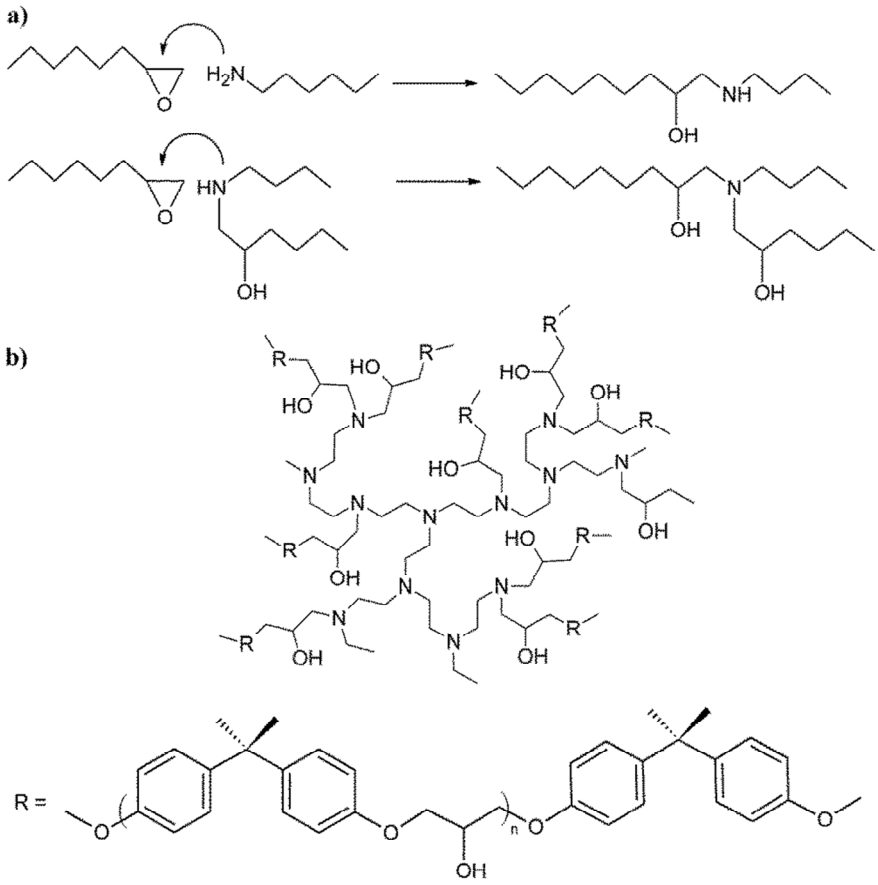

Figure IV.5.3 a) Simplified scheme of the epoxy-amine condensation mechanism and b) the final structure of the hyperbranched-modified shape-memory polymer.

Various formulations were prepared with different contents of diglycidyl ether of bisphenol A (DGEBA), Jeffamine® D400 (D400) and Lupasol® FG (LP800) (Table IV.5.1). The proportions of reactants in each formulation were selected to obtain a molecular structure made up of stoichiometric DGEBA-D400 and DGEBA-LP800 networks. The sample nomenclature XD400-YLP used in Table IV.5.1 indicates the weight fraction of the stoichiometric DGEBA-D400 (X) and DGEBA-LP800 (Y) networks. This study looked at only three of the previously

reported formulations [20]. In order to study the effect of the Lupasol® content on the network, formulations with the lower, intermediate and higher LP content were chosen (90D400-10LP, 60D400-40LP and 30D400-70LP respectively). The crosslinking density ν_c is calculated assuming that all amine groups turn into crosslinks using the following expression:

$$\nu_c\,(\text{mol/g}) = \frac{m_{D400}\cdot\left(eqN_{D400}/\text{g}\right) + m_{LP800}\cdot\left(eqN_{LP800}/\text{g}\right)}{m_T} \qquad \text{(IV.5.1)}$$

where m_{D400} is the mass of Jeffamine® D400, $\left(eqN_{D400}/\text{g}\right)$ is the total amine in Jeffamine® D400 (0.0041-0.0047 eqN/g), m_{LP800} is the mass of Lupasol® FG and $\left(eqN_{LP800}/\text{g}\right)$ is the total amine in Lupasol® FG (0.0231 eqN/g) calculated using the ratio previously indicated.

Table IV.5.1 Composition of the formulations studied. ν_c is the crosslinking density calculated assuming that all amine groups turn into crosslinks

Sample	wt. % DGEBA	wt. % D400	wt. % LP800	D400:LP800 amine ratio[a]	ν_c (mol/g)
90D400-10LP	63.5	34.8	1.7	4.010	0.001915
60D400-10LP	70.2	23.2	6.6	0.668	0.002551
30D400-70LP	76.8	11.6	11.6	0.191	0.003187

[a] Total primary, secondary and tertiary amine groups present in the crosslinking agent.

The components were mixed manually in a glass vial and then poured into an open mould covered with Teflon to avoid the presence of bubbles and to facilitate sample release. The samples were cured for 2h at 120 ºC and then slowly cooled to room temperature inside the oven. This curing time was optimized on the basis of differential scanning calorimetry. To do so it was necessary to determine the time needed to

ensure the complete disappearance of any exothermic peak related to residual crosslinking reactions. The samples were then polished with sandpaper to obtain uniform final dimensions.

2.2 Thermomechanical Characterization

The thermomechanical properties were evaluated using a DMA Q800 (TA Instruments) equipped with a 3-point bending clamp. Prismatic rectangular samples of ca. 30 mm x 5.5 mm x 2.5 mm were analysed from 30 ºC to 150 ºC at 1 Hz, 0.1% strain and a heating rate of 3 ºC/min. The glass transition temperature was determined from the peak in tan δ. The values of storage modulus *E'* below and above glass transition were evaluated. The onset of the glass transition temperature $T_g^{E'}$ was determined as the onset in the storage modulus decrease during mechanical relaxation. According to Yakacki *et al.* [29], a peak in the deformability of shape-memory acrylate-based polymer can be obtained at a temperature coinciding with the onset of the glass transition temperature. Feldkamp and Rousseau [12] demonstrated that this phenomenon is also present in epoxy-based networks.

The coefficient of thermal expansion (CTE) was measured using a TMA/SDTA 840 (Metler Toledo). Samples of ca. 3 mm x 3 mm x 2 mm were analysed with a contact force of 0.01 N from 30 ºC to T_g + 30 ºC at a heating rate of 3 ºC/min. Three different samples were subjected to two consecutive heating-cooling processes in order to erase thermal history. The CTE was defined as the slope of the curve. The average value of the CTE in glassy and rubbery state was determined.

2.3 Mechanical Properties

The mechanical properties at $T_g^{E'}$ were measured using a DMA Q800 equipped with a film-tension clamp in force-controlled mode. Prismatic rectangular samples of ca. 20 mm x 2.5 mm x 0.5 mm were analysed at $T_g^{E'}$ at a force rate of 1 N/min. In both experiments, strain was calculated

as the total elongation (L_f - L_0) (displacement of the crosshead) with respect to the initial length (L_0) (Equation IV.5.2).

$$\varepsilon(\%) = \frac{L_f - L_0}{L_0} \cdot 100 \qquad \text{(IV.5.2)}$$

2.4 Shape-Memory Properties

The shape-memory properties were measured using a DMA Q800 (TA Instruments) with a force-controlled mode and equipped with a film-tension clamp. Prismatic rectangular samples of ca. 20 mm x 2 mm x 0.5 mm were used in the shape-memory performances. The method for creating a temporary shape and triggering the shape-memory effect is a thermomechanical procedure called 'programming'. The programming consists of various steps and can be carried out under stress free conditions (Figure IV.5.4 and Figure IV.5.5, path 1-4a) or under constrained conditions (Figure IV.5.4 and Figure IV.5.5, path 1-4b). The programming under stress free conditions was carried out by heating the sample to the programming temperature T_{prog} and deforming it to a prescribed value of maximum stress σ_m. In this stage the deformation of the sample was ε_m. The next step was to cool it to a low temperature T_{low} below the transition temperature in order to fix the temporary shape. After fixation the stress was released (σ_0 = 0) and the deformation of the sample was ε_u. The shape-memory effect was triggered by heating the sample to a recovery temperature $T_{recovery}$, which is above the transition temperature.

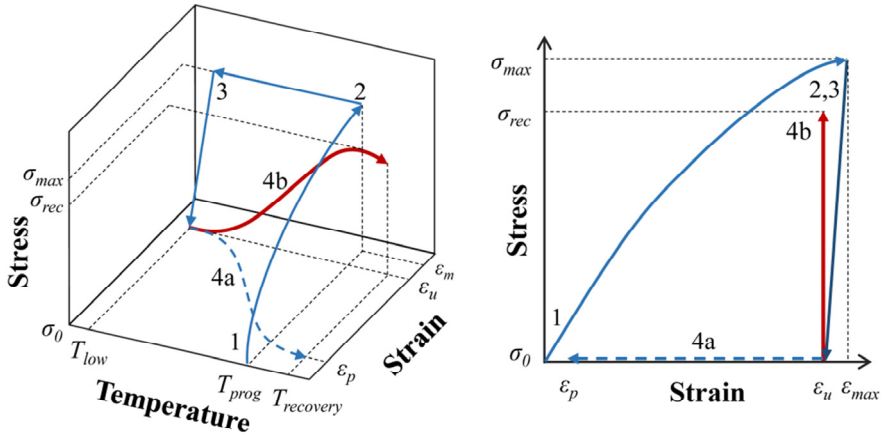

Figure IV.5.4 Schematic representation of the thermomechanical programming under free recovery conditions (dashed line) and under fully constrained conditions, which generates a recovery stress (solid line).

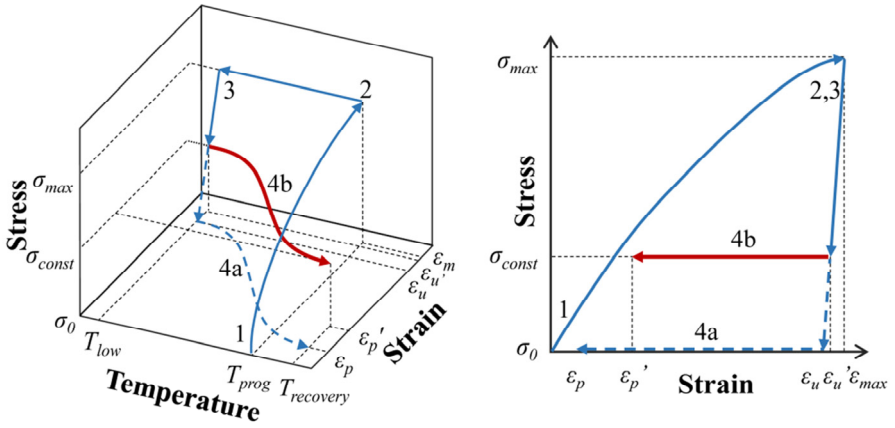

Figure IV.5.5 Schematic representation of the thermomechanical programming under free recovery conditions (dashed line) and under partially constrained conditions, which generates mechanical work (solid line).

The programming under constrained conditions is different depending on whether the aim is to determine recovery stress (Figure IV.5.4, path 1-4b) or mechanical work (Figure IV.5.5, path 1-4b). In order to evaluate recovery stress, the deformation after unloading ε_u was held constant while the sample was heated to the recovery temperature $T_{recovery}$. The recovery stress increased as the temperature increased to a maximum value noted as σ_{rec}. To evaluate the mechanical work, the sample was not unloaded to σ_0 during the unloading stage but it was unloaded to a constraining stress σ_{const}. The constraining stress was held constant while the sample was heated to $T_{recovery}$ and the strain recovered under constraining stress $\varepsilon_u' - \varepsilon_p'$ was measured. The work calculated during the constrained recovery was the work performed per unit volume (kJ/m^3) and it was calculated using Equation IV.5.3:

$$W_a(\mathrm{kJ/m^3}) = \sigma_{const} \cdot (\varepsilon_u' - \varepsilon_p') \qquad \text{(IV.5.3)}$$

In the experiments to determine recovery stress, five different maximum stresses were chosen (2, 4, 6, 8 and 10 MPa) in order to analyse how maximum applied stress during path 1-2 of the programming affected recovery stress generation. In the experiments performed to determine the mechanical work, the maximum stress applied during programming was chosen as 0.75 of the stress at break in order to perform a comparative study with the same level of load for each sample. Four different constraining stresses (σ_{const}) were chosen: 20, 40, 60 and 80% of the maximum stress applied to deform the sample during deformation stage. The programming temperature T_{prog} was chosen as the onset of the glass transition temperature $T_g^{E'}$ for each sample in both kinds of experiment (recovery stress and mechanical work). The low temperature T_{low} was chosen as room temperature (~25 ºC) and the heating rate during recovery was 3 ºC/min. The deformation rate chosen during the loading and unloading stages was 1 MPa/min.

3. Results and Discussion

3.1 Thermomechanical Properties

Thermomechanical results are summarized in Table IV.5.2 and Figure IV.5.6. The glass transition temperatures can be controlled by varying chemical composition. T_g's are 60, 87 and 117 ºC for formulations 90D400-10LP, 60D400-40LP and 30D400-70LP respectively. A higher LP800 content implies a higher crosslinking density (Table IV.5.1) because of the higher number of reactive amine groups per unit mass and the presence of internal branching points. This leads to a decrease in the average chain length between netpoints and a more restricted molecular mobility, thus increasing the T_g. As Table IV.5.2 and Figure IV.5.6 show, an increase in LP800 also causes a lowering and a broadening of the peak of tan δ. LP800 leads to a more heterogeneous network structure due to the inherently dispersed nature of the hyperbranched poly(ethyleneimine) and the presence of different types of crosslinks coming from the pre-existing tertiary amines and reacted primary and secondary amines of LP800. The decrease in tan δ peak and area when the amount of LP800 increases is also indicative of a more densely crosslinked network with restricted mobility.

All formulations show very high values of storage modulus at the glassy region around 3 GPa (Table IV.5.2 and Figure IV.5.6), which is higher than most of the shape-memory epoxy resins found in the literature. The storage modulus at rubbery region E'_r increases as the LP800 content increases. According to the theory of rubber elasticity, E'_r is roughly proportional to the crosslinking density and it is therefore expected to increase in line with the crosslinking density (Table IV.5.2). However, the hyperbranched structure of LP800 can cause mobility restrictions due to the high number of internal branching points and very short ethylene segments within. In contrast to the long, flexible aliphatic structure of Jeffamine®, one can expect mobility restrictions and lower

deformability as the LP800 content in the cured thermosets is increased [30].

Table IV.5.2 Thermomechanical data obtained by DMA: glass transition temperature (T_g), onset temperature of the glass transition temperature (T_g^E), storage modulus at glassy and rubbery regions (E'_g and E'_r respectively)

Sample	T_g [a] [ºC]	$T_g^{E'}$ [ºC]	tan δ peak	FWHM [b] [ºC]	tan δ area [c] [ºC]	E'_g [d] [MPa]	E'_r [e] [MPa]	$\frac{E'_g}{E'_r}$
90D400-10LP	60	50	0.96	15.45	14.83	2878	16	183
60D400-40LP	87	71	0.62	21.11	13.09	3149	29	110
30D400-70LP	117	98	0.41	24.58	10.08	2858	52	55

[a] measured as the peak of tan δ
[b] full width at half maximum
[c] determined as the product of tan δ peak and FWHM
[d] measured at T_g – 40 ºC
[e] measured at T_g + 40 ºC

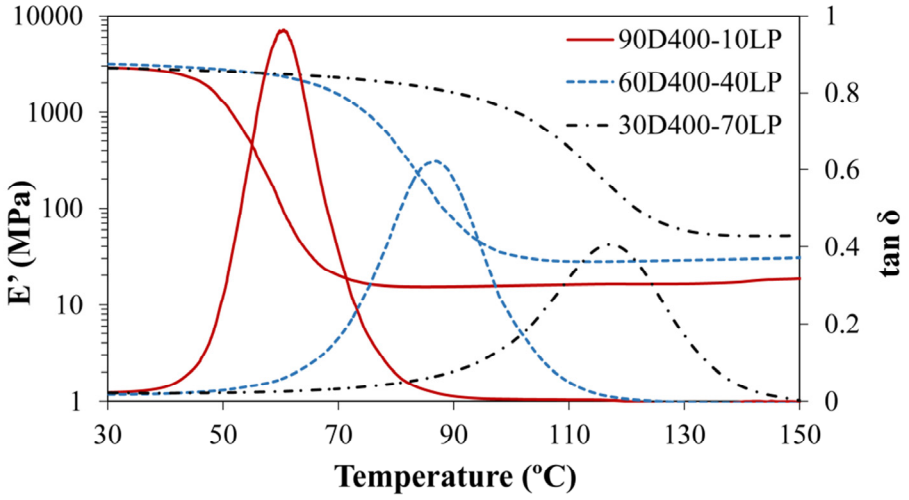

Figure IV.5.6 Storage modulus E' and tan δ as a function of temperature for each formulation.

In order to analyse the effect of thermal expansion during heating, the coefficient of thermal expansion (CTE) was evaluated. Table IV.5.3

J. Polym. Sci. Part B: Polym. Phys. 2016, 54, 1002-1013

shows the CTE in the glassy and rubbery region. The CTE in glassy region slightly decreases from $101x10^{-6}$ to $86x10^{-6}$ 1/ºC as the content of LP increases. With a higher content of hyperbranched polymer the molecular motion is more restricted and thus the volume gained during heating is lower. The CTE in the rubbery region is more than two times the CTE in the glassy region. This is caused by the increase in the free-volume when heated above the T_g. The impact of thermal expansion on fully constrained recoveries will be discussed in later sections.

Table IV.5.3 Average value of the coefficient of thermal expansion (CTE) for each formulation

Sample	90D400-10LP	60D400-40LP	30D400-70LP
CTE glassy region ($^oC^{-1}$ x 10^{-6})	101±2	91±1	86±2
CTE rubbery region ($^oC^{-1}$ x 10^{-6})	204±3	193±2	201±1

3.2 Mechanical Properties

Table IV.5.4 shows the mechanical properties evaluated at $T_g^{E'}$. All formulations show very high values of stress at break, around 12 MPa for 90D400-10LP and 60D400-30LP and 15 MPa for formulation 30D400-70LP. Tensile modulus reveals a more rigid network with increasing LP800 content, which implies a decrease in strain at break: from 58% for 90D400-10LP to 17% for 30D400-70LP.

The tensile modulus values shown in Table IV.5.4 correlate well with the relaxed modulus of the materials shown in Table IV.5.2. Although the behaviour of the material is not at all comparable in small/oscillatory and large/tensile deformation experiments, this is consistent with the fact that $T_g^{E'}$ is a temperature at which the material is already relaxed or has a relatively short relaxation time in comparison with the timescale of the tensile experiment. Generally speaking, an

increase in the crosslinking density results in a less mobile and ductile network, leading to a lower failure strain and a higher stress at break on a macroscopic level, as reported in Table IV.5.4. These results can be explained by taking into account the internal hyperbranched structure of LP800 with short ethylene segments within, with lower deformability than the long, flexible Jeffamine® structure.

Table IV.5.4 shows that by lowering the LP800 content, the elastic energy density stored before break can be increased (with a maximum value of $3.7x10^3$ kJ/m^3). This stored elastic energy density is an important metric of shape-memory behaviour because it provides an estimated upper boundary for recoverable elastic energy; that is, the material's capability to perform mechanical work against external loads in the recovery stage. The ability of SMPs to stabilize deformed shapes and perform mechanical work upon shape recovery is limited by the strength and density of the bonds created during shape stabilization. Consequently, reducing crosslinking density helps to improve this capability. Formulation 90D400-10LP showed the highest elastic energy density ($3.7x10^3$ kJ/m^3), which decreases to $1.3x10^3$ kJ/m^3 in formulation 30D400-70LP.

Table IV.5.4 Tensile data $T_g^{E'}$ obtained by uniaxial tensile testing: stress at break (σ_b), deformation at break (ε_b), elastic energy density and tensile modulus

Sample	σ_b (MPa)	ε_b (%)	Elastic energy density (kJ/m^3)	Tensile modulus (MPa)
90D400-10LP	12.7	58.0	$3.7x10^3$	19.6
60D400-40LP	12.3	29.5	$1.8x10^3$	38.4
30D400-70LP	15.4	17.2	$1.3x10^3$	84.4

3.3 Recovery Stress Quantification

This section studies the recovery stress generation during fully constrained shape recovery. Five different maximum prescribed stresses

were used in recovery stress performances: 2, 4, 6, 8 and 10 MPa. Figure IV.5.7a shows the shape-memory cycles with fully constrained recoveries for each maximum stress applied. For the sake of simplicity, only the cycles of formulation 90D400-10LP are represented.

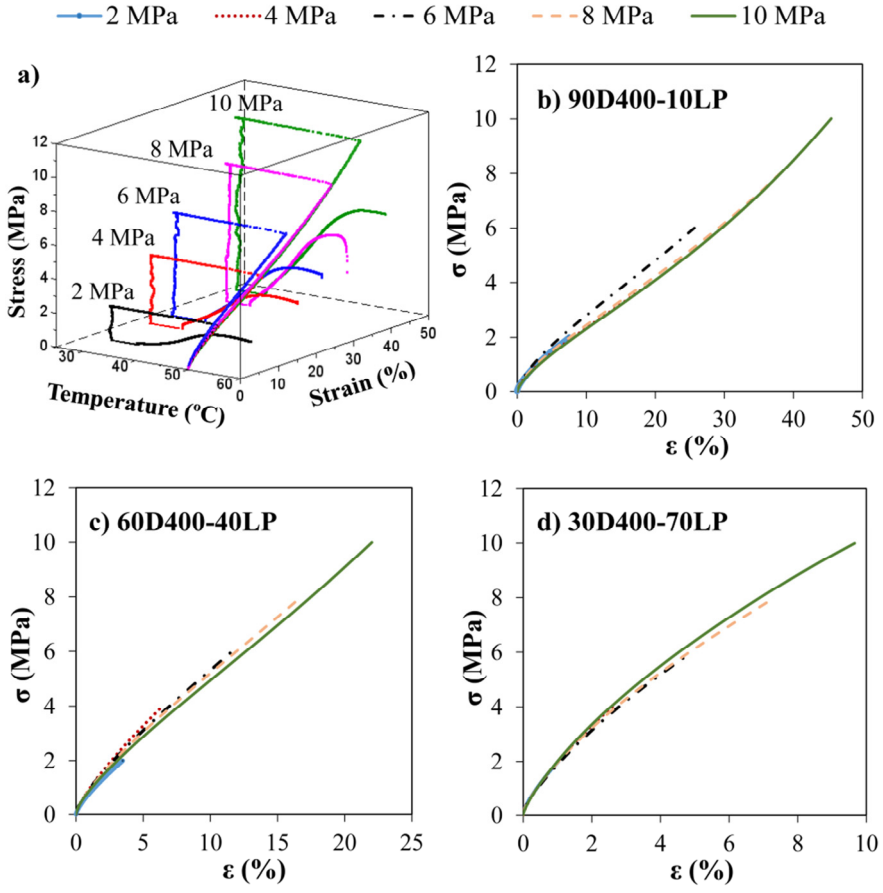

Figure IV.5.7 a) Three dimensional graphic of the fully constrained recovery process and recovery stress generation of formulation 90D400-10LP for all different σ_m; Stress-strain curves of the deforming stage during programming (step 1-2 in Figure IV.5.4 and Figure IV.5.5) in recovery stress performances for formulation 90D400-10LP (a), 60D400-40LP (b) and 30D400-70LP (c).

Figure IV.5.7b, Figure IV.5.7c and Figure IV.5.7d show the stress-strain curves of the deforming stage of programming (step 1-2 in Figure

IV.5.4) with each σ_m. As noted in section 3.2, formulations with a higher content of hyperbranched polymer present a more rigid structure and thus the deformation achieved during programming is lower.

Keeping in mind the values of stress at break at $T_g^{E'}$ for each formulation (Table IV.5.4), specific maximum prescribed stresses were selected to ensure a comparative study of the effect of σ_m within the failure limits of each formulation. With 10 MPa, formulations 90D400-10LP and 60D400-40LP were stretched to around 80% of their failure strain. For formulation 30D400-70LP, it was possible to apply higher values of σ_m; however, the other formulations could not be stretched to the same values and thus a comparative study could not be carried out.

Figure IV.5.8 shows the recovery stress generation as a function of temperature during the recovery stage of programming (step 4b in Figure IV.5.4). The recovery stress progressively increases with increasing temperature until reaching a maximum at $T_{\sigma rec}$ (indicated in Figure IV.5.8 with a cross). Two thermomechanical processes are involved in recovery stress generation during fully constrained recovery: the shape-memory effect and the thermal expansion.

Some studies have reported the influence of thermal expansion on constrained recoveries [31,32]. As the programming of the temporary shape was carried out in tension, the constrained thermal expansion produces a stress with an opposite sign to the recovery stress generated. The constrained thermal expansion stress can be observed as a compression plateau in experiments performed on formulation 30D400-70LP with σ_m = 2 and 4 MPa. While thermal expansion dominates in the low temperature range, the recovery stress shifts toward positive values due to the activation of the shape-memory effect as the temperature increases.

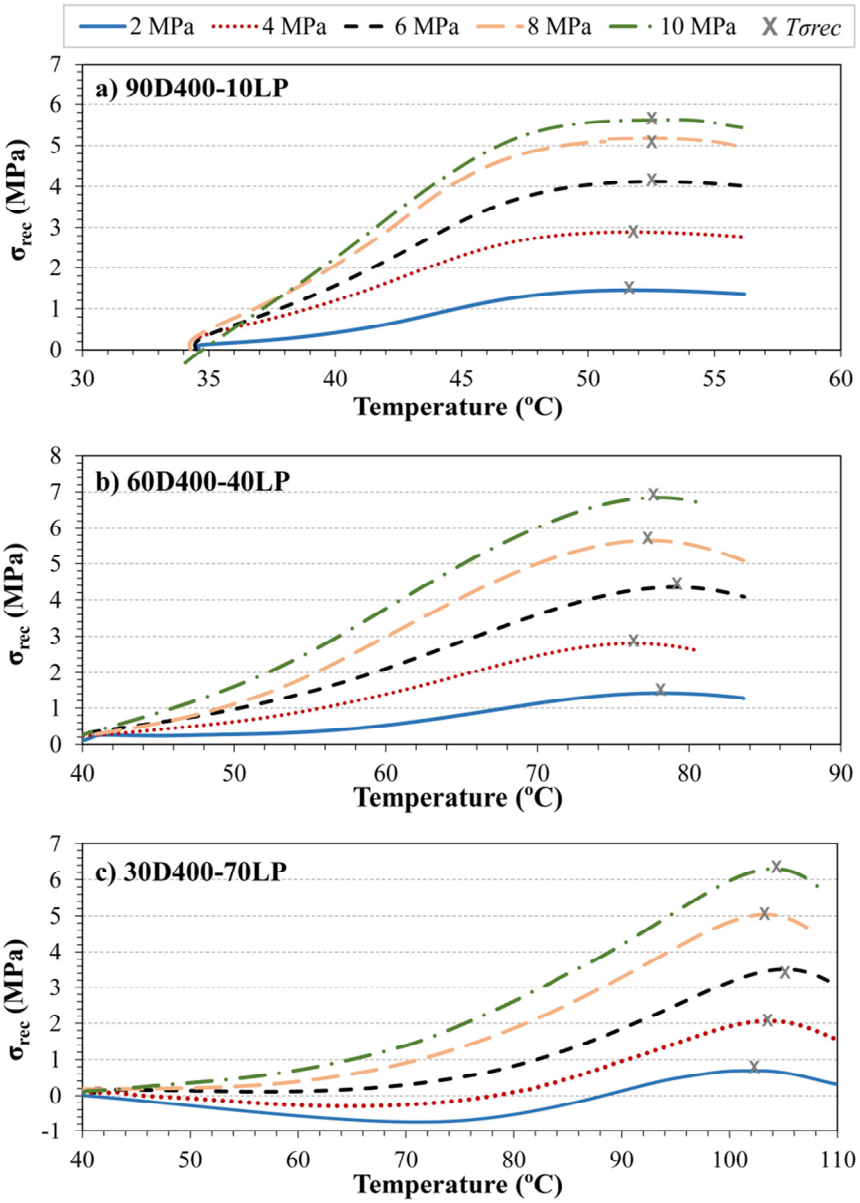

Figure IV.5.8 Recovery stress generation as a function of temperature during the recovery stage of all formulations and the temperature corresponding to maximum σ_{rec} ($T_{\sigma rec}$) indicated with a cross (X).

This effect is not observed with higher σ_m. Similar results were obtained by Arrieta et al. [25], where the compression regime disappears as the applied strain increases. As σ_m is increasing, the maximum deformation achieved during programming increases and leads to a higher chain orientation which results in a higher entropy gain during recovery stage. Thus, the progressive increase of σ_{rec} upon heating is stronger and soon surpasses the compressive stress due to thermal expansion.

Although there are barely any differences between the formulations regarding the coefficient of thermal expansion (Table IV.5.3), the compressive plateau is also absent from formulations 60D400-40LP and 90D400-10LP. The transition temperatures of such formulations are lower than in formulation 30D400-70LP and thus the stress generation begins at lower temperatures and the recovery stress overrides the compressive stress, even at lower temperatures.

Table IV.5.5 lists the temperatures at which the maximum recovery stresses are obtained ($T_{\sigma rec}$), the programming temperature of each formulation T_{prog} and the switching temperature T_{sw} in free recovery conditions. An almost linear relationship between $T_{\sigma rec}$ and T_{prog} was found. The ratio between $T_{\sigma rec}/T_{prog}$ presents very similar values for all formulations: 1.02, 1.09 and 1.06 for formulations 90D400-10LP, 60D400-40LP and 30D400-70LP respectively.

The switching temperatures (T_{sw}) of free recovery performances were obtained as the inflexion point in the strain-temperature curve during shape recovery [20] and mark the beginning of shape recovery. The recovery stress generation in constrained recovery begins at temperatures much lower than in free recovery (Figure IV.5.8). For example, with formulation 90D400-10LP, a recovery stress is obtained at a temperature 15 ºC below the glass transition temperature (60 ºC), which is equal to 50% of the maximum programming stress. This result has important implications for the design of applications because it makes it

possible to quickly generate recovery stress even at temperatures lower than the glass transition temperature of the materials.

Table IV.5.5 Programming temperature T_{prog}, average maximum recovery stress temperature $T_{\sigma rec}$ of each formulation and switching temperature T_{sw}

Sample	90D400-10LP	60D400-40LP	30D400-70LP
T_{prog} [a] (ºC)	50	71	98
$T_{\sigma rec}$ [b] (ºC)	52	78	104
T_{sw} [c] (ºC)	50	70	98

[a] $T_{prog} = T_g^{E'}$
[b] Average value of $T_{\sigma rec}$
[c] T_{sw} obtained as the inflection point in strain-temperature curve during free shape recovery obtained from [20]

Figure IV.5.9 shows the maximum recovery stress σ_{rec} generated during the fully constrained recovery stage as a function of the maximum applied stress σ_m during programming. In each formulation σ_{rec} increases as σ_m increases. As σ_m increases, the maximum deformation acquired during programming increases and leads to a higher chain orientation which results in a higher entropy gain during recovery stage [24]. Thus, the maximum recovery stress increases and reaches values of almost 7 MPa in formulation 60D400-40LP. Some authors have reported maximum recovery stress values during fully constrained recovery in SMPs programmed in tension mode, but values as high as those reported in the present paper are not found in the literature. Arrieta *et al.* [25] reported recovery stress of around 6 MPa in an acrylic based shape-memory polymer pre-strained to 55%. Ortega *et al.* [33] reported recovery stress of almost 4 MPa in (meth)acrylated based shape-memory polymers. Cui *et al.* [24] reported values of 3.7 MPa in a polyether urethane modified with 20% of $BaSO_4$ microparticles.

Such high values of recovery stress presented in Figure IV.5.9 come from a combination of high maximum stress applied during the programming of the temporary shape and the high driving recovery

forces exercised by the crosslinked network in comparison with other SMPs. On one hand, the high values of breaking stress of these materials (Table IV.5.4) enable the application of high maximum stresses σ_m (up to 12 MPa) and thus obtaining such good values of recovery stress. On the other hand, if one bears in mind the structure of the hyperbranched poly(ethyleneimine), the presence of different types of crosslinks can be found within its structure, coming from the reacted primary and secondary amine and the pre-existing tertiary amines. Some of these crosslinking points are connected by short aliphatic structures, which lead to zones with a high crosslinking density. This generates high local concentrations of branching points within the structure of the polymer which may produce higher driving forces than those produced by conventional shape-memory epoxy polymers.

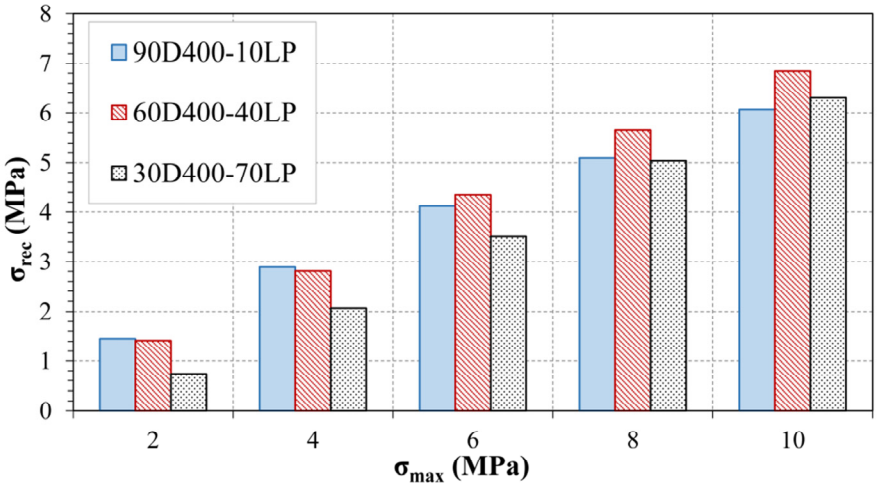

Figure IV.5.9 Maximum recovery stress developed: σ_{rec} as a function of the maximum stress σ_m of each formulation.

In Figure IV.5.9, with low values of σ_m (2 and 4 MPa), formulation 90D400-10LP shows the highest values of σ_{rec} However, with σ_m = 6 MPa to 10 MPa, formulation 60D400-40LP shows higher values of σ_{rec} than formulation 90D400-10LP; and with σ_{rec} = 10 MPa formulation 30D400-

70LP shows higher σ_{rec} than formulation 90D400-10LP. Some studies have shown that crosslinking density is the governing factor in recovery stress generation due to the larger driving entropy recovery forces [23,33]. However, it seems that with low levels of deformation, the higher molecular mobility of formulation 90D400-10LP overrides the higher crosslinking density of formulations 60D400-40LP and 30D400-70LP. With increasing values of σ_m the crosslinking density acquires more importance and the entropy recovery forces predominate over the ease of movement of more homogeneous networks.

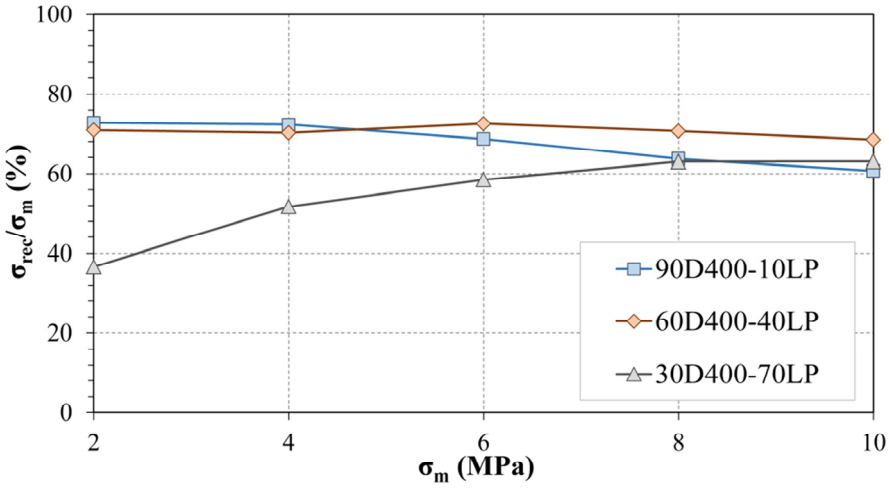

Figure IV.5.10 σ_{rec}/σ_m ratio as a function of the maximum stress applied during programming of each formulation.

Figure IV.5.10 clearly shows the tendency mentioned above. This figure plots the ratio of the maximum recovery stress σ_{rec} to the maximum stress applied σ_m (σ_{rec}/σ_m) as a function of the maximum stress applied. The formulation 90D400-10LP shows a high σ_{rec}/σ_m ratio (around 73%) with σ_m = 2 MPa, which decreases to σ_{rec}/σ_m = 61% with σ_m = 10 MPa; formulation 60D400-40LP shows a constant ratio around 70% and formulation 30D400-70LP shows an increasing ratio from 34% to 63% with increasing σ_m.

It should be taken into account that in order to enhance the recovery stress, the closer to failure that the SMPs are programmed the greater the recovery stress generation. For example, formulation 30D400-70LP can support higher σ_m and thus obtain higher σ_{rec}. Moreover, for those applications in which SMPs have to work under fully constrained conditions, a compromise should be reached between crosslinking density, which exerts sufficient driving recovery force, and a sufficiently homogeneous network that allows molecular mobility.

3.4 Work Output

The present section studies the mechanical work output during shape recovery with different constraining stresses. In order to perform a comparative study with the same level of load for each sample, each sample was stretched during shape-memory programming to a prescribed maximum stress (σ_m) corresponding to 75% of the stress at break ($\sigma_m = 0.75 \cdot \sigma_b$). Table IV.5.6 lists the prescribed maximum stress, σ_m, and the corresponding maximum deformation reached, ε_m, for each material.

Table IV.5.6 Prescribed stress for shape-memory programming (σ_m) and strain corresponding to σ_m (ε_m) for work output performances

Sample	σ_m (MPa)	ε_m (%)
90D400-10LP	10	46
60D400-40LP	9	20
30D400-70LP	12	11

Figure IV.5.11a shows the shape-memory cycles with partially constrained recoveries for each constraining stress applied. For the sake of simplicity, only the cycles of formulation 90D400-10LP are represented.

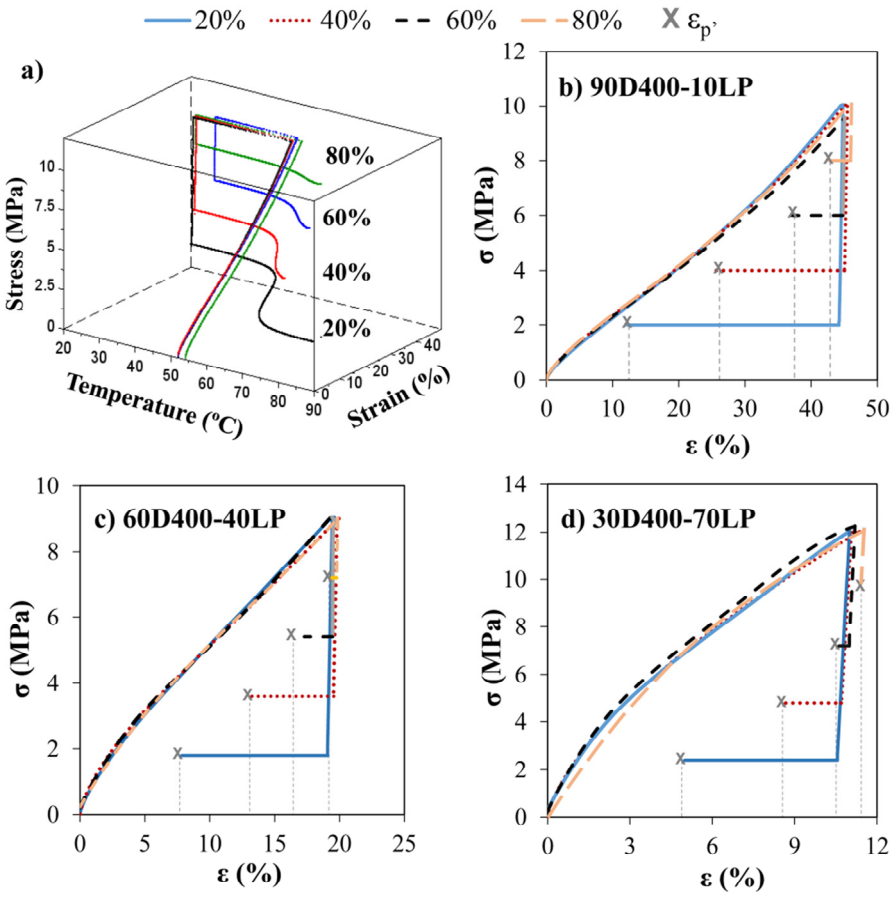

Figure IV.5.11 a) Three dimensional graphic of the partially constrained recovery and mechanical work generation of formulation 90D400-10LP; partially constrained shape-memory programming of formulation 90D400-10LP (a), 60D400-40LP (b) and 30D400-70LP (c).

Figure IV.5.11b-d show shape recovery processes under different constraining stresses for each formulation. Four different constraining stresses were selected which correspond to 20, 40, 60 and 80% of the maximum prescribed stress applied during programming. The parameter used to quantify shape recovery is the shape recovery ratio R_r, which was calculated using Equation IV.4.4. Note that R_r was calculated with the irrecoverable deformation at the end of the partially constrained

recoveries ε_p'. This value is indicated in Figure IV.5.11b, Figure IV.5.11c and Figure IV.5.11d with a cross for a better clarity.

$$R_r(\%) = \frac{\varepsilon_m - \varepsilon_p'}{\varepsilon_m} \qquad \text{(IV.4.4)}$$

Figure IV.5.12 shows the shape recovery ratio as a function of the constraining level for all formulations. As expected, the shape recovery ratio decreases with increasing constraint. However the decrease on shape recovery is more acute the greater the presence of hyperbranched polymer within the network. While the formulation 90D400-10LP still showed an R_r = 20% with 60% of constraint, in formulation 60D400-40LP this falls to R_r = 10% and in formulation 30D400-70LP it was almost R_r = 0%.

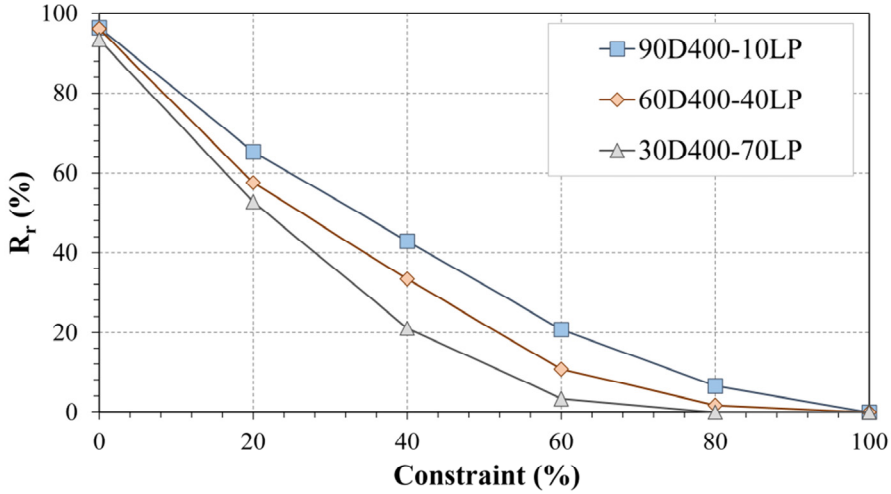

Figure IV.5.12 Shape recovery ratio as a function of the constraining level in each formulation.

The R_r values of these materials under free recovery conditions (constraint = 0%) were obtained from a previous study [20]. Although some studies have indicated the influence of crosslinking density on shape-memory properties [34,35], we conclude that network relaxation

dynamics rather than the theoretical crosslinking density is the key parameter governing the shape-memory properties, including shape recovery, shape fixity and shape recovery rate. The heterogeneous structure of the HBP, which contains short ethylene segments, means that it has restricted molecular dynamics which may even adversely affect shape recovery. This was observed when the shape recovery ratio decreased as the Lupasol® content within the network increased. The application of both constraining stress and a higher content of Lupasol® may be the reason why the shape recovery ratio in formulation 60D400-40LP and, above all, in formulation 30D400-70LP falls so drastically as the level of constraint is increased.

Figure IV.5.13 shows the results of work output for each formulation. It should be noted that there is no work output when the recovery is performed under free conditions, because there is no constraining stress $\sigma_{const} = 0$, or under fully constrained conditions, because there is no recovery $\varepsilon_u' - \varepsilon_p' = 0$. W_a increases from zero to a maximum and then decreases to zero again. The peak is observed when the constraint is 40% of the maximum stress applied in formulations 90D400-10LP but it shifts toward lower values of constraint, to 20% in formulation 30D400-70LP. This shift from the maximum toward lower values of constraint might be due to the fall in shape recovery as the LP content increases (Figure IV.5.12).

Formulation 90D400-10LP shows the highest values of work density (750 kJ/m^3). To the best knowledge of the authors, values as high as these have not been recorded in the literature. Lakhera *et al.* [28] reported values of almost 300 kJ/m^3 in compression programmed acrylate-based thermosets; Rapp and Baier [26] reported 280 kJ/m^3 in polystyrene-based Veriflex®; and Kolesov *et al.* [27] reported 175 kJ/m^3 in ethylene-1-octenecopolymers. Such high values of formulation 90D400-10LP come from a combination of excellent mechanical and shape-memory properties. The high stress and deformation at break (almost 13

MPa and 60% respectively) and the excellent shape recovery ratio (96%) allow the application of high constraining stresses and recovery from a large amount of deformation.

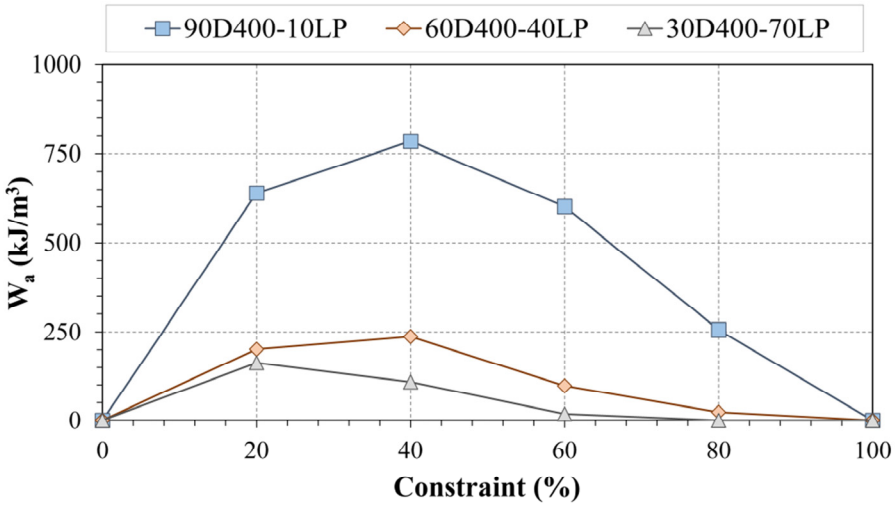

Figure IV.5.13 Work output as a function of the constraining level of all formulations.

The absolute value of work output is larger in formulations with lower HBP content because the corresponding deformation when stretched at σ_m is higher and thus so too is the deformation recovered. Therefore it is necessary to quantify the efficiency of the work output process. To do so, the ratio of work generated during partially constrained recovery W_a to the work required to program the sample W_p was determined. W_p was calculated using Equation IV.5.5:

$$W_p(\mathrm{kJ/m^3}) = \sigma_m \cdot \varepsilon_m \qquad \text{(IV.5.5)}$$

Figure IV.5.14 shows the W_a/W_p ratio as a function of the constraining level of all formulations. The shape of the curve of W_a/W_p is the same as W_a, showing a maximum of 40% for formulations 90D400-10LP and 60D400-40LP and 20% for formulation 30D400-70LP.

Formulation 90D400-10LP shows the highest W_a/W_p ratio, with a peak of 17%, and decreases as the content of LP increases. This trend may be explained by different shape recovery behaviours between formulations (Figure IV.5.12). The ability to recover deformation against a constraining stress is lower in formulations with higher HBP content and thus the ability to perform mechanical work during a partially constrained recovery is limited. Network homogeneity emerges as a critical factor in mechanical work output.

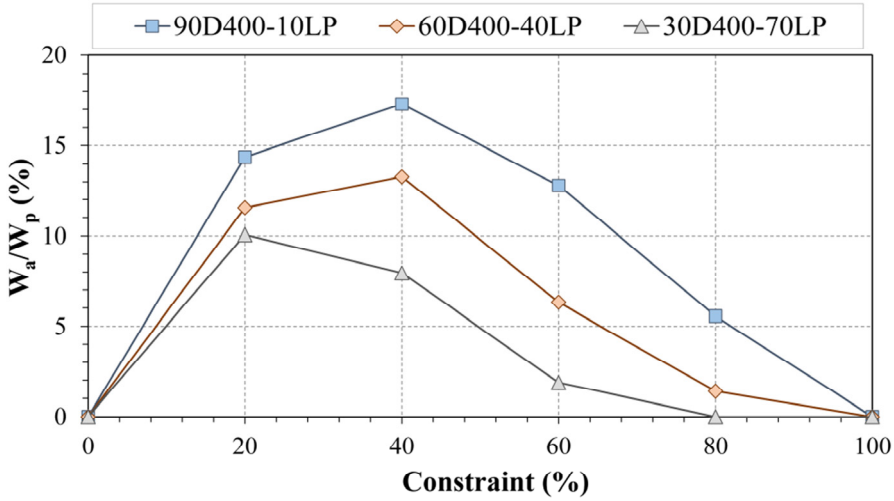

Figure IV.5.14 Ratio of work generated W_a to the work required to program the sample W_p.

Conclusions

Partially and fully constrained shape-memory recovery performances were performed on hyperbranched-modified shape-memory epoxy thermosets. The effect that the network structure, the maximum programming stress and constraining stress have on the recovery stress and work output were analysed and discussed.

The maximum recovery stress generated during fully constrained recovery increased as the maximum stress applied during programming

increased, until it reaches the unusually high values of almost 7 MPa for formulation 60D400-40LP when programmed to σ_m = 10 MPa. The thermal expansion of the sample submitted at fixed strain shape recovery produced undesirable compressive stresses at lower maximum applied stress. A compromise between crosslinking density and a homogeneous network needs to be reached in order to guarantee sufficient driving recovery force and to allow molecular mobility.

The application of constraining stress during shape recovery caused a drastic fall in the shape recovery ratio. This decrease was more acute in formulations with a higher content of hyperbranched polymer due to their lower molecular mobility. This shifted the maximum work generated toward lower constraining levels and decreased the efficiency of the process. The work density performed during partially constrained recovery showed remarkably high values of more than 750 kJ/m^3. The network structure plays an important role in work output performances.

According to the results obtained, the molecular morphology of SMPs that are intended for use as thermomechanical actuators must be thoroughly studied to ensure both high recovery forces and sufficient molecular mobility. Hyperbranched poly(ethyleneimine)-modified shape-memory epoxy thermosets are promising materials for actuator-like applications. By correctly selecting the chemical composition either high recovery stress or high mechanical work can be achieved.

Acknowledgement

The authors would like to thank MINECO (Ministerio de Economía y Competitividad) (MAT2014-53706-C03-01) and Generalitat de Catalunya (2014-SGR-67) for giving financial support.

References

[1] A. Lendlein and S. Kelch, *Angew. Chem. Int. Ed.* **2002**, *41*, 2034–2057.

[2] S. Chen, S. Yang, Z. Li, S. Xu, H. Yuan, S. Chen, and Z. Ge, *Polym. Compos.* **2015**, *36*, 439–444.

[3] D. Yang, W. Huang, X. He, and M. Xie, *Polym. Int.* **2012**, *61*, 38–42.

[4] A. Lendlein, H. Jiang, O. Jünger, and R. Langer, *Nature*, **2005**, *434*, 879–882.

[5] D. W. Zhang, J. J. Zhang, R. Wei, J. W. Xia, D. N. Jiao, and Y. X. Pan, *Appl.Mech. Mat.* **2013***, 333–335*, 1926-1929.

[6] M. Behl, K. Kratz, U. Noechel, T. Sauter, and A. Lendlein, *Proc. Natl. Acad. Sci. U. S. A.* **2013**, *110*, 12555–12559.

[7] J. Reeder, M. Kaltenbrunner, T. Ware, D. Arreaga-Salas, A. Avendano-Bolivar, T. Yokota, Y. Inoue, M. Sekino, W. Voit, T. Sekitani, and T. Someya, *Adv. Mater.* **2014**, *26*, 4967–4973.

[8] K. J. Cha, E. Lih, J. Choi, Y. K. Joung, D. J. Ahn, and D. K. Han, *Macromol. Biosci.* **2014**, *14*, 667–678.

[9] C. Liu, H. Qin, and P. T. Mather, *J. Mater. Chem.* **2007**, 17, 1543–1558.

[10] I. A. Rousseau, *Polym. Eng. Sci.* **2008**, *48*, 2075–2089.

[11] K. S. Santhosh Kumar, R. Biju, and C. P. Reghunadhan Nair, *React. Funct. Polym.* **2013**, *73*, 421–430.

[12] D. M. Feldkamp and I. A. Rousseau, Macromol. Mater. Eng. **2010**, *295*, 726–734.

[13] D. M. Feldkamp and I. A. Rousseau, *Macromol. Mater. Eng.* **2011***, 296*, 12, 1128–1141.

[14] A. B. Leonardi, L. A. Fasce, I. A. Zucchi, C. E. Hoppe, E. R. Soulé, C. J. Pérez, and R. J. J. Williams, *Eur. Polym. J.* **2011**, *47*, 362–369.

[15] T. Xie and I. A. Rousseau, *Polymer* **2009**, *50*, 1852–1856.

[16] D. Santiago, M. Morell, X. Fernández-Francos, A. Serra, J. M. Salla, and X. Ramis, *React. Funct. Polym.* **2011**, *71*, 380–389.

[17] D. Santiago, X. Fernández-Francos, X. Ramis, J. M. Salla, and M. Sangermano, *Thermochim. Acta* **2011**, *526*, 9–21.

[18] X. Fernández-Francos, D. Santiago, F. Ferrando, X. Ramis, J. M. Salla, A. Serra, and M. Sangermano, *J. Polym. Sci. Part B Polym. Phys.* **2012**, *50*, 1489–1503.

[19] M. Flores, X. Fernández-Francos, F. Ferrando, X. Ramis, and A. Serra, *Polym. United Kingd.* **2012**, *53*, 5232–5241.

[20] D. Santiago, X. Fernández-Francos, F. Ferrando, and S. De la Flor, *J. Polym. Sci. Part B Polym. Phys.***2015**, *53*, 924–933.

[21] M. Bothe and T. Pretsch, *J. Mater. Chem.*, **2013**, 1, 14491–14497.

[22] J. J. Song, H. H. Chang, and H. E. Naguib, *Eur. Polym. J.* **2015**, *67*, 186–198.

[23] C. M. Yakacki, R. Shandas, D. Safranski, A. M. Ortega, K. Sassaman, and K. Gall, *Adv. Funct. Mater.***2008**, *18*, 2428–2435.

[24] J. Cui, K. Kratz, and A. Lendlein, *Smart Mater. Struct.***2010**, 19, 065019.

[25] J. S. Arrieta, J. Diani, and P. Gilormini, *J. Appl. Polym. Sci.* **2014**, *131*, 39813

[26] S. Rapp and H. Baier, *Smart Mater. Struct.* **2010**, *19*, 045018.

[27] I. S. Kolesov, K. Kratz, A. Lendlein, and H.-J. Radusch, *Polymer* **2009**, *50*, 5490–5498.

[28] N. Lakhera, C. M. Yakacki, T. D. Nguyen, and C. P. Frick, *J. Appl. Polym. Sci.* **2012**, *126*, 72–82.

[29] C. M. Yakacki, S. Willis, C. Luders, and K. Gall, *Adv. Eng. Mater.***2008**, *10*, 112–119.

[30] D. Ratna, R. Varley, and G. P. Simon, *J. Appl. Polym. Sci.* **2003**, *89*, 2339–2345.

[31] Y. Liu, K. Gall, M. L. Dunn, A. R. Greenberg, and J. Diani, *Int. J. Plast.* **2006**, *22*, 279–313.

[32] X. Chen and T. D. Nguyen, *Mech. Mater.***2011**, *43*, 127–138.

[33] A. M. Ortega, C. M. Yakacki, S. A. Dixon, R. Likos, A. R. Greenberg, and K. Gall, *Soft Matter* **2012**, *8*, 7381–7392.

[34] I. A. Rousseau and T. Xie, *J Mater Chem.* **2010**, *20*, 3431–3441.

[35] X. L. Wu, S. F. Kang, X. J. Xu, F. Xiao, and X. L. Ge, *J. Appl. Polym. Sci.* **2014**, *131,* 40559.

UNIVERSITAT ROVIRA I VIRGILI
EXPERIMENTAL CHARACTERIZATION OF SHAPE-MEMORY POLYMERS: INFLUENCE OF PROCESSING METHODS AND CHEMICAL STRUCTURE
David Manuel Santiago Abraira

IV.6. Thermomechanical Characterization of Hyperbranched-Modified Epoxy Thermosets with Enhanced Mechanical and Shape-Memory Properties

David Santiago, Francesc Ferrando, Silvia De la Flor

Journal of Materials Science ***2016****, under review*

UNIVERSITAT ROVIRA I VIRGILI
EXPERIMENTAL CHARACTERIZATION OF SHAPE-MEMORY POLYMERS: INFLUENCE OF PROCESSING METHODS AND CHEMICAL STRUCTURE
David Manuel Santiago Abraira

J. Mater. Sci. 2016, *under review*

Thermomechanical Characterization of Hyperbranched-Modified Epoxy Thermosets with Enhanced Mechanical and Shape-Memory Properties

David Santiago[1], Francesc Ferrando[1], Silvia De la Flor[1]

[1]Department of Mechanical Engineering, Universitat Rovira i Virgili, Av. Països Catalans 26, 43007 Tarragona, Spain

Abstract

In this study a complete characterization of the thermomechanical and shape-memory properties of epoxy shape-memory polymers modified with hyperbranched polymer and aliphatic diamine was performed. Focusing on the mechanical properties that are highly desirable for shape-memory polymers, tensile behaviour until break was analysed at different temperatures and microhardness and impact strength were determined at room temperature. As regards shape memory performance, the synthetized materials were fully characterized at different programming temperatures to study how this influenced the recovery ratio, fixity ratio, shape-recovery velocity and switching temperature. Tensile testing revealed a peak in deformability and in the stored energy density at the onset of the glass transition temperature, demonstrating that this is the best programming temperature for obtaining the best shape-memory performances. The Young's moduli revealed more rigid structures in formulations with higher hyperbranched polymer content, while microhardness testing showed higher values with increasing hyperbranched polymer content due to the increased crosslinking density. Impact strength was greatly improved as the aliphatic diamine content increases due to the energy dissipation capability of its flexible structure. As regards the shape-memory properties, increasing the programming temperature of the shape-memory performances has a minor effect on formulations with a lower hyperbranched polymer content and worsens

the shape-memory properties when the hyperbranched polymer content is increased.

Keywords: *Shape-memory polymers, epoxy, hyperbranched, mechanical properties, tensile, impact strength, microhardness*

1. Introduction

Shape-memory polymers (SMPs) are materials that are capable of changing their shape when an external stimulus is applied. The polymer can be processed into its permanent shape by conventional techniques and be deformed into a second or temporary shape via a step known as programming [1]. This temporary shape will remain stable until the appropriate stimulus is applied. This effect is called the shape-memory effect (SME) and is usually thermally induced but can also be induced by an electrical current, magnetic field or light [2-4].

SMPs can be classified into four different classes according to their chemical structure and transition temperature [5]. Of these, chemically crosslinked glassy thermosets (class I SMPs) are characterized by a high degree of shape fixity due to the high modulus at the glassy region and a high degree of shape recovery due to excellent rubber elasticity at the rubbery region and the absence of chain slippage. Epoxy-based SMPs and acrylate-based SMPs are the most common examples of this class [6,7].

Epoxy resins are widely used in many applications (coatings, adhesives and matrix in composites) because of their chemical resistance, thermal stability and good mechanical properties [8]. However, their brittle behaviour and low elongation at break greatly limit their use as SMPs. A number of studies have focused on overcoming this limitation by choosing suitable shape-memory thermal conditions and through chemical composition adjustments [9,10]. Although the toughness of epoxies is greatly improved in these kinds of network, achieving high

mechanical properties in terms of tensile strength may remain a limitation for more mechanically demanding shape-memory applications such as thermomechanical actuators. There is therefore a need to explore new structures that combine high mechanical properties while showing excellent shape-memory properties.

Our research group recently published details of a new kind of hyperbranched-modified shape-memory epoxy polymers with excellent mechanical and shape-memory properties [11]. Hyperbranched polymers (HBPs) are a class of dendritic polymers that show promise as polymeric modifiers because of their densely-branched structure, which makes them less viscous than their linear counterparts of the same molecular weight, and their high concentration of surface reactive groups that can be modified to tune their physical/chemical compatibility to a variety of matrices and substrates [12]. Preliminary tests showed that the presence of HBPs in the network led to excellent mechanical properties, with stress at break rising to 15 MPa and 60% failure strain at high temperature. Shape-memory properties showed excellent results, with shape-recovery and shape-fixity ratios up to 97% and 98% respectively and a fast recovery rate.

Thus HBPs have proved to be excellent crosslinking agents for shape-memory epoxy thermosets. The effects of the HBP in terms of kinetics, network structure and thermomechanical and shape-memory properties have been studied recently [11,13,14], but a thorough characterization of the mechanical properties of these materials has yet to be carried out.

Several studies on enhanced mechanical properties in terms of the deformability of epoxy-based shape-memory thermosets can be found in the literature [9,15-17]. However, only a few consider other mechanical properties such as impact strength or hardness that might be interesting for the design of shape-memory applications [18,19]. Some SMP applications like biomedical applications (*i.e.* cardiovascular stents, smart

sutures) may require the material operate in a conditioned environment [20]. However, bearing in mind other applications such as thermomechanical actuators and self-deployable structures, it is likely that SMPs will have to operate in an aggressive mechanically-demanding environment. Thus the mechanical requirements go beyond the showing of high values for stress and strain at break.

It is for this purpose that the present study explores and discusses the mechanical properties of hyperbranched-modified epoxy SMPs. A series of materials with shape-memory properties are synthetized using an epoxy resin modified with a commercial hyperbranched poly(ethyleneimine) and an aliphatic polyetheramine as crosslinking agents with different weight fractions of each reactant. Tensile strength is investigated at different testing temperatures, the effect of HBPs on the Young's modulus values, hardness and impact strength are studied and the analysis of fracture is performed using SEM microscopy. In our previous study [11] the shape-memory properties of hyperbranched-modified SMPs were evaluated using the onset of the glass transition temperature as the programming temperature. As mentioned earlier, one of the objectives of this research is to study tensile strength at different temperatures. Consequently, this study aims to determine how using those different testing temperatures as programming temperatures will affect the shape-memory properties.

This study is carried out with the aim of providing a complete characterization of the mechanical properties of hyperbranched-modified epoxy shape-memory polymers. The results demonstrate that these materials combine high values of tensile and impact strength and high values of stored elastic energy and hardness while presenting excellent shape-memory properties.

2. Experimental Methods

2.1 Materials

Diglycidyl ether of bisphenol A (Araldite GY 240, Huntsman) with a weight per epoxy equivalent of 182 g mol^{-1} was used as the base epoxy resin (Figure IV.6.1a). A commercial hyperbranched poly(ethyleneimine) (Lupasol® FG, BASF) with M_w = 800 g mol^{-1} (Figure IV.6.1b) and an aliphatic diamine (Jeffamine® D400, Huntsman) with M_w = 430 g mol^{-1} (Figure IV.6.1c) were used as crosslinking agents.

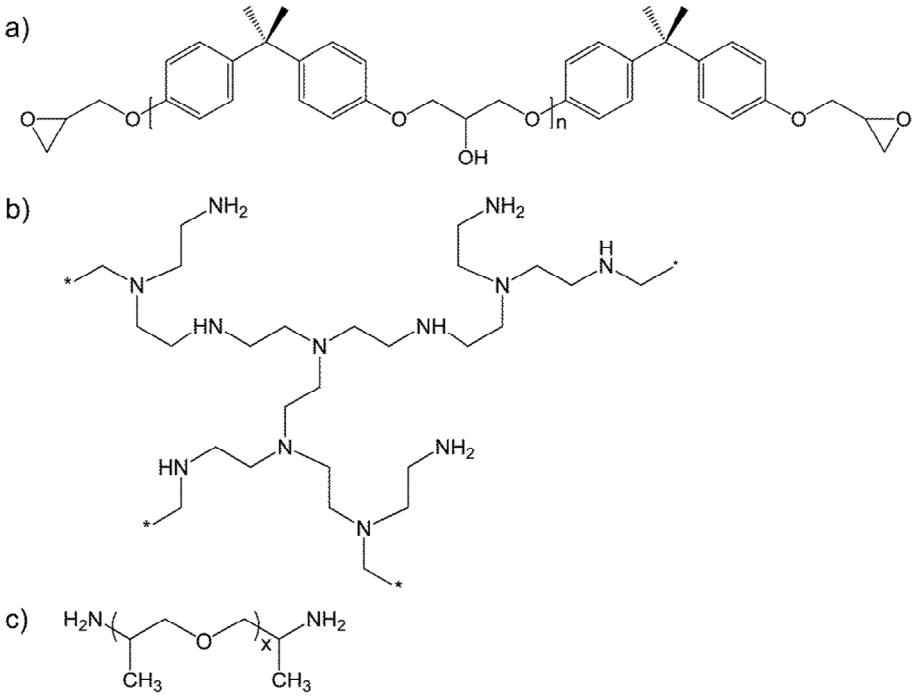

Figure IV.6.1 a) Chemical structure of DGEBA (n = 0.08); b) chemical structure of Jeffamine® D400 (x ≈ 6.1); c) chemical structure of Lupasol® FG.

Various formulations with different contents of diglycidyl ether of bisphenol A (DGEBA), Jeffamine® D400 (D400) and Lupasol® FG (LP) were prepared (Table IV.6.1). The proportions of the reactants in each

formulation were selected to obtain a molecular structure formed by stoichiometric DGEBA-D400 and DGEBA-LP800 networks. The sample nomenclature XD400-YLP used in Table IV.6.1 indicates the weight fraction of stoichiometric DGEBA-D400 (X) and DGEBA-LP800 (Y) networks.

The components were mixed manually in a glass vial and then poured into an open mould covered with Teflon to avoid the presence of bubbles and facilitate sample release. The samples were cured for 2h at 120 ºC in an oven and then slowly cooled to room temperature. This curing time was optimized on the basis of differential scanning calorimetry, determining the time necessary to ensure the complete disappearance of any exothermic peak related to residual crosslinking reactions. The samples were then polished with sandpaper to obtain uniform final dimensions.

Table IV.6.1 Composition of the formulations studied. ν_c is the crosslinking density calculated assuming that all amine groups turn into crosslinks

Sample	wt. % DGEBA	wt. % D400	wt. % LP800	D400: LP800 amine ratio[a]	ν_c [mol/g]
90D400-10LP	63.5	34.8	1.7	4.010	0.001915
80D400-20LP	65.7	31.0	3.3	1.782	0.002127
70D400-30LP	67.9	27.1	5.0	1.040	0.002339
60D400-40LP	70.2	23.2	6.6	0.668	0.002551
50D400-50LP	72.4	19.4	8.3	0.446	0.002763
40D400-60LP	74.6	15.5	9.9	0.297	0.002975
30D400-70LP	76.8	11.6	11.6	0.191	0.003187

[a] Total primary, secondary and tertiary amine groups present in the crosslinking agent.

2.2 Thermomechanical Characterization

The thermomechanical properties were measured using a DMA Q800 (TA Instruments) equipped with a 3-point bending clamp. Prismatic

rectangular samples of ca. 30 mm x 5.5 mm x 2.5 mm were analysed at 1 Hz, 0.1% strain and a heating rate of 3 ºC min^{-1}. The glass transition temperature was determined from the peak in tan δ. The values of storage modulus *E'* below and above glass transition were evaluated. The onset of glass transition temperature $T_g^{E'}$ was determined as the onset in the storage modulus decrease during mechanical relaxation, as seen in Figure IV.6.2.

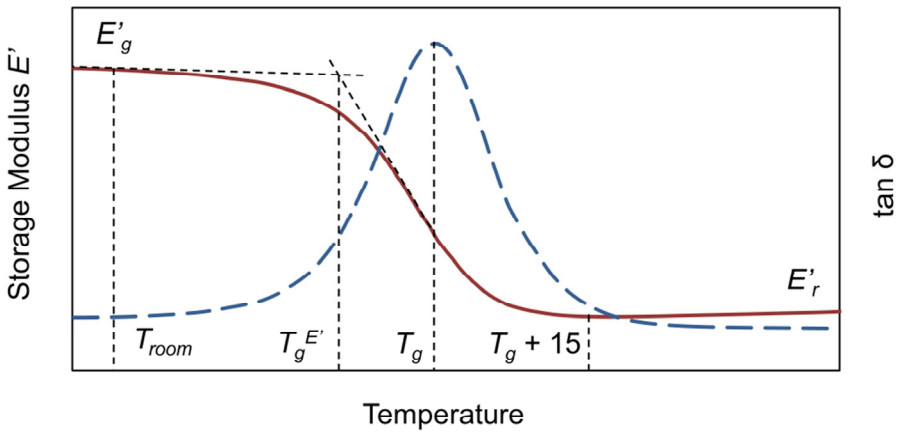

Figure IV.6.2 Determination of the temperatures $T_g^{E'}$, T_g and T_g+15 from the results obtained with DMA analysis.

2.3 Mechanical Characterization

Tensile tests

The mechanical properties at room temperature (~25 ºC) were evaluated using an electromechanical universal testing machine (Zwick 1445) with specially designed grips. The size of the specimens was adapted from ASTMD638 requirements, adopting a Type IV dog-bone shape. The experiments were performed at a crosshead speed of 1 mm min^{-1}.

The mechanical properties at $T_g^{E'}$, T_g and T_g + 15 ºC of each formulation were evaluated using a DMA Q800 (TA Instruments) equipped with a film-tension clamp in force-controlled mode. Prismatic rectangular samples of ca. 20 mm x 2.5 mm x 0.5 mm were used at a

force rate of 1N min^{-1}. In each experiment, strain was calculated as the total elongation (displacement of the crosshead) with respect to the initial length (Equation IV.6.1).

$$\varepsilon(\%) = \frac{L_f - L_0}{L_0} \cdot 100 \qquad \text{(IV.6.1)}$$

Impact strength

The impact test was performed at room temperature by means of a Zwick 5110 impact tester, according to ASTM D4508-10 using rectangular samples (25 mm x 15 mm x 2 mm). 10 measurements were made for each formulation and the pendulum employed had a kinetic energy of 1 J. The impact strength was calculated from the energy absorbed by the sample upon fracture as:

$$\text{Impact Strength } \left(\frac{\text{kJ}}{\text{m}^2}\right) = \frac{E - E_0}{S} \qquad \text{(IV.6.2)}$$

Where E is the energy loss of the pendulum with the sample, E_0 is the energy loss of the pendulum with no sample and S is the cross section of the sample.

Young's modulus

The Young's modulus was calculated under flexural conditions with a DMA Q800 (TA Instruments) equipped with a 3-point bending clamp. The Young's modulus was calculated at room temperature, with a ramp force of 1 N min^{-1} up to 15 N.

Hardness

Microhardness was measured with a Wilson Wolpert (Micro-Vickers 401MAV) microhardness tester with a micro-Vickers indenter and a 200 g load. In order to obtain a microhardness value, ten micro-Vickers indentations were performed on each specimen. A statistical calculation

with a 95% confidence level was then carried out to determine the upper and lower limits.

SEM Microscopy

The fracture areas of the samples were metallized with gold and observed with a Jeol JSM 6400 scanning electron microscope (SEM). The samples were fractured by impact testing at room temperature.

2.4 Characterization of Shape-Memory Properties

The shape-memory properties were measured using a DMA Q800 with a force-controlled mode and equipped with a film-tension clamp. Prismatic rectangular samples of ca. 20 mm x 2.5 mm x 0.5 mm were used in shape-memory performances. The method for creating a temporary shape and triggering the shape-memory effect is a thermomechanical procedure called programming. This consists of various steps:

1. The sample is heated to programming temperature T_{prog} and deformed to a prescribed value of maximum stress σ_m at 1 MPa min^{-1}. σ_m was selected as 75% of the stress at break ($\sigma_m = 0.75\sigma_b$) of each formulation at the corresponding T_{prog} in order to perform a comparative study with the same level of load for each sample. In this stage the deformation of the sample is ε_m.
2. The sample is cooled to low temperature T_{low} (~25 ºC) in order to fix the temporary shape.
3. After fixation the stress is released at the same stress rate of 1 MPa min^{-1}. Once the sample is unloaded, the deformation of the sample is ε_u.
4. The shape-memory effect is triggered by heating the sample to recovery temperature $T_{recovery}$. The heating rate during shape recovery was 3 ºC min^{-1} and the final recovery temperature was T_g + 10 ºC to ensure complete recovery. The amount of non-recoverable deformation at the end of programming is ε_p.

$$R_r(\%) = \frac{\varepsilon_m - \varepsilon_p}{\varepsilon_m} \cdot 100 \qquad \text{(IV.6.3)}$$

The shape-fixity ratio quantifies the ability of the SMP to fix the temporary shape. It was computed as the deformation after the stress was released with respect to the maximum deformation (Equation IV.6.4):

$$R_f(\%) = \frac{\varepsilon_u}{\varepsilon_m} \cdot 100 \qquad \text{(IV.6.4)}$$

The shape-recovery velocity (V_r) quantifies the velocity at which the permanent shape is recovered. V_r was calculated as the time interval between 15% and 85% of strain recovered (Equation IV.6.5):

$$V_r(\%/\text{min}) = \frac{\left(\frac{\varepsilon_{rec,15\%} - \varepsilon_{rec,85\%}}{\varepsilon_{rec,15\%}}\right) \cdot 100}{\Delta t_{15\%-85\%}} \qquad \text{(IV.6.5)}$$

3. Results and Discussion

3.1 Thermomechanical Properties

The thermomechanical results are summarized in Table IV.6.2 and Figure IV.6.3. The glass transition temperature T_g of the materials can be controlled by varying the chemical composition of the formulation. T_g shows values ranging from 60 ºC to 117 ºC as the LP content increases, and therefore these epoxy thermosets can be used in applications requiring a broad range of transition temperatures. A higher LP content implies a higher crosslinking density (Table IV.6.1) because of the higher number of reactive amine groups per unit mass and the presence of internal branching points. This leads to a decrease in the average chain length between netpoints and a more restricted molecular mobility, thus increasing the T_g. As Table IV.6.2 and Figure IV.6.3 show, an increase in LP also causes a lowering and a broadening of the peak of tan δ. LP leads

to a more heterogeneous network structure due to the inherently dispersed nature of the hyperbranched poly(ethyleneimine). The decrease in tan δ peak and area when the amount of LP increases is also indicative of a more densely crosslinked network with restricted mobility.

Table IV.6.2 Thermomechanical data obtained by DMA: glass transition temperature (T_g), onset temperature of the glass transition temperature (T_g^E), storage modulus at glassy and rubbery regions (E'_g and E'_r respectively)

Sample	T_g[a] (ºC)	$T_g^{E'}$ (ºC)	tan δ peak	FWHM[b] (ºC)	tan δ area[c] (ºC)	E'_g[d] (MPa)	E'_r[e] (MPa)	$\frac{E'_g}{E'_r}$
90D400-10LP	60	50	0.96	15.45	14.83	2878	16	183
80D400-20LP	68	57	0.82	17.82	14.61	2880	17	166
70D400-30LP	77	63	0.71	20.29	14.41	3105	23	137
60D400-40LP	87	71	0.62	21.11	13.09	3149	29	110
50D400-50LP	96	80	0.54	23.33	12.60	3110	34	91
40D400-60LP	104	88	0.50	23.66	11.83	3221	41	79
30D400-70LP	117	98	0.41	24.58	10.08	2858	52	55

[a] Measured as the peak of tan δ

[b] Full Width at Half Maximum

[c] determined as the product of tan δ peak and FWHM

[d] measured at T_g – 40 ºC

[e] measured at T_g + 40 ºC

All formulations show very high values of storage modulus at the glassy region around 3 GPa (Table IV.6.2 and Figure IV.6.3), which is higher than most of the shape-memory epoxy resins found in the literature. The storage modulus at rubbery region E'_r increases as the LP content increases. According to the theory of rubber elasticity, E'_r is roughly proportional to the crosslinking density and is therefore expected to increase in line with it (Table IV.6.2).

Almost all the samples in the present work show a difference between the storage modulus at glassy and rubbery regions of around 2 orders of magnitude. This important difference in mechanical properties

between the glassy and rubbery states is crucial if a polymer is required to present SME.

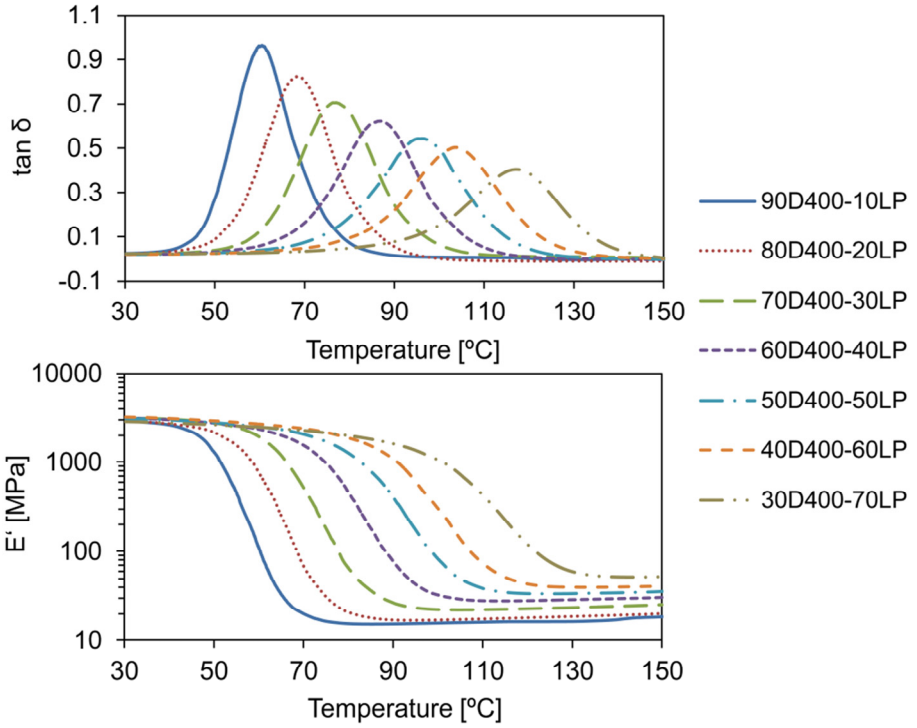

Figure IV.6.3 Tan δ and storage modulus *E'* as a function of temperature for all formulations.

3.2 Mechanical Properties

Tensile strength

Figure IV.6.4 shows the results of the stress and strain at break obtained from tensile tests at T_{room}, $T_g^{E'}$, T_g and T_g + 15 for each formulation. Below the glass transition temperature (Figure IV.6.4a), the values of stress at break increase almost linearly with increasing crosslinking density and T_g up to sample 40D400-60LP, where it reaches its highest value (around 55 MPa). Regarding the strain at break, this seems not to be differently affected by crosslinking density, with two distinctive regions observed: from 90D400-10LP to 60D400-20LP, with a strain value of around 3.6%,

and from 50D400-50LP to 30D400-70LP, with a strain value of around 5%. These results suggest that the increase in the stress and strain at break seems to be possible up to a certain value when the increasing crosslinking density limits the deformability and stress capability of the network.

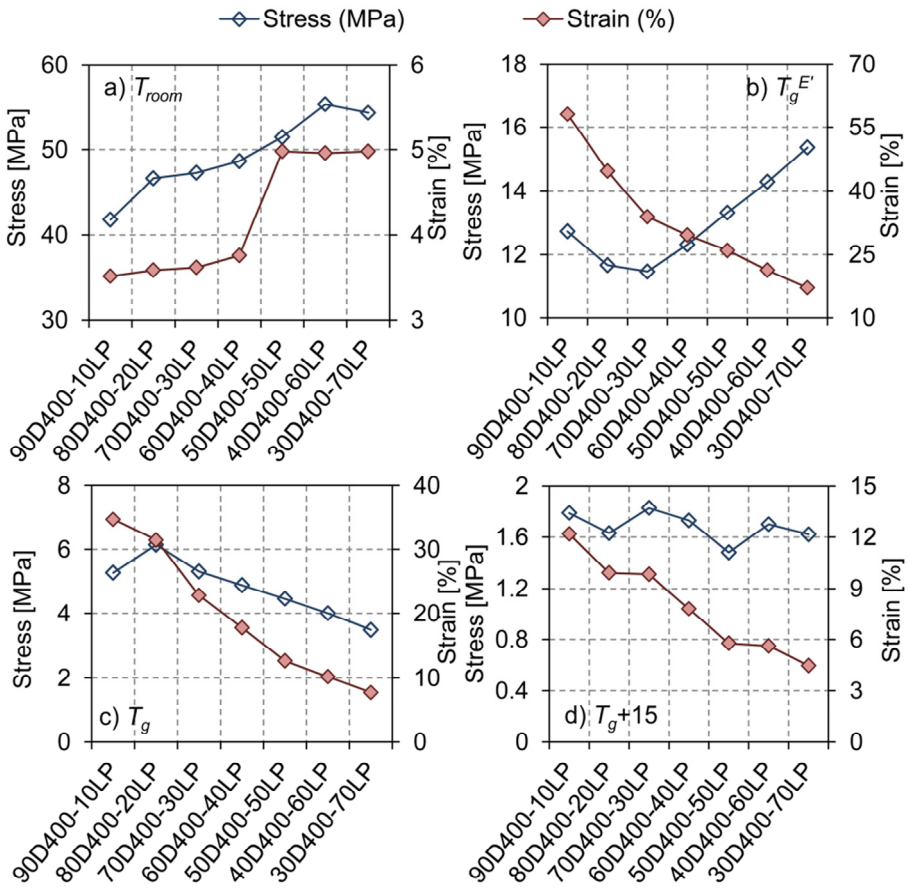

Figure IV.6.4 Stress at break and strain at break at T_{room} (a), $T_g^{E'}$ (b), T_g (c) and T_g+15 (d) for all formulations.

At the onset of the glass transition temperature $T_g^{E'}$ (Figure IV.6.4b), the crosslinking density acquires significant relevance. An increase in the LP content causes an increase in the crosslinking density,

which results in a less mobile and ductile network leading in the macroscopic scale to lower values of failure strain and higher values of stress at break: ε_b decreases from 58.1% to 17.2% and σ_b increases from 12.7 MPa to 15.4 MPa.

The values of σ_b and ε_b at $T \geq T_g$ (Figure IV.6.4c and Figure IV.6.4d) decrease as the LP content increases. At transition temperature T_g, the values of stress at break decrease from 5.3 MPa (formulation 90D400-10LP) to 3.5 MPa (30D400-70LP), despite a slight increase for formulation 80D400-20LP (6.1 MPa), and the strain at break decreases from 34.7% (formulation 90D400-10LP) to 7.7% (formulation 30D400-70LP). At $T = T_g + 15$, the values of stress at break are not greatly affected by the LP content, the trend is not clear and σ_b shows values of around 1.68 MPa; the values of strain at break decrease from 12.1% (formulation 90D400-10LP) to 4.5% (formulation 30D400-70LP).

The mechanical properties of hyperbranched-modified epoxy SMPs greatly depend on the testing temperature. Well into the glassy regime (Figure IV.6.4a), both the stress at break and strain at break increase as the LP content increases. The mechanical properties below the transition temperatures in epoxy-based thermosets depend on the cohesive forces, the presence of local mobility and the difference between the test temperature and T_g. However, the role of crosslinking density is not clear [21]. As can be observed in Table IV.6.1, on increasing the LP content, the DGEBA content also increases and leads to an increase in the number of hydroxyl groups which contribute to the cohesion of the network structure. The internal flexible structure of LP, with certain but limited local mobility below the T_g, may contribute to the observed behaviour. Well into the rubbery regime (Figure IV.6.4c and Figure IV.6.4d), both the stress at break and the strain at break decrease as the LP content increases. At $T \geq T_g$, the increasing crosslinking density restricts molecular mobility resulting in lower values of failure strain. Although formulations with higher crosslinked density should show

higher values of stress at break [22], it seems that the disperse nature of the hyperbranched structure of LP causes a reduction in the stress capability of these materials, and thus the stress at break decreases as the LP content increases.

At the onset of the glass transition temperature $T_g^{E'}$ (Figure IV.6.4b) the stress at break increases and the strain at break decreases as the LP content increases. This temperature coincides with the beginning of the mechanical relaxation of the materials, and the effect of the crosslinking density is different to that shown well into the glassy and rubbery regimes. An increase in the crosslinking density results in a less mobile and ductile network, leading in the macroscopic scale to a lower failure strain and a higher stress at break.

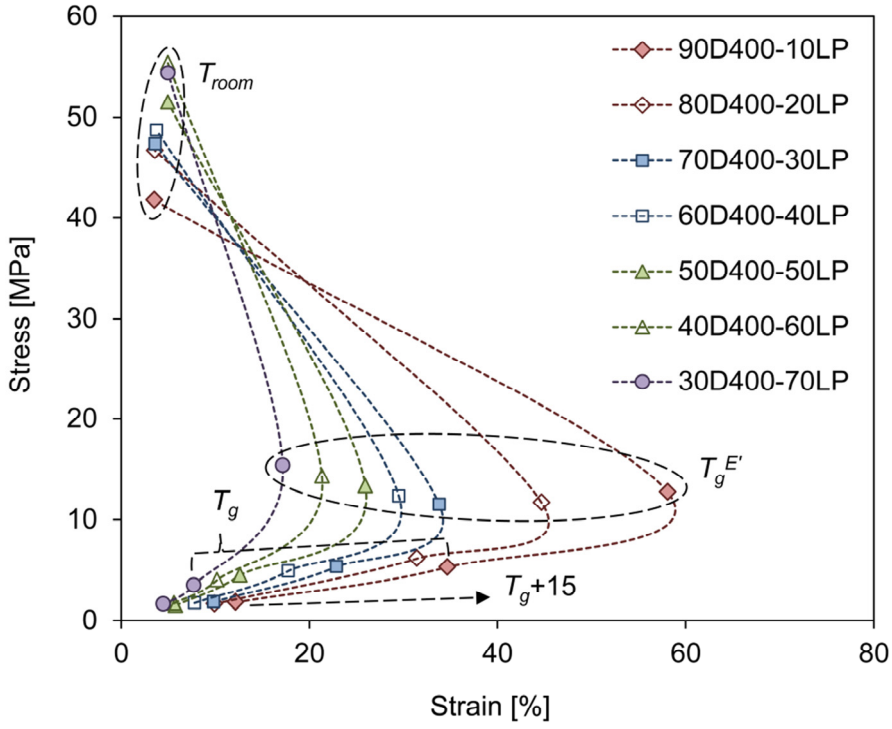

Figure IV.6.5 Values of stress at break (right) and strain at break (left) of each formulation as a function of testing temperature (T_{room}, $T_g^{E'}$, T_g and T_g + 15).

The above results are clearly observed in Figure IV.6.5. The highest values of strain at break are obtained when tested at $T_g^{E'}$ in each formulation. This result is in accordance with previous results reported by Yakacki *et al.* [22] in their acrylate-based SMPs and Feldkamp and Rousseau [9] in their epoxy-based SMPs and has important implications for the design SMP applications. By selecting the programming temperature to match the onset of the glass transition temperature, an increase in the strain capacity is expected.

The mechanical properties in terms of stress at break and strain at break give important information for the limit values when programming the temporary shape of the SMP. However, another important mechanical parameter to characterize SMPs is the elastic energy density. Calculated as the area under the stress-strain curves, this is shown in Figure IV.6.6. The stored elastic energy density is an important metric of shape-memory behaviour because it estimates an upper boundary for recoverable elastic energy, *i.e.* the material's capability to perform mechanical work against external loads in the recovery stage. The ability of SMPs to stabilize deformed shapes and perform mechanical work upon shape recovery is limited by the strength and density of the bonds created during shape stabilization [23]. Hence reducing crosslinking density helps to improve this capability: at $T_g^{E'}$, T_g and T_g + 15, the elastic energy density decreases on increasing the LP content due to the decrease in the strain at break (around 70% in each temperature). At T_{room}, the increasing stress at break values cause an increase in the stored energy density of formulations with higher LP content (from 0.73 MJ m^{-3} to 1.35 MJ m^{-3}).

The highest values for elastic energy density are obtained at $T_g^{E'}$: from 3.7 MJ m^{-3} (formulation 90D400-10LP) to 1.3 MJ m^{-3} (formulation 30D400-70LP). These results are in accordance with those shown in Figure IV.6.5, where a peak in deformability was observed when the materials were stretched at $T_g^{E'}$. These high values of stored energy

density at $T_g^{E'}$ come from the combination of relatively high deformation at break values (up to 60%) and remarkably high stress at break values (up to 15 MPa).

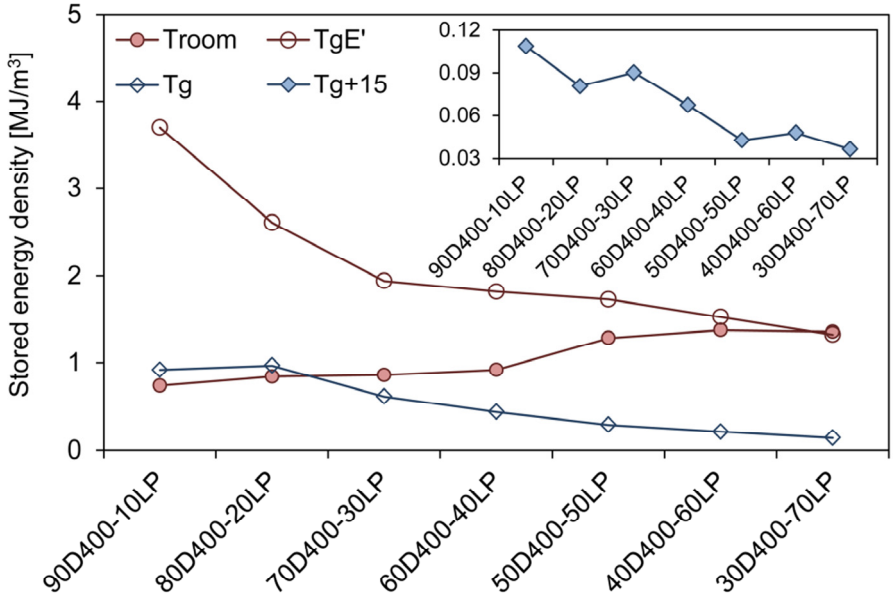

Figure IV.6.6 Stored energy density of each formulation for testing temperatures T_{room}, $T_g^{E'}$, T_g and T_g+15.

The elastic energy density when stretched at T_{room} shows relatively high values, higher than those shown at T_g, T_g + 15 and even higher at $T_g^{E'}$ for formulation 30D400-70LP. These results are due to the excellent stress at break values, between 42 and 53 MPa. Some studies have reported shape-memory programming procedures which use T_{prog}s below the transition temperature of the materials [24,25]. This non-conventional technique known as cold-working programming consists of deforming the materials above their yielding point in order to maintain a significant amount of deformation after fixation. This deformation can be partially or totally recovered when heating the SMP above its transition temperature. The cold-working programming cannot obtain the same

extent of shape fixation as traditional programming, but it does present some advantages such as the high stress capacity of the materials.

Young modulus

Figure IV.6.7 shows the Young's modulus of all formulations obtained by flexural tests E_f. Determining the Young's modulus using the 3-point bending test has some advantages with respect to tensile testing, *i.e.* easier sample preparation and testing. Determining the Young's modulus in plastics by tensile testing is complicated due to the difficulty of determining distinctly the proportional part of the elastic deformation. This proportional part is more clearly observed by 3-point bending testing because the whole test can be performed in the elastic regime. Moreover, obtaining the strain by tensile testing with the displacement of the crosshead may lead to inaccuracies in the calculation of the Young's modulus.

The values of the Young's modulus increase almost linearly from 1161 MPa for formulation 90D400-10LP to 2103 MPa for formulation 30D400-70LP. These results are in accordance with the tensile properties at room temperature shown in Figure IV.6.4a, in which the stress and strain at break increase linearly as the Lupasol® content increases. This is clearly observed from formulation 90D400-10LP to formulation 70D400-30LP. However, taking the error bars into account, it is difficult to establish differences in the Young's modulus from formulation 70D400-30LP to 30D400-70LP, with values around 1800 MPa. This trend of the Young's modulus correlates well with the trend of the values of the storage modulus at glassy region E'_g (Table IV.6.2), where there is no significant difference between the formulations.

As mentioned earlier, the mechanical properties below the transition temperature mainly depend on the cohesive forces of the network. As can be observed in Table IV.6.1, on increasing the LP content the DGEBA content also increases, thereby increasing the number of hydroxyl groups coming from the epoxy-amine condensation

and contributing to the cohesion of the network structure. The increase in network cohesion is clearly observed from formulation 90D400-10LP to 70D400-30LP and from this point forwards the crosslinking and cohesive forces have no significant effect on the rigidity of the materials studied.

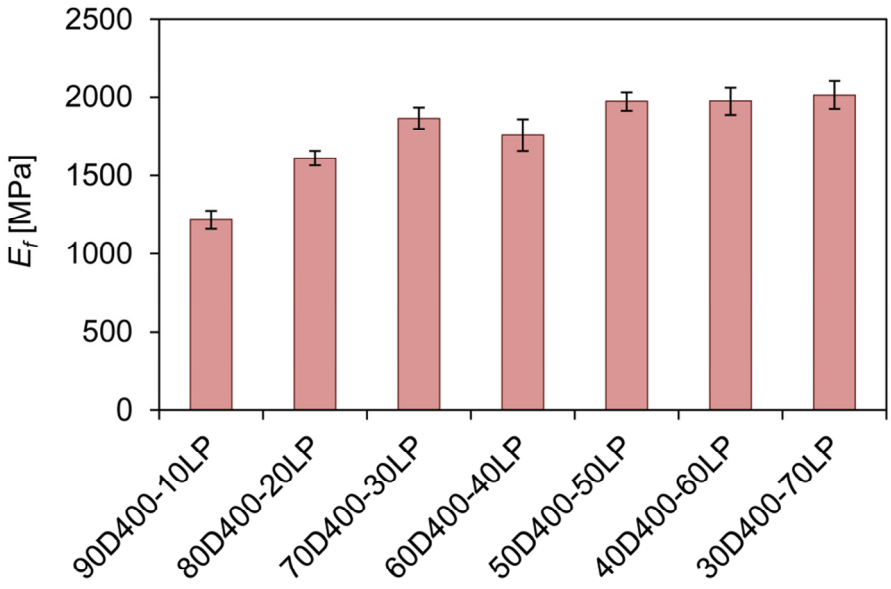

Figure IV.6.7 Young modulus E_f of all formulations obtained by flexural tests.

Hardness

Another mechanical property of interest for SMPs is the hardness. Some applications may require the temporary shape of the SMP to be programmed at a different site from the one in which it will operate or the storage of the programmed specimen during a period of time. Any surface damage produced by scratches or splits may have undesirable effects on the shape-memory properties of the material. Figure IV.6.8 shows the hardness values for all formulations.

The hardness progressively increases from formulation 90D400-10LP (HV0.2 = 5.4) to formulation 30D400-70LP (HV0.2 = 13.5). However, as in the case of the Young's modulus values, it is difficult to

establish differences in the hardness values of the intermediate formulations (from 80D400-20LP to 40D400-60LP). These results can be explained by taking into account the structure of the materials. Flores *et al.* [26] reported a decrease in hardness in epoxy resins modified with hyperbranched polyesters with long aliphatic chains due to the flexibility added by this modifier. As can be observed in Table IV.6.1, on increasing the LP content the D400 content decreases and the DGEBA content increases. Thus the lower presence of the plasticizing effect of the D400 flexible structure along with the increasing crosslinking density of formulations with higher LP and DGEBA content could explain the observed increase in hardness.

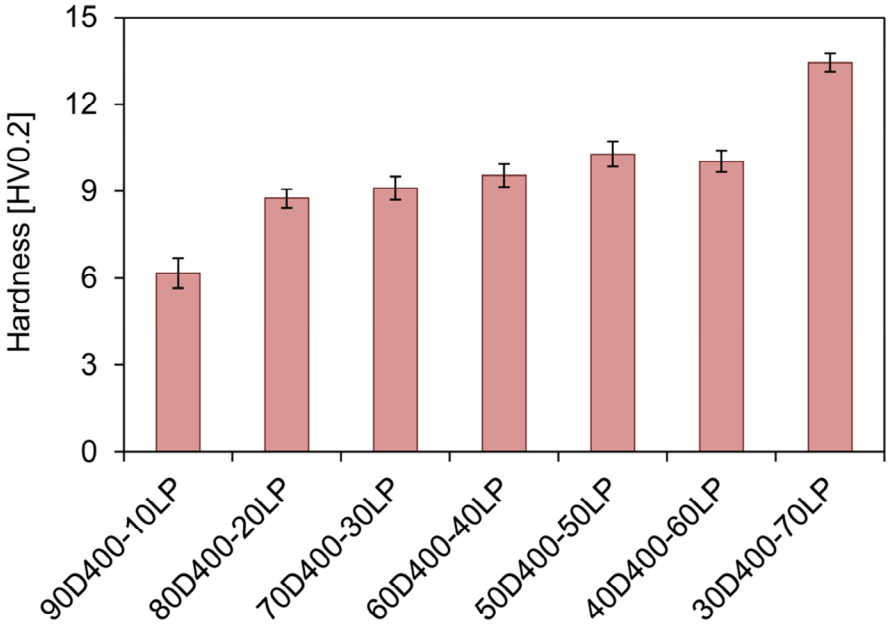

Figure IV.6.8 Hardness values of all formulations.

Impact strength

As in the case of hardness, the impact strength of the SMPs is an interesting mechanical property for those applications in which they have to operate in a different place from that in which they were programmed

or be stored for a period of time before operation. High impact strength may be desirable in order to avoid cracks during shipping or storage which can damage the SME of the material. Figure IV.6.9 shows the impact strength of formulations 30D400-70LP, 60D400-40LP and 90D400-10LP and the neat epoxy-D400 formulation 100D400. Given the slight differences in the Young's modulus and hardness testing of the intermediate formulations, for impact testing we only tested the formulations with the lowest and highest LP content (90D400-10LP and 30D400-70LP respectively) and one intermediate formulation (60D400-40LP). 100D400 is a formulation synthetized by stoichiometric DGEBA and Jeffamine® D400 with no LP content, used as a benchmark value in order to analyse the effect of HBP on impact strength.

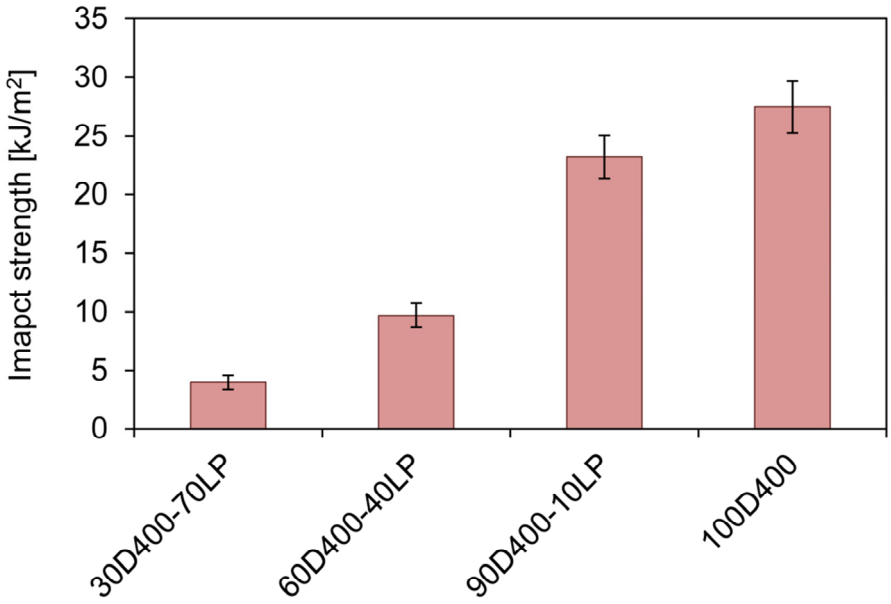

Figure IV.6.9 Impact strength of formulations 30D400-70LP, 60D400-40LP, 90D400-10LP and 100D400.

In order to improve the impact resistance of a material, it is important to introduce mechanisms that can contribute to energy

dissipation, thereby impeding crack propagation. It has been demonstrated that the use of HBPs can effectively enhance the impact strength of epoxy materials [27-29]. However, the addition of LP decreases the impact strength in comparison to the neat epoxy-D400 formulation (100D400). With 1.7% LP content (formulation 90D400-10LP) the impact strength slightly decreases from 27.5 kJ m^{-2} (formulation 100D400) to 23.2 kJ m^{-2}, and with 11.6% (formulation 30D400-70LP) decreases to 4 kJ m^{-2}. Following these results, the good impact resistance of these materials in comparison to similar networks based on hyperbranched-modified epoxies can be established. Morell *et al.* [27] reported values of impact strength lower than 4 kJ m^{-2} in epoxy thermosets modified with hyperbranched poly(ester-amide)s. Flores *et al.* [28] and Acebo *et al.* [29] reported values lower than 10 kJ m^{-2} and 4 kJ m^{-2} respectively in epoxy networks modified with undecenoyl-modified hyperbranched polymers. Looking into shape-memory networks modified with HBPs, Han *et al.* [30] reported values of impact strength up to 13 kJ m^{-2} in epoxy resins modified with a hyperbranched polyester.

As can be observed in Table IV.6.1, formulations with lower LP content have higher D400 content. The trend observed in impact strength values is caused by the greater effect of Jeffamine® D400 on the impact strength than Lupasol®. Its long flexible aliphatic structure increases the length of polymer chains between crosslinking points and the free volume of network structure [31]. Thus formulations with a higher D400 content can dissipate a great deal of energy upon impact due to their higher molecular motion.

SEM Microscopy

The results of impact strength can be explained in terms of the morphology of the samples observed by SEM microscopy. The micrographs of the fracture surfaces of impacted samples of formulations 30D400-70LP, 60D400-40LP, 90D400-10LP and 100D400 are shown in

Figure IV.6.10. The analysis of the surface fracture reveals a more rigid behaviour as the LP content increases. The crack propagation spreads from right to left. The surface fracture can be clearly divided into two halves, the right half corresponding with the pendulum impact and fracture initiation and the left half corresponding with the fracture propagation. The initiation of the fracture of formulations with no or low LP content (Figure IV.6.10a and Figure IV.6.10b) begins with crazes which propagate parallel to the direction of fracture propagation until they combine with adjacent cracks. As the LP content increases, the large smooth zones (which indicate a more ductile fracture) tend to disappear due to the increased number of crazes formed. Formulations with higher LP content (Figure IV.6.10c and Figure IV.6.10d) do not show fracture bands in the fracture initiation because the fracture spreads into several planes. The zone of fracture propagation (left half) is characterized by the formation of brittle failure bands and splintering chips. Local deviations of these bands from the main direction of fracture propagation (clearly observed in Figure IV.6.10c) corroborate the brittle behaviour of formulations with a high LP content.

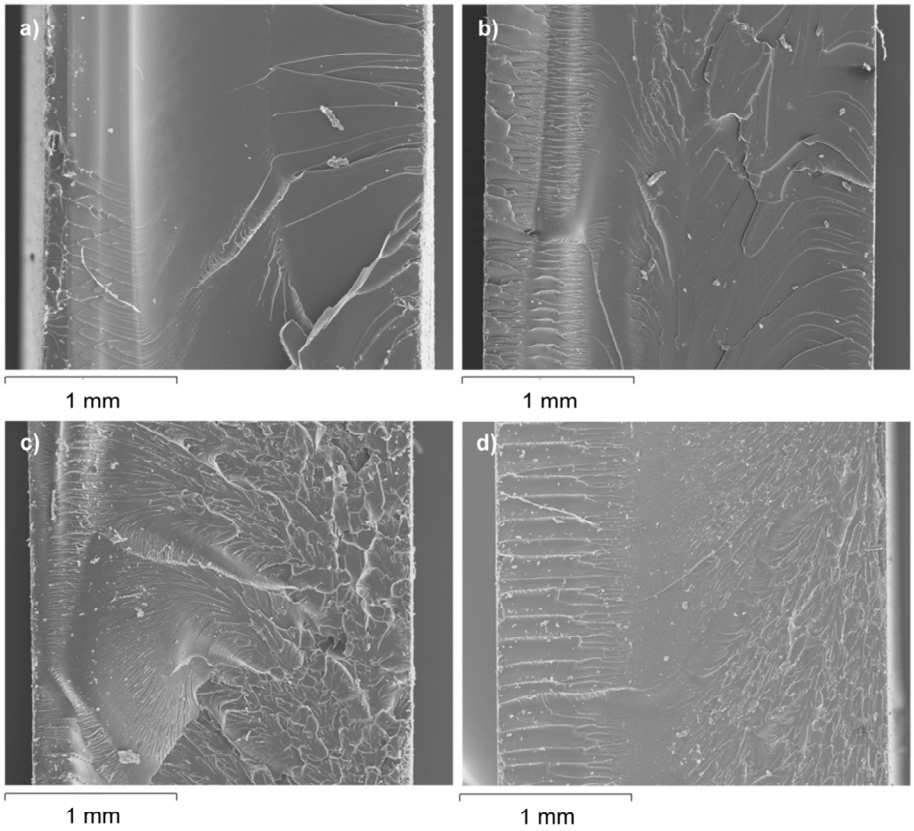

Figure IV.6.10 SEM micrographs of fracture surfaces of the formulations 100D400 (a), 90D400-10LP (b), 60D400-40LP (c) and 30D400-70LP (d).

3.3 Shape-Memory Properties

As observed in Figure IV.6.4, Figure IV.6.5 and Figure IV.6.6, the deformability and ability of hyperbranched-modified epoxy SMPs to store elastic energy density during deformation are greatly improved when the deformation temperature matches the onset of the glass transition temperature ($T_g^{E'}$) of the materials. In our previous study of hyperbranched-modified SMPs, shape-memory properties were fully characterized at $T_{prog} = T_g^{E'}$ [11]. According to the results of both research studies, $T_g^{E'}$ reveals itself to be a desirable programming temperature for shape-memory applications, with good mechanical properties in terms of

stress and strain at break and showing excellent shape-memory properties. However, it is possible that in real applications the programming temperature may not be adjusted at $T_g^{E'}$. Therefore it is important to study the implications for shape-memory properties with other temperatures as T_{prog}.

Table IV.6.3 lists the shape-memory properties of formulations 90D400-10LP, 60D400-40LP and 30D400-70LP at different T_{prog}s (T_{room}, $T_g^{E'}$, T_g and T_g + 15). The shape-memory properties of formulation 90D400-10LP show no significant changes with different T_{prog}s: R_r shows values around 96.5%, R_f shows values around 98% and V_r shows values around 20% min^{-1}. However, the shape-memory properties of formulation 60D400-40LP and especially formulation 30D400-70LP are adversely affected when increasing T_{prog}. The R_r, R_f and V_r decrease when increasing T_{prog} from $T_g^{E'}$ to T_g + 15. In the case of formulation 30D400-70LP, the shape-recovery velocity could not even be calculated (according to Equation IV.6.5) when programmed at T_g + 15 because shape-recovery was under 85%.

One of the main conclusions of our previously study [11] was that the shape-recovery and shape-fixity ratios decrease slightly when increasing the LP content, because this restricts chain-conformational changes during deformation and molecular dynamics, adversely affecting the shape-recovery and shape-fixity ratios and the shape-recovery velocity. Moreover, it should be noted that the maximum deformation achieved in formulations 60D400-40LP and 30D400-70LP when stretched to σ_m at $T_{prog} = T_g$ and T_g + 15 is relatively low: 12.0%, 5.6% and 5.4%, 3.4% respectively. Therefore the elastic energy stored and the driving recovery forces in such cases are very low and do not allow suitable shape-recovery and shape-recovery velocity.

In the case of shape-fixity ratio R_f, a significant decrease is observed when increasing T_{prog}. This is caused by a spontaneous elastic recovery during the beginning of the cooling step.

T_{sw} shows values around the $T_g^{E'}$ of each formulation (50 ºC, 71 ºC and 98 ºC for formulations 90D400-10LP, 60D400-40LP and 30D400-70LP respectively). $T_g^{E'}$ coincides with the onset of the glass transition temperature (Figure IV.6.2) and is thus a temperature at which the molecular motion becomes significant and marks the beginning of shape recovery. A slight increase in T_{sw} is observed in formulations 60D400-40LP (from 70 ºC to 74 ºC) and 30D400-70LP (from 98 ºC to 105 ºC). This may be caused by the drop in V_r. T_{sw} is determined as the inflexion point in a strain-temperature curve during the recovery stage, and a decrease in V_r may cause the determination of such a point to shift to higher temperatures.

Table IV.6.3 Shape-recovery ratio (R_r), shape-fixity ratio (R_f), shape-recovery velocity (V_r) and switching temperature (T_{sw}) of formulation 90D400-10LP at different T_{prog}s

Sample	T_{prog} (ºC)		R_r (%)	R_f (%)	V_r (%/min)	T_{sw} (ºC)
90D400-10LP	$T_{prog} = T_g^{E'}$	50	96.4	98.0	21.6	50
	$T_{prog} = T_g$	60	96.3	98.8	19.7	51
	$T_{prog} = T_g + 15$	75	96.7	96.7	20.8	51
60D00-40LP	$T_{prog} = T_g^{E'}$	71	96.1	97.3	17.7	70
	$T_{prog} = T_g$	87	97.1	96.1	14.8	71
	$T_{prog} = T_g + 15$	102	93.7	90.5	14.9	74
30D400-70LP	$T_{prog} = T_g^{E'}$	98	93.4	94.6	14.7	98
	$T_{prog} = T_g$	117	89.4	88.2	10.3	103
	$T_{prog} = T_g + 15$	132	76.9	78.9	-	105

According to the results in Table IV.6.3 the programming temperature has little effect on the shape-memory properties of formulations with low LP content. However, as the LP content increases, increasing the programming temperature causes a significant drop in

shape-memory properties caused by restricted chain-conformational changes and low driving recovery forces.

Conclusions

In this study the thermal and mechanical characterization of hyperbranched-modified epoxy shape-memory polymers was performed. The thermomechanical properties were analysed by dynamic mechanical analysis and the mechanical properties were studied through tensile, flexural, hardness and impact testing. The surface fracturing was analysed by SEM microscopy and the shape-memory properties were quantified at different programming temperatures.

The thermomechanical measurements showed that increasing the Lupasol® content led to more heterogeneous networks with higher crosslinking density and higher glass transition temperatures. Tensile testing revealed good values for stress at break and strain at break at different temperatures. A peak in deformability and stored elastic energy density was observed at the onset of the glass transition temperature $T_g^{E'}$. The values of the Young's modulus revealed more rigid structures on formulations with a higher content of Lupasol®. Hardness testing showed higher values in formulations with a higher DGEBA and Lupasol® content due to increased crosslinking density and less presence of the plasticizing effect of the Jeffamine® D400 flexible structure. Impact strength increased as Jeffamine® D400 content increased due to the high energy dissipation upon impact provided by its long aliphatic flexible structure. The analysis of the surface fracture confirmed the higher rigid structure of formulations with a higher Lupasol® content.

Increasing the programming temperature during shape-memory programming has a minor effect in formulations with a lower Lupasol® content and but significantly worsens the shape-memory properties when the Lupasol® content is increased.

According to the results obtained, hyperbranched-modified epoxy shape-memory polymers can be used in applications requiring a broad range of transition temperatures. Measurements of the mechanical properties revealed that these materials can operate under highly mechanically-demanding conditions while still showing good shape-memory properties.

Acknowledgements

The authors would like to thank MICINN (MAT2014-53706-C03-01) and the Generalitat de Catalunya (2014-SGR-67) for their financial support.

References

[1] Lendlein A and Kelch S (2002) Shape-Memory Polymers, Angew Chem Int Ed 41: 2034-2057.

[2] Wang Y, Zhu G, Cui X, Liu T, Liu Z and Wang K (2014) Electroactive shape memory effect of radiation cross-linked SBS/LLDPE composites filled with carbon black, Colloid Polym Sci 292:2311-2317.

[3] Cai Y, Jiang J-S, Liu Z-W, Zeng Y and Zhang W-G (2013) Magnetically-sensitive shape memory polyurethane composites crosslinked with multi-walled carbon nanotubes, Compos Part Appl Sci Manuf 53:16-23.

[4] Sodhi JS, Cruz PR and Rao IJ (2015) Inhomogeneous deformations of light activated shape memory polymers, Int J Eng Sci 89:1-17.

[5] Liu C, Qin H and Mather PT (2007) Review of progress in shape-memory polymers, J Mater Chem 17:1543-1558.

[6] Belmonte A, Guzmán D, Fernández-Francos X and De la Flor S (2015) Effect of the network structure and programming temperature on the shape-memory response of thiol-epoxy 'click' systems, Polymers 7:2146-2164.

[7] Santiago D, De la Flor S, Ferrando F, Ramis X and Sangermano M (2016) Thermomechanical properties and shape-Memory behavior of bisphenol A diacrylate-based shape-memory polymers, Macromol Chem Phys 217:39-50.

[8] Santhosh Kumar KS, Biju R and Reghunadhan Nair CP (2013) Progress in shape memory epoxy resins, Netw Polym High Perform Mater 73:421-430.

[9] Feldkamp DM and Rousseau IA (2010) Effect of the deformation temperature on the shape-memory behavior of epoxy networks, Macromol Mater Eng 295:726-734.

[10] Jing X, Liu Y, Liu Y, Liu Z and Tan H (2014) Toughening-modified epoxy-amine system: cure kinetics, mechanical behavior, and shape memory performances, J Appl Polym Sci 131:40853.

[11] Santiago D, Fernández-Francos X, Ferrando F and De la Flor S (2015) Shape-memory effect in hyperbranched poly(ethyleneimine)-modified epoxy thermosets, J Polym Sci Part B Polym Phys 53:924-933.

[12] Voit B (2000) New developments in hyperbranched polymers, J Polym Sci Part Polym Chem 38:2505-2525.

[13] Santiago D, Fernández-Francos X, Ramis X, Salla JM and Sangermano M (2011) Comparative curing kinetics and thermal-mechanical properties of DGEBA thermosets cured with a hyperbranched poly(ethyleneimine) and an aliphatic triamine, Thermochim Acta 526:9-21.

[14] Fernández-Francos X, Santiago D, Ferrando F, Ramis X, Salla JM, Serra A and Sangermano M (2012) Network structure and thermomechanical properties of hybrid DGEBA networks cured with 1-methylimidazole and hyperbranched poly(ethyleneimine)s, J Polym Sci Part B Polym Phys 50:1489-1503.

[15] Leonardi AB, Fasce LA, Zucchi IA, Hoppe CE, Soulé ER, Pérez CJ and Williams RJJ (2011) Shape memory epoxies based on

networks with chemical and physical crosslinks, Eur Polym J 47:362-369.

[16] Voit W, Ware T, Dasari RR, Smith P, Danz L, Simon D, Barlow S, Marder SR and Gall K (2010) High-strain shape-memory polymers, Adv Funct Mater 20:162-171.

[17] Fan M, Liu J, Li X, Zhang J and Cheng J (2014) Thermal, mechanical and shape memory properties of an intrinsically toughened epoxy/anhydride system, J Polym Res 21:376.

[18] Park C, Yul Lee J, Chul Chun B, Chung Y-C, Whan Cho J and Gyoo Cho B (2004) Shape memory effect of poly(ethylene terephthalate) and poly(ethylene glycol) copolymer cross-linked with glycerol and sulfoisophthalate group and its application to impact-absorbing composite material, J Appl Polym Sci 94:308-316.

[19] Deka H and Karak N (2010) Shape-memory property and characterization of epoxy resin-modified Mesua ferrea L. seed oil-based hyperbranched polyurethane, J Appl Polym Sci 116:106-115.

[20] Tandon GP, Goecke K, Cable K and Baur J (2009) Durability assessment of styrene- and epoxy-based shape-memory polymer resins, J Intell Mater Syst Struct 20:2127-2143.

[21] Pascault JP, Sautereau H, Verdu J, Williams RJJ (2002) Thermosetting Polymers. Marcel Dekker, New York.

[22] Yakacki CM, Willis S, Luders C and Gall K (2008) Deformation limits in shape-memory polymers, Adv Eng Mater 10.112-119.

[23] Anthamatten M, Roddecha S and Li J (2013) Energy storage capacity of shape-memory polymers, Macromolecules 46:4230-4234.

[24] Li G and Xu W (2011) Thermomechanical behavior of thermoset shape memory polymer programmed by cold-compression: Testing and constitutive modelling, J Mech Phys Solids 59:1231-1250.

[25] Pandini S, Bignotti F, Baldi F and Passera S (2013) Network architecture and shape memory behavior of cold-worked epoxies, J Intell Mater Syst Struct 24:1583-1597.

[26] Flores M, Fernández-Francos X, Jiménez-Piqué E, Foix D, Serra A and Ramis X (2012) New epoxy thermosets obtained from diglycidylether of bisphenol a and modified hyperbranched polyesters with long aliphatic chains cured by diisocyanates, Polym Eng Sci 52:2597-2610.

[27] Morell M, Erber M, Ramis X, Ferrando F, Voit B and Serra, A (2010) New epoxy thermosets modified with hyperbranched poly(ester-amide) of different molecular weight, Eur Polym J 46:1498-1509.

[28] Flores M, Fernández-Francos X, Ferrando F, Ramis X and Serra A (2012) Efficient impact resistance improvement of epoxy/anhydride thermosets by adding hyperbranched polyesters partially modified with undecenoyl chains, Polymer 53:5232-5241.

[29] Acebo C, Fernández-Francos X, De La Flor S, Ramis X and Serra A (2015) New anhydride/epoxy thermosets based on diglycidyl ether of bisphenol A and 10-undecenoyl modified poly(ethyleneimine) with improved impact resistance, Prog Org Coatings 85:52-59.

[30] Han C, Liu Y and Tan H (2011) Preparation and investigation on properties of shape memory epoxy modified by hyperbranched polyester, Adv Mater Res 335-336:851-855

[31] Yang J-P, Chen Z-K, Yang G, Fu S-Y and Ye L (2008) Simultaneous improvements in the cryogenic tensile strength, ductility and impact strength of epoxy resins by a hyperbranched polymer, Polymer 49:3168-3175.

UNIVERSITAT ROVIRA I VIRGILI
EXPERIMENTAL CHARACTERIZATION OF SHAPE-MEMORY POLYMERS: INFLUENCE OF PROCESSING METHODS AND CHEMICAL STRUCTURE
David Manuel Santiago Abraira

IV.7. Thermomechanical Properties and Shape-Memory Behaviour of Bisphenol A Diacrylate-Based Shape-Memory Polymers

David Santiago, Silvia De la Flor, Francesc Ferrando, Xavier Ramis, Marco Sangermano

Macromolecules Chemistry and Physics ***2016****, 217, 39-50*

UNIVERSITAT ROVIRA I VIRGILI
EXPERIMENTAL CHARACTERIZATION OF SHAPE-MEMORY POLYMERS: INFLUENCE OF PROCESSING METHODS AND CHEMICAL STRUCTURE
David Manuel Santiago Abraira

Macromol. Chem. Phys. 2016, 217, 39-50

Thermomechanical Properties and Shape-Memory Behaviour of Bisphenol A Diacrylate-Based Shape-Memory Polymers

David Santiago[1], Silvia De la Flor[1], Francesc Ferrando[1], Xavier Ramis[2], Marco Sangermano[3]

[1] Department of Mechanical Engineering, Universitat Rovira i Virgili, Av. Països Catalans 26, 43007 Tarragona, Spain

[2] Thermodynamics Laboratory, Heat Engines Department, ETSEIB, Universitat Politècnica de Catalunya, Av. Diagonal 647, 08028, Barcelona, Spain

[3] Dipartamento di Scienza Applicata e Tecnologia, Politecnico di Torino, C.so Duca degli Abruzzi 24, 10129, Turin, Italy

Abstract

A series of acrylate-based shape-memory materials are synthesized from bisphenol A diacrylate monomers as crosslinking agents. Networks are synthesized by keeping constant the content of bisphenol A-based crosslinking agent and systematically varying the content ratio of different mono-functional chain builder monomers. The implications of the structure of bisphenol A-based monomers and the chemical structure and content of mono-functional monomers on thermomechanical properties are discussed. Thermomechanical properties are analysed using dynamic mechanical analyses and mechanical properties are studied at room temperature and at the onset of the glass transition temperature. Shape-memory performances under isothermal and transient temperature conditions are also carried out. Tensile tests show excellent values of stress at break up to 45 and 15 MPa at room and high temperature respectively. The measurements show excellent shape recovery and shape fixity ratios, around 95 % and 97 % respectively. These materials also

show very high recovery velocities under transient temperature conditions, up to 24 % min^{-1}, and very short recovery times, up to 1.5 seconds, under isothermal conditions in a water bath. The results confirm that networks synthesized from bisphenol A crosslinkers are promising shape-memory materials.

Keywords: *acrylate, bisphenol A, isothermal, mechanical properties, shape-memory polymers*

1. Introduction

Shape-memory polymers (SMPs) are a class of materials that have the capability of changing their shape upon application of an appropriate external stimulus. These polymers can be processed in a permanent or original shape by conventional techniques and then, deformed in a new or temporary shape that can remain stable until the stimulus is applied [1]. The shape changing is usually driven by heat but it can also be driven by light, magnetic field or an electrical current [2-4]. In the recent years, SMPs have attracted a lot of interest due to their wide range of applications including self-deployable structures for aerospace applications, smart fibers and fabrics for smart clothing, electronics or biomedical devices [5-8].

Usually SMPs are classified depending on their chemically nature (thermoplastic or thermosets) and transition temperature (glass or melting transition temperature). The most common SMPs are usually thermoplastics due to their high deformability and easy processing, making them suitable for a great variety of potential applications [9,10]. However, in recent years some studies have reported shape memory thermosets with excellent mechanical and shape memory properties such as epoxy-based or UV-polymerized acrylate-based shape memory polymers [11,12].

UV-polymerization is growing in importance due to their wide fields of applications including surface coatings, adhesives, printing inks or composites materials [13-16]. Radical UV-polymerization possesses many advantages in front of traditional thermal curing: faster polymerization rates, lower energy consumption because it is usually carried out at room temperature and it is environmental friendly due to the use of solvent-free formulations [17].

The primary backbone of acrylate-based shape-memory networks are formed through free radical polymerization of crosslinking monomers and pendant segments formed by mono-functional chain builder monomers [18]. Several works have focused on the use of acrylate-based shape-memory polymers for biomedical applications due to their high degree of biocompatibility [19]. Smith *et al.* [20] investigated how the mechanical properties of methacrylate networks are influenced by physiological conditions by using poly(ethylene glycol) dimethacrylate and different mono-functional monomers. Ortega *et al.* [21] studied the effect that crosslinking and long-term storage have on shape memory properties of different formulations formed by the copolymerization of *tert*-butyl acrylate with poly(ethylene glycol) dimethacrylate with different molecular weights. Smith *et al.* [22] studied the relationship between mechanical properties and chemical structure of materials synthesized from poly(ethylene glycol) dimethacrylate and three different mono-functional monomers deformed in air and under hydrated conditions.

Other works have focused on studying thermal, mechanical and shape memory properties of these networks as well as the influence of the functionality and the concentration of the monomers on such properties. Yakacki *et al.* [23] investigated the influence of the polymer network on free and constrained recovery under isothermal and transient temperature conditions in materials obtained from synthesizing methyl-methacrylate and poly(ethylene glycol) dimethacrylate. Arrieta *et al.* [12] studied the shape memory properties of a network formed by benzyl

methacrylate and poly(ethylene glycol) dimethacrylate. They programmed the temporary shape at different programming temperatures and performed free and constrained recovery at different heating rates.

Accordingly, acrylate-based shape-memory networks synthesized from poly(ethylene glycol)-based monomers as crosslinking agents are fully characterized and have demonstrated their excellent mechanical and shape-memory properties. However, minus work has been done with different crosslinking agents, such as bisphenol A-based diacrylate monomers. Networks formed by this kind of monomers are commonly used in many applications due to their good adhesion, hardness and thermal and chemical resistance [24]. By substituting poly(ethylene glycol)-based acrylate crosslinkers for bisphenol A-based crosslinkers with higher cohesive energy density (CED), it is expected higher glass transition temperatures as well as an increase of the mechanical properties due to the presence of aromatic rings within the structure. In this sense, this study proposes the use of bisphenol A-based bi-functional monomers as crosslinking agents for shape-memory thermosets.

A few works have explored the use of bisphenol A-based crosslinking agents for shape-memory materials. Safranski and Gall [18] studied the effect of chemical structure and crosslinking density on the thermal and mechanical properties of (meth)acrylate networks. The authors proposed different mono-functional monomers as chain builder and different multi-functional monomers as crosslinking agents, including bisphenol A-based monomers. Voit *et al.* [25] studied the transition of acrylate-based materials from thermoplastic to thermosets in order to obtain high strain shape-memory polymers. For this purpose, these authors suggested to minimize the concentration of bisphenol A ethoxylate di(meth)acrylate crosslinking agent until less than 0.25%. However, it is necessary a further investigation of the implications that the presence of this kind of monomers have on thermomechanical properties and a deep study of the shape-memory properties.

Therefore, in the present study a family of shape-memory materials is synthesized from three different mono-functional monomers as chain builders, and two different bisphenol A-based bi-functional monomers as crosslinking agents. The networks are synthesized by keeping the content of crosslinking agent constant and systematically varying the content ratio of different mono-functional monomers. The implications of the chemical structure of bisphenol A-based monomers and mono-functional monomers on the thermomechanical and viscoelastic properties are analyzed and discussed. Tensile tests and shape-memory performances have revealed shape-memory materials with good mechanical properties, both at room and high temperatures, and excellent shape-memory properties with very high recovery and fixity ratios and fast recovery velocities under isothermal and transient temperature conditions.

2. Experimental Section

2.1 Materials

Diglycidyl ether of bisphenol A diacrylate (Ebecryl® 605, Allnex) (based on 75/25 w/w bisphenol A diacrylate/tripropylene glycol diacrylate) with M_w = 500 g mol^{-1} (Figure IV.7.1a) and diglycidyl ether of bisphenol A ethoxylate diacrylate (Sigma-Aldrich) with M_n = 512 g mol^{-1} (Figure IV.7.1b) were used as crosslinker agents. Methyl methacrylate (Sigma-Aldrich) (Figure IV.7.1c), ethyl methacrylate (Sigma-Aldrich) (Figure IV.7.1d) and poly(ethylene glycol) methylether methacrylate (Sigma-Aldrich) with M_n = 475 g mol^{-1} (Figure IV.7.1e) were used as mono-functional chain builders. Darocur® 1173 (BASF) was used as photoinitiator (Figure IV.7.1f).

The CED was calculated for MMA, EMA and PGM in order to discuss thermal and mechanical properties of the materials prepared. CED parameter characterizes the intermolecular interactions in polymers using the group contributions according to the method outlined by Van

Krevelen [26]. The CED values for MMA, EMA and PGM were 398 MPa, 385 MPa and 340 MPa respectively.

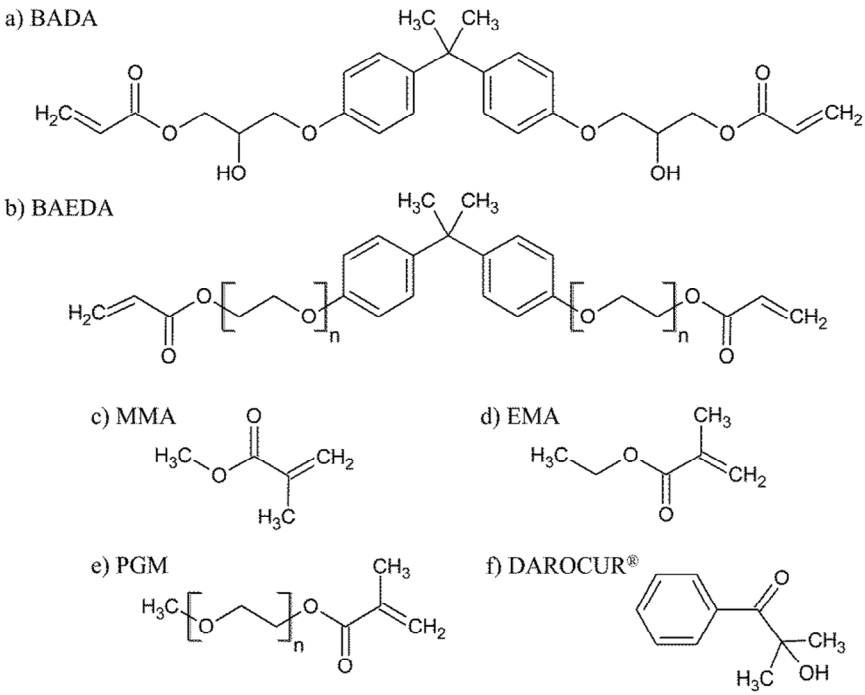

Figure IV.7.1 a) Chemical structure of Bisphenol A diacrylate; b) chemical structure of Bisphenol A ethoxylate diacrylate; c) chemical structure of methyl methacrylate; d) chemical structure of ethyl methacrylate; e) chemical structure of poly(ethylene glycol) methylether methacrylate; f) chemical structure of Darocur® 1173.

Various formulations with different content of each reactant were prepared and are summarized in Table IV.7.1. The formulations were prepared by mixing 50 wt. % of bisphenol A diacrylate (BADA) or bisphenol A ethoxylate diacrylate (BAEDA) which acted as crosslinker agents and 50 wt. % of a mixture of methyl methacrylate (MMA), ethyl methacrylate (EMA) or poly(ethylene glycol) methylether methacrylate (PGM) which acted as mono-functional chain builders. The content of

crosslinking agent was kept constant in both set of formulations in order to avoid the effect of different crosslinking densities within the networks. Preliminary studies concluded that formulations with BADA synthesized with no presence of PGM or with BAEDA synthesized with a MMA:PGM or EMA:PGM ratio of 1:3 were not suitable for shape-memory performances because they showed too high and too low values of stiffness respectively. The photoinitiator 2-hydroxy-2-methyl-1-phenyl-propan-1-one (Darocur® 1173, BASF) was added at a concentration of 2 wt. % of the total formulation weight. The reactants were mixed manually in an opaque plastic vial until fully dissolved and poured in an open mould with dimensions 30 mm x 3.75 mm x 0.75 mm. The polymerization took place by exposing the configuration to UV light (Helios Italquartz) for 2 min at an intensity of ~100 mW cm^{-2} (measured with an EIT UV-meter) in a nitrogen atmosphere. Finally the samples were polished to obtain the final dimensions for each test.

Table IV.7.1 Composition of the formulations studied

	Sample	wt. % BADA	wt. % BAEDA	wt. % MMA	wt. % EMA	wt. % PGM
1	BA-1M-3P	50	0	12.5	0	37.5
2	BA-2M-2P	50	0	25	0	25
3	BA-3M-1P	50	0	37.7	0	12.5
4	BA-1E-3P	50	0	0	12.5	37.5
5	BA-2E-2P	50	0	0	25	25
6	BA-3E-1P	50	0	0	37.5	12.5
7	BAE-2M-2P	0	50	25	0	25
8	BAE-3M-1P	0	50	37.5	0	12.5
9	BAE-M	0	50	50	0	0
10	BAE-2E-2P	0	50	0	25	25
11	BAE-3E-1P	0	50	0	37.5	12.5
12	BAE-E	0	50	0	50	0

2.2 Thermomechanical Characterization

Thermomechanical properties were measured using a DMA Q800 (TA Instruments) equipped with a film-tension clamp. Prismatic rectangular samples of ca. 20 mm x 2 mm x 0.5 mm were analysed at 1 Hz, 0.1% strain and a heating rate of 3 ºC min^{-1} from -30 to 150 ºC. The glass transition temperature T_g, the onset of the glass transition temperature $T_g^{E'}$ and the storage modulus below and above the glass transition temperature were evaluated (E'_g and E'_r respectively) (Figure IV.7.2). The glass transition temperature was determined from the peak in the loss factor tan δ. The onset of the glass transition temperature $T_g^{E'}$ was determined as the point at which the storage modulus E' started to decrease during mechanical relaxation.

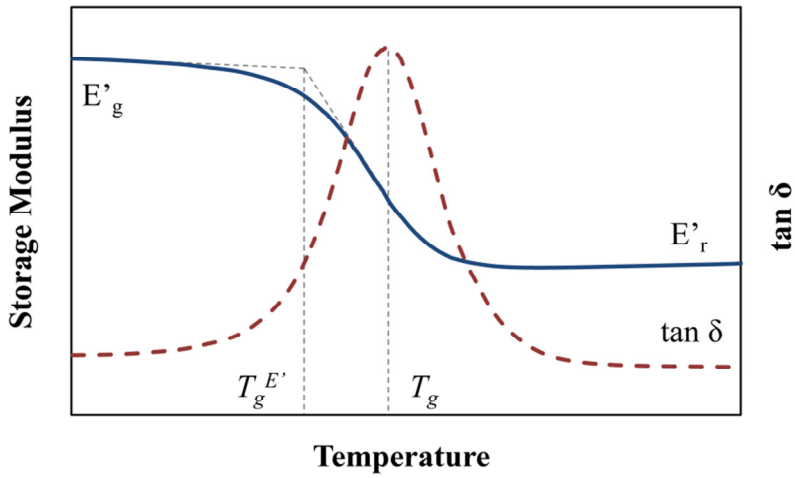

Figure IV.7.2 Determination of the temperatures T_g and $T_g^{E'}$ from the results obtained with DMA analysis.

2.3 Fourier Transform Infrared Spectroscopy (FT-IR) Characterization

Final conversion of each formulation was evaluated by Fourier transform infrared spectroscopy (FT-IR). Each formulation was irradiated using a FT-IR Thermo-Nicolet 5700 model. The formulations were coated onto

a sample holder (around 50 μm) and exposed to UV-light at an intensity of ~25 mW cm^{-2}. After 30 seconds of UV irradiation, the sample was irradiated with IR which analysed the extent of the reaction and then irradiated again during 30 seconds with UV-light. This process was repeated until final conversion. The disappearance of the peak corresponding to acrylate double bond at 1635 cm^{-1} was monitored and, as the IR absorbance is proportional to the monomer concentration, the final conversion could be obtained.

2.4 Mechanical Characterization

Mechanical properties at room temperature were evaluated using a universal testing machine (Instron 3366) equipped with a 10 kN load cell. Dog-bone shape samples were cut according to ASTM D638 Type IV requirements. Experiments were performed at a crosshead speed of 1 mm min^{-1}. Mechanical properties at high temperature were measured using a DMA Q800 (TA Instruments) equipped with a film-tension clamp in the force controlled mode. Dog-bone shape samples of ca. 20 mm x 2 mm x 0.5 mm were analysed at $T_g^{E'}$ at a force rate of 1 N min^{-1}. In both experiments, three different samples were used and the average values are shown, and strain was calculated as the total elongation ($L_f - L_0$) (displacement of the crosshead) with respect to the initial length (L_0) (Equation IV.7.1).

$$\varepsilon(\%) = \frac{L_f - L_0}{L_0} \cdot 100 \qquad \text{(IV.7.1)}$$

2.5 Shape-Memory Characterization

The shape-memory properties were measured using a DMA Q800 with a force-controlled mode and equipped with a film-tension clamp. Dog-bone shape samples of ca. 20 mm x 2 mm x 0.5 mm were used in shape-memory tests. The procedure for imposing a temporary shape to the SMP was a thermomechanical cycle called programming and consisted in

various steps (Figure IV.7.3). The programming began with heating up the sample to the programming temperature T_{prog} and deforming to a prescribed value of maximum stress σ_m at a 1 MPa min^{-1}. The deformation of the sample once had been stretched was ε_m. The next step was cooling down the sample into a temperature below the transition temperature T_{low} (0 ºC) in order to fix the temporary shape. After fixation, the stress was released at the same stress rate of 1 MPa min^{-1}. There was an amount of deformation that the SMP cannot fix and the deformation of the sample after unloading was ε_u. The recovery process was activated by heating up the sample to a recovery temperature $T_{recovery} = T_g + 10$. The heating rate during shape recovery was 3 ºC min^{-1}. The deformation at the end of programming was ε_p which is the amount of deformation that the SMP cannot recover. At this point a new cycle began by adjusting the temperature again to T_{prog}. Three consecutive cycles were performed to each sample.

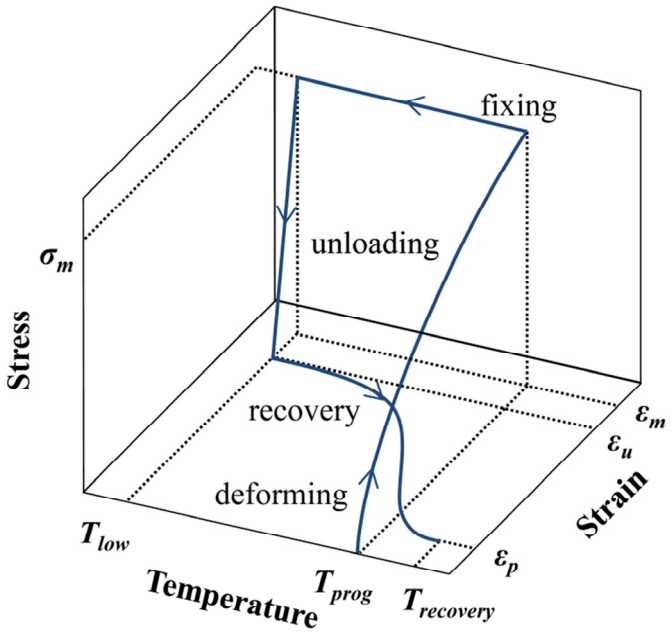

Figure IV.7.3 Scheme of the thermomechanical programming.

The programming temperature was selected as the onset of the glass transition temperature $T_g^{E'}$ (Figure IV.7.2). According to Yakacki *et al.* [27] a maximum in the deformability of shape-memory acrylate-based polymer can be obtained at a temperature coinciding with the onset of glass transition temperature.

Every sample was stretched into a determined value of maximum stress σ_m, corresponding to a 75% of the stress at break σ_b ($\sigma_m = 0.75\sigma_b$) in order to perform a comparative study with the same level of load for each sample.

The most significant parameters for quantifying shape-memory properties are the shape-recovery ratio (R_r) and the shape-fixity ratio (R_f). The shape-recovery ratio (Equation IV.7.2) quantifies the ability of the SMP to recover its original shape and it was calculated as the total deformation recovered with respect to the maximum deformation reached during the programming. The values of shape-recovery ratio presented correspond to the average value of the three consecutive cycles.

$$R_r(\%) = \frac{\varepsilon_m - \varepsilon_p}{\varepsilon_m} \cdot 100 \qquad \text{(IV.7.2)}$$

The shape-fixity ratio, calculated from Equation IV.7.3, quantifies the ability of the SMP to fix the temporary shape. It was computed as the deformation after the stress was released with respect to the maximum deformation.

$$R_f(\%) = \frac{\varepsilon_u}{\varepsilon_m} \cdot 100 \qquad \text{(IV.7.3)}$$

Another parameter of interest to evaluate the shape memory ability is the shape recovery velocity (V_r). The shape recovery velocity quantifies the velocity at which the permanent shape is recovered. V_r was calculated

as the time interval that it takes from 15% to 85% of strain recovered (Equation IV.7.4).

$$V_r\,(\%/\mathrm{min}) = \frac{\left(\frac{\varepsilon_{rec,15\%} - \varepsilon_{rec,85\%}}{\varepsilon_{rec,15\%}}\right) \cdot 100}{\Delta t_{15\%-85\%}} \qquad \text{(IV.7.4)}$$

Where $\varepsilon_{rec,15\%}$ is the deformation corresponding to a shape recovery of 15%, $\varepsilon_{rec,85\%}$ is the deformation corresponding to a shape recovery of 85% and $\Delta t_{15\%-85\%}$ is the time interval between these two points. The difference between deformations corresponding to a shape recovery of 15% and 85%, $\varepsilon_{rec,15\%} - \varepsilon_{rec,85\%,}$ was calculated with respect to $\varepsilon_{rec,15\%}$ in order to avoid the influence of the maximum deformation on V_r.

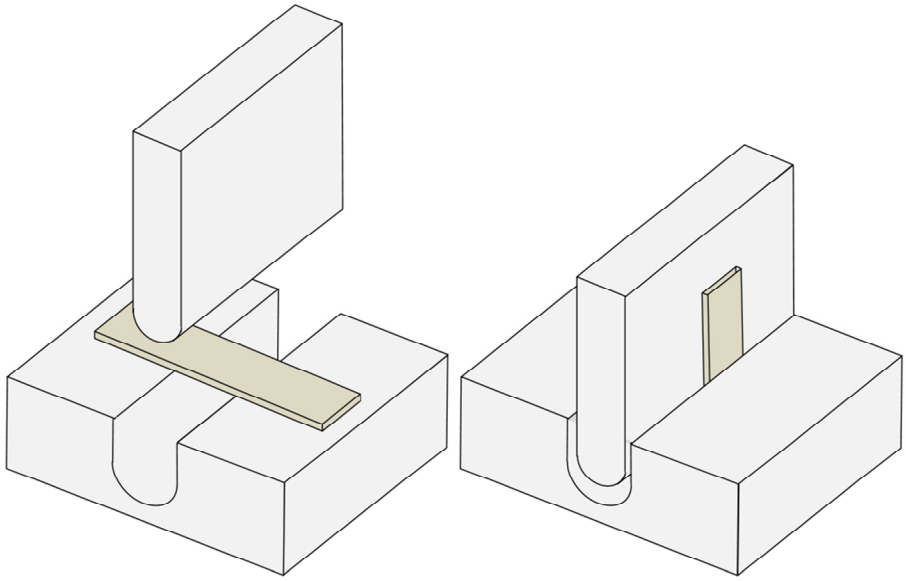

Figure IV.7.4 Schematic representation of the deformation of the sample with the U-shaped fixture.

Self-deploy shape-memory tests were also performed in order to evaluate the recovery process under isothermal conditions. Prismatic rectangular samples of ca. 30 mm x 3.75 mm x 0.75 mm were used. The

samples were immersed in a hot water bath at $T_{prog} = T_g$ of each formulation and held for 30 seconds. After heating, the samples were deformed into "U" shape (which corresponded to an angle of $\theta = 180º$) with a specially designed device (Figure IV.7.4). Then, the samples were immersed in cold water ($T_{low} = 10$ ºC) for 5 minutes while maintaining the "U" shape. In order to evaluate the shape recovery process, the samples were immersed again in hot water at different $T_{recovery}$. The angle θ was monitored in each time of the recovery until the sample reached a complete recovery ($\theta = 0º$) or until finalised the recovery process.

3. Results and Discussion

3.1 Thermomechanical Properties

Table IV.7.2 summarizes the thermomechanical properties of all formulations. The glass transition temperature of the network increases with increasing content of methyl methacrylate (MMA) or ethyl methacrylate (EMA) and decreasing content of poly(ethylene glycol) methylether methacrylate (PGM). Each set of formulations (either with BADA or BAEDA) have the same backbone because they have the same type and amount of crosslinking agent and thus the pendant side group is the one that determines the T_g [18]. Since the pendant side group is changed from long and mobile PGM segments to short and rigid MMA or EMA segments, the molecular mobility of the network is restricted and thus causing a delaying in the transition from glassy to rubbery state. This result can be rationalized in terms of cohesive energy density (CED) of the mono-functional monomers. The CED parameter reflects the cohesive strength of the network and, as the T_g, is a parameter governing the yield response of glassy networks [28]. The higher CED parameter of monomers MMA and EMA (398 and 385 MPa) with respect to the CED parameter of the PGM (340 MPa) leads to formulations with a more cohesive structure and thus with higher glass transition temperatures.

The shape of the tan δ peak during the material relaxation can also be correlated with its network structure. The peak height is an indicator of the viscous character of the material during the relaxation and the total peak area is related with the total amount of the energy dissipated during relaxation [29]. As can be observed in Table IV.7.2 and Figure IV.7.5, an increase in the content of PGM causes a broadening of the width of the transition and a lowering of the peak height and area of tan δ. This trend indicates that the presence of PGM leads to a more heterogeneous network due to the longer length of the polymeric chain of PGM.

Table IV.7.2 Thermomechanical results obtained by DMA

Sample	T_g[a] [ºC]	$T_{gE'}$ [ºC]	FWHM[b] [ºC]	tan δ height	tan δ area[c]	E'_g[d] [MPa]	E'_r[e] [MPa]	E'_g/E'_r
BA-1M-3P	45	21	32	0.53	17	2125	30	71
BA-2M-2P	67	44	27	0.65	18	2214	25	87
*BA-3M-1P	80	61	22	0.90	20	2741	20	140
BA-1E-3P	41	15	29.	0.53	15	1799	31	59
BA-2E-2P	53	30	28	0.64	18	2246	27	84
*BA-3E-1P	69	50	23	0.81	19	2676	24	111
BAE-2M-2P	44	24	22	0.77	17	2244	21	106
*BAE-3M-1P	62	44	21	0.86	18	2750	20	138
*BAE-M	87	72	19	1.01	19	2712	16	166
BAE-2E-2P	33	15	23	0.78	18	2095	23	91
*BAE-3E-1P	50	34	19	0.90	17	2565	21	122
*BAE-E	70	49	21	0.96	20	2593	17	152

[a]Measured as the peak of tan δ; [b]Full With at Half Maximum; [c]Determined as the product of tan δ peak and FWHM; [d]Measured at T_g – 50 ºC; [e]Measured at T_g + 50 ºC; *Formulations selected for shape-memory analysis

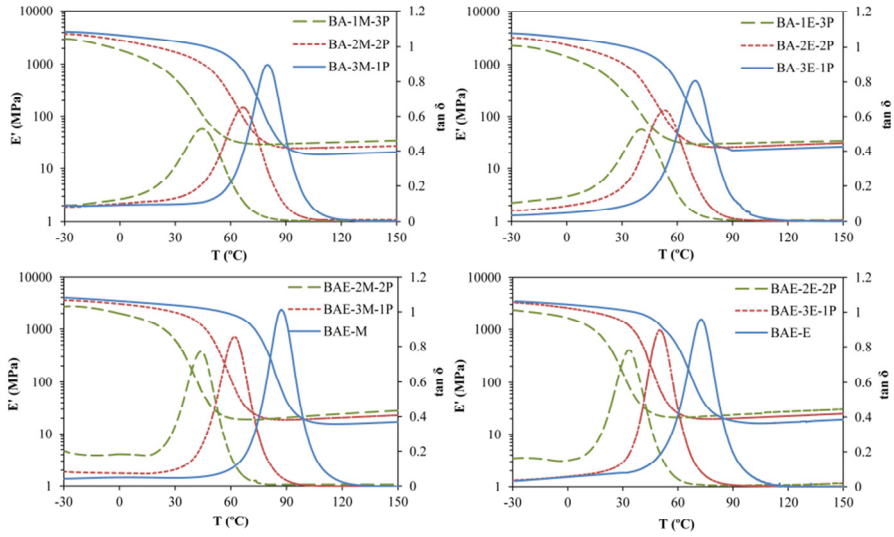

Figure IV.7.5 Storage modulus *E'* and tan δ as a function of temperature of all formulations.

The trend of the glass transition temperature contrasts with the trend of the storage modulus at rubbery region *E'*, which decreases with increasing content of MMA or EMA (Figure IV.7.6). This trend could be explained in terms of the architecture of the polymer chain between crosslinks. As the content of crosslinking agent is kept near constant, each set of formulations (either with BADA or BAEDA) has the same crosslinking points. Thus, as the content of MMA or EMA increases, the distance between crosslinking points increases and the length of the pendant side group decreases. Consequently the rubbery modulus decreases due to the higher molecular motion of formulations with higher content of MMA or EMA. Other factors may also contribute to this behaviour, as the formation of physical crosslinks or molecular interactions between the poly(ethylene glycol) side-chains of PGM units.

The storage modulus at glassy region increases as the content of PGM decreases and the content of MMA/EMA increases, according to the lower CED values of PGM.

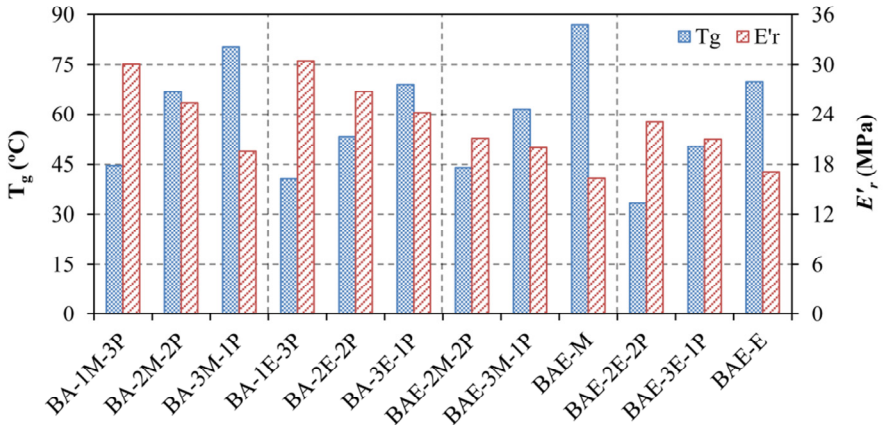

Figure IV.7.6 Glass transition temperature T_g and storage modulus E' in the rubbery region of all formulations.

Comparing the behaviour of formulations with bisphenol A ethoxylate diacrylate (BAEDA) and with bisphenol A diacrylate (BADA), the first have lower glass transition temperatures, around 20 ºC in formulations with the same type of mono-functional monomer and content ratio. The shape of the transition indicates a more homogeneous and mobile network with BAEDA than with BADA: the width of the transition is narrower and the peak height is higher (Table IV.7.2 and Figure IV.7.5). In addition, the storage modulus at rubbery region E'_r shows lower values with BAEDA than with BADA. The existence of hydrogen-bond interactions in formulations with BADA and the presence of flexible oxyethylene groups in formulations with BAEDA lead to a lower T_g and a more flexible and mobile structure in the relaxed state.

Among all the formulations analysed in Table IV.7.2, only those that show a difference between the storage modulus at glassy and rubbery region around 2 orders of magnitude were chosen to further studies (denoted by * in Table IV.7.2). This important difference in mechanical properties between the glassy and rubbery states is crucial if a polymer is

required to present shape-memory effect [30]. Although the formulation BAE-2M-2P has a properly E'_g/E'_r ratio, it has low glass transition temperature (44 ºC) and cold storage of the temporary shape would be necessary in order to guarantee acceptable fixation. For this reason these formulation were not selected for further studies.

3.2 IR Characterization

In Table IV.7.3 are noted the values of final conversion of the selected formulations. The polymerization rate is extremely fast and within the first 30 seconds of irradiation the conversion reached values around 90% in all cases.

Table IV.7.3 Conversion values of the selected formulations obtained by FT-IR

Sample	BA-3M-1P	BA-3E-1P	BAE-3M-1P	BAE-M	BAE-3E-1P	BAE-E
Conversion (%)	97	98	98	93	100	95

3.3 Mechanical Properties

Mechanical properties at room temperature (~21 ºC) are showed in Table IV.7.4 and Figure IV.7.7. Figure IV.7.7 clearly shows two different behaviours between formulations with BADA and BAEDA. Whereas formulations with BAEDA show a large plateau of plastic deformation with deformations at break of almost 30% (except in the case of the formulations BAE-E), formulations with BADA barely show plastic deformation, with failure strain around 11%. In the case of ultimate strength, formulations with the same type and content ratio of mono-functional monomers, the ultimate strength is more than a 100% higher in formulations with BADA than with BAEDA. Properties below the glass transition temperature depend on a combination of factors such as the cohesive forces and presence of local mobility [31]. This different behaviour may be attributed to the presence of flexible and mobile

oxyethylene groups of BAEDA and the existence of hydrogen-bonds in formulations with BADA.

Table IV.7.4 Tensile data at room temperature obtained by uniaxial tensile testing: ultimate strength (σ_{max}), corresponding strain at ultimate strength ($\varepsilon_{\sigma max}$), stress at break (σ_b), deformation at break (ε_b), elastic modulus and difference between T_g - T_{room}

Sample	σ_{max} [MPa]	$\varepsilon_{\sigma max}$ [%]	σ_b [MPa]	ε_b [%]	Elastic modulus [MPa]	T_g - T_{room} [ºC]
BA-3M-1P	42.8±0.4	8.1±0.8	42.0±0.4	9.4±0.9	853.4±5.2	59
BA-3E-1P	24.4±0.2	7.9±0.9	23.4±0.1	12.5±0.2	510.7±4.9	48
BAE-3M-1P	20.6±0.1	6.3±0.5	18.2±0.3	18.2±0.9	477.0±1.7	40
BAE-M	45.9±0.9	6.4±0.3	39.1±0.1	25.5±0.3	948.9±2.5	66
BAE-3E-1P	9.7±0.4	5.2±0.7	12.4±0.5	29.0±0.2	216.6±4.1	29
BAE-E	31.4±0.4	7.2±0.8	26.3±0.3	15.7±0.1	916.3±5.0	49

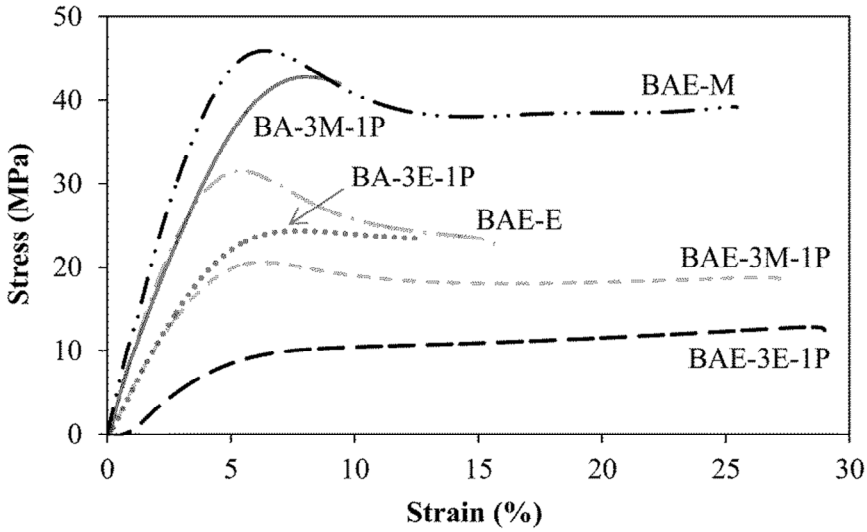

Figure IV.7.7 Stress-strain experiments of the selected formulations at room temperature.

In both cases, either with BADA or BAEDA as crosslinking agents, the ultimate strength σ_{max} is higher in formulations with MMA than with EMA. This difference is more accused in the presence of PGM (75% higher in BA-3M-1P than in BA-3E-1P and 100% higher in BAE-3M-1P than in BAE-3E-1P) than in formulations without PGM (50% higher in BAE-M than in BAE-E).

As stated above, mechanical properties depend on different factors and among them the difference between the test temperature and T_g. The observed tendency clearly shows that the strength and elastic modulus increases almost linearly with increasing T_g - T_{room}.

Table IV.7.5 summarizes the mechanical properties evaluated at $T_g^{E'}$. All formulations show high values of stress at break, higher than 10 MPa in all cases and up to 15 MPa for the formulation BAE-3E-1P. The values of stress at break at the onset of the glass transition temperature of formulations with poly(ethylene glycol)-based crosslinking agents are usually much lower, which in no case exceed 10 MPa [19,22,27].

Table IV.7.5 Tensile data at $T_g^{E'}$ obtained by DMA: onset of the glass transition temperature $T_g^{E'}$, stress at break (σ_b), deformation at break (ε_b), tensile modulus, prescribed stress for shape memory programming (σ_m) and strain corresponding to σ_m (ε_m)

Sample	$T_g^{E'}$ [ºC]	σ_b [MPa]	ε_b [%]	Tensile modulus [MPa]	σ_m [MPa]	ε_m [%]
BA-3M-1P	61	12.1±0.9	32.0±0.2	34.8±1.2	9.1	24.0
BA-3E-1P	50	10.0±0.5	27.2±0.3	34.3±0.5	7.5	20.4
BAE-3M-1P	44	11.2±0.6	41.5±0.1	25.3±0.9	8.4	31.1
BAE-M	72	13.5±0.6	50.7±0.2	24.3±0.2	10.1	38.0
BAE-3E-1P	34	15.4±0.5	57.0±0.3	26.6±0.8	11.5	42.8
BAE-E	49	11.8±0.7	40.4±0.9	26.9±0.7	8.9	30.3

The tensile modulus reveals two different behaviours depending on the crosslinking agent used. Formulations with BADA show a tensile modulus around 34 MPa while formulations with BAEDA show tensile modulus around 25 MPa. This leads to a higher deformation at break to formulations with BAEDA. This different behaviour is due to the presence of oxyethylene groups within the structure of BAEDA and the presence of hydrogen bonds in formulations with BADA. These results correlated well with the results of the mechanical properties evaluated at room temperature, where two different behaviours were also observed between formulations with BADA and BAEDA.

3.4 Shape-Memory Properties

In order to perform a comparative study with the same level of load for each sample, every sample was stretched during shape-memory programming to a prescribed maximum stress (σ_m) corresponding to 75% of the stress at break ($\sigma_m = 0.75\sigma_b$). Table IV.7.5 presents the prescribed maximum stress and the corresponding maximum deformation reached, ε_m, for each material. Figure IV.7.8 shows the average shape-recovery ratio (R_r) and shape-fixity ratio (R_f) of three consecutive cycles when programming under these conditions (σ_m and $T_g^{E\backslash}$) of each formulation.

All formulations show shape-recovery ratios around 95%, except formulation BAE-3E-1P which shows 91%, and shape-fixity ratios around 97%. Shape-memory properties can also be correlated with thermomechanical properties and network structure. During the programming step, the material can be easily deformed with a significant decrease in the entropy of the system due to chain conformation rearrangement. When the applied external stress is released at low temperature, the lower mobility of the network structure prevents chain rearrangement and holding the remaining deformation. Once the temperature exceeds the T_g, the network chains gain sufficient mobility and thus the SMP is able to recover its original shape. Therefore, it can

be assumed that network relaxation dynamics is the key parameter governing the recovery process [32].

In the case of formulation BAE-3E-1P, although the tensile test at $T_g^{E'}$ (Table IV.7.5) do not reveal significant differences among all formulations, the accumulation of plastic deformation may be the cause of the lower recovery ratio with respect to the rest of formulations.

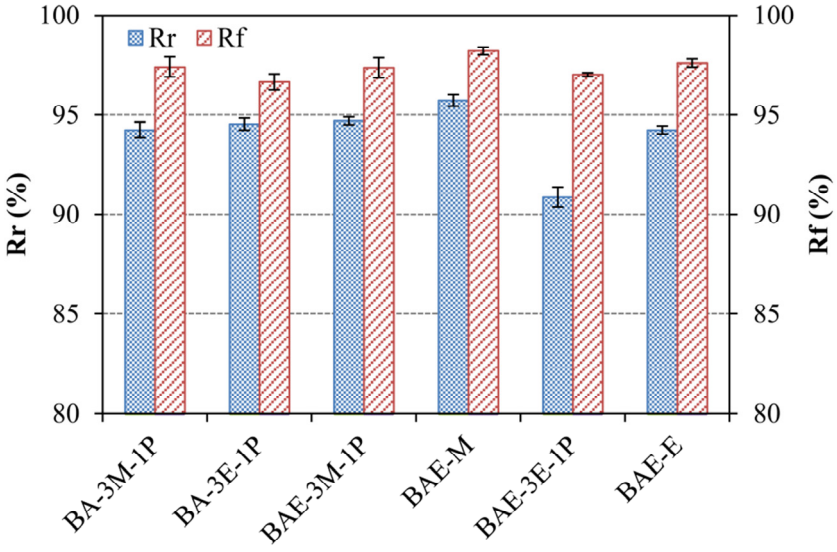

Figure IV.7.8 Shape-recovery ratio and shape-fixity ratio of each formulation.

Figure IV.7.9 shows the strain recovered ε_{rec} during the recovery stage (Figure IV.7.9a) and the shape-recovery velocity V_r (Figure IV.7.9b) for all samples. The recovery speed shows very high values for all formulations; it is possible to obtain a 95% of shape recovery in a few minutes and in a narrow interval of temperatures. As the maximum deformation during stretching has no influence on this parameter, the values and trend of V_r can be explained in viscoelastic terms. Although no significant differences were observed in terms of recovery and fixation between the studied formulations, it seems that the recovery velocity is more sensitive to small changes in the thermomechanical properties and

network structure between formulations. It can be observed that formulations with BADA show lower values of V_r (around 18 % min^{-1}) than formulations with BAEDA (around 22 % min^{-1}). Formulations with BAEDA have a more homogeneous and mobile network due to the presence of flexible oxyethylene groups, thus it will take shorter to release the stored internal stresses during the recovery process (Table IV.7.2 and Figure IV.7.5). Formulation BAE-3E-1P presented lower shape-recovery velocity in comparison with the other formulations with BAEDA. The accumulation of plastic deformation during the deformation stage of programming, that also lowered the shape-recovery ratio (Figure IV.7.8), may also be the cause of the difference on V_r with respect to the rest of formulations with BAEDA.

Formulations BAE-M and BAE-E show the highest values of V_r (21.40 % min^{-1} and 22.62 % min^{-1} respectively). The presence of PGM within the networks (Table IV.7.2 and Figure IV.7.5) leads to more heterogeneous networks, with shorter chain length between crosslinks and long pendant chains that slow down the recovery velocity.

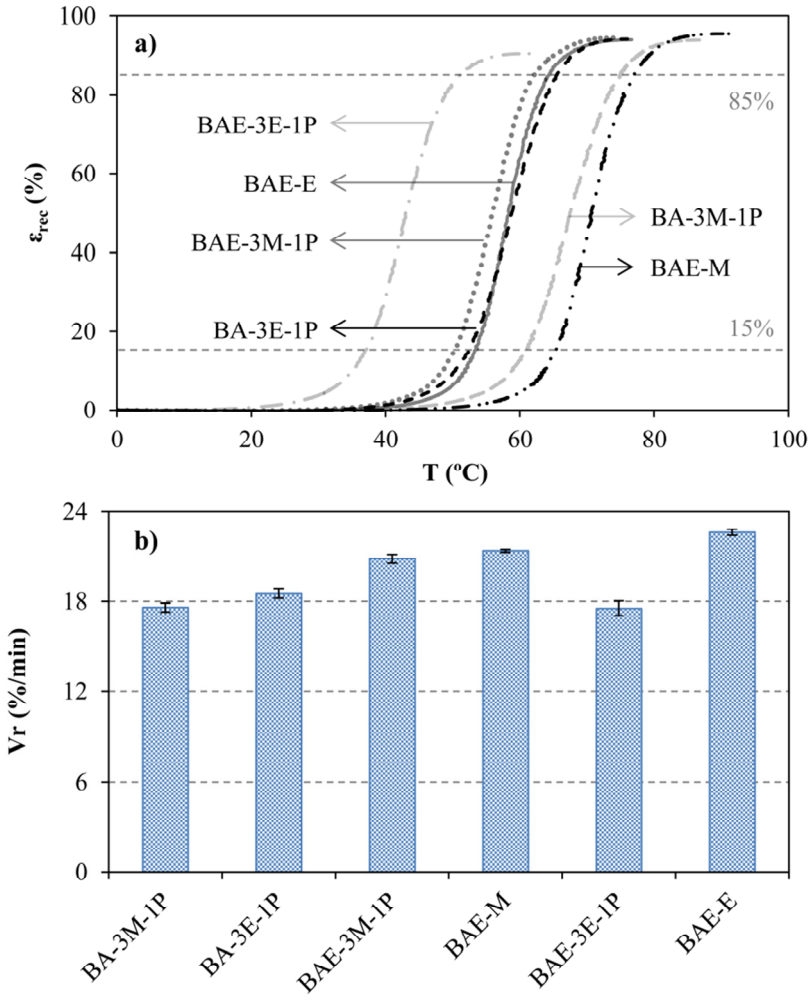

Figure IV.7.9 Strain recovered ε_{rec} during heating (a) and shape-recovery velocity V_r (b) of all formulations.

In order to evaluate the recovery velocity under isothermal conditions, self-deploy experiments were performed. The interest of isothermal recovery performances lies in the fact that in many applications the recovery process is triggered at a constant temperature [33]. Results demonstrate the excellent recovery velocities also in isothermal conditions: samples need just a few seconds to reach their

original shape and to achieve a complete recovery. Figure IV.7.10 shows the recovery process of the formulation BAE-M at $T_{recovery} = T_g$. The sample only takes 3 seconds (including the immersion time) to regain its original shape.

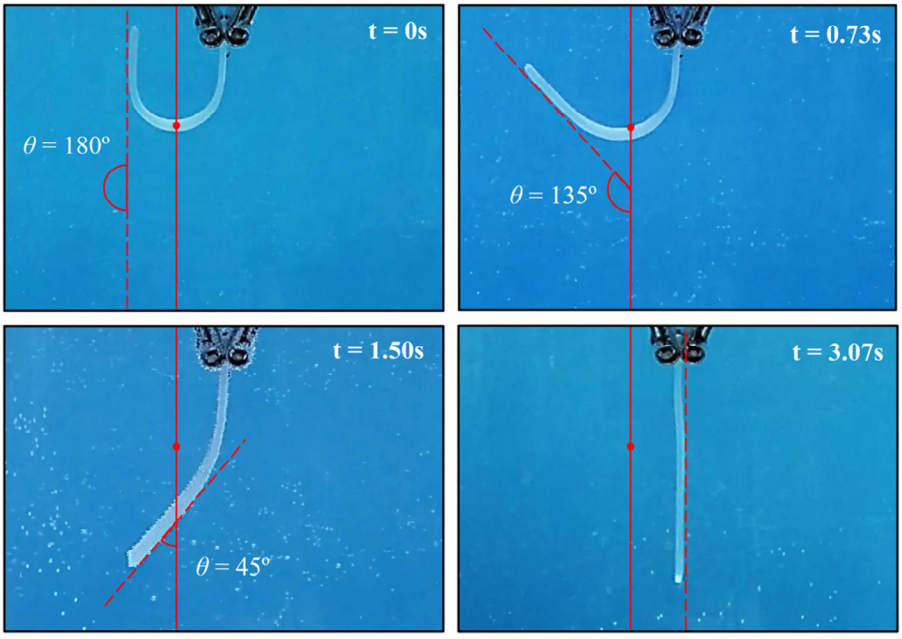

Figure IV.7.10 Recovery process of the formulation BAE-M at $T_{recovery} = T_g$.

Figure IV.7.11 shows the recovered angle θ versus time for each formulation at three different recovery temperatures. The results show extremely short recovery times. Even when the recovery temperature is lower than the glass transition temperature, the majority of the formulations achieve a complete recovery in less than 10 seconds. Although formulations BAE-3M-1P and BAE-M do not reach a complete recovery at $T_{recovery} = T_g$ - 10, the recovery times are quite fast (less than 30 seconds) with corresponding recoveries of 92%.

As expected, it takes less time to achieve a complete recovery with increasing recovery temperature. With an increase in the recovery temperature, the thermal motion of the polymer chains is accentuated

and thus the recovery force increases [34]. When $T_{recovery} = T_g$ and $T_{recovery} = T_g + 10$, the recovery process is almost instantaneous with recovery times around 2.5 and 1.5 seconds respectively.

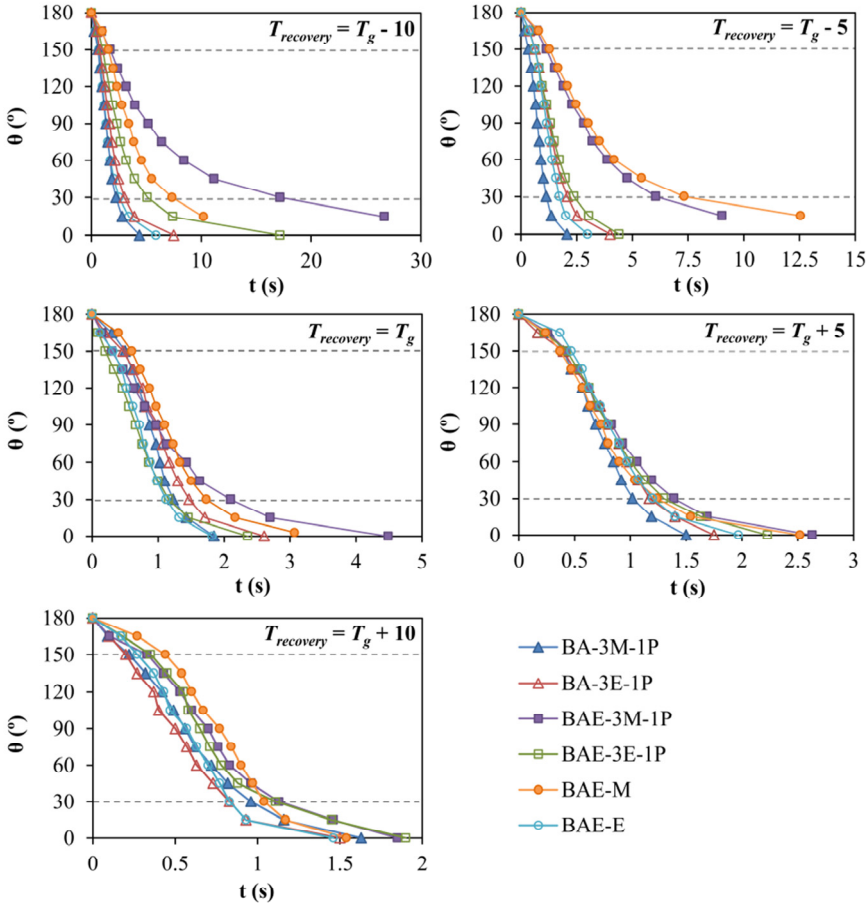

Figure IV.7.11 Recovered angle as a function of time of each selected formulation and at different $T_{recovery}$.

Three stages of recovery can be distinguished from the slope of the curve in each test. The first stage comprises the recovery from 180º to 150º, the second stage comprises from 150º to 30º and the third one comprises from 30º until final recovery. During the first stage, the recovery process is triggered and friction between polymer chains is

causing a relatively low recovery velocity. In the second stage, the gradual arrangement of segments reduces the friction and thus the slope of the curve increases. In the last stage of recovery the slope of the curve reduces significantly due to the most of the constrained force has been released. Other authors studied the isothermal recovery process and highlighted the presence of various zones during the recovery [35-38]. However their results are not comparative because in the present work the use of a hot water bath entails different heat transfer between the environment and the samples.

At $T_{recovery} = T_g - 10$ it can be observed differences on the slope of the curves between formulations, especially in formulations BAE-3M-1P and BAE-M. Below the glass transition temperature the molecular motion are restricted, thus the differences can be attributed to greater difficulty of these formulations in releasing internal stress due to the network architecture. With $T_{recovery} \geq T_g$ differences in recovery velocity between formulations become less significant and only during the third stage can be observed slight differences in the recovery time. In the case of $T_{recovery} = T_g + 10$ the differences between formulations are less than 0.5 seconds and all of them achieved complete recovery around 1.5 seconds.

4. Conclusions

A series of acrylate-based shape-memory thermoset materials were synthesized using bisphenol A-based crosslinking agents and different mono-functional monomers as chain builders. Thermal, mechanical and shape-memory properties were systematically studied and the results were discussed.

The thermomechanical measurements revealed a more heterogeneous network and lower glass transition temperatures with increasing content of PGM and decreasing content of MMA or EMA. Formulations with BAEDA showed lower glass transition temperatures and more homogeneous networks than formulations with BADA. The

thermomechanical properties of acrylate-based shape-memory thermosets can be tuned according to the CED parameter at the mono-functional monomers and the rigidity of the crosslinking agent used.

Mechanical properties at room temperature showed two different behaviours: formulations with BAEDA showed a large plateau of plastic deformation with failure strains of almost 30% than formulations with BADA, with failure strains around 11%. At the programming temperature $T_g^{E'}$, all formulations showed high values of stress at break higher than 10 MPa and up to 15 MPa. Formulations with BAEDA showed lower tensile modulus than formulations with BADA and thus higher failure strains due to the presence of mobile oxyethylene units in BAEDA and the existence of hydrogen-bond interactions in formulations with BADA.

Shape-memory properties showed very good values of shape recovery and shape fixity ratios around 95% and 97% respectively. These materials showed very fast recovery velocities in transient temperature conditions (up to 24 % min^{-1}) and very short recovery times in isothermal conditions (up to 1.5 seconds).

In accordance with these results, acrylate-based shape-memory networks synthesized from bisphenol A-based crosslinking agents are promising shape-memory materials that combine excellent mechanical properties and with very high recovery and fixity ratios as well as very fast recovery velocities.

Acknowledgments

The authors would like to thank MICINN (MAT2014-53706-C03-01 and MAT2014-53706-C03-02) for its financial support.

References

[1] A. Lendlein, S. Kelch, Angew. *Chem. Int. Ed.* **2002**, *41*, 2034–2057.
[2] J. S. Sodhi, P. R. Cruz, I. J. Rao, *Int. J. Eng. Sci.* **2015**, *89*, 1–17.
[3] D. Yang, W. Huang, X. He, M. Xie, *Polym. Int.* **2012**, *61*, 38–42.

[4] S. Chen, S. Yang, Z. Li, S. Xu, H. Yuan, S. Chen, Z. Ge, *Polym. Compos.* **2015**, *36*, 439–444.

[5] Y. Liu, H. Du, L. Liu, J. Leng, *Smart Mater. Struct.* **2014**, *23*, 023001.

[6] A. Gugliuzza, E. Drioli, *J. Membr. Sci.* **2013**, *446*, 350–375.

[7] J. Reeder, M. Kaltenbrunner, T. Ware, D. Arreaga-Salas, A. Avendano-Bolivar, T. Yokota, Y. Inoue, M. Sekino, W. Voit, T. Sekitani, T. Someya, *Adv. Mater.* **2014**, *26*, 4967–4973.

[8] K. J. Cha, E. Lih, J. Choi, Y. K. Joung, D. J. Ahn, D. K. Han, *Macromol. Biosci.* **2014**, *14*, 667–678.

[9] K. K. Julich-Gruner, C. Löwenberg, A. T. Neffe, M. Behl, A. Lendlein, *Macromol. Chem. Phys.* **2013**, *214*, 527–536.

[10] G. J. Berg, M. K. McBride, C. Wang, C. N. Bowman, *Polymer* **2014**, *55*, 5849–5872.

[11] D. Santiago, X. Fernández-Francos, F. Ferrando, S. De la Flor, *J. Polym. Sci. Part B Polym. Phys.* **2015**, *53*, 924–933.

[12] J. S. Arrieta, J. Diani, P. Gilormini, *J. Appl. Polym. Sci.* **2014**, *131*, 39813.

[13] R. Bongiovanni, G. Malucelli, M. Sangermano, A. Priola, *Macromol. Symp.* **2002**, *187*, 469–479.

[14] P. Puomi, H. M. Fagerholm, A. Sopanen, Anti-Corros. *Methods Mater.* **2001**, *48*, 160–170.

[15] M. Sangermano, M. Sturari, A. Chiappone, I. Roppolo, *Macromol. Mater. Eng.* **2015**, *300*, 340–345.

[16] R. Nazar, S. Ronchetti, I. Roppolo, M. Sangermano, R. M. Bongiovanni, *Macromol. Mater. Eng.* **2015**, *300*, 226–233.

[17] M. Sangermano, N. Razza, J. V. Crivello, *Macromol. Mater. Eng.* **2014**, *299*, 775–793.

[18] D. L. Safranski, K. Gall, *Polymer* **2008**, *49*, 4446–4455.

[19] K. Gall, C. M. Yakacki, Y. Liu, R. Shandas, N. Willett, K. S. Anseth, J. *Biomed. Mater. Res. Part A.* **2005**, *73*, 339–348.

[20] K. E. Smith, S. S. Parks, M. A. Hyjek, S. E. Downey, K. Gall, *Polymer* **2009**, *50*, 5112–5123.

[21] A. M. Ortega, C. M. Yakacki, S. A. Dixon, R. Likos, A. R. Greenberg, K. Gall, *Soft Matter.* **2012**, *8*, 7381–7392.

[22] K. E. Smith, J. S. Temenoff, K. Gall, *J. Appl. Polym. Sci.* **2009**, *114*, 2711–2722.

[23] C. M. Yakacki, R. Shandas, D. Safranski, A. M. Ortega, K. Sassaman, K. Gall, *Adv. Funct. Mater.* **2008**, *18*, 2428–2435.

[24] C.-H. Park, S.-W. Lee, J.-W. Park, H.-J. Kim, *React. Funct. Polym.* **2013**, *73*, 641–646.

[25] W. Voit, T. Ware, R. R. Dasari, P. Smith, L. Danz, D. Simon, S. Barlow, S. R. Marder, K. Gall, *Adv. Funct. Mater.* **2010**, *20*, 162–171.

[26] D. W. van Krevelen, Properties of polymers, Elsevier, Amsterdam, 1972.

[27] C. M. Yakacki, S. Willis, C. Luders, K. Gall, *Adv. Eng. Mater.* **2008**, *10*, 112–119.

[28] A. J. Lesser, K. J. Calzia, *J. Polym. Sci. Part B Polym. Phys.* **2004**, *42*, 2050–2056.

[29] X. L. Wu, S. F. Kang, X. J. Xu, F. Xiao, X. L. Ge, *J. Appl. Polym. Sci.* **2014**, *131*, 40559.

[30] C. Liu, H. Qin, P. T. Mather, *J. Mater. Chem.* **2007**, *17*, 1543–1558.

[31] J. P. Pascault, H. Sautereau, J. Verdu, R. J. J. Williams, Thermosetting Polymers. Marcel Dekker, New York, 2002.

[32] J. Diani, P. Gilormini, C. Frédy, I. Rousseau, *Int. J. Solids Struct.* **2012**, *49*, 793–799.

[33] C. Azra, C. J. G. Plummer, J.-A. E. Månson, *Smart Mater. Struct.* **2011**, *20*, 082002.

[34] D. Zhang, Y. Liu, K. Yu, J. Leng, *J. Intell. Mater. Syst. Struct.* **2011**, *22*, 2147–2154.

[35] Y. Liu, C. Han, H. Tan, X. Du, *Mater. Sci. Eng.* **2010**, *527*, 2510–2514.

[36] S. Pandini, F. Bignotti, F. Baldi, S. Passera, *J. Intell. Mater. Syst. Struct.* **2013**, *24*, 1583–1597.

[37] M. Fan, H. Yu, X. Li, J. Cheng, J. Zhang, *Smart Mater. Struct.* **2013**, *22*, 055034.

[38] M. Fan, J. Liu, X. Li, J. Zhang, J. Cheng, *J. Polym. Res.* **2014**, *21*, 376.

Chapter V

Conclusions and Future Work

V.1. Conclusions

This thesis presents an experimental study of the influence of the thermomechanical conditions and chemical structure of thermoplastic and thermosetting shape-memory polymers. Below the most important conclusions obtained during this thesis are described.

Effect of thermomechanical programming conditions on thermoplastic shape-memory polymers:

- The thermomechanical cyclic conditions strongly affect the shape-recovery ratio R_r of the SMPs and their stabilization with cycling. When the SMP was subjected to successive cycles, R_r degraded because of the accumulation of irrecoverable deformation. Higher maximum prescribed stress σ_m and higher programming temperature T_{prog} accentuated this degradation. Higher σ_m delayed the stabilization of R_r. However, T_{prog} did not affect the stability of R_r. The stress holding time t_H caused considerable degradation of R_r over successive cycles even if t_H was applied just for a few seconds. It is strongly recommended to quench the temperature as fast as possible in order to reduce the effect of the t_H.
- The shape fixity ratio R_f and the switching temperature T_{sw} showed similar values at each σ_m. If $T_{prog} > T_g$, the SMP showed better values of fixation than $T_{prog} < T_g$ and T_{sw} increased with increasing T_{prog}.

With low σ_m, neither R_f nor T_{sw} were affected by cycling beyond instable behaviour during the first cycles. R_f and T_{sw} were not affected by the t_H over successive cycles.

- A progressive strain-hardening was observed when the SMP was programmed over successive cycles. This phenomenon was more pronounced when $T_{prog} < T_g$. With high σ_m the strain-hardening was prolonged for more cycles and the percentage of hardening was higher. Specimens subjected to t_H softened considerably during the first cycle and the strain-hardening showed the same magnitude regardless of the t_H applied.

Thermomechanical characterization of hyperbranched-modified epoxy-based shape-memory polymers:

- The presence of hyperbranched poly(ethyleneimine)s (Lupasol®) in the epoxy networks led to more heterogeneous structures with higher crosslinking density and higher glass transition temperatures. Formulations modified with the high molecular weight Lupasol® PR8515 had lower T_gs but wider transitions than formulations modified with the low molecular weight Lupasol® FG. The ratio between the glassy modulus and the rubbery modulus E'_g/E'_r decreased as the hyperbranched polymer content was increased in the materials, in accordance with the increase in crosslinking density.

- The tensile tests revealed excellent mechanical properties in terms of very high strain and stress at break values at different temperatures. Tensile testing at room temperature (in the glassy regime) showed that an increase in Lupasol® resulted in an increase in the stress at break and strain at break. In the rubbery regime, an increase in the Lupasol® content decreased the values of stress and strain at break. A deformability peak was found at the onset of the glass transition temperature $T_g^{E'}$, showing noteworthy values up to

60% and 15 MPa. At this temperature, the stress at break increased and the strain at break decreased due to an increase in the crosslinking density. The higher crosslinking density and the presence of possible molecular interactions of formulations with Lupasol® PR8515 resulted in slightly lower values of stress at break and strain at break than formulations with Lupasol® FG.

- The characterization of less conventional mechanical properties for shape-memory polymers provided interesting information for their use in real applications. Young's modulus values revealed more rigid structures in formulations with a higher Lupasol® content and hardness test results showed higher values of hardness in formulations with a higher DGEBA and Lupasol® content due to increased crosslinking density and less presence of the plasticizing effect of Jeffamine® D400 flexible structure. Formulations with a lower Lupasol® content (and thus a higher Jeffamine® D400 content) showed higher values of impact strength due to the energy dissipation effect of the aliphatic flexible structure of Jeffamine® D400. The analysis of the surface fracture by SEM microscopy confirmed the more rigid structure of formulations with a higher Lupasol® content.

Shape-memory properties under free and constrained conditions of hyperbranched-modified epoxy-based shape-memory polymers:

- The shape-memory properties of hyperbranched-modified epoxy-based SMPs showed excellent values: shape recovery and shape fixity were as high as 97% and 98%, respectively. R_r and R_f decreased slightly when the Lupasol® content was increased because it restricted chain-conformational changes during deformation and molecular dynamics, adversely affecting the shape-memory properties. Formulations with Lupasol® PR8515 presented slightly lower shape-memory properties because they

were more heterogeneously structured than formulations with Lupasol® FG.

- The thermomechanical procedures under constrained recovery conditions showed exceptionally high values of recovery stress and work output (up to 7 MPa and 750 kJ/m^3, respectively).The recovery stress generated during fully constrained recovery increased as the maximum stress applied during programming increased. A peak in the generation of mechanical work was observed in partially constrained shape recovery. A higher Lupasol® content reduced the shape recovery ratio and shifted the maximum work generated toward lower constraining levels and decreased the efficiency of the process. A compromise between crosslinking density and a homogeneous network needs to be reached in order to guarantee sufficient driving recovery force and to allow molecular mobility.

Thermomechanical and shape-memory properties of bisphenol A-based acrylate-based shape-memory polymers:

- Thermomechanical measurements of bisphenol A-based acrylate-based shape-memory thermosets revealed more heterogeneous networks and lower glass transition temperatures when PGM content was increased and the MMA or EMA content decreased. Formulations with BAEDA showed lower glass transition temperatures and more homogeneous networks than formulations with BADA.

- Mechanical properties evaluated at room temperature showed that formulations with BAEDA presented a larger plateau of plastic deformation than formulations with BADA. At the onset of the glass transition temperature $T_g^{E'}$, all formulations showed high values of stress at break (up to 15 MPa). Formulations with BAEDA showed lower tensile modulus than formulations with

BADA and thus higher failure strains due to the presence of mobile oxyethylene units in BAEDA and the existence of hydrogen-bond interactions in formulations with BADA.

- Shape-memory properties showed very good values of R_r and R_f of around 95% and 97%, respectively. These materials showed very fast recovery velocities in transient temperature conditions and very short recovery times in isothermal conditions.

The results obtained during this thesis give an overview of the combination of thermomechanical programming conditions that maximized the shape-memory properties of thermoplastic shape-memory polymers over the highest number of cycles. Furthermore, the thermal, mechanical and shape-memory characterization of hyperbranched-modified epoxy-based shape-memory polymers revealed that these materials look promising for potential actuator-like applications. Acrylate-based shape-memory thermosets modified with bisphenol A-based crosslinking agents can be used to enhance the thermomechanical and shape-memory properties of this kind of material.

V.2. Future work

The work carried out during this thesis has raised certain questions that require further study in the future. For example:

- Chapter III studied the influence of some thermomechanical parameters on shape-memory properties when the SMP is subjected to several shape-memory cycles. The thermomechanical parameters studied were the programming temperature, the maximum stress and the stress-holding time. However, other parameters were not looked at. The effect of deformation rates, heating and cooling rates, or the fixing and recovery temperatures have been the focus of several research studies. Moreover, further work can look at the effect of these thermomechanical parameters on the stabilization of the shape-memory properties when successive shape-memory cycles are performed.
- Chapter IV studied the effect of hyperbranched polymers on the shape-memory properties of epoxy-based shape-memory polymers. In general terms, hyperbranched polymers enhanced mechanical and shape-memory properties. However, the content and molecular weight of hyperbranched polymers should be controlled because their structure increases the heterogeneity of the shape-memory networks and adversely affects the shape-memory properties. Two different hyperbranched polymers with different molecular weights were studied in this dissertation: Lupasol® FG with 800 g/mol and Lupasol® PR8515 with 2000 g/mol. In order to properly understand the effect of the hyperbranched structure, hyperbranched polymers with higher and lower molecular weights can be used. Diethylene triamine can act as a very low molecular weight hyperbranched polymer (103 g/mol) and Lupasol® WF as a higher molecular weight modifier (25000 g/mol).

- Some members of our research group have done some excellent work on synthesizing star-shaped polymers, which are promising modifiers for thermosetting shape-memory polymers. Star-shape polymers consist of at least three linear polymer chains connected to a central core (Figure V.2.1). The results obtained suggest that they can significantly toughen epoxy resins without such undesirable effects as a drop in the storage modulus in the glassy region or an increase in the viscosity of the blends. Therefore, the thermomechanical and viscoelastic properties of star-shaped polymers could be studied and their applicability as modifiers for shape-memory polymers analysed.

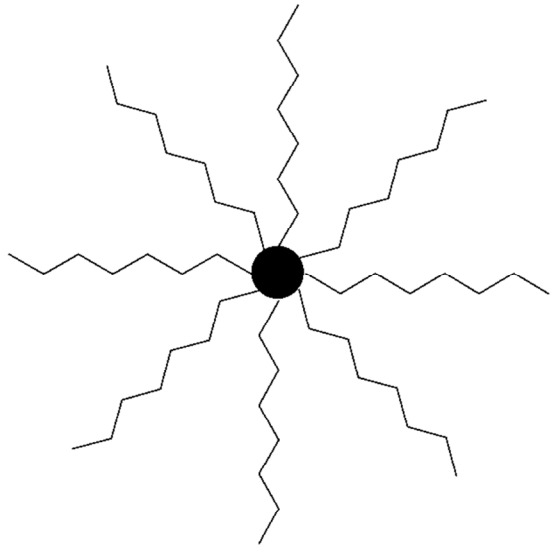

Figure V.2.1 Schematic representation of the structure of star-shaped polymers.

UNIVERSITAT ROVIRA I VIRGILI
EXPERIMENTAL CHARACTERIZATION OF SHAPE-MEMORY POLYMERS: INFLUENCE OF PROCESSING METHODS AND CHEMICAL STRUCTURE
David Manuel Santiago Abraira

Appendix A

A.1. Supporting information

Table A.1 Technical data of Tecoflex® EG-72D

Properties	ASTM Test	Tecoflex® EG-72D
Shore hardness	D2240	67D
Specific gravity	D792	1.11
Flexural modulus (MPa)	D790	634
Ultimate tensile (MPa)	D412	56
Ultimate elongation (%)	D412	310
Tensile modulus (MPa)		
100%	D412	23
200%		33
300%		49
Mold shrinkage (%)	D955	0.4-0.6

Table A.2 Specifications of Lupasol® FG and Lupasol® PR8515

Properties	Lupasol® FG	Lupasol® PR8515
Form	Liquid	Liquid
Odour	Faint odour	Faint odour
Colour	Colourless to yellowish	Colourless to yellowish
Water content (%)	1.5 max.	2 max.
Solidification temperature (ºC)	-20	~-10
Boiling temperature (ºC)	-	> 200
Thermal decomposition (ºC)	> 250	> 250
Solubility in water	Fully soluble	Fully soluble
Viscosity @ 20 ºC (mPa·s)	800-5000	10000-20000
Density (20 ºC) (g/cm^3)	1.03 (DIN 51757)	1.05 (DIN 51757)
Pour point (ºC)	-20	-9
pH	10-12 (DIN 19268)	10-12
Dry content (%)	-	98
Molecular weight (g/mol)	800	2000
Common chemical name	Polyethyleneimine (PEI)	Polyethyleneimine (PEI)
CAS number	25987-06-8	25987-06-8

Table A.3 Specifications of Araldyte® GY 240

Properties	Araldyte® GY 240
Characteristics	Bisphenol A
Viscosity (25 ºC) (mPa·s)	7000-9000
Epoxy index (eq/kg)	5.45-5.56
Epoxy equivalent (g/eq)	180-183
Colour (Gardner)	≤ 2

Table A.4 Specifications of Jeffamine® D-400

Properties	Jeffamine® D-400
Appearance (25 ºC)	Colourless to pale yellow liquid with slight haze permitted
Colour (Pt-Co)	30 max.
Primary amine (%)	97 min.
Total acetylatables (meq/g)	4.2-4.9
Total amine (meq/g)	4.1-4.7
Amine hydrogen equivalent (g/eq)	115
Density (g/ml)	0.972
pH (5% aqueous solution)	11.6
Water content (%)	0.25 max.
CAS number	9046-10-0

Table A.5 Specifications of Ebecryl® 605

Properties	Ebecryl® 605
Dilution	20 TPGDA
Viscosity @ 25 ºC (mPa·s)	7500
Colour	2
Molecular weight (g/mol)	500
Functionality	2

Table A.6 Specifications of bisphenol A ethoxylate diacrylate

Properties	Bisphenol A ethoxylate diacrylate
Colour	Colourless to light yellow
Form	Viscous liquid
Molecular weight (g/mol)	512
Viscosity (25 ºC) (cps)	800-1200
Density (25 ºC) (g/ml)	1.14
CAS number	64401-02-1

Table A.7 Specifications of methyl methacrylate

Properties	Methyl methacrylate
Colour	Colourless
Form	Liquid
Molecular weight (g/mol)	100
MEHQ as inhibitor (ppm)	8-30
CAS number	80-62-6

Table A.8 Specifications of ethyl methacrylate

Properties	Ethyl methacrylate
Colour	Colourless
Form	Liquid
Molecular weight (g/mol)	114
MEHQ as inhibitor (ppm)	15-20
CAS number	97-63-2

Table A.9 Specifications of poly(ethylene glycol) methylether methacrylate

Properties	Poly(ethylene glycol) methylether methacrylate
Colour	Colourless
Form	Viscous liquid
Molecular weight (g/mol)	500
MEHQ as inhibitor (ppm)	100
BHT as inhibitor (ppm)	200
Density (25 ºC) (g/ml)	1.08
CAS number	26915-72-0

A.2. List of figures

A.3. List of tables

UNIVERSITAT ROVIRA I VIRGILI
EXPERIMENTAL CHARACTERIZATION OF SHAPE-MEMORY POLYMERS: INFLUENCE OF PROCESSING METHODS AND CHEMICAL STRUCTURE
David Manuel Santiago Abraira

A.4. List of publications

- **David Santiago**, Francesc Ferrando, Silvia De la Flor. *"Effect of different shape-memory processing methods on the thermomechanical cyclic properties of a shape-memory polyurethane"*. Journal of Materials Engineering and Performance **2014**, *23*, 2561-2566.
- **David Santiago**, Francesc Ferrando, Silvia De la Flor. *"Influence of holding time on shape recovery in a polyurethane shape-memory polymer"*. Journal of Materials Engineering and Performance **2014**, *23*, 2567-2573.
- **David Santiago**, Xavier Fernández-Francos, Francesc Ferrando, Silvia De la Flor. *"Shape-memory effect in hyperbranched poly(ethyleneimine)-modified epoxy thermosets"*. Journal of Polymer Science. Part B: Polymer Physics **2015**, *53*, 924-933.
- **David Santiago**, Silvia De la Flor, Francesc Ferrando, Xavier Ramis, Marco Sangermano. *"Thermomechanical properties and shape-memory behavior of bisphenol A diacrylate-based shape-memory polymers"*. Macromolecular Chemistry and Physics **2016**, *217*, 39-50.
- **David Santiago**, Albert Fabregat-Sanjuan, Francesc Ferrando, Silvia De la Flor. "*Recovery stress and work output in hyperbranched poly(ethyleneimine)-modified shape-memory epoxy polymers"*. Journal of Polymer Science. Part B: Polymer Physics **2016**, *54*, 1002-1013

- **David Santiago**, Albert Fabregat-Sanjuan, Francesc Ferrando, Silvia De la Flor. *"Improving mechanical and shape memory properties in hyperbranched epoxy shape memory polymers"*. Shape Memory and Superelasticity **2016**, DOI: 10.1007/s40830-016-0067-y.

- **David Santiago**, Francesc Ferrando, Silvia De la Flor. *"Thermomechanical characterization of hyperbranched-modified epoxy thermosets with enhanced mechanical and shape-memory properties"*. Journal of Polymer Science **2016**, *under review*.

A.4.1. Previous publications related to this thesis

- **David Santiago**, Mireia Morell, Xavier Fernández-Francos, Àngels Serra, Josep M. Salla, Xavier Ramis. *"Influence of the end groups of hyperbranched poly(glycidol) on the cationic curing and morphology of diglycidylether of bisfenol A thermosets"*. Reactive & Functional Polymers **2011**, *71*, 380-389.

- **David Santiago**, Xavier Fernández-Francos, Xavier Ramis, Josep M. Salla, Marco Sangermano. *"Comparative curing kinetics and thermal-mechanical properties of DGEBA thermosets cured with a hyperbranched poly(ethyleneimine) and an aliphatic triamine"*. Thermochimia Acta **2011**, *526*, 9-21.

- Xavier Fernández-Francos, **David Santiago**, Francesc Ferrando, Xavier Ramis, Josep M. Salla, Àngels Serra, Marco Sangermano. *"Network structure and thermomechanical properties of hybrid DGEBA networks cured with 1-methylimidazole and hyperbranched poly(ethyleneimine)s"*. Journal of Polymer Science, Part B: Polymer Physics **2012**, *50*, 1489-1503.

A.5. Meeting contributions

- **David Santiago**, Francesc Ferrando, Silvia De la Flor. *"Thermomechanical Cyclic Properties by Different Shape Memory Processing in Polyurethane Shape Memory Polymer"*. The International Conference on Shape Memory and Superelastic Technologies (SMST). Prague, Czech Republic, May 2013. Poster presentation.
- **David Santiago**, Francesc Ferrando, Silvia De la Flor. *"Influence of Holding Time on Shape Recovery in a Polyurethane Shape-Memory Polymer"*. The International Conference on Shape Memory and Superelastic Technologies (SMST). Prague, Czech Republic, May 2013. Poster presentation.
- **David Santiago**, Xavier Fernández-Francos, Francesc Ferrando, Silvia De la Flor. *"Efecto de memoria de forma en resinas epoxy modificadas con polietileniminas hiperramificadas"*. XIII Reunión del Grupo Especializado de Polímeros (GEP) de la RSEQ y RSEF. Girona, España, Septiembre 2014. Presentación oral.
- **David Santiago**, Francesc Ferrando, Silvia De la Flor. *"Influencia de los parámetros de ensayo en las propiedades termomecánicas de polímeros con memoria de forma"*. XX Congreso Nacional de Ingeniería Mecánica (CNIM). Málaga, España, Septiembre 2014. Presentación oral.

- Silvia De la Flor, **David Santiago**, Albert Fabregat-Sanjuan, Francesc Ferrando, Xavier Fernández-Francos. *"Enhancing Mechanical and Shape Memory Properties in Hyperbranched Epoxy Shape Memory Polymers"*. Shape-Memory and Superelastic Technologies (SMST). Oxfordshire, United Kingdom, May 2015. Poster presentation.
- **David Santiago**, Francesc Ferrando, Silvia De la Flor. *"Recovery stress quantification developed in epoxy-based shape-memory polymers"*. 1st French-Spanish Joint Congress for Young Researches in Polymers. Donostia-San Sebastián, Spain, September 2015. Oral presentation.
- **David Santiago**, Francesc Ferrando, Silvia De la Flor. *"Evolución de las propiedades termomecánicas con el ciclado en poliuretanos con memoria de forma"*. XII Congreso Iberoamericano de Ingeniería Mecánica. Guayaquil, Ecuador, Noviembre 2015. Presentación oral.

A.6. Internship

University: Politecnico di Torino
Dipartamento di Scienza Applicata e Tecnologia
Corso Duca degli Abruzzi 24, 10129, Turin, Italy
Advisor: Dr. Marco Sangermano
Period: October 4th 2104 – January 15th 2015

The work developed at *Politecnico di Torino* included thermomechanical and shape-memory properties characterization of shape-memory thermosetting polymers synthesized by bisphenol A-based diacrylates as crosslinking agents and various (meth)acrylate monomers as chain builders.

UNIVERSITAT ROVIRA I VIRGILI
EXPERIMENTAL CHARACTERIZATION OF SHAPE-MEMORY POLYMERS: INFLUENCE OF PROCESSING METHODS AND CHEMICAL STRUCTURE
David Manuel Santiago Abraira

UNIVERSITAT ROVIRA I VIRGILI
EXPERIMENTAL CHARACTERIZATION OF SHAPE-MEMORY POLYMERS: INFLUENCE OF PROCESSING METHODS AND CHEMICAL STRUCTURE
David Manuel Santiago Abraira